VOLUME 14 (1959) No. 2

NUCLEAR PHYSICS

JOURNAL DEVOTED TO THE EXPERIMENTAL AND THEORETICAL STUDY OF THE FUNDAMENTAL CONSTITUENTS OF MATTER AND THEIR INTERACTIONS

EDITOR: L. ROSENFELD · COPENHAGEN

G. R. ALLCOCK, Topics in the theory of dispersion relations 177

J. E. ALBERGHINI and R. M. STEFFEN, Transverse polarization of K-conversion electrons following the beta decay of Hg^{203} 199

I. R. GATLAND, Schwinger's meson and the μ-mesic atom 205

J. R. BIRD and J. R. WATERS, The use of digital recording on magnetic tape for the study of γ-rays from resonant neutron capture in platinum 212

A. M. SEGAR and R. RUBINSTEIN, Neutral meson production by 930 MeV protons. 222

P. MENOTTI, Wigner's inequalities for relativistic scattering 232

DOUGLAS MILLER, Coupled errors on scattering phase shifts 238

LESLIE COHEN and RALPH A. TOBIN, Lifetime of the 3.56-MeV state of Li^6 . . 243

A. S. MELIGY, Isotope shift from non-uniform nuclear charge distributions . . 248

G. BARTON, D. M. BRINK and L. M. DELVES, Quadrupole enhancement in O^{17} and F^{17} 256

J. SUCHER, An asymptotic causality requirement for systems with constrained inputs 263

R. J. BELL, T. W. BONNER and F. GABBARD, The disintegration of Ne^{20} by fast neutrons 270

FLETCHER GABBARD, H. BICHSEL and T. W. BONNER, The disintegration of nitrogen by fast neutrons 277

H. E. HALL and T. W. BONNER, Gamma radiations from inelastic scattering of fast neutrons in C^{12}, N^{14} and O^{16}. 295

F. KASCHLUHN, Eine feldtheoretische Verallgemeinerung der Impulsnäherung 314

YU. A. BUDAGOV, S. WIKTOR, V. P. DZELEPOV, P. F. YERMOLOF and V. I. MOSKALEV, β-decay of negative pions 339

J. VON BEHR und H. MARSCHALL, Zur Depolarisation der μ-Mesonen beim Auger-Einfang in Wasserstoff 342

NORTH-HOLLAND PUBLISHING COMPANY - AMSTERDAM

December (2) 1959

EDITORIAL BOARD

AUSTRALIA & NEW ZEALAND:	H. Messel (Sydney), M. L. Oliphant (Canberra)
AUSTRIA:	B. Karlik, (Vienna), H. Thirring (Vienna)
BELGIUM:	M. de Hemptinne (Louvain), J. Verhaeghe (Ghent)
CANADA:	G. Volkoff (Vancouver)
DENMARK:	C. Møller (Copenhagen), S. Rozental (Copenhagen), G. Brown (Copenhagen)
FINLAND:	L. Simons (Helsinki)
FRANCE:	A. Berthelot (Saclay), S. Gorodetzky (Strasbourg)
GERMANY (DEM. REP.):	G. Hertz (Leipzig)
GERMANY (FED. REP.):	W. Gentner (Freiburg i. B.), J. H. D. Jensen (Heidelberg)
GREAT BRITAIN:	S. Devons (Manchester), T. H. R. Skyrme (Harwell)
HUNGARY:	L. Janossy (Budapest)
INDIA:	H. Bhabha (Bombay), R. Ramanna (Trombay)
IRISH REPUBLIC:	J. McConnell (Maynooth)
ISRAEL:	G. Racah (Jerusalem)
ITALY:	E. Amaldi (Rome)
JAPAN:	S. Kikuchi (Tokyo), S. Tomonaga (Tokyo)
MEXICO:	M. Moshinsky (Mexico)
NETHERLANDS:	H. Brinkman (Groningen), S. R. de Groot (Leiden)
NORWAY:	E. Hylleraas (Oslo), A. Lundby (Oslo), H. Wergeland (Trondheim)
POLAND:	L. Infeld (Warsaw)
PORTUGAL:	J. M. Araújo (Porto), J. R. de Almeida Santos (Coimbra)
SOUTH AMERICA:	G. Beck (Saõ Paulo), J. Leite Lopes (Rio de Janeiro)
SPAIN:	J. M. Otero (Madrid), C. Sanchez del Rio (Madrid)
SWEDEN:	O. Klein (Stockholm), K. Siegbahn (Uppsala), I. Waller (Uppsala)
SWITZERLAND:	P. Huber (Basel), P. Scherrer (Zürich)
U.A.R. & ARAB COUNTRIES:	F. El Bedewi (Alexandria), M. G. Nooh (Cairo)
U.S.A.	H. H. Barschall (Madison, Wisconsin), V. Weisskopf (Cambridge, Mass.)
U.S.S.R.:	M. A. Markov (Moscow), I. S. Shapiro (Moscow), D. V. Skobeltzyn (Moscow)
YUGOSLAVIA:	I. Supek (Zagreb)

CONTRIBUTIONS may be sent to the Editor, Professor L. Rosenfeld, NORDITA, Blegdamsvej 17, Copenhagen Ø, either directly, or preferably through the intermediary of one of the members of the Editorial Board of the country or region in which the author is working. They may be written in English, French or German.

NUCLEAR PHYSICS is published in fortnightly issues. The subscription price per volume of 700 pages is fl 57.00; 114s; $ 15.00. Post-free.

SUBSCRIPTIONS should be sent to the publishers, NORTH-HOLLAND PUBLISHING COMPANY, P.O.Box 103, Amsterdam or to any subscription-agent.

BOOKS FOR REVIEW should be sent to Professor Rosenfeld.

No part of this issue may be reproduced in any form, by print, photoprint, microfilm or any other means without written permission from the publisher. Reprints, photoprints or microfilms are obtainable at cost from the publisher.

Printed in the Netherlands

7.A

Nuclear Physics **14** (1959/60) 177—198; © *North-Holland Publishing Co., Amsterdam*

Not to be reproduced by photoprint or microfilm without written permission from the publisher

TOPICS IN THE THEORY OF DISPERSION RELATIONS

G. R. ALLCOCK

Department of Theoretical Physics, University of Liverpool

Received 4 September 1959

Abstract: The mathematics and physics of the theory of dispersion relations are discussed, with particular reference to the quantized field description of the scattering by a fixed centre. Various known analytic continuations of physical data are examined for mathematical stability, and the dispersion relation at fixed momentum transfer is proved by a simple method which is throughout susceptible to the operations of numerical analysis. It is suggested that such stability is a necessary feature of a satisfactory proof.

The scattering problem is formulated entirely in terms of the fields at large but finite distances from the scatterer, and this leads to a direct and perspicuous treatment of the "unphysical" region. The effect of finite violations of microscopic causality is expressed quantitatively through a new dispersion relation which, while still dealing only with accessible scattering data, embodies within itself a fundamental length.

1. Introduction

There are many articles on the derivation of dispersion relations from the principle of relativistic microscopic causality †. Yet all the known proofs, even those which are rigorous [1–3, 17]) use mathematical constructions whose physical motivation does not seem particularly clear or direct. There is not in evidence that degree of simplicity for which one might reasonably hope, having in mind the relatively straightforward structure of the dispersion relations themselves. More serious is a frequent failure to make a clear distinction between the radically different properties enjoyed by analytic functions on the one hand, and the numerical data of physics on the other. Matters arising in this connection are discussed at some length in section 2 of the present paper, the main point of that section being to indicate that the analytic continuation of a physical function, such as a scattering amplitude, is in the nature of the case an essentially arbitrary operation, dependent upon the preference of the author responsible.

The delicacy of analytic continuation has often been stressed, but it has generally been argued that just because of this it is necessary to use "exact" expressions for the physical functions represented, in order to obtain their "correct" continuation. Such an approach entails mathematical considerations of a type unfamiliar in other branches of theoretical physics. The present work

† See refs.[1–4]) and further references given therein, also ref. [8]).

shows a different and less recondite approach to the problem. There is really no such thing as a "correct" analytic continuation of a physical function, except purely as a matter of convention. Hence there arises the possibility of using "not quite exact" expressions for the function represented, designed to give more useful analytic continuations than the "exact" one. The advantages of this point of view are illustrated in the following, taking, by way of example, the fixed-target scattering of a relativistic neutral spin-zero boson with non-zero rest mass. It is anticipated that the simple but rigorous treatment given in section 4 will, with suitable adaptation, be applicable to meson-nucleon scattering.

The scattering amplitude is expressed "almost exactly" as a functional of the fields at large enough but nevertheless finite distances from the scatterer. (Similar "not quite exact" representations of scattering amplitudes have been used in dispersion theory by Joffé [5]), Gasiorowicz and Ruderman [6]), and Bohr and Mottelson [7]). This device is, of course, quite in accord with the physical nature of a scattering process. It gives immediately a useful representation of the scattering amplitude as a function simultaneously analytic in the energy ω and the momentum transfer Δ, so that, in particular, dispersion relations with fixed momentum transfer follow at once. The representation ensures that the domain of analyticity already extends throughout the region of unphysical energies, and the usual difficulties here are avoided from the beginning. The contribution of this region, though generally obscured, has long been known to be in the end determined entirely by the long-distance behaviour of the bound-state and scattering-state wave functions. It is a merit of the new representation that it manifests this feature directly.

When dealing with analytic continuations of physical data, etc., certain problems of *stability* invariably arise. A continuation may be said to be *stable* if any small change in the data produces only a small change in the continuation. Various examples are examined for stability according to this simple criterion in section 2. In the present approach to dispersion relations the scattering amplitude is expressed in terms of operators for particle flux through distant surfaces surrounding the scatterer, and instability of the continuation may arise with respect to the shape and size of these surfaces. The demand that every quantity appearing in the fixed momentum-transfer dispersion relation be stable sets the usual upper limit 2α to the momentum transfer Δ. Here α is the reciprocal exponential range of the interaction which produces the scattering. Within this range of momentum transfer, the contribution of the continuum part of the unphysical region is a stable functional of the space-time data, and can be expressed as a function of the scattering phase shifts. Nevertheless, as shown in section 2, and again in section 4, it is *not* a stable functional of experimentally accessible angular distribution data. The conclusion drawn from this is that the dispersion relations with non-zero momentum transfer are

in principle unusable, except when supplemented by some sort of effective range theory. Effective range theory can supply the required theoretical *assumptions* as to the behaviour of all the higher phase shifts, which can never be measured with the requisite accuracy. Thus only the forward scattering dispersion relations make unequivocal statements about experimental data.

The derivation of the dispersion relations proceeds through the application of microscopic causality at macroscopic distances. The precise meaning of the causality condition is discussed in section 3. The present treatment brings out clearly the facts that the dispersion relations do not depend on the canonical commutation relations, nor on the assumption of microscopic causality within the collision region. These are not new results †. However, dispersion relations modified to allow for finite violations of microscopic causality are presented (eq. (48)), and it is believed that these are new. The wave front is allowed to jump forward by a distance not exceeding l as it passes acausally through the collision region, and the parameter l is built into the dispersion relations explicitly. It is noteworthy that the modified dispersion relations (48) for forward scattering express only relationships between l and directly observable quantities. Thus, given good enough experimental data, it should become possible to obtain information as to the magnitude of possible violations of microscopic causality.

2. Analytic Continuation and Extrapolation

The original derivations of the relativistic dispersion relations [8]) amply demonstrated the heuristic value of the method of analytic continuation; nevertheless the proper formulation of the method requires great care, on account of a certain lack of *stability*. A simple demonstration of this instability is afforded by the problem of constructing a function $T(\omega)$ analytic in the upper half of the ω-plane, given $T(\omega)$ on the real ω-axis. If $T(\omega)$ on the real axis is changed by the addition of some small but rapidly oscillating term, the extension into the complex plane may be completely altered. One such term which is large in the upper half-plane is $\varepsilon \exp(-i\omega/\varepsilon)$, with ε arbitrarily small. A similar term $\varepsilon \exp(i\omega/\varepsilon)$ makes virtually no change in the upper half-plane, but is large in the lower half-plane. Many similar trivial examples may be written down. In general, therefore, although it is meaningful to refer to the continuation of an *analytic* function $T(\omega)$ into a larger domain, such a continuation is unstable, being infinitely sensitive to the given function $T(\omega)$. By the same argument it is not meaningful or legitimate, without further specification, to refer to analytic continuations or extrapolations of the data and constructs of physics, for these are essentially numerical functions. It is clear that the analytic continuation or extrapolation even of very accurate

† See refs. [5–7]).

numerical data is in itself wholly undefined, no matter how small the distance of extrapolation, and no matter how fine the mesh on which the data are set.

Continuations of numerical data may, however, be constructed, as a matter of convention, through specific formulae expressing the continuations as stable explicit functions of the data. But the instability latent in the problem implies that such stable conventions are not by any means unique, and correspondingly the continuations which they give may have no mathematical or physical significance. Their utility must be judged by the extent to which they facilitate the derivation of relationships between stable and physically accessible functions of the data.

The above elementary considerations are relevant to dispersion theory. Van Kampen [9, 10]) seems to have been the first to discuss these matters, and has made some pertinent observations in this connection, pointing out in particular that the instability encountered in analytic continuation is precisely that which appears in the solution of an elliptic differential equation subjected to hyperbolic boundary conditions.

The conventions by which analytic continuations are set up in dispersion theory depend to some extent upon how the dynamical problem is formulated. Below a few examples are discussed, to exhibit various kinds of instability which may arise.

2.1. EFFECTIVE RANGE DISPERSION THEORY

The work of Heisenberg [11]) on the analytic properties of the partial-wave scattering matrix $S(k)$, showing the bound states as poles and zeros on the imaginary k-axis, occupies a prominent position among the various formal developments of a similar character which ultimately led to the heuristic derivations [8]) of the meson-nucleon dispersion relations. In the context of this problem the exact solution of the Schroedinger equation with complex energy eigenvalue $k^2/2\kappa$ provides a possible convention by which the analytic continuation of $S(k)$ may be given concrete definition. But Ma [12]) found that $S(k)$ so defined in the complex plane depends in an erratic way on the long-range part of the scattering potential. Thus, an exponential potential $V_0 \exp(-\alpha r)$ gives an analytic S-matrix having redundant poles and zeros, not descriptive of bound states. If, however, the same potential be cut off at a large radius R, and the Schroedinger equation be again solved exactly, a new analytic S-matrix is obtained, agreeing with the previous one within the strip $|\mathrm{Im}\, k| < \frac{1}{2}\alpha$, with neglect only of insignificant rapidly fluctuating terms of the order R^{-1}. Outside this strip the two S-matrices differ completely, in particular the second does not have redundant poles and zeros. Evidently, therefore, the continuation of the partial-wave S-matrix by exact solution of the Schroedinger equation is unstable with respect to arbitrarily small changes in the long distance tail of the potential. That is to say, it cannot be expressed as an explicit functional of the

potential unless the latter be completely cut off (or given some explicit analytic space dependence) outside some large but finite distance.

It will be seen that in this problem the "inexact" continuation, based on a cut off potential, is better than that derived from the exact potential, in that the zeros and poles of the former continuation all correspond to existing bound states. Neither continuation, however, is necessarily very significant, for they are both hypersensitive to the potential at large but finite distances. The situation improves if it is known *a priori*, say, on the basis of a specific theory, that the potential can be neglected completely outside some small radius a. This case has been treated, *inter alia*, by Hu [13]), Van Kampen [10]), and Knight and Toll [14]). Exact resonance formulae and dispersion relations follow. They involve the factor $\exp(ika)$, but if a is sufficiently small this factor can often be regarded as independent of k over large ranges of k, in which case the formulae may exhibit a physically useful structure. Van Kampen [10]) makes the interesting observation that these resonance formulae and dispersion relations are stable against the introduction of a small long range tail on the potential, while the analytic functions $S(k)$ from which they are derived do not at all possess such stability, except of course on the real k-axis. Similar instabilities appear in all dispersion theory based on analytic continuation, but are often quite harmless provided they are recognized.

2.2. ANGULAR DISTRIBUTION ANALYSIS

A second example to illustrate the idea of stability is afforded by the analytic continuation of a scattering amplitude T, considered as a function of $\cos\theta$ at fixed energy. This problem has been treated by various authors [15–20]). Writing $\cos\theta = x$, it has been shown that the data of quite a variety of non-relativistic and relativistic scattering mechanisms permit the stable definition of a function $T(x)$ analytic and regular within an ellipse in the complex x-plane, with foci at $x = \pm 1$. This analytic function $T(x)$ coincides with the actual scattering amplitude in the real domain $-1 \leqq x \leqq 1$.

Neumann's theorem [21]) on the expansion of analytic functions asserts that the analytic function $T(x)$ can always be represented within the ellipse by a convergent series of Legendre polynomials in x:

$$T(x) = \sum_n a_n P_n(x). \tag{1}$$

The coefficients a_n are given by the formula

$$2\pi i a_n = (2n+1) \oint T(x) Q_n(x) \mathrm{d}x, \tag{2}$$

the integral being taken around the ellipse, and the $Q_n(x)$ being Legendre functions of the second kind. Eqs. (1) and (2) are essentially a statement of Cauchy's integral. They express $T(x)$ within the ellipse as a *stable* functional of its boundary values on the circumference of the ellipse.

The functions $Q_n(x)$ are analytic except for a cut along the real axis from -1 to 1, on which the discontinuity is $-i\pi P_n(x)$. Hence, shrinking the elliptical integration contour in eq. (2), one obtains an alternative representation of the a_n,

$$a_n = \tfrac{1}{2}(2n+1)\int_{-1}^{1} T(x)P_n(x)\mathrm{d}x. \tag{3}$$

Eqs. (1) and (3) express the analytic function $T(x)$ as an *unstable* functional of its values on the real axis in the interval from -1 to 1. The instability arises in an obvious manner, from large n-values. As n is increased, $P_n(x)$ becomes ever smaller and more rapidly oscillatory within the real interval from -1 to 1, but ever larger for all complex x and for all real x outside this interval. The net effect is that if $T(x)$ is given numerically in the interval from -1 to 1 on the real axis, eq. (3) determines the a_n with an accuracy such that the expansion (1) is useful nowhere at all in the complex plane except in the same real interval.

The above-described instability may be examined quantitatively through a sequence of "approximate" continuations $T_N(x)$ defined by the equation

$$T_N(x) \equiv \int_{-1}^{1} K_N(x, x')T(x')\mathrm{d}x', \tag{4}$$

where the kernel K_N for the N^{th} approximation is defined by

$$K_N(x, x') \equiv \sum_{n=0}^{N} P_n(x)(n+\tfrac{1}{2})P_n(x'). \tag{5}$$

The recursion formulae for the Legendre polynomials [21]) can be used here to give for $K_N(x, x')$ an expression better adapted for the present discussion, namely,

$$K_N(x, x') = \tfrac{1}{2}(x-x')^{-1}(N+1)\{P_{N+1}(x)P_N(x')-P_N(x)P_{N+1}(x')\}. \tag{6}$$

This permits the behaviour of the K_N for large N to be ascertained by inserting the asymptotic expansions of the Legendre polynomials [22]). In particular, if x is real and greater than 1, with x' lying in the interval between -1 and 1, eq. (6) gives, for large enough N,

$$K_N(x, x') \sim \frac{\exp\{(N+\tfrac{1}{2})\cosh^{-1}x\}}{2\pi(x-x')(x^2-1)^{\frac{1}{4}}(1-x'^2)^{\frac{1}{4}}}$$

$$\cdot\,[\exp\{\cosh^{-1}x\}\cos\{(N+\tfrac{1}{2})\cos^{-1}x'-\tfrac{1}{4}\pi\}-\cos\{(N+\tfrac{3}{2})\cos^{-1}x'-\tfrac{1}{4}\pi\}]. \tag{7}$$

As N is increased, the kernels (7) exhibit more and more fully the wild behaviour expected of the members of a sequence whose limiting member K_∞ is designed to accomplish the impossible!

In spite of the lack of stability demonstrated above, formulae (1) and (3) have repeatedly been suggested, without further specifications, as a means

whereby experimental angular distribution data may be extrapolated beyond the physically available region, namely beyond the segment of the real axis enclosed by the points ± 1. Extrapolations of this type are required to evaluate the continuum contributions in the unphysical region of the dispersion relations with fixed non-zero momentum transfer. It is clear that such extrapolations, if they are to be meaningful, must embody theoretical assumptions as to the a_n for large n. Moreover, the errors or uncertainties δa_n in the assumed or measured a_n must be such that $\sum_n P_n(x)|\delta a_n|$ is small throughout the region of extrapolation. Again using the asymptotic expansions of the Legendre polynomials [22]) one finds that so far as large n are concerned the above series behaves like

$$(x^2-1)^{-\frac{1}{4}} \sum_n (2n\pi)^{-\frac{1}{2}} \exp\{(n+\tfrac{1}{2})\cosh^{-1}x\}|\delta a_n|, \tag{8}$$

if x is real and greater than unity. The requirement that such a series be not only convergent but also small clearly sets very stringent limitations on the δa_n, which are not provided by the theorems of refs. [15–20]).

In view of the above facts, it is noteworthy that the highly successful extrapolations of experimental angular distribution data which Chew and others have recently made [23]) to determine meson-nucleon coupling constants do indeed invoke suitable theoretical assumptions in the form of the extrapolation curve used. All the a_n with n larger than some critical value n_0 are assumed to be given accurately by the renormalized Born approximation, as explicit functions of a single coupling constant. This serves to establish a convention for the otherwise undetermined extrapolation, but its physical import is concerned with the ranges and strengths of various contributions to the scattering interaction, and the way these affect the angular distribution in the physical region of x. The analysis of angular distribution data by these methods can therefore be accomplished without introducing the formal extrapolation out of the physical region [24]), and it seems to the present writer that such a procedure is less likely to lead to misconceptions. As to the choice of n_0, it is, from a practical point of view, apparent that it must at the same time be large enough to permit a satisfactory experimental fit, yet small enough that inaccuracies in the data do not make the problem indeterminate. But such an empirical criterion as this is obviously insufficient. If it indicates a value of n_0 lower than that expected on purely theoretical grounds, the analysis is completely unreliable, and can only be made useful with the help of better experimental data †.

2.3. DISPERSION RELATIONS AT FIXED MOMENTUM TRANSFER

Another important application of the notion of stability is to the various formulae which have been used to construct analytic continuations of the

† The author wishes to thank Dr. M. J. Moravcsik for an illuminating discussion on this matter.

scattering amplitude, considered as a function of the energy at fixed momentum transfer. Three examples of such continuations are discussed below.

The scattering of a non-relativistic particle by a local static potential has been treated by Khuri [15]), who investigates the Schroedinger equation with complex energy, and expresses its solution as a Fredholm quotient. In this way the scattering amplitude at fixed momentum transfer and complex energy is explicitly exhibited as a stable functional of the scattering potential, analytic in the infinite upper half of the energy plane. The scattering of a Dirac particle by a local static potential has been treated in a similar manner by Khuri and Treiman [16]). [It may be worth while to remark at this juncture that the Dirac equation with local potential is hyperbolic in the relativistic sense, and so embodies fully the content of the principle of relativistic microcausality. Nevertheless it is not altogether clear whether the conditions of applicability of Khuri's method bear any close relationship to the relativistic microcausality principle, nor is it clear whether any recognizable vestige of this principle survives in the non-relativistic Schroedinger equation †.]

The treatment of problems in field theory necessarily proceeds by methods rather different from that just described, because in field theory neither the field equations nor their solutions are properly known. In these problems, in order to envisage something concrete to be investigated, it seems appropriate to consider the field operators in space-time to be given as numerical data. Such an attitude to the fields may perhaps give an impression of undue empiricism, but whether or not this be so, its legitimacy may be argued on the grounds that the equations of theoretical physics ought to be susceptible to numerical analysis.

The first dispersion relation to be derived from the principles of field theory was that for the forward scattering of photons. The appropriate scattering amplitude can be expressed as a Fourier transform of the space-time data, and the microcausality condition implies that the space-time integrals concerned continue to converge when the energy of the photon acquires a positive imaginary part [25]). Provided the numerical space-time data are strictly causal they specify in this way a stable analytic continuation of the scattering amplitude. It can be shown that this continuation is, however, unstable with respect to small violations of microcausality, while the dispersion relation to which it gives rise is not so affected. The situation here is quite analogous to that noted at the end of subsection 2.1.

When the momentum transfer, or the mass of the scattered particle, are greater than zero, the integrals over the space-time data give every appearance of trying to diverge at space-like infinity, for all energies such that the momentum becomes complex. Thus, without some modification such as that proposed in section 4 of the present work, the method which was so successful for the

† Van Kampen [10]) has found a causality principle for this equation.

forward scattering of photons fails in these cases to provide an analytic extension of the scattering amplitude.

In order to circumvent this obstacle to a rigorous proof of the dispersion relations, Bogoliubov considered the scattering amplitude for a particle with imaginary mass, for which analytic extensions and dispersion relations follow as for the forward scattering of photons. Both sides of the dispersion equation so obtained were shown to be analytic functions of the mass, so that the dispersion equation continues up to the physical mass [2,3]) †. It is not easy to see that the equalities established in this proof are stable with respect to small acausal changes in the space-time data, and that they really remain so during the analytic continuation of the dispersion relation from imaginary to real masses; nevertheless such stability can, in fact, be made manifest. Apart from these awkward features, the method does not seem to lend itself to a perspicuous treatment of the unphysical region, which indeed causes most of the difficulty in establishing the above stability.

An alternative rigorous treatment of forward scattering, due to Symanzik [1]), avoids the complicated intermediary constructions of Bogoliubov's proof. It consists in performing the space integrations at a later state in the calculations. Again, however, the evaluation of the contribution of the unphysical region suffers from a lack of simplicity. Symanzik proceeds with the help of an analytic continuation of the vertex function, specified as a stable functional of momentum space data through a vertex dispersion relation.

3. Asymptotic Microcausality

Several authors [26]) have discussed the modifications which acausality necessitates in the dispersion relations. An essential point here was made by Joffé [5]), and subsequently by Gasiorowicz and Ruderman [6]) and Bohr and Mottelson [7]). It is that the dispersion relations really depend on the covariant microscopic causality condition, namely

$$[\phi(x), \phi(x')] = 0 \quad \text{for} \quad (x-x')^2 < 0, \tag{9}$$

only at considerable distances from the region of collision; moreover the dependence is such that $|\mathbf{r}-\mathbf{r}'|$ in (9) can be kept as large as required. For such applications the terminology *asymptotic microcausality* seems appropriate. The appellation *macroscopic causality* is unsuitable here, since the proof of the dispersion relations still depends upon the assumption that in asymptotic space regions far from the collision the causality condition deviates from (9) only to within a microscopic extent. In other words, it is still necessary to assume that the timing of any significantly non-zero value of the commutator,

† The essentials of Bogoliubov's method have been illustrated in a simpler context by Gasiorowicz and Noyes [17]), but the unphysical region is not much discussed there.

in the asymptotic region, disagrees with the time limitations set in eq. (9) only by a microscopic amount. A microscopic time implies here one not exceeding a small fraction of the periodic times of the wave motions making large contributions to the dispersion integral.

Joffé [5]) has remarked that these facts permit the covariant introduction of a fundamental length in the proof of the usual dispersion relations. For the less restrictive condition

$$[\phi(x), \phi(x')] = 0 \quad \text{for} \quad (x-x')^2 < -\lambda^2 \tag{10}$$

becomes indistinguishable from (9) provided $|\mathbf{r}-\mathbf{r}'|$ is chosen large enough to make $\lambda^2/|\mathbf{r}-\mathbf{r}'|$ microscopically small. With the fundamental lengths λ usually contemplated such values of $|\mathbf{r}-\mathbf{r}'|$ can lie well within atomic dimensions.

In the following a still less stringent causality condition will be used at distant points, namely

$$[\phi(x), \phi(x')] = 0 \quad \text{for} \quad |t-t'| < |\mathbf{r}-\mathbf{r}'|-l. \tag{11}$$

This non-covariant condition will be applied in the frame of reference of the fixed target. It asserts that the appearance of a scattered wave at a distant point can anticipate the appropriate retarded time by an amount not exceeding the constant l. In view of the hyperbolic character of the Klein-Gordon equation, which will be assumed to be obeyed by $\phi(x)$ to all intents and purposes, except near the scatterer, a sharply delineated time of arrival of a scattered wave implies an equally precise time for its emission at the effective edge of the scatterer. The real implication of eq. (11) is therefore that the scattered wave is generated in the scattering region in advance of the retarded time by an amount not exceeding l, after which it propagates away by the causal Klein-Gordon equation. The causality condition (11) will be shown to give rise to modified dispersion relations, which are as susceptible to experimental test as the customary ones, and permit in principle the evaluation of l.

4. Derivation of a Dispersion Relation

The present section treats the scattering of a neutral spin-zero boson by a spherically symmetrical fixed centre, placed at the origin of the space coordinates. Self interactions are ignored, so that the self-adjoint boson field operator $\phi(x)$ is taken to obey the Klein-Gordon equation

$$(\partial_\mu \partial^\mu + \kappa^2)\phi = 0 \tag{12}$$

at large enough distances from the scatterer. This statement concerning the Klein-Gordon equation will later be qualified in connection with the unphysical region in the dispersion relations.

4.1. THE SCATTERING AMPLITUDE

The amplitude $T(k, k')$ for scattering of a boson from momentum k' to k is essentially obtained by identifying

$$2\pi i\delta(\omega-\omega')T(k, k') \tag{13}$$

with the time-ordered expression

$$\lim_{t\to\infty}\,[\lim_{t'\to\infty}\langle 0|\mathrm{T}\{a(t, k)-a(-t, k)\}\{\bar{a}(-t', k')-\bar{a}(t', k')\}|0\rangle]. \tag{14}$$

Here $k = (\omega, \mathbf{k})$ denotes a positive energy four-momentum satisfying the Klein-Gordon condition, and $\bar{a}(t, k)$ signifies the normalized operator for creation of a boson with momentum k at time t;

$$\bar{a}(t, k) = \int_t \phi(x) i\overleftrightarrow{\partial_0}\, \mathrm{e}^{-ikx}\mathrm{d}^3\mathbf{r}, \tag{15}$$

with

$$\overleftrightarrow{\partial_0} \equiv \partial/\partial t-\overleftarrow{\partial}/\partial t.$$

The sequence of limits in (14) is clearly legitimate within the context of wave packets. It eliminates some transients, factoring out a δ-function to express energy conservation.

It is customary at this stage to link up the past and future space integrations in expressions like (14), by adding in suitable three-dimensional integrals at space-like infinity, such that application of Green's formula in four dimensions serves to replace all the three-dimensional integrations by four-dimensional ones [27]). This procedure eliminates transients which would otherwise arise from the limits of the space integrations in (14). It is followed in the present development, with, however, one essential modification. The crucial step is to exclude the regions

$$r < R, \quad r' < R' \tag{16}$$

from the integrations over $\mathbf{r}$ and $\mathbf{r}'$ in (14). Here R and R' are two non-infinite radii, large enough that beyond them a boson may be regarded as free of interaction in any realizable scattering situation. Later R' will be chosen larger than R, but this is not essential at present. The next step is to link up the past and future space integrations in the usual way, and apply Green's formula firstly to the space-time region $r > R$, and secondly to the region $r' > R'$. In this way the integrals in (14) are successively shifted onto the hyper-cylinders $r = R$, $r' = R'$. The discontinuity in the T-product gives rise to an additional contribution from the region $r' > R'$. By these manipulations (14) is reduced to

$$\begin{aligned}-\lim_{t\to\infty}\int_{-t}^{t}\mathrm{d}t\int_{r=R}\mathrm{d}\sigma_\alpha\int_{-\infty}^{\infty}\mathrm{d}t'\,\mathrm{e}^{ikx}i\overleftrightarrow{\nabla_\alpha}\Big\{\int_{r'=R'}\mathrm{d}\sigma'_\beta\langle 0|\mathrm{T}\phi(x)\phi(x')|0\rangle i\overleftrightarrow{\nabla'_\beta}\mathrm{e}^{-ik'x'}\\ +\int_{r'>R'}\mathrm{d}^3\mathbf{r}'\langle 0|\mathrm{T}\phi(x)\phi(x')|0\rangle i(\overleftarrow{\partial'_\mu}\partial'^\mu+\kappa^2)\mathrm{e}^{-ik'x'}\Big\}.\end{aligned} \tag{17}$$

Here $d\boldsymbol{\sigma}$ and $d\boldsymbol{\sigma}'$ are elements of two-dimensional area pointing outward from the spheres $r = R$, $r' = R'$.

For the derivation of dispersion relations the time-ordered products in (17) must be replaced by retarded commutators. Proceeding in a now standard way [1, 4]), this may be achieved by subtracting from (14) the vanishing quantity

$$\lim_{t\to\infty}\,[\lim_{t'\to\infty}\langle 0|\{\tilde{a}(-t', k')-\tilde{a}(t', k')\}\{a(t, k)-a(-t, k)\}|0\rangle]. \tag{18}$$

This expression is also subjected to the manipulations described above. The net effect is then to replace $T\phi(x)\phi(x')$ in (17) by

$$T\phi(x)\phi(x')-\phi(x')\phi(x) = \theta(t-t')[\phi(x), \phi(x')], \tag{19}$$

where θ denotes the unit positive step function.

Finally, taking account of time translational invariance, and equating the result to (13), the scattering amplitude T appears in the form

$$\begin{aligned} T(k, k') = i\int_{r=R} d\sigma_\alpha \int_{-\infty}^{\infty} dt' e^{-i\mathbf{k}\cdot\mathbf{r}} i\overleftrightarrow{\nabla}_\alpha \\ \cdot\Big\{\int_{r'=R'} d\sigma'_\beta \langle 0|\theta(-t')[\phi(0, \mathbf{r}), \phi(t', \mathbf{r}')]|0\rangle i\overleftrightarrow{\nabla}'_\beta e^{-ik'x'} \\ +\int_{r'>R'} d^3\mathbf{r}' \langle 0|\theta(-t')[\phi(0, \mathbf{r}), \phi(t', \mathbf{r}')]|0\rangle i(\overleftarrow{\partial'_\mu \partial'^\mu} + \kappa^2) e^{-ik'x'}\Big\}. \end{aligned} \tag{20}$$

The above eq. (20) can be interpreted as follows. The operator $\phi(0, \mathbf{r})$ corresponds to the particle flux at radius R at time $t = 0$. It is related to past particle fluxes at radius R' through the first term on the right hand side of (20). The second term on the right hand side of (20), which contributes only at $t' = 0$ through the discontinuity of the step function $\theta(-t')$, relates the flux at radius R at time $t = 0$ to the state of affairs external to R' at time $t' = 0$. The two terms, taken together, will be seen to represent a flux measurement at radius R at time $t = 0$ in a state which has been properly prepared by making suitable operations in the region $r' \geqq R'$, $t' \leqq 0$.

The formula (20) is considerably simplified if R' is chosen to exceed R by an amount sufficient to make the zero-time commutators in the second term on the right hand side vanish. If the microcausality condition (10) is used the appropriate limitation on R' is

$$R' > R+\lambda. \tag{21}$$

For canonical theories λ is zero, so that it then suffices to take R' greater than R. If the weak microcausality condition (11) is used, the limitation on R' will again be of the form (21), with λ suitably identified.

In the following an inequality such as (21) will therefore be understood, so that the second term on the right hand side of (20) will not appear.

4.2. ANALYTIC PROPERTIES AT FIXED MOMENTUM TRANSFER

It is convenient to set

$$\begin{aligned} \mathbf{k} &= \mathbf{K} - \tfrac{1}{2}\boldsymbol{\Delta}, \\ \mathbf{k}' &= \mathbf{K} + \tfrac{1}{2}\boldsymbol{\Delta}, \end{aligned} \tag{22}$$

so that $\boldsymbol{\Delta}$ is the momentum transfer vector. Energy conservation gives

$$\mathbf{K} \cdot \boldsymbol{\Delta} = 0, \tag{23}$$

and the magnitude of $\mathbf{K}$ is given in terms of the energy ω by

$$\mathbf{K}^2 = \omega^2 - \kappa^2 - \tfrac{1}{4}\boldsymbol{\Delta}^2. \tag{24}$$

Eqs. (23) and (24) are solved, to within the freedom left by the rotation group, by taking the x, y and z components of $\boldsymbol{\Delta}$ and $\mathbf{K}$ as follows:

$$\boldsymbol{\Delta} = (0, \Delta, 0), \quad \mathbf{K} = (K, 0, 0); \quad K \equiv (\omega^2 - \kappa^2 - \tfrac{1}{4}\Delta^2)^{\frac{1}{2}}. \tag{25}$$

The momentum transfer Δ will be taken real. The square root in (25) will be understood, as a matter of definition, to be analytic in the upper half of the ω-plane, and positive for ω real and greater than $(\kappa^2 + \frac{1}{4}\Delta^2)^{\frac{1}{2}}$. It will therefore be negative for ω real and less than $-(\kappa^2 + \frac{1}{4}\Delta^2)^{\frac{1}{2}}$, and positive imaginary in the unphysical region which lies in between.

On substituting (22) and (25) into (20), one obtains

$$\begin{aligned} T(\omega, \Delta) = -i \int_{r=R} \mathrm{d}\sigma_\alpha \int_{-\infty}^{0} \mathrm{d}t' \int_{r'=R'>R+\lambda} \mathrm{d}\sigma'_\beta \, \mathrm{e}^{-i(Kx - \frac{1}{2}\Delta y)} \\ \cdot \overleftrightarrow{\nabla}_\alpha \langle 0 | [\phi(0, \mathbf{r}), \phi(t', \mathbf{r}')] | 0 \rangle \overleftrightarrow{\nabla'}_\beta \, \mathrm{e}^{i(Kx' + \frac{1}{2}\Delta y') - i\omega t'}. \end{aligned} \tag{26}$$

Eq. (26) expresses the scattering amplitude as a sum of exponentials analytic in ω, weighted by the given space-time data. Since R and R', although perhaps large, are nevertheless finite, the expression (26) can become divergent only through the semi-infinite time integration, and this will necessarily converge in the region Im $\omega > 0$. Thus (26) defines a function $T(\omega, \Delta)$ analytic and regular in the *finite* upper half of the ω-plane. Singularities on the real ω-axis are not excluded, however, and indeed it is clear by inspection that the purely harmonic bound state time dependences which may be present in the commutator will lead to poles on the real ω-axis. Such singularities may, however, be smoothed out by restricting the time integration to a very long but finite interval. This device will be understood in the following. It is not necessary to the argument, but it does simplify the application of Cauchy's integral by enabling the contour to run along the real axis without indentation.

For sufficiently large $|\omega|$ the exponentials in the integrand in (26) behave like

$$\exp\{\tfrac{1}{2}i\Delta(y + y') - i\omega(t' + x - x') + i(\kappa^2 + \tfrac{1}{4}\Delta^2)(x - x')/2\omega + \mathrm{O}(\omega^{-3})\}. \tag{27}$$

The first term of the exponent here is finite, since y and y' lie on spheres of

radii R and R'. The third and higher terms are finite for a similar reason, and moreover they tend to zero as $|\omega|$ tends to infinity. The second term of the exponent is limited by the causality condition (11), according to which the exponential (27) is needed only for points such that

$$t' \leqq -\{|x-x'|-l\}. \tag{28}$$

It follows that the exponential (27) cannot increase with $\operatorname{Im}\omega$ for large $|\omega|$ faster than $\exp(-i\omega l)$, or equivalently, $\exp(-iKl)$. If a causality condition of the form (10) is used, the parameter l here may be replaced by $\lambda^2(R'-R)^{-1}$. This is in fact an over-estimate, but it can still be made as small as desired by making R' sufficiently large. Thus, the causality condition (10) is seen to be quite as effective as the canonical causality condition (9), so far as the dispersion relation is concerned.

The limiting behaviour of $T(\omega, \Delta)$ for large $|\omega|$ will now be considered. As argued in subsection 2.3, it is legitimate to suppose the space-time data to be set numerically on a space-time mesh of finite grain. In this case $T(\omega, \Delta)$, defined in terms of the numerical data by eq. (26), is bounded for large $|\omega|$ in the same way as $\omega^{-1}\exp(-iKl)$. This behaviour arises because the integration of the exponential (27) over a small cell of the five-dimensional region of integration brings in a factor $\omega^{-1}K^{-2}$, while each operator $\overleftrightarrow{\nabla}$ in eq. (26) brings in a factor K.

Introducing now a positive number η, and a length d, such that

$$d \geqq l, \tag{29}$$

and applying Cauchy's integral formula to the analytic function $T(\omega, \Delta)\exp(iKd)(\omega-\omega'+i\eta)^{-1}$ taken on a contour consisting of the real axis and a semicircular arc at infinity in the upper half-plane, one obtains

$$\int_{-\infty}^{\infty} \frac{1}{\omega-\omega'+i\eta} T(\omega, \Delta)e^{iKd}d\omega = 0. \tag{30}$$

In the limit $\eta \to 0$ eq. (30) yields the Hilbert relation

$$\operatorname{Re}\{T(\omega', \Delta)e^{iK'd}\} = \frac{1}{\pi}\int_{-\infty}^{\infty} \frac{\mathrm{P}}{\omega-\omega'} \operatorname{Im}\{T(\omega, \Delta)e^{iKd}\}d\omega, \tag{31}$$

and the reciprocal Hilbert relation for the imaginary part.

4.3. SUBTRACTIONS

If the principal value integral in (31) converges at infinity only by virtue of the coarseness of the mesh on which the numerical space-time data are set, its convergence may be improved by making subtractions, as described, for example, in refs. [1–4]). A finite number of subtractions will suffice if the "exact" space-time data contain nothing more singular then derivatives of δ-functions to finite order.

4.4. AN ALTERNATIVE DERIVATION OF THE HILBERT RELATION; NECESSITY OF THE UNPHYSICAL REGION

An alternative derivation of (30) comes very simply by replacing the plane wave in the right hand side of (26) by the following linear combination of plane waves:

$$\int_{-\infty}^{\infty} (\omega-\omega'+i\eta)^{-1} \exp\{\tfrac{1}{2}i\Delta(y+y')-iK(x-x')-i\omega t'+iKd\}\mathrm{d}\omega. \qquad (32)$$

For, in view of eq. (29), the above combination vanishes exactly in the region $t' < -\{|x-x'|-l\}$, as may be seen by applying Cauchy's theorem. Therefore it gives zero when substituted into the right hand side of (26). Eq. (30) then follows on interchanging the order of integration, which procedure may be justified by arguments similar to the foregoing.

The essential point about the linear combination (32) is that it vanishes outside a sharply defined space-time region. Bohr and Mottelson [7]) have noted that this property can only be achieved by the inclusion of the full range of real ω. A wave packet built from physical frequencies alone (i.e. $\omega^2 \geqq \kappa^2+\frac{1}{4}\Delta^2$) cannot travel near the edge of the region (28) without spilling over. This reflects the well-known feature that the group velocities carried by a wave with mass are always less than unity.

4.5. CROSSING SYMMETRY

For real ω the function K satisfies the relation

$$iK(-\omega) = \{iK(\omega)\}^*. \qquad (33)$$

Hence, taking the conjugate of (26), one finds

$$T(-\omega, \Delta) = T(\omega, -\Delta)^* = T(\omega, \Delta)^*, \qquad (34)$$

the last step following from rotational invariance. Taking into account the crossing symmetries (33) and (34), the two halves of the integration in the Hilbert relation (31) can be folded together to give

$$\mathrm{Re}\{T(\omega', \Delta)\mathrm{e}^{iK'd}\} = \frac{2}{\pi}\int_0^{\infty} \frac{\omega \mathrm{P}}{\omega^2-\omega'^2} \mathrm{Im}\{T(\omega, \Delta)\mathrm{e}^{iKd}\}\mathrm{d}\omega \qquad (35)$$

4.6. ABSORPTIVE CHARACTER OF Im $T(\omega, \Delta)$

In the unphysical region K is given by

$$K = i(\omega_0^2-\omega^2)^{\frac{1}{2}}, \qquad (36)$$

where ω_0 separates the physical and unphysical regions:

$$\omega_0 = (\kappa^2+\tfrac{1}{4}\Delta^2)^{\frac{1}{2}}. \qquad (37)$$

In the unphysical region, therefore, the factor $\mathrm{Im}\{T(\omega, \Delta)e^{iKd}\}$ in the integral in (35) reduces to

$$\exp\{-d(\omega_0{}^2-\omega^2)^{\frac{1}{2}}\}\mathrm{Im}\, T(\omega, \Delta), \tag{38}$$

which entails only the imaginary part of $T(\omega, \Delta)$. As well known, the imaginary part of $T(\omega, \Delta)$ is *absorptive*, that is to say it is determined solely by energy conserving intermediate states. This important and simplifying feature follows from time-translation and rotation invariance, which can be used to express the conjugate of eq. (26) in the form

$$\begin{aligned} T(\omega, \Delta)^* = i\int_{r=R'} \mathrm{d}\sigma_\alpha \int_0^\infty \mathrm{d}t' \int_{r'=R<R'-\lambda} \mathrm{d}\sigma'_\beta\, e^{-i(Kx-\frac{1}{2}\Delta y)} \\ \cdot \overleftrightarrow{\nabla}_\alpha \langle 0|[\phi(0, \mathbf{r}), \phi(t', \mathbf{r}')]|0\rangle \overleftrightarrow{\nabla}'_\beta e^{i(Kx'+\frac{1}{2}\Delta y')-i\omega t'}. \end{aligned} \tag{39}$$

The rotations used in deriving (39) consist of one rotation through an angle π about the x-axis, with an additional rotation through π about the y-axis when ω lies in the unphysical region (where $K^* = -K$). It will be seen that (39) differs from (26) in the limits of the time integration, and also in the interchange of R and R'. With regard to the latter point it is quite permissible to symmetrize all the preceding formulae with respect to R and R' †. If this be done, $\mathrm{Im}\, T(\omega, \Delta)$ appears in the form

$$\begin{aligned} \mathrm{Im}\, T(\omega, \Delta) &= \tfrac{1}{2}i\{T(\omega, \Delta)^* - T(\omega, \Delta)\} \\ &= -\tfrac{1}{4}\left\{\int_{r=R} \mathrm{d}\sigma_\alpha \int_{r'=R'} \mathrm{d}\sigma'_\beta + \int_{r=R'} \mathrm{d}\sigma_\alpha \int_{r'=R} \mathrm{d}\sigma'_\beta\right\} \\ &\cdot e^{-i(Kx-\frac{1}{2}\Delta y)} \overleftrightarrow{\nabla}_\alpha \langle 0|[\phi(0, \mathbf{r}), \int_{-\infty}^{\infty} \phi(t', \mathbf{r}')e^{-i\omega t'}\mathrm{d}t']|0\rangle \overleftrightarrow{\nabla}'_\beta e^{i(Kx'+\frac{1}{2}\Delta y')}. \end{aligned} \tag{40}$$

Eq. (40) expresses fully the absorptive character of $\mathrm{Im}\, T(\omega, \Delta)$.

4.7. BOUND STATE CONTRIBUTIONS TO $\mathrm{Im}\, T(\omega, 0)$

For simplicity an s-wave bound state will be treated. Most of the following remarks will apply equally to bound states of higher angular momentum.

The bound state $|\mathrm{B}\rangle$ may be characterized by a wave function $\psi_\mathrm{B}(\mathbf{r})$, defined by,

$$\langle 0|\phi(t, \mathbf{r})|\mathrm{B}\rangle \equiv \psi_\mathrm{B}(\mathbf{r})\exp(-i\omega_\mathrm{B}t), \tag{41}$$

it being understood that $|\mathrm{B}\rangle$ is normalized to unity. At large distances from the origin $\psi_\mathrm{B}(\mathbf{r})$ has an asymptotic expansion

$$\psi_\mathrm{B}(\mathbf{r}) \sim \psi_\mathrm{B}{}^{(0)}(\mathbf{r}) + \psi_\mathrm{B}{}^{(1)}(\mathbf{r}) + \ldots, \tag{42}$$

in which the leading term $\psi_\mathrm{B}{}^{(0)}$ derives from a solution of the Klein-Gordon equation. Thus, for an s-wave bound state, $\psi_\mathrm{B}{}^{(0)}$ has the structure

$$\psi_\mathrm{B}{}^{(0)}(\mathbf{r}) = g_\mathrm{B}(4\pi r)^{-1} \exp\{-r(\kappa^2-\omega_\mathrm{B}{}^2)^{\frac{1}{2}}\}, \tag{43}$$

† The radii R and R' interchange if the sequence of time limits in (14) is reversed.

where g_B is a normalization constant. Asymptotic expansions of the above type always appear if the interaction at large distances can be represented as a local potential $V(r)$ falling off more rapidly than a Coulomb potential. Moreover, in this case the next term in the expansion is determined by the equation

$$(\kappa^2-\omega_B{}^2-\nabla^2)\psi_B{}^{(1)}(\mathbf{r}) = -2\kappa V(r)\psi_B{}^{(0)}(\mathbf{r}). \tag{44}$$

It will be useful to invoke eq. (44) to provide a concrete model for the discussion of $\psi_B{}^{(1)}$. But the existence of the asymptotic expansion does not hinge upon the potential assumption. It is rather concomitant to the very existence of a scattering matrix.

When the commutator in (40) is split by insertion of a complete set of states, the state $|B\rangle$ gives a factor $2\pi\delta(\omega-\omega_B)$, through the infinite time integration, and this ensures exact energy conservation. The contribution of $|B\rangle$ to Im $T(\omega, \Delta)$ is therefore primarily determined by the following surface integral:

$$\int d\sigma_\alpha \exp\{(\kappa^2+\tfrac{1}{4}\Delta^2-\omega_B{}^2)^{\frac{1}{2}}x+\tfrac{1}{2}i\Delta y\}\overleftrightarrow{\nabla}_\alpha\psi_B(\mathbf{r}). \tag{45}$$

The form of this expression shows that the bound state contribution depends only on the long-distance behaviour of the bound-state wave function. But it is necessary to study the stability of the surface integral against changes of the more or less arbitrary surface of integration. For the exponential factor in (45) becomes ever larger as the surface of integration recedes to infinity.

The contribution of the leading term $\psi_B{}^{(0)}$ will first be evaluated. It will be seen from eq. (43) that $\psi_B{}^{(0)}$ obeys the equation

$$(-\nabla^2-\omega_B{}^2+\kappa^2)\psi_B{}^{(0)}(\mathbf{r}) = g_B\delta^3(\mathbf{r}), \tag{46}$$

while the exponential factor in the surface integral (45) obeys the same differential equation, without the inhomogeneous term. A straightforward application of Green's formula, using these two differential equations, shows that $\psi_B{}^{(0)}(\mathbf{r})$ contributes to the surface integral (45) exactly the number $-g_B$, irrespective of the precise whereabouts and shape of the surface of integration.

The contribution of $\psi_B{}^{(1)}$ in (45) will now be considered. For forward scattering ($\Delta = 0$), the decay of $\psi_B{}^{(1)}$ is faster than that of $\psi_B{}^{(0)}$, and more than compensates the growth of the exponential factor in (45). For sufficiently distant surfaces therefore, the contributions of $\psi_B{}^{(1)}$ and higher terms drop out. Thus the bound-state contribution to Im $T(\omega, 0)$ is stable, and is equal to

$$\pi|g_B|^2\delta(\omega-\omega_B). \tag{47}$$

4.8. DISPERSION RELATION FOR FORWARD SCATTERING

On inserting (47) into the Hilbert relation (35) for forward scattering one obtains

$$\mathrm{Re}\{T(\omega', 0)\mathrm{e}^{iK(\omega')d}\} = \sum_{\mathrm{B}} \frac{2\omega_{\mathrm{B}}|g_{\mathrm{B}}|^2}{\omega_{\mathrm{B}}{}^2-\omega'^2} \exp\{-d(\kappa^2-\omega_{\mathrm{B}}{}^2)^{\frac{1}{2}}\} + \frac{2}{\pi}\int_{\kappa}^{\infty} \frac{\omega \mathrm{P}}{\omega^2-\omega'^2} \mathrm{Im}\{T(\omega, 0)\mathrm{e}^{iK(\omega)d}\}\mathrm{d}\omega. \tag{48}$$

The stability of all quantities appearing in this dispersion relation is already established. Apart from the length $d(d \geqq l)$, it involves only experimentally accessible parameters, and may therefore in principle be used to obtain information as to the fundamental length l. The meaning and interpretation of l has been discussed in section 3.

4.9. BOUND STATE CONTRIBUTIONS TO Im $T(\omega, \Delta)$

As soon as the momentum transfer Δ is non-zero, the possibility of instability arises, and this can only be resolved by appeal to the form of $\psi_{\mathrm{B}}{}^{(1)}$. Let the surface integral (45) be evaluated on two different surfaces. The *difference* between these two evaluations can be expressed, using Green's formula, as the volume integral of the density

$$\exp\{(\kappa^2+\tfrac{1}{4}\Delta^2-\omega_{\mathrm{B}}{}^2)^{\frac{1}{2}}x+\tfrac{1}{2}i\Delta y\}(\kappa^2-\omega_{\mathrm{B}}{}^2-\nabla^2)\psi_{\mathrm{B}}{}^{(1)}(\mathbf{r}) \tag{49}$$

over the volume enclosed between the two surfaces. For stability it is necessary that this density decays sufficiently rapidly with increasing distance from the scatterer. If the potential assumption (44) is accurate at large distances, and if moreover $V(r)$ tails off within limits of the form

$$|V(r)| < Ar^{-n}\exp(-\alpha r) \quad \text{for large} \quad r, \tag{50}$$

with $\alpha \geqq 0$, $n > 1$, and A finite, eqs. (43) and (44) enable definite statements to be made concerning the limiting behaviour of the density (49). In this way the surface integral (45) is found to be stable if, and only if

$$(\kappa^2+\tfrac{1}{4}\Delta^2-\omega_{\mathrm{B}}{}^2)^{\frac{1}{2}} \leqq \alpha+(\kappa^2-\omega_{\mathrm{B}}{}^2)^{\frac{1}{2}},$$

i.e.

$$\Delta^2 \leqq 4\alpha^2+8\alpha(\kappa^2-\omega_{\mathrm{B}}{}^2)^{\frac{1}{2}}. \tag{51}$$

If Δ does not satisfy (51) the density (49) grows with increasing distance, so that (45) becomes ever more unstable against small deformations of the surface of integration as this recedes to larger distances. If on the other hand Δ does satisfy (51), the contribution of $\psi_{\mathrm{B}}{}^{(1)}$ and higher terms in (45) can be made as small as desired by working at a sufficiently great distance. For eq. (44) implies that

$$|\psi_{\mathrm{B}}{}^{(1)}(\mathbf{r})| \leqq \frac{2\kappa A r^{-n}\mathrm{e}^{-\alpha r}\psi_{\mathrm{B}}{}^{(0)}(\mathbf{r})}{\alpha^2+2\alpha(\kappa^2-\omega_{\mathrm{B}}{}^2)^{\frac{1}{2}}} \quad \text{for} \quad \alpha \neq 0, \tag{52a}$$

and

$$|\psi_{\mathrm{B}}{}^{(1)}(\mathbf{r})| \leqq \frac{\kappa A r^{-n+1}\psi_{\mathrm{B}}{}^{(0)}(\mathbf{r})}{(n-1)(\kappa^2-\omega_{\mathrm{B}}{}^2)^{\frac{1}{2}}} \quad \text{for} \quad \alpha = 0, \tag{52b}$$

so that the stable limit of (45) is due entirely to $\psi_B^{(0)}$. Therefore, provided (51) is satisfied, the bound state contribution to Im $T(\omega, \Delta)$ is given by (47), as for forward scattering.

4.10. CONTINUUM CONTRIBUTIONS TO Im $T(\omega, \Delta)$.

When Δ is non-zero, ω can lie in the unphysical region $\kappa < \omega < \omega_0$, and the intermediate states in the expression (40) for Im $T(\omega, \Delta)$ are then scattering states. The stability of the contribution of any such state in (40) can be analysed by the method used in subsection 4.9 for bound states. The only difference now is that the wave functions propagate to infinity instead of decaying exponentially, and this makes the stability condition more stringent than the bound-state condition (51). It is readily seen to be

$$(\kappa^2+\tfrac{1}{4}\Delta^2-\omega^2)^{\frac{1}{2}} \leqq \alpha, \tag{53}$$

which, in view of the relevant range of ω, implies that

$$\Delta^2 \leqq 4\alpha^2. \tag{54}$$

Before the above argument can be used to infer the stability of Im $T(\omega, \Delta)$ itself, it is necessary to show that one may delay the sum over intermediate states until the space integrations have been performed. For this purpose it seems useful to invoke the properties of plane-wave scattering states. It can surely be postulated that the wave function of each plane-wave scattering state of energy ω is bounded in the asymptotic region. Then the sum over states, amounting as it does merely to an integration over angles, can certainly be postponed, and the stable limit for each plane-wave contribution will be effectively reached at some large but finite radius R common to all the states concerned. These stable limits will also necessarily be bounded, and the subsequent angular integration for the sum over states cannot introduce any instability.

From the above simple considerations the stability of Im $T(\omega, \Delta)$ follows for $\Delta^2 \leqq 4\alpha^2$. Since this condition implies the bound-state stability condition (51), it is a sufficient condition for stability of the integrand in the right hand side of the Hilbert relation (35). This limitation $\Delta^2 \leqq 4\alpha^2$ on the momentum transfer in the Hilbert relation is the same as that found in the work of Khuri and Treiman [16]), Gasiorowicz and Noyes [17]) and Klein and Zemach [20]). When it is obeyed, the Hilbert relation (35) exhibits $T(\omega, \Delta)$ as a stable regular analytic function of ω in the whole of the upper half of the ω-plane. It follows that the real part of $T(\omega, \Delta)$ on the unphysical section of the real ω-axis is likewise stable, for it derives from the boundary value of the above stable analytic function. These properties of stability will be seen to be consequential to the combined effects of causality and spectrum; the latter being invoked especially through the exponential decay of the wave functions of bound intermediate states.

It seems worth while to remark that the limitation (54) on the momentum transfer persists even when the continuum states extend to energies lower than κ, as happens when exothermic reactions are possible. For, barring possible complications from self fields, the stability of the contribution of any state with energy less than κ is evidently decided, not by (53), but by (51), which takes account of the exponential decay of the matrix elements of $\phi(\mathbf{r})$ in all such states.

4.11. PHASE SHIFT EXPANSION FOR Im $T(\omega, \Delta)$

Using the methods of subsection 4.9, it may readily be shown that, when the stability condition (54) is obeyed, the asymptotic expansion of the wave function of each scattering state of energy ω enters into Im $T(\omega, \Delta)$ only through its leading term. The higher terms from all scattering states of energy ω can be made arbitrarily small by taking R sufficiently large.

Now the leading term in the asymptotic expansion of the wave function of each plane-wave state at some large radius R, being a bounded function of angle, and having no doubt reasonable continuity properties, may certainly be expressed through a phase-shift expansion. Its contribution to Im $T(\omega, \Delta)$ is obviously bounded since R is non-infinite, and appears likewise as a function of the phase shifts, and the sum over states, which brings in only a further angular integration, gives another finite function of the phase shifts. It follows that for $\Delta^2 \leqq 4\alpha^2$ the absorptive part Im $T(\omega, \Delta)$ can be expressed as a convergent function of the scattering phases †, these being defined in terms of the angular decomposition of the wave function in the asymptotic region, at a large but finite radius R.

It will be seen that the above rigorous proof of the convergence of the phase-shift expansion of Im $T(\omega, \Delta)$ is really quite trivial. All that has been done, in fact, is to demonstrate that Im $T(\omega, \Delta)$ has a well defined meaning in terms of configuration space angular data. Then, naturally, it continues to have meaning when this data is carried by phase shifts.

4.12. INSTABILITY WITH RESPECT TO MEASURED ANGULAR DISTRIBUTION DATA

The phase-shift expansion serves essentially to extrapolate Im $T(\omega, \Delta)$ to angles with cosine less than minus one. Therefore, as the work of subsection 2.2 indicates, it does *not* furnish a means whereby Im $T(\omega, \Delta)$ can be experimentally determined in terms of measured angular distribution data alone. Further quantitative information is required as to the behaviour of the phase shifts for high angular momenta. This feature may be seen directly in the present formu-

† Khuri [15]) and Khuri and Treiman [16]) found for the phase-shift expansion of Im $T(\omega, \Delta)$ only the range $\Delta^2 \leqq \alpha^2$. Gasiorowicz and Noyes [17]) enlarged the domain to $\Delta^2 \leqq 2\alpha^2$. The full range $\Delta^2 \leqq 4\alpha^2$ was found by Klein and Zemach [20]). A similarly large domain for the phase-shift expansion of Im $T(\omega, \Delta)$ in the context of relativistic meson-nucleon scattering was discovered by Lehmann [18]).

lation. The object under discussion is a surface integral at a large but finite radius R. The integral involves a scattering-state wave function weighted by a factor $\exp\{(\kappa^2+\frac{1}{4}\Delta^2-\omega^2)^{\frac{1}{2}}x+\frac{1}{2}i\Delta y\}$. For large R, this factor has $\approx R\Delta$ oscillations of magnitude $\approx \exp\{(\kappa^2+\frac{1}{4}\Delta^2-\omega^2)^{\frac{1}{2}}R\}$ per unit solid angle. Evidently, although the integral is perfectly well defined, it exhibits a pathological behaviour similar to that shown in eq. (7), the large parameter R being somewhat analogous to the large parameter N in that equation. To overcome this difficulty it will be necessary to use a small R, invoking some model by which the effect of the potential outside R can be properly calculated.

The above discussion indicates a very essential difference between the dispersion relation for forward scattering ($\Delta = 0$) and the dispersion relation with fixed non-zero momentum transfer ($0 < \Delta^2 \leqq 4\varkappa^2$). The former expresses relationships between observable quantities, while the latter requires an extrapolation and can only be compared to experiment with the help of rather specific assumptions as to the ranges and strengths of the various terms in the potential tail. It seems that the physical content of dispersion theory in general is much enhanced by bringing in such assumptions, but the matter will not be pursued here.

4.13. DISPERSION RELATIONS FOR $\Delta^2 > 4\varkappa^2$

It is not clear whether the Hilbert relation (35) can be useful for $\Delta^2 > 4\varkappa^2$. There seems no reason to question the stability of the principal value integration through the physical region, and the left hand side is also stable when ω' lies in the physical region. Therefore, since (35) is exact for arbitrarily large Δ, the integration through the unphysical region has the property that it is stable whenever ω' is physical, in spite of the instability of the integrand.

5. Conclusions

It is hoped that the preceding discussion may help to clarify the status of analytic functions in quantum field theory. Apart from this, some general conclusions may be drawn.

Perhaps most satisfying is the demonstration that the theory of dispersion relations can be put on a sound footing using only elementary mathematics. This desirable objective is achieved here by avoiding over-idealized limits both in the small and in the large, taking into consideration the nature of the supposed physical situation. Physics indicates that in the small, the space-time data can always be *well enough* represented as bounded continuous functions. Likewise, in the large, it indicates that the scattering process can always be limited to a finite region of space-time. With these factors taken into account, there is no necessity to invoke such refined theorems as, e.g., the Titchmarsh theorem, the power and precision of which can be embarrassing rather than helpful in the analysis of physical data!

It is also pleasing that the unphysical region can be treated properly in a direct manner, as foreshadowed in the work of Bohr and Mottelson [7]). This development depends essentially upon being able to distinguish the asymptotic region from the scattering region. Such a distinction has not yet appeared in the treatment of relativistic problems, but it can undoubtedly be made there as well. The use of a finite space region also helps; with an infinite space region the unphysical contributions are only too liable to appear in the form $0 \times \infty$!

Finally, it is interesting that a quantitative experimental check on deviations from asymptotic microcausality is in principle possible.

References

1) K. Symanzik, Phys. Rev. **105** (1957) 743
2) N. N. Bogoliubov, B. V. Medvedev and M. K Polivanov, Fortschr. d. Phys. **7** (1958) 169; N. N. Bogoliubov and D. V. Shirkov, Introduction to the theory of quantized fields (Interscience 1959) 597
3) H. J. Bremermann, R. Oehme and J. G. Taylor, Phys. Rev. **109** (1958) 2178
4) M. L. Goldberger, Y. Nambu and R. Oehme, Annals of Phys. **2** (1957) 226
5) B. L. Joffé, Journ. Exp. Theor. Phys. **31** (1956) 583; Soviet Physics, J.E.T.P. **4** (1957) 534
6) S. Gasiorowicz and M. A. Ruderman, Phys. Rev. **110** (1958) 261
7) A. Bohr, Proceedings of the 1958 Annual International Conference on High Energy Physics at CERN (CERN 1958) 213
8) M. L. Goldberger, H. Miyazawa and R. Oehme, Phys. Rev. **99** (1955) 986; R. Karplus and M. A. Ruderman, Phys. Rev. **98** (1955) 771
9) N. G. Van Kampen, Phil. Mag. **42** (1951) 851
10) N. G. Van Kampen, Phys. Rev. **91** (1953) 1267; Physica **20** (1954) 115
11) W. Heisenberg, Zeits. f. Phys. **120** (1943) 513, 673; see also C. Møller, Mat. Fys. Medd. Dan. Vid. Selsk. **23**, No. 1 (1945)
12) S. T. Ma, Phys. Rev. **71** (1947) 195; see also J. Meixner, Zeits. f. Naturforsch. **3a** (1948) 75
13) N. Hu, Phys. Rev. **74** (1948) 131
14) J. M. Knight and J. S. Toll, Ann. Phys. **3** (1958) 49
15) N. N. Khuri, Phys. Rev. **107** (1957) 1148
16) N. N. Khuri and S. B. Treiman, Phys. Rev. **109** (1958) 198
17) S. Gasiorowicz and H. P. Noyes, Nuovo Cimento **10** (1958) 78
18) H. Lehmann, Nuovo Cimento **10** (1958) 579
19) R. Oehme and J. G. Taylor, Phys. Rev. **113** (1959) 371
20) A. Klein and C. Zemach, Annals of Physics **7** (1959) 440
21) E. T. Whittaker and G. N. Watson, A Course of Modern Analysis, 4th ed. (C. U. P., 1927) 319—322
22) E. W. Hobson, The Theory of Spherical and Ellipsoidal Harmonics (C. U. P., 1931) 300, 306
23) G. F. Chew, Phys. Rev. **112** (1958) 1380; J. G. Taylor, M. J. Moravcsik and J. L. Uretsky, Phys. Rev. **113** (1959) 689
24) P. Cziffra, M. H. MacGregor, M. J. Moravcsik and H. P. Stapp, U.C.R.L. 8510 (1958)
25) M. L. Goldberger, Phys. Rev. **97** (1955) 508
26) R. Oehme, Phys. Rev. **100** (1955) 1503; D. Ito, S. Minami and H. Tanaka, Nuovo Cimento **9** (1958) 461
27) H. Lehmann, K. Symanzik and W. Zimmermann, Nuovo Cimento **6** (1957) 319

8.A

Nuclear Physics **14** (1959/60) 199—204; © *North-Holland Publishing Co., Amsterdam*

Not to be reproduced by photoprint or microfilm without written permission from the publisher

TRANSVERSE POLARIZATION OF K-CONVERSION ELECTRONS FOLLOWING THE BETA DECAY OF Hg^{203}

J. E. ALBERGHINI † and R. M. STEFFEN

Department of Physics, Purdue University, Lafayette, Indiana ††

Received 3 September 1959

Abstract: The degree of transverse polarization of the K-conversion electrons following the first-forbidden beta decay of Hg^{203} has been measured. The electron polarization has been observed by means of the left-right asymmetry in a Mott-scattering process. The degree of polarization of the conversion electrons was determined as $P_\perp(\theta) = (0.35 \pm 0.07)(v/c) \sin\theta$, where θ is the angle between the beta particle direction and the conversion electron direction. The analysis of the result within the framework of the ξ-approximation for non-unique first-forbidden beta decay gives strong support to the decay scheme $(\frac{3}{2})\ \beta\ (\frac{3}{2})$ c.e. $(\frac{1}{2})$.

Rose and Becker [1–3]), and independently Beresteckij and Rudik [4]), have shown that, as a consequence of the non-conservation of parity in weak interactions, internal conversion electrons following a beta transition possess an appreciable longitudinal and also transverse polarization. The latter is in the plane of the momentum vectors $\mathbf{p}_\beta$ and $\mathbf{p}_e$ of the beta particle and the conversion electron, respectively.

For a beta transition followed by an M1+E2 mixture according to the decay scheme $(I_1)\beta(I)$ c.e. (I_2), the transverse polarization of the K-conversion electrons is of the form

$$P_\perp(\theta) = \sum_{k=1}^{n} \frac{{\alpha_k}^\beta}{{\alpha_0}^\beta} B_k^{\text{c.e.}} P_k^1(\cos\theta), \tag{1}$$

where

$$B_k^{\text{c.e.}} = \frac{1}{\sqrt{2k+1}} \frac{b_{k\perp}(\text{M1}) F_k(11I_2I) + 2\tilde{\delta} b_{k\perp}(\text{M1, E2}) F_k(12I_2I) + \tilde{\delta}^2 b_{k\perp}(\text{E2}) F_k(22I_2I)}{1+\tilde{\delta}^2}, \tag{2}$$

$${a_k}^\beta = \sqrt{2k+1} \sum_{L_1L'_1} F_k(L_1L'_1I_1I) b_k(L_1L'_1). \tag{3}$$

The $F_k(L_1L_2I_2I_1)$ are the F-coefficients which appear in the theory of angular correlations, $b_k(L_1L'_1)$ are the beta-particle parameters of Alder [5]), $b_{k\perp}(\pi L)$,

† Sponsored by the Hughes Master of Science Fellowship Program.

†† Supported by the U. S. Atomic Energy Commission.

$\pi = \mathrm{M}, \mathrm{E}$, are the conversion electron particle parameters of Rose [3]), and $\bar{\delta}^2$ is the relative conversion electron intensity ratio E2 to M1. A positive polarization $P_\perp$ is in the direction of $\mathbf{p}_c \times (\mathbf{p}_\beta \times \mathbf{p}_c)$; θ is the angle between $\mathbf{p}_\beta$ and $\mathbf{p}_c$. For allowed beta decays, and for first-forbidden beta transitions which are characterized by the ξ-approximation [6-8]) ($\xi = \alpha Z/2R \gg 1$), only $\alpha_0{}^\beta$ and $\alpha_1{}^\beta$ are non-vanishing:

$$\frac{\alpha_1{}^\beta}{\alpha_0{}^\beta} = \frac{2}{\sqrt{3}} \frac{p_\beta}{W} \frac{-F_1(11I_1I) - \delta_{I_1I}\sqrt{3}X}{1+X^2} \tag{4}$$

where

$$X = \frac{C_V \int 1}{C_A \int \boldsymbol{\sigma}} \tag{5}$$

for the allowed beta decay, and

$$X = \frac{-C_A \int i\gamma_5 - \xi C_A \int \boldsymbol{\sigma} \cdot \mathbf{r}}{C_V \int i\boldsymbol{\alpha} - (C_V \int \mathbf{r} - C_A \int i\boldsymbol{\alpha} \times \mathbf{r})\xi} \tag{6}$$

for first-forbidden beta decay.

The transverse polarization of the K-conversion electrons following the beta decay of Hg^{203} was measured with the use of the vacuum chamber shown in fig. 1. Hg^{203} was chosen since it has a relatively large internal conversion coefficient and the K-shell conversion peak is well separated from the continuous beta spectrum. Also, Hg^{203} has a convenient half life and has no competing beta transitions of significant intensity. The Hg^{203} sources were prepared by depositing pure Hg metal from $Hg(NO_3)_2$ onto 0.8 mg/cm² mylar backing foil.

The left-right asymmetry in a Mott scattering process on a thin gold foil (180 μg/cm²) was determined as a measure of the polarization of the conversion electrons. The energy spectrum of the scattered electrons as observed with the conversion electron detector is shown in fig. 2. The single channel analyzer window was adjusted to accept the K-conversion peak. The beta particles travelled through a 0.8 mg/cm² mylar window and were recorded by the beta detector whose position was alternated at constant time intervals (15 min or 60 min) between $\alpha = 90°$ and $\alpha = 270°$ (refer to fig. 1). The average energy of the beta particles accepted by this counter was $\bar{E}_\beta = 0.14$ MeV, corresponding to $(p/W)_{av} = (v/c)_{av} = 0.62$. The average angle θ between $\mathbf{p}_\beta$ and $\mathbf{p}_c$ was 117°. Control measurements were made by replacing the 0.18 mg/cm² gold foil by a 3.4 mg/cm² aluminium foil which was chosen to give the same (very small) plural scattering probability as the gold foil. To assure maximum symmetry and a plane average scattering surface in both cases, the foils were rotated continuously about a vertical axis. The beta-conversion electron coincidence counting rates $C_{\beta C}(\alpha)$ were corrected for the presence of a small background

(including coincidences with conversion electrons scattered from the walls of the vacuum chamber, etc.) which was measured with the scattering foil removed and the source in position.

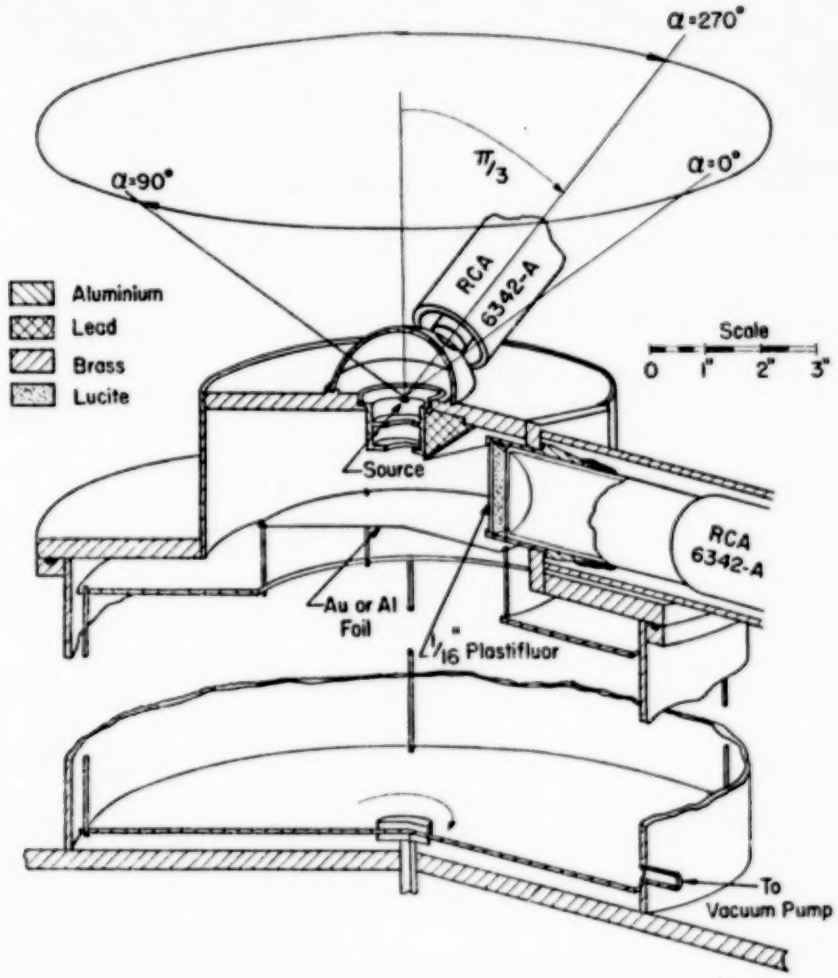

Fig. 1. Vacuum chamber and detector arrangement used for transverse polarization measurements of conversion electrons.

The experimental results for the asymmetry $a = [C_{\beta C}(90°) - C_{\beta C}(270°)]/[C_{\beta C}(90°) + C_{\beta C}(270°)]$ are summarized in table 1. The polarization, $P_\perp(117°) = +0.19 \pm 0.04$, of the Hg^{203} conversion electrons was calculated according to the method of Wegener [9]). The geometrical corrections resulting from the finite sizes of the beta detector and of the conversion electron detector (Au scatterer) have been taken into account on the basis of the θ-dependence given in eq. (1).

The measurements yield for the degree of transverse polarization of the Hg^{203} K-conversion electrons:

$$P_\perp(\theta) = (0.35 \pm 0.07)(v/c) \sin \theta \qquad (7)$$

(including coincidences with conversion electrons scattered from the walls of the vacuum chamber, etc.) which was measured with the scattering foil removed and the source in position.

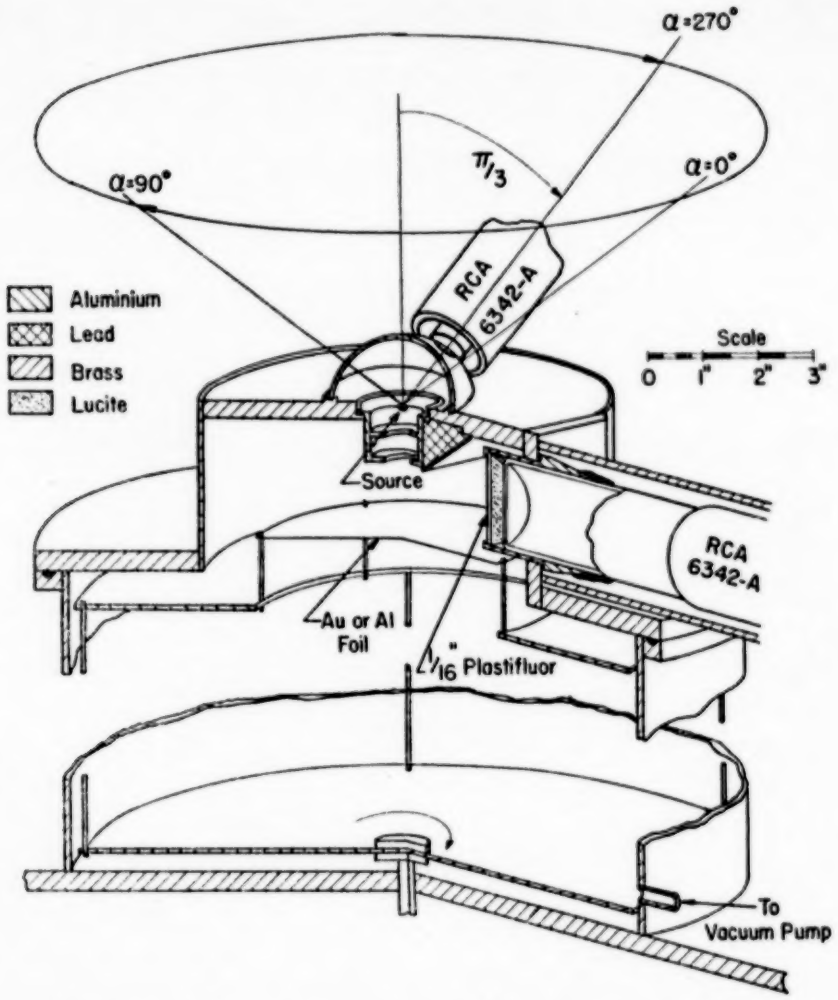

Fig. 1. Vacuum chamber and detector arrangement used for transverse polarization measurements of conversion electrons.

The experimental results for the asymmetry $a = [C_{\beta C}(90°) - C_{\beta C}(270°)]/[C_{\beta C}(90°) + C_{\beta C}(270°)]$ are summarized in table 1. The polarization, $P_{\perp}(117°) = +0.19 \pm 0.04$, of the Hg^{203} conversion electrons was calculated according to the method of Wegener [9]). The geometrical corrections resulting from the finite sizes of the beta detector and of the conversion electron detector (Au scatterer) have been taken into account on the basis of the θ-dependence given in eq. (1).

The measurements yield for the degree of transverse polarization of the Hg^{203} K-conversion electrons:

$$P_{\perp}(\theta) = (0.35 \pm 0.07)(v/c) \sin \theta \qquad (7)$$

Several arguments indicate that the beta decay of Hg^{203} is a first-forbidden transition although the *ft*-value is relatively small ($\log ft = 6.4$): from shell model considerations a parity change is expected in the transition $_{80}Hg^{203} \rightarrow {}_{81}Tl^{203}$. Furthermore, the beta-gamma directional correlation of Hg^{203} exhibits a small anisotropy [12]), $W_{\beta\gamma}(\theta) = 1-(0.0022\pm0.0009)P_2(\cos\theta)$, and it is very unlikely that this anisotropy could be caused by higher order effects in an allowed beta transition [13]).

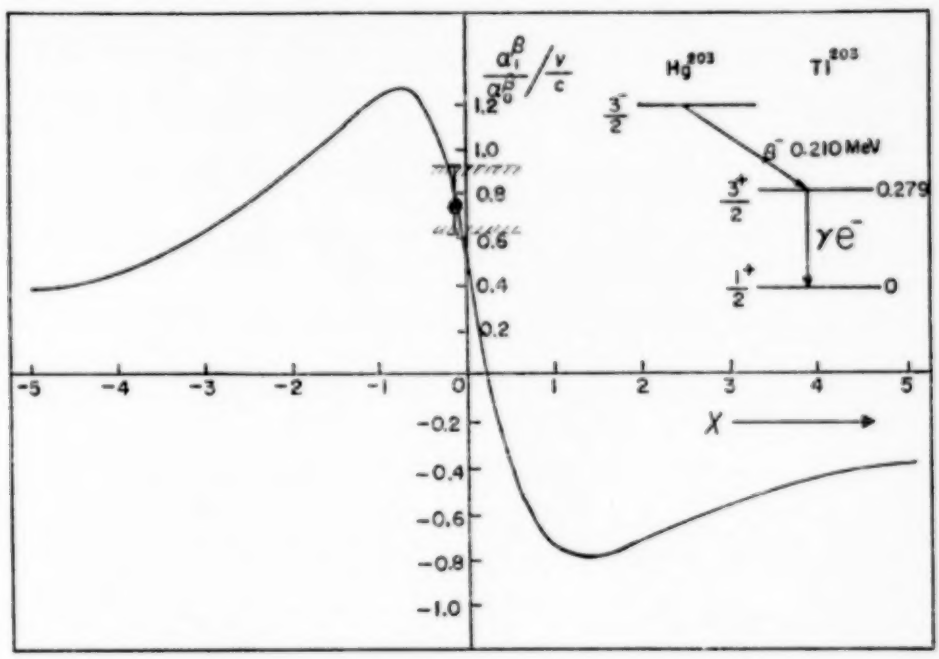

Fig. 3. The beta particle parameter ratio α_1^β/a_0^β for a $\frac{3}{2} \rightarrow \frac{3}{2}$ beta transition as a function of the nuclear matrix element ratio X.

Since the Hg^{203} beta spectrum has an allowed shape [10]) and $\xi \approx 15 \gg 1$, the use of the ξ-approximation for this first-forbidden beta decay seems to be appropriate. In this approximation (refer to eq. (4)), $\alpha_1^\beta/\alpha_0^\beta = -0.775v/c$ for the $(\frac{5}{2})-(\frac{3}{2})-(\frac{1}{2})$ spin sequence, $\alpha_1^\beta/\alpha_0^\beta = 1.29v/c$ for the $(\frac{1}{2})-(\frac{3}{2})-(\frac{1}{2})$ spin sequence, and $\alpha_1^\beta/\alpha_0^\beta = [(0.514-2X)/(1+X^2)](v/c)$ for the $(\frac{3}{2})-(\frac{3}{2})-(\frac{1}{2})$ spin sequence. For the latter decay scheme, fig. 3 shows a plot of $\alpha_1^\beta/\alpha_0^\beta$ versus the nuclear matrix element ratio X. Hence, within the framework of the validity of the ξ-approximation the experimental result of $P_\perp$ gives strong support to the $(\frac{3}{2})-(\frac{3}{2})-(\frac{1}{2})$ spin sequence and also indicates † $X = -0.01\pm0.01$. This result agrees satisfactorily with the beta-gamma directional correlation measurements [12]) and with the beta-gamma circular polarization correlation experiments [14]).

During the progress of this work it came to our attention that a similar experiment has been performed in Russia [15]).

† The second possible solution $X \approx -2.5$ is considered rather improbable.

The authors are indebted to Dr. M. E. Rose for communicating the results of his calculations prior to publication and for his helpful cooperation in the theoretical analysis. Discussions with Dr. R. W. King have been of considerable value in the interpretation of the experimental data.

References

1) M. E. Rose and R. L. Becker, Phys. Rev. Letters **1** (1958) 116
2) R. L. Becker and M. E. Rose, Bull. Am. Phys. Soc. **4** (1958) 79
3) R. L. Becker and M. E. Rose, Nuovo Cimento **13** (1959) 1182
4) V. B. Beresteckij and A. P. Rudik, Nuovo Cimento **10** (1958) 375
5) Alder, Stech and Winther, Phys. Rev. **107** (1957) 728
6) T. Kotani and M. Ross, Phys. Rev. Letters **1** (1958) 140
7) T. Kotani and M. Ross, Progr. Theoret. Phys. **20** (1958) 643
8) T. Kotani, Phys. Rev. **113** (1959) 622
9) H. Wegener, Z. Physik **151** (1958) 252
10) N. Marty, Compt. Rend. **240** (1955) 291
11) F. K. McGowan and P. H. Stelson, Phys. Rev. **109** (1958) 901
12) R. M. Steffen, to be published
13) R. M. Steffen, Phys. Rev. Letters **3** (1959) 277
14) F. Boehm and A. H. Wapstra, Phys. Rev. **109** (1957) 456
15) V. A. Lyubimov and M. E. Vishnevskii, JETP **9** (1959) 1103

8.B *Nuclear Physics* **14** (1959/60) 205—211; © *North-Holland Publishing Co., Amsterdam*
Not to be reproduced by photoprint or microfilm without written permission from the publisher

SCHWINGER'S MESON AND THE μ-MESIC ATOM

I. R. GATLAND
Department of Mathematics, Imperial College, London

Received 22 August 1959

Abstract: The properties of Schwinger's meson (σ), which is supposed to interact with muons and cascade particles, have been estimated by calculating
(i) the muon self mass and comparing this with the muon-electron mass difference,
(ii) the anomalous effect on the bound state levels of μ-mesic atoms and comparing this with the experimental data.
These and other results have been used to obtain values of the σ-meson mass and the strength of its coupling to muons and baryons.

1. Introduction

It has been suggested by Schwinger and others that the mass difference between electrons and muons may be due to the existence of a new meson (σ) which interacts with muons but not with electrons. The σ-meson is also expected to interact with baryons and, if it interacts with cascade particles but not directly with nucleons, its existence may also explain the N—Ξ mass difference. Now, this would introduce a new interaction between nucleons and muons, through the cascade particle and σ-meson fields, in addition to that through the photon field. However, the properties of the muon, such as scattering, bremstrahlung etc., have been explained reasonably well in terms of the electromagnetic interaction alone and the small anomalous effects observed may be due to experimental errors and inadequacies in the theories of nuclear charge distribution. Hence the interaction through the σ-meson field can only play a small part except, of course, in the muon and cascade particle self masses.

From this and other information it may be possible to fix the σ-meson properties. Thus, we expect the σ-particle to be a meson, probably with spin zero. Since it has not been observed in emulsions or cloud chambers it must be uncharged and have a fast decay to pions, say. The mass (κ) of the σ-meson together with the coupling constants g and b for the $\bar{\mu}\mu\sigma$ and $\bar{\Xi}\Xi\sigma$ interactions, respectively, may be estimated by comparing the large self mass of the muon with the small μ—N interaction through the σ-meson field.

In this paper we consider in particular the muon self mass, muon scattering and the properties of the μ-mesic atom.

2. The Muon Self Mass

The value of the self mass of the muon obtained from the usual self energy graph is given in a paper by Cowland [1]). However, in the case when the $\bar{\mu}\mu\sigma$ and $\bar{\Xi}\Xi\sigma$ interactions are scalar the tadpole graphs with either a closed muon or cascade particle loop also contribute. The self energy graphs are shown in fig. 1. Thus in the case when both the $\bar{\mu}\mu\sigma$ and $\bar{\Xi}\Xi\sigma$ interactions are scalar we have for the self mass $\delta\mu$ of the muon

$$\begin{aligned}\delta\mu = &\frac{gb}{4\pi}\frac{M}{\pi}\left[\frac{\lambda^2}{\kappa^2}-\frac{M^2}{\kappa^2}\ln\left(1+\frac{\lambda^2}{M^2}\right)\right]\\ &+\frac{g^2}{4\pi}\frac{\mu}{\pi}\left[\frac{\lambda^2}{\kappa^2}-\frac{\mu^2}{\kappa^2}\ln\left(1+\frac{\lambda^2}{\mu^2}\right)\right]\\ &+\frac{g^2}{4\pi}\frac{3\mu}{4\pi}\ln\left(\frac{\kappa}{\lambda}\right)+\mathrm{O}\left(\frac{\mu^2}{\kappa^2}\right)\end{aligned} \tag{1}$$

where M is the mass of the cascade particle, μ the mass of the muon and λ the cut off. The third term is given by eq. (6) of ref. [1]).

Put

$$\frac{M}{\mu}=13, \qquad \frac{\lambda}{\kappa}=\rho, \qquad \frac{\kappa}{\mu}=\tau;$$

then,

$$\begin{aligned}\frac{\delta\mu}{\mu}\approx &\frac{gb}{4\pi}\frac{13\rho^2}{\pi}\left[1-\frac{169}{\rho^2\tau^2}\ln\left(1+\frac{\rho^2\tau^2}{169}\right)\right]\\ &+\frac{g^2}{4\pi}\frac{\rho^2}{\pi}\left[1-\frac{3}{4\rho^2}\ln\rho-\frac{1}{\rho^2\tau^2}\ln\left(1+\rho^2\tau^2\right)\right].\end{aligned} \tag{2}$$

If the $\bar{\mu}\mu\sigma$ interaction is scalar and the $\bar{\Xi}\Xi\sigma$ interaction is pseudoscalar the diagram with a closed cascade particle loop does not contribute and the first term in eq. (1) is absent. The case where both the $\bar{\mu}\mu\sigma$ and $\bar{\Xi}\Xi\sigma$ interactions are pseudoscalar has been adequately treated in ref. [1]) and found to be inconsistent with the small anomalous magnetic moment.

3. The μ-Mesic Atom

The muon-nucleon interaction through the σ-meson field will add a Yukawa type potential to the field of the nucleus to which the muon is bound. For low charge values ($Z \leqq 35$) the energy levels due to the electromagnetic potential may be calculated by applying corrections for the finite charge radius and for relativistic effects to the solution of the Schrödinger equation for the point nucleus and muon only. Since the transition energies given by this theory differ

little from the experimental results the Yukawa potential can only play a small part and may thus be treated as a perturbation on the wave function given by the Schrödinger equation in the electromagnetic case.

For the 2p—1s transition the experimental results and those from electromagnetic theory are given in papers by Fitch and Rainwater [2]) and Cooper and Henley [3]). These are tabulated here in table 1 for $Z < 35$.

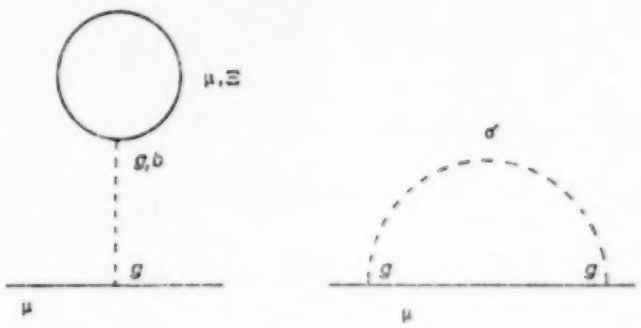

Fig. 1.

TABLE 1

Experimental and calculated 2p—1s transition energies in MeV

Element Z	Experimental results E_{exp}(2p—1s)	Point nucleus			Extended nucleus			Average E(2p—1s)
		E(1s)	$E(2p_{\frac{3}{2}}—1s)$	$E(2p_{\frac{1}{2}}—1s)$	E(1s)	$E(2p_{\frac{3}{2}}—1s)$	$E(2p_{\frac{1}{2}}—1s)$	
13	0.35	0.4849	0.3631	0.3628				0.3630
14	0.41	0.5614	0.4214	0.4209				0.4212
22	0.955	1.3917	1.0455	1.0432	1.282	0.935	0.933	0.934
29	1.55	2.4300	1.8277	1.8208	2.12	1.52	1.51	1.52
30	1.60	2.6026	1.9579	1.9500				

The correction due to the Yukawa potential is calculated as follows. The Schrödinger equation for the point nucleus and muon with the photon interaction only is

$$H^0\psi^0_{nlm} = E_n{}^0\psi^0_{nlm}, \quad \text{where} \quad H^0 = -\frac{\nabla^2}{2\mu} - \frac{Ze^2}{4\pi}\frac{1}{r}. \tag{3}$$

This may be solved in the same way as that for the hydrogen atom. The fundamental system of units is used, i.e., $\hbar = c = 1$. Now, the Yukawa potential gives a perturbation Hamiltonian

$$H' = \frac{Agb'}{4\pi}\frac{e^{-\kappa r}}{r}, \tag{4}$$

where A is the mass number of the nucleus, and b' the effective coupling constant for the $\overline{N}N\sigma$ interaction through the π, K and Ξ fields. Since the nu-

cleons are coupled strongly to the cascade particle, $|b'| \approx b$, where b is the $\bar{\Xi}\Xi\sigma$ interaction coupling constant. However, since pseudo-scalar particles are involved the sign of b' is not known.

Now, the transitions usually observed are of the form [2,3])

$$n = p+1, \quad l = p \to n = p, \quad l = p-1 \qquad (p > 0).$$

Hence we require the energy correction, ε_n, to the n^{th} energy level assuming $l = n-1$. Using eq. (4) perturbation theory gives

$$\varepsilon_n = \frac{Agb' Ze^2}{16\pi^2} \frac{\mu}{n^2} \left(\frac{\alpha_n}{\kappa+\alpha_n}\right)^{2n}, \tag{5}$$

where

$$\alpha_n = 2\mu Ze^2/4\pi n. \tag{6}$$

Put

$$\kappa = \tau\mu \text{ (as above)}, \quad \frac{e^2}{4\pi} = \tfrac{1}{137}, \qquad \mu = 106 \text{ MeV}.$$

Then

$$\varepsilon_n = \tfrac{106}{137} \frac{Agb'}{4\pi} \frac{Z^{2n+1}}{(68.5\tau n+Z)^{2n}} \text{MeV}. \tag{7}$$

For the 2p $\to$ 1s transition the energy correction is

$$\begin{aligned} \varepsilon_2-\varepsilon_1 &= \tfrac{106}{137} \frac{gb'}{4\pi} AZ^3 \left[\frac{Z^2}{4(137\tau+Z)^4} - \frac{1}{(68.5\tau+Z)^2}\right] \\ &\approx -\tfrac{106}{137} \frac{gb'}{4\pi} \frac{AZ^3}{(68.5\tau+Z)^2} \text{MeV} \end{aligned} \tag{8}$$

for $\tau \geqq 3$, $Z \leqq 35$.

Now, if we suppose that with this correction the theoretical and experimental results agree we require

$$E_{\text{exp}} = E_{\text{EM}}+\varepsilon_2-\varepsilon_1, \tag{9}$$

where E_{EM} is the transition energy given by the electromagnetic theory which is tabulated in the last column of table 1. From table 1 we see that $E_{\text{exp}} > E_{\text{EM}}$. Hence we require

$$\varepsilon_2-\varepsilon_1 > 0, \ \therefore b' < 0, \qquad \text{i.e.} \qquad b' \approx -b.$$

Thus,

$$\varepsilon_2-\varepsilon_1 = E_{\text{exp}}-E_{\text{EM}} \approx \frac{106gbAZ^3}{137\times 4\pi(68.5\tau+Z)^2} \tag{10}$$

Hence

$$\frac{gb}{4\pi} = (E_{\text{exp}}-E_{\text{EM}})\rho_Z(\tau+\beta_Z)^2 \tag{11}$$

where

$$\rho_Z = \frac{137(68.5)^2}{106AZ^3} \quad \text{and} \quad \beta_Z = \frac{Z}{68.5} \ll 3 \leqq \tau.$$

The values of these functions of Z are given in table 2 and these figures indicate that $(E_{\text{exp}}-E_{\text{EM}})\rho_Z$ is not independent of Z as required by eq. (11) ($\beta_Z \ll \tau$), so that the assumption that the Yukawa potential alone is responsible for the discrepancies between the experimental results and those given by electromagnetic theory cannot be valid. However, we may place limits on the strength of the Yukawa potential by using the most stringent result.

TABLE 2

Test of eq. (11)

Z	$E_{\text{exp}}-E_{\text{EM}}$	ρ_Z	β_Z	$(E_{\text{exp}}-E_{\text{EM}})\rho_Z$
13	1.3×10^{-2}	10.0×10^{-2}	0.19	13×10^{-4}
14	1.1×10^{-2}	7.1×10^{-2}	0.20	8×10^{-4}
22	2.1×10^{-2}	1.2×10^{-2}	0.32	2.5×10^{-4}
29	3.0×10^{-2}	0.4×10^{-2}	0.42	1.2×10^{-4}

From the results for $Z = 29$ we have

$$\frac{gb}{4\pi} \leqq 1.2\tau^2\times10^{-4}. \tag{12}$$

We now substitute this relation between g, b and τ into eq. (2) and put $\delta\mu/\mu = 1$ since we assume that the muon and electron have the same bare mass. Also we suppose that

$$\eta = b/g \approx 1.$$

Then,

$$\begin{aligned} 1 \leqq{}& 1.2\times10^{-4}\tau^2\rho^2\frac{13}{\pi}\left[1-\frac{169}{\tau^2\rho^2}\ln\left(1+\frac{\tau^2\rho^2}{169}\right)\right] \\ &+\frac{1.2\times10^{-4}}{\eta}\frac{\tau^2\rho^2}{\pi}\left[1-\frac{3}{4}\frac{\ln\rho}{\rho^2}-\frac{1}{\rho^2\tau^2}\ln(1+\tau^2\rho^2)\right]. \end{aligned} \tag{13}$$

If the first term dominates, as is probably the case if the $\bar{\Xi}\Xi\sigma$ interaction is scalar, we have

$$11.9 \leqq \left[\frac{\tau^2\rho^2}{169}-\ln\left(1+\frac{\tau^2\rho^2}{169}\right)\right]. \tag{14}$$

Hence

$$\tau\rho \geqq 50. \tag{15}$$

Now, we expect the cut off λ to be of the same order as κ i.e. $\rho \approx 1$, but the value of τ is rather sensitive to that of ρ in eq. (15). However, if we take 2κ as an

upper bound for λ we have

$$2\frac{\kappa}{\mu} = 2\tau \geqq \rho\tau \geqq 50.$$

Thus,

$$\kappa > 3 \text{ proton masses.}$$

Also, for the coupling constants we have

$$\frac{gb}{4\pi} \leqq 1.2\times(25)^2\times 10^{-4} \approx \tfrac{1}{13}.$$

If, however, the second term dominates, as will be the case when the $\bar{\Xi}\Xi\sigma$ interaction is pseudoscalar, we have

$$2.62\eta\times 10^4 \leqq \left[\rho^2\tau^2\left(1-\tfrac{3}{4}\frac{\ln\rho}{\rho^2}\right) - \ln(1+\tau^2\rho^2)\right].$$

Then, for $\rho > 1$,

$$\tfrac{3}{4}\frac{\ln\rho}{\rho^2} < \tfrac{1}{7}.$$

Also,

$$\rho^2\tau^2 \gg 1, \therefore \ln(1+\rho^2\tau^2) \ll \rho^2\tau^2.$$

Thus,

$$\rho\tau \geqq 162\eta^{\frac{1}{2}},$$

and, assuming as before $\rho \leqq 2$,

$$\tau \geqq 81\eta^{\frac{1}{2}}.$$

For the coupling constants we have

$$\frac{g^2}{4\pi} \leqq 1.2\times 10^{-4}\times(81)^2 = 0.8.$$

It is not possible to estimate η in general but since the Ξ—N mass difference is similar to the muon self mass we expect $b \approx g$ i.e. $\eta \approx 1$. Thus,

$$\tau \geqq 81, \quad \text{i.e.} \quad \kappa \geqq 9 \text{ proton masses.}$$

4. Muon Scattering

The anomalous muon-nucleon scattering has been calculated in a previous paper [4]) where it is shown that for $\kappa = 3$ proton masses and $gb/4\pi \approx \sqrt{2}$ the anomalous cross section is of the order of 10^{-29} cm^2. The new calculations based on results for the μ-mesic atom require either a larger mass or smaller coupling constants and both these modifications produce even smaller anomalous scattering cross sections.

5. Conclusion

If the tadpole graphs both contribute it is possible to obtain the large muon self mass with only a moderately weak $\mu-\sigma-\Xi$ interaction. However, the restrictions imposed by the data on the μ-mesic atom still require a very large mass for the σ-meson and, even if the σ-meson exists, it cannot do much to explain the possible anomalous properties of the muon other than the muon-electron mass difference.

It has been pointed out that the accurate determination of the muon mass is dependent on the interpretation, through electromagnetic theory alone, of the transition energies in μ-mesic phosphorus [5]). But as the transition in question is for $n = 3 \rightarrow n = 2$, the correction is negligible compared with the $n=2 \rightarrow n=1$ transition, investigated in this paper, as is shown by eq. (8). However, it is worth noting that the determination of the muon mass by this method is affected by the possible existence of the σ-meson.

I am indebted to Professor A. Salam for discussions on this problem and to Dr. P. T. Matthews for the remark on the muon mass measurement.

References

1) W. S. Cowland, Nuclear Physics **8** (1958) 397
2) V. L. Fitch and J. Rainwater, Phys. Rev. **92** (1953) 789
3) L. N. Cooper and E. M. Henley, Phys. Rev. **92** (1953) 801
4) I. R. Gatland, Nuclear Physics **9** (1958/59) 267
5) A. Petermann and Y. Yamaguchi, Phys. Rev. Letters **2** (1959) 359

3.A:6.A *Nuclear Physics* **14** (1959/60) 212—221; © *North-Holland Publishing Co., Amsterdam*
Not to be reproduced by photoprint or microfilm without written permission from the publisher

THE USE OF DIGITAL RECORDING ON MAGNETIC TAPE FOR THE STUDY OF γ-RAYS FROM RESONANT NEUTRON CAPTURE IN PLATINUM

J. R. BIRD and J. R. WATERS
A.E.R.E., *Harwell, Didcot, Berks.*

Received 31 August 1959

Abstract: The high energy γ-ray spectra resulting from resonant neutron capture in platinum have been investigated for neutron energies up to 600 eV. 63 channels of γ-ray energy and 255 of neutron time of flight were recorded simultaneously as binary numbers on magnetic tape giving a total of 16 000 combinations. These define the γ-ray spectra for the resonances and the background between them. The 47, 68.5 and 98 eV resonances give spectra for neutron capture in Pt^{192}, Pt^{195} and Pt^{198}. These show dominant transitions which can be explained in terms of the shell model. Typical spectra for higher energy resonances are also shown. It was found that the intensity of the ground state transition for capture in Pt^{195} showed large fluctuations from resonance to resonance.

1. Introduction

A number of experiments have been performed recently [1–4]) to investigate the γ-ray spectra from resonant neutron capture in heavy elements. Corge *et al.* [1]) and Hughes *et al.* [2]) have studied the time-of-flight of neutrons which give rise to γ-rays in a narrow energy range close to the binding energy of the particular isotope. This method is of interest because, for certain nuclei, the ground state transition is allowed for only one of the two possible spins of the capturing states formed by neutron capture. However, the results of Kennett, Bollinger and Carpenter [3]) and Bird [4]) show that more information can be obtained by studying the γ-ray energy spectrum for particular neutron resonances. Since each resonance must, in general, be observed individually, this involves a long series of experiments to study a number of resonances and the γ-ray background between them. However, all the information required is contained in the three-dimensional dependence of the number of counts on both neutron energy and γ-ray energy so that it would be advantageous to be able to record both these quantities simultaneously.

Rae and Firk [5]) used magnetic tape to record two pulses whose amplitudes were proportional to γ-ray energy and neutron time-of-flight. This record was replayed at high speed, the data being analysed directly with multi-channel pulse height analyzers. This method introduces an additional spread in the energy and time resolutions which makes it more difficult to study the closely

spaced γ-rays from heavy nuclei. Moreover high stability equipment is required for both the recording and the analysis of the information, both of which may involve long times for low counting rate experiments.

If, instead of recording an analogue of the desired information, it is converted into binary numbers, these may be recorded and subsequently analysed with no loss of accuracy. The only critical part of the circuit is the analogue-to-digital converter. The remaining electronics consists of standard digital computer circuit blocks which can be transistorised for greater reliability. The use of this method of recording data on magnetic tape has a number of advantages. For example [6]):

(a) Since analysis can be carried out at at least 100 times the recording speed, a great deal of data can be handled by the repeated application of an analyser of limited capacity. The saving of analysis time also means that one analyser can be used in conjunction with a number of recorders. This saves equipment when many experiments are performed at the same time.

(b) Data from several counters can be recorded at the same time thus enabling coincidence experiments to be performed. Similarly several independent variables may be recorded as described in this experiment. This can result in a large saving in accelerator time and reduces the problems of electronics stability and monitoring.

(c) Since a permanent record of the data is made, if a sudden failure occurs in the equipment during a long run, it is usually possible to salvage the recorded data up to the point of failure. Also it is possible to analyse the data, or parts of it, several times in order to determine the most interesting parts and the best method of presentation. On the other hand, when an experiment is complete, the magnetic tape can be erased and reused.

A digital recording system based on that described by Wells [7]) has been used in a study of the high energy gamma rays from neutron capture in platinum.

2. Experimental Procedure

A four inch sodium iodide crystal, with 10 % resolution for Cs^{137} gamma rays, was used to detect the gamma rays from neutron capture in platinum. A 3 mm thick sample was placed at $6\frac{1}{2}$ metres from the target of the Harwell 15 MeV Electron Linear Accelerator which gives $\frac{1}{4}$ microsecond wide neutron pulses 400 times per second. The details of shielding and detection equipment have been described previously [8]). The pulse height distribution from the detector was analysed by an amplitude-to-time converter as used in the A.E.R.E. Type 1524 100 channel pulse height analyser. This gives out a train of pulses, the number of which is proportional to the amplitude of the input pulse. A 100 channel display unit was used in conjunction with the converter, for calibration and monitoring purposes.

A second train of pulses was generated to define the time of flight of a neutron which gave rise to a pulse in the detector. This was done by passing a regular series of $\frac{1}{4}$ microsecond pulses through a gate which was opened 20 microseconds after the start of the accelerator pulse, and closed by the arrival of the detector pulse. A linear gate was used to prevent the amplitude to time converter from operating except during the correct time interval. These two trains of pulses, one defining a gamma ray energy and the other the associated neutron time of flight, were passed into two binary scalars. The resulting binary numbers were recorded on 14 tracks in line across the width of 1″ wide magnetic tape †. Six tracks were used to give 63 channels of gamma ray energy covering the range from 4.5 to 9.0 MeV. Eight tracks gave 255 channels of time of flight information covering the neutron energy range from 30 to 600 eV with a resolution of 0.05 microseconds per metre.

A recording speed of 1″ per second was used so that a reel of 7200 feet of magnetic tape lasted for 24 hours. At this speed the dead time of the equipment was 5 msec. and since the total counting rate was 5 per second, the counting losses were small. Approximately 7×10^5 pulses were recorded during a total running time of 100 hours.

The analysis was carried out with a 1023 channel analyser †† which accepted the information from four gamma-ray energy channels simultaneously. The information was stored in a ferrite core memory with a capacity of 1023 counts per channel. Sixteen replays were necessary to obtain the total of 16 000 numbers. Since the analysis tape speed was 100 inches per second, the total time for analysis was one sixth of the recording time. The contents of the memory were punched on to paper tape in the form of octal numbers. These were then converted into decimal numbers and running totals calculated using a Hollerith 555 computer. Time of flight curves for each gamma-ray energy channel were plotted on an automatic graph plotter.

The positions of the resonances were found from the curves and the background (determined by the counting rate between resonances) was obtained as a function of both neutron time of flight and gamma ray energy. The area in each resonance was calculated from the tabulated running totals and the background subtracted. Curves of area versus gamma-ray energy then give the gamma-ray spectrum for each resonance. Alternatively a three dimensional model can be constructed which displays directly the variation of the count rate with both variables (fig. 1).

3. Results

The time of flight curves for three gamma ray energy channels are shown in fig. 2. The neutron energies for the various peaks observed are listed in table 1.

† Minnesota Mining and Manufacturing Co. Number 150 Instrumentation Tape.

†† Built by E.M.I. Ltd., Hayes, Middlesex.

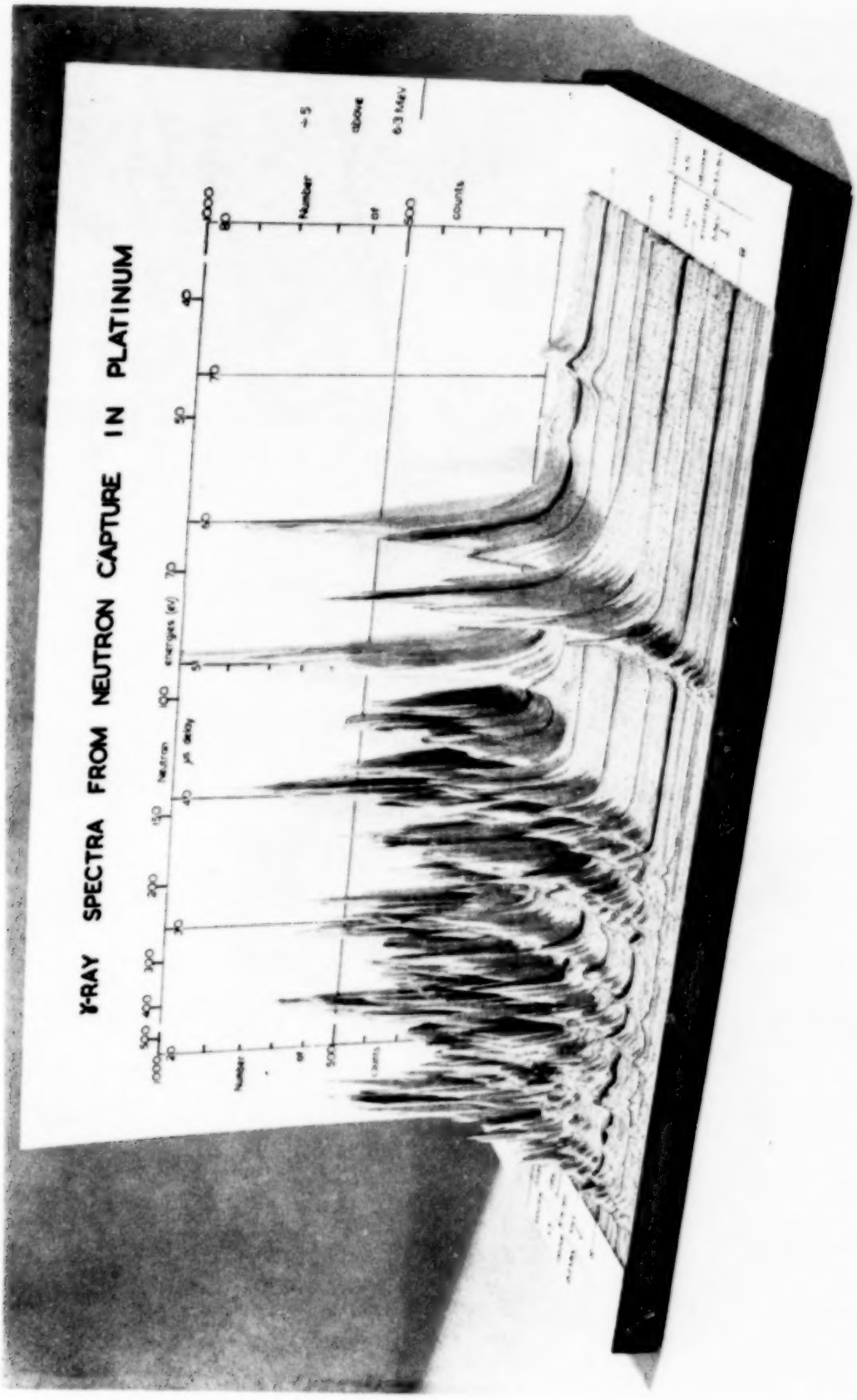

Fig. 1. Model of the γ-ray spectra from neutron capture in platinum. The plot is neutron energy vs. γ-ray energy vs. number of counts.

The errors quoted are probable errors from the determination of time of flight and systematic errors of a similar magnitude may also occur. The results are in satisfactory agreement with the results of Corge *et al.* [1]) although the limited resolution means that only the prominent features of the spectrum are observed.

Information on the isotopic allocation of the resonances is given in table 1

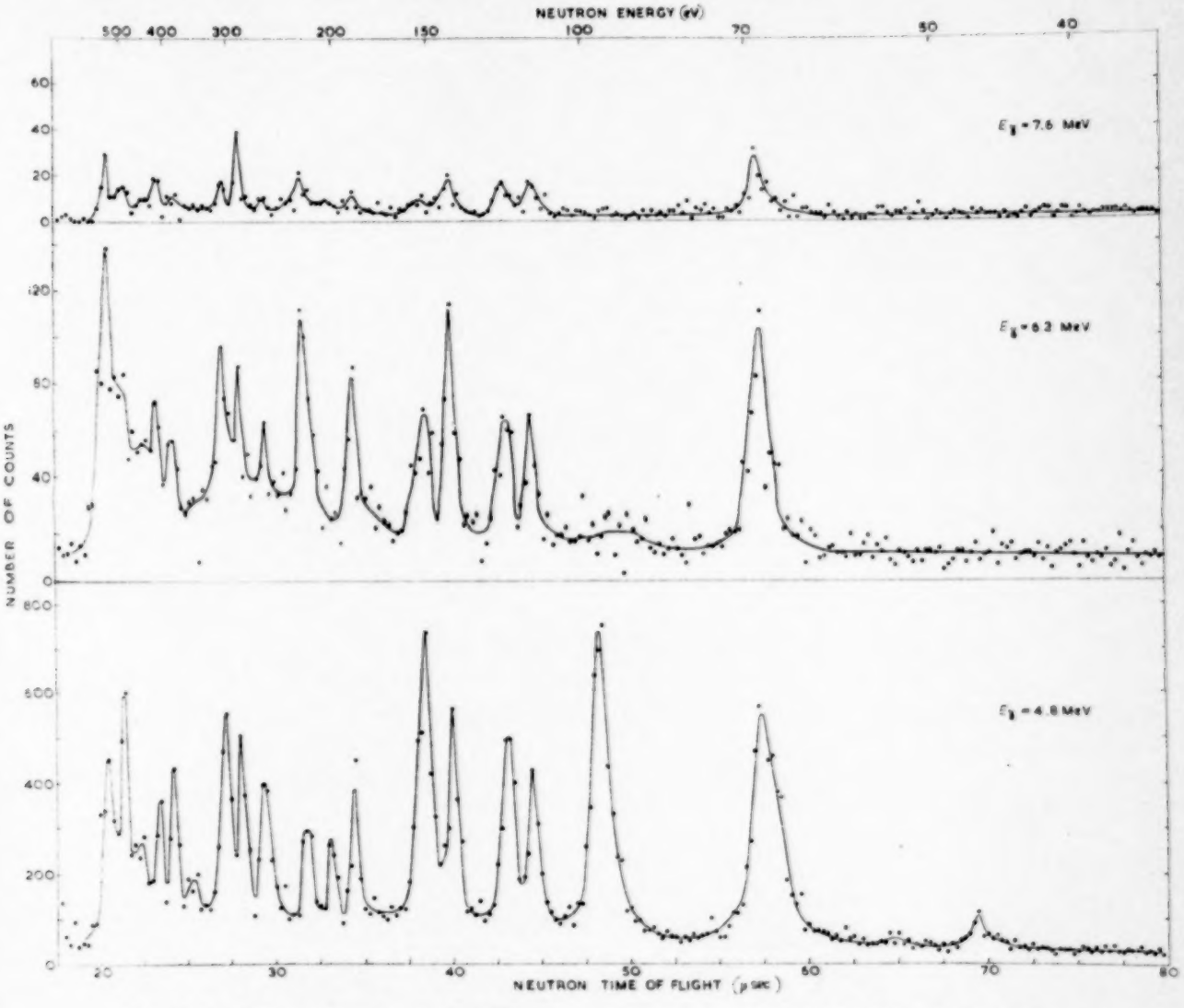
NEUTRON ENERGY (eV)
500 400 300 200 150 100 70 50 40
E_γ = 7.6 MeV
E_γ = 6.2 MeV
E_γ = 4.8 MeV
NUMBER OF COUNTS
NEUTRON TIME OF FLIGHT (μsec)
20 30 40 50 60 70 80

Fig. 2. Typical neutron time of flight curves at γ-ray energies of 4.8, 6.2 and 7.6 MeV.

using the results of Stolovy and Harvey [9]) and Chrien [10]). Further information has been obtained from a study of the low energy gamma ray spectra. Capture in Pt^{195} leads to the formation of an even-even nucleus and enhanced transitions are observed between low lying excited states [11]). A 345 keV peak is observed for Pt^{195} resonances and this can be explained as a combination of gamma-rays from the first excited state to the ground state (331 keV) and from the second excited state to the first excited state (354 keV). We have observed such a peak for those resonances marked with an asterisk in table 1 and the relative intensi-

ties of the peaks are given in brackets. When the relative intensity is less than 1, it is probable that there are two or more unresolved resonances and that these, are not all due to Pt^{195}.

Gamma-ray spectra can be drawn for each of the peaks in the time of flight spectrum, thus providing information that would have involved more than 20 times as much accelerator time to collect by normal methods. Spectra for the first four resonances are shown in fig. 3. The gamma ray energy scale gives

TABLE 1

Energies and isotopic allocations for the neutron resonances in platinum

Resonance energy (eV)	Isotopic allocation
47 ± 0.5	Pt^{192}
54 ± 0.5	
68.5 ± 0.6	Pt^{195} *(1.0)
98 ± 1	Pt^{198}
115 ± 1.3	*(1.7)
123 ± 1.4	Pt^{195} *(0.5)
142 ± 1.8	*(1.2)
155 ± 2	Pt^{195} *(0.5)
192 ± 3	*(1.0)
209 ± 3	*(0.8)
228 ± 4	*(1.0)
263 ± 4	*(1.1)
290 ± 5	*(0.7)
312 ± 6	*(0.5)
356 ± 7	
394 ± 8	
426 ± 9	
450 ± 10	
508 ± 12	
568 ± 14	

* 345 keV gamma ray peak observed indicating contribution from capture in Pt^{195}. Relative intensities are given in parenthesis.

the position of the extrapolated upper edge of the spectrum of single gamma rays [8]). The complex nature of the spectra from a sodium iodide crystal and the close spacing of gamma rays from neutron capture in heavy elements means that it is not possible to isolate individual gamma rays in most cases. However, the main features of the spectra in fig. 2 give useful information on the capture process in individual platinum isotopes. In table 2, data concerning capture in the various isotopes are given, including the energy and multipolarity expected for a ground state transition in each case.

The 96 eV resonance, which is due to capture in Pt^{198}, shows a very strong gamma ray at 5.5 MeV. However the calculated binding energy is 6.5 MeV and

the ground state transition is expected to be magnetic quadrupole so that this is probably responsible for the very low count rate observed above 5.5 MeV. The 5.5 MeV gamma ray is probably a transition to an excited state at 1 MeV in Pt^{199}. The shape of the spectrum is very similar to that observed for gamma rays from a polonium-beryllium source, which implies that there is only one strong gamma ray in the energy region studied.

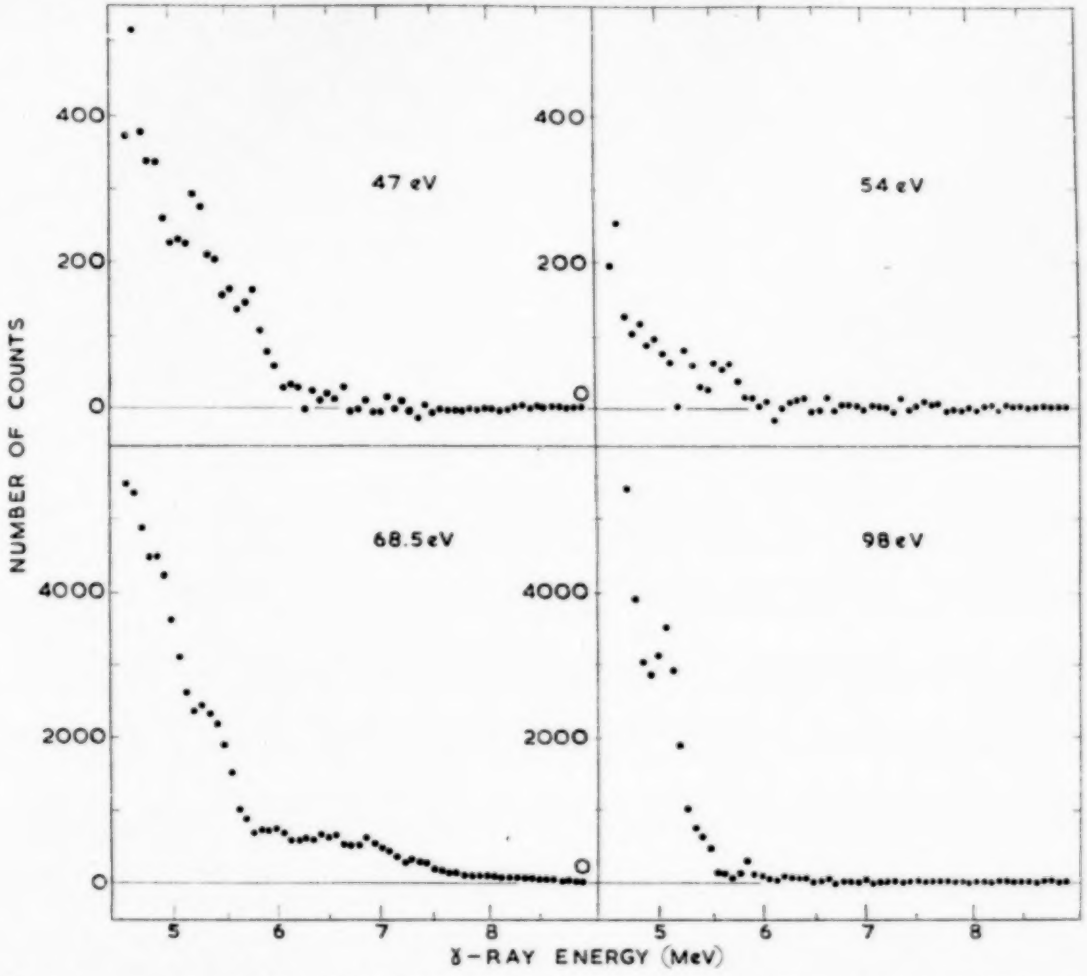

Fig. 3. γ-ray spectra for the 47, 54, 68.5 and 98 eV resonances. The ordinates are the total number of counts under the resonance peak.

The 68.5 eV resonance is due to capture in Pt^{195} and shows gamma rays with significant intensity up to an energy of 7.8 MeV. This is close to the highest energy gamma ray observed for thermal neutron capture in platinum (7.92 MeV) which agrees with the binding energy calculated from mass measurements. The presence of a ground state transition proves that this resonance leads to the formation of a spin 1 capturing state in Pt^{196}. The transitions to the ground and the first two excited states (at 354 and 685 keV respectively) are relatively weak and the first strong gamma ray occurs at 5.7 MeV followed by others at

lower energies. These are probably transitions to excited states at 2.2 MeV and above.

The 47 eV resonance is due to Pt^{192} and the strong gamma ray at 6.1 MeV is therefore the ground state transition. The spectrum shows some structure which suggests that there are only a few gamma rays above 5 MeV. The 54 eV resonance is so weak that its end point is poorly defined but it appears to be at approximately 5.9 MeV so that it may be due to capture in Pt^{192}, Pt^{194} or Pt^{196}.

TABLE 2

Neutron capture characteristics for the platinum isotopes

Isotope	Abundance (%)	Ground state spin		Multipolarity of ground state gamma ray	Binding energy (MeV)
		Target nucleus	Final nucleus		
Pt^{190}	0.012	0+	$\frac{1}{2}-$	E1	6.4
Pt^{192}	0.78	0+	$\frac{1}{2}-$	E1	6.1
Pt^{194}	32.8	0+	$\frac{1}{2}-$	E1	6.09
Pt^{195}	33.7	$\frac{1}{2}-$	1+	E1	7.92
			0+	forbidden	
Pt^{196}	25.4	0+	$\frac{1}{2}-$	E2	5.7
Pt^{198}	7.23	0+	$\frac{5}{2}-$	M2	6.5

Taken from L. V. Groshev *et al.*[12]).

The shapes of the spectra for different isotopes can be satisfactorily explained by a consideration of the shell model interpretation of nuclei in this mass region. The configurations suggested by Elliott and Lane [13]) indicate that successive even nuclei are formed by the addition of pairs of neutrons to the $i_{\frac{13}{2}}$ shell, while the intervening odd-neutron nuclei mostly have their odd neutron in the $p_{\frac{1}{2}}$ shell. For even target nuclei, the capturing state will have spin $\frac{1}{2}$, and E1 transitions with strengths approaching the single particle estimates may be expected to occur to final states which are predominantly composed of the target nucleus as a core plus one $p_{\frac{1}{2}}$ neutron. This would explain the strong ground state transition for capture in Pt^{192}. On the other hand Pt^{199} does not have an odd neutron in the $p_{\frac{1}{2}}$ shell, but has one neutron missing from the lower $f_{\frac{5}{2}}$ shell. Thus the ground state transition for capture in Pt^{198} is no longer favoured. Hence the excited state at 1 MeV which receives strong radiation probably consists of a Pt^{198} core plus a $p_{\frac{1}{2}}$ neutron. For capture in Pt^{195}, the strong gamma rays again occur to excited states, this time to levels above the pairing energy so that a similar explanation can be applied. It may be noted that the same conditions which favour strong transitions also favour the direct capture process which may, therefore, make some contribution to the cross section.

The results in table 1 suggest that the peaks in the time of flight spectrum between 100 and 300 eV neutron energy are either partly or entirely due to one

or more resonances in Pt^{195}. It is not surprising therefore that their γ-ray spectra are comparable with that for the 68.5 eV resonance. Typical spectra are shown in fig. 4. The 209 eV spectrum shows very few counts above 7 MeV which is what would be expected for a zero spin capturing state. However, the observed intensities in this region show considerable fluctuations from resonance to resonance so that it is not possible to prove the zero spin. The intensities observed in the

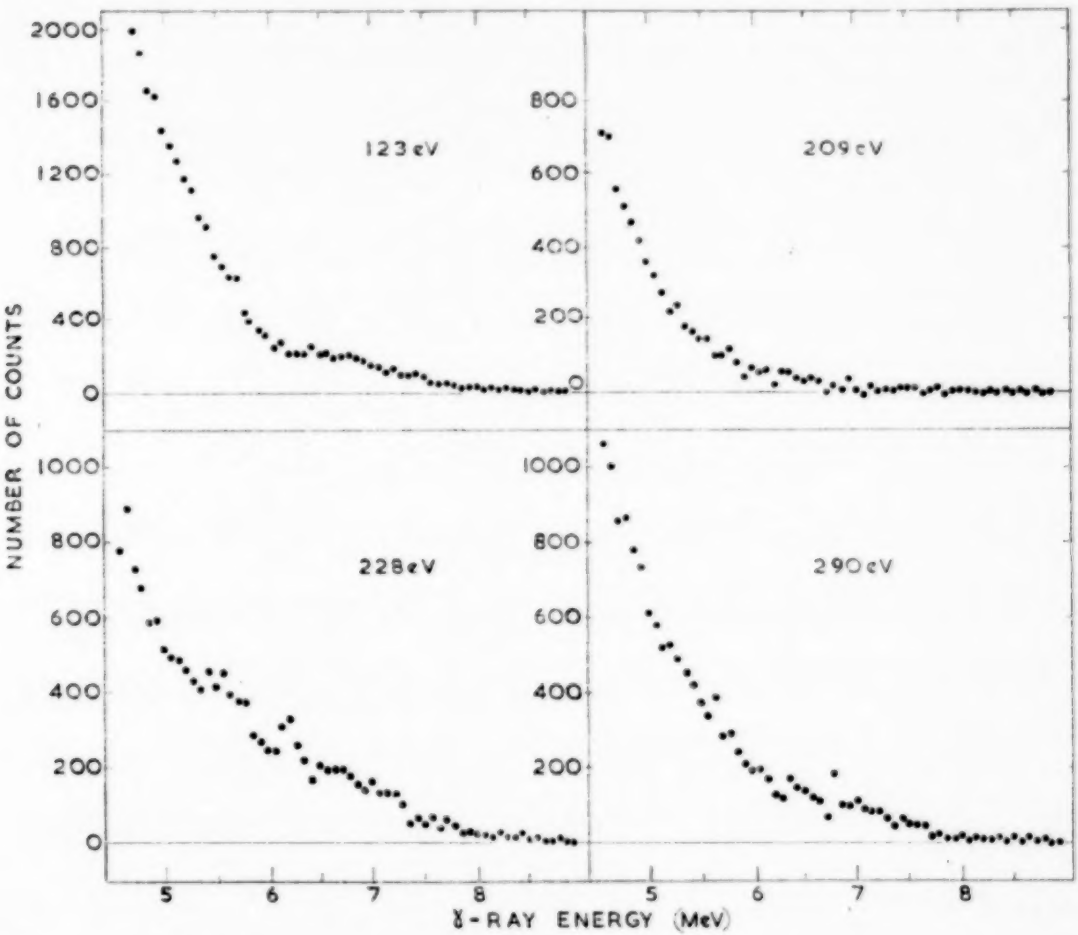

Fig. 4. γ-ray spectra for the 123, 209, 228 and 290 eV resonances. The ordinates are the total number of counts under the resonance peak.

energy interval from 7.6 to 8.0 MeV, which should involve ground state transitions only, are given in table 3. The ratios of these to the total capture areas are also given after normalisation to unity for the 68 eV resonance. The capture areas are the combined results of the intensities observed for all gamma rays above 4.5 MeV and of independent measurements made including lower gamma ray energies. The results in parenthesis have been corrected to allow for the amount of capture due to Pt^{195} as indicated by the study of low energy gamma rays (see table 1). Considerable fluctuations in intensity are observed and

in most cases these show similar trends to the results of Corge *et al.* [1]). However, the presence of spin 0 resonances and the unknown contribution from unresolved resonances means that the present results will not indicate the true distribution of partial radiation widths.

The intensities observed in the energy interval from 7.0 to 8.0 MeV are also given in table 3 together with the ratio of these results to those for the ground state transition. Measurements over similar energy intervals to those used in columns B and C in table 3 have been made using the polonium-beryllium

TABLE 3

γ-ray intensities from platinum resonances

Resonance energy (eV)	Capture area (normalised) A	Counts in energy interval		Normalised ratio C/A	Ratio B/C
		7.0–8.0 MeV B	7.6–8.0 MeV C		
68.5	1.00	3271±60	721±40	1.00	4.5±0.25
115	0.26±0.02	749±40	184±20	1.00±0.15	4.1±0.5
123	0.40±0.02	1073±50	256±25	0.89±0.11 (1.8 ±0.4)	4.2±0.5
142	0.33±0.02	902±45	230±25	0.97±0.13	3.9±0.4
155	0.60±0.03	660±50	169±35	0.36±0.06 (0.7 ±0.2)	3.9±0.7
192	0.12±0.02	449±40	79±20	0.61±0.14	5.7±1.5
209	0.14±0.02	103±35	25±17	0.25±0.17	4.1±3.3
228	0.17±0.02	1088±45	275±25	2.25±0.35	4.0±0.4
263	0.23±0.02	300±35	61±20	0.37±0.12	5.0±1.7
290	0.23±0.02	730±35	170±20	1.03±0.15 (1.5 ±0.4)	4.3±0.6
312	0.30±0.02	765±45	181±20	0.83±0.12 (1.6 ±0.4)	4.2±0.6

The errors given are statistical.

gamma ray. A ratio of 4 : 1 was observed for the counts in the two intervals. Thus the numbers, in the last column in table 3 indicate that the contributions to the spectra from transitions to the first and second excited states are relatively small.

4. Conclusions

Experiments involving the study of several parameters, such as the neutron time of flight and gamma-ray energy distributions for resonant neutron capture, can be greatly facilitated by the use of digital recording techniques and there is no consequent loss of resolution. The results obtained in this way for capture in three isotopes of platinum show the dominance of transitions to final states which probably have strong single particle p configurations. A comparison of the results for a number of resonances in one isotope (Pt^{195})

gives information on the spins associated with a number of the resonances and shows the presence of fluctuations of at least 5 : 1 in individual partial radiation widths.

Our thanks are due to F. H. Wells and J. G. Page for the design and construction of the recording equipment and assistance in setting it up, and also to P. A. Egelstaff and J. W. Hall for the use of the 1023 channel analyser.

References

1) C. Corge, V. D. Huynh, J. Julien, S. Mirza, F. Netter and J. Simic, Comptes Rendus Acad. Sci. **249** (1959) 413
2) D. J. Hughes, M. K. Brussel, J. D. Fox and R. L. Zimmerman, Phys. Rev. Letters **2** (1959) 505
3) T. J. Kennett, L. M. Bollinger and R. T. Carpenter, Phys. Rev. Letters **1** (1958) 76
4) J. R. Bird, Proc. 2nd Int. Conf. Peaceful Uses of Atomic Energy, Geneva, **14** (1958) 294
5) E. R. Rae and F. W. K. Firk, Nuclear Instruments **1** (1957) 227
6) P. E. Cavanagh and D. A. Boyce, Rev. Sci. Instr. **27** (1956) 1028
7) F. H. Wells, Nuclear Instruments **2** (1958) 165
8) J. R. Bird, C. Moxon and F. W. K. Firk, Nuclear Physics **13** (1959) 525
9) A. Stolovy and J. A. Harvey, Phys. Rev. **108** (1957) 353
10) R. E. Chrien, private communication
11) J. E. Draper, Phys. Rev. **114** (1959) 268
12) L. V. Groshev, A. M. Demidov, V. N. Lutsenko and V. I. Pelekhov, Atlas of capture γ-ray Spectra (Pergamon Press, London, 1959)
13) J. P. Elliott and A. M. Lane, Handbuch der Physik **39** (1957) 241

7.C *Nuclear Physics* **14** (1959/60) 222—231; © *North-Holland Publishing Co., Amsterdam*
Not to be reproduced by photoprint or microfilm without written permission from the publisher

NEUTRAL MESON PRODUCTION BY 930 MeV PROTONS

A. M. SEGAR and R. RUBINSTEIN
Department of Physics, The University, Birmingham, England

Received 28 August 1959

Abstract: The production of neutral mesons in p—C and p—Al collisions has been studied using total absorption Čerenkov counters.

The counters were tested in gamma ray beams arising from π^0 production in internal targets in the synchrotron.

Total cross sections for π^0 production from carbon at 930 and 660 MeV were 69 ± 14 and 21 ± 9 mb. The angular distribution of gamma rays, in the nucleon-nucleon centre of mass, at 930 MeV, was $1-(0.2\pm0.3)\ \cos\theta+(0.9\pm0.3)\cos^2\theta$.

From this the angular distribution of mesons in proton-nucleon collisions is deduced as being

$$1+(2.6\pm1.6)\cos^2\theta.$$

1. Introduction

Pion production in nucleon-nucleon collisions is of greater current interest than that in nucleon-nucleus collisions because of the simplicity of the theoretical analysis. However, production in nucleon collisions with complex nuclei does reveal some features of the two particle process whilst at the same time providing much higher counting rates.

The intense absorption of pions in nuclear matter ensures that all pions observed are produced in nucleon-nucleon interactions at the edge of the nucleus. At the edge, the bound nucleon is little affected by other nucleons. Therefore, the production is expected to have the same characteristics as two particle production, except for the effects of absorption of the incident nucleons.

Most work on neutral meson production at energies well above threshold, but below the energy where there is appreciable double pion production, has been done by groups using the 680 MeV synchrocyclotron at Dubna [1]). Production at these energies is best described by a resonance model, in which all production is supposed to occur via the lowest resonant state of the pion nucleon system ($J=\frac{3}{2}$, $T=\frac{3}{2}$). Calculations of excitation functions and angular distributions for this case have been given by Mandelstam [2]), and by Lindenbaum and Sternheimer [3]). The former author considers only a limited number of angular momentum states, in fact only those for which the resonant isobar and the free nucleon are in relative S and P states. The latter authors adopt a statistical approach, expected to be valid only at high energies.

The total cross section for the reaction

$$p+p \rightarrow p+p+\pi^0$$

which we denote $\sigma(pp0)$, increases monotonically up to 660 MeV in good agreement with Mandelstam's calculation (see Dunaitzev and Prokoshkin [4]). The behaviour of $\sigma(np0)$ is similar [5]). The angular distribution of mesons from both reactions is isotropic at the higher energies [4]), in agreement with the calculations of Mandelstam. The total cross sections for meson production in nuclei vary as the $\frac{2}{3}$ power of the atomic weight, as one would expect for surface production.

In the nucleon-nucleon centre of mass system, the angular distributions measured at Dubna are peaked in the backward direction, the backward/forward asymmetry having values between 1 for the proton and 3.4 for lead [1]). This asymmetry arises because of the surface production. Mesons going forward are produced at the forward surface of the nucleus by a beam attenuated by passage through the nucleus, while those going backward are produced by the unattenuated beam. This asymmetry provides a very direct measure of the nucleon absorption in nuclear matter.

Measurement of π^0 production using synchrotron beams needs very much longer counting periods than do experiments with a synchrocyclotron. The experiments described here used a beam of about 10^5 protons per 10 second synchrotron cycle. Under these conditions, it was possible to study production on nuclei only, and even then the counting rate was about 0.1 per minute. It is planned to measure production on nucleons when a more intense external proton beam is available.

2. Experimental Method

Fig. 1 shows the target, and the counter telescopes. Not shown are the beam focussing and collimating arrangements, and the monitor counters. The counter telescopes each contain three counters, arranged to select gamma rays. Counter $\bar{1}$ rejects charged particles. Gamma rays convert in the lead radiator producing electron pairs which count in 2, and which then initiate a shower in the glass of 3.

Counter $\bar{1}$ has a 4″ dia. plastic scintillator, and is placed in anticoincidence, resolving time 1.5×10^{-8} sec, with counter 2, a 1″ or $1\frac{1}{2}$″ dia. plastic scintillator. 3 is a lead glass total absorption Čerenkov counter, the glass being a $4\frac{1}{2}$″ dia. by 8″ cylinder. Coincidences $\bar{1}$, 2, 3, resolving time 4×10^{-8} sec, are used to gate pulses from 3, the gated pulses being displayed on a pulse height analyser.

Fig. 2 shows a spectrum obtained from π^0 decay γ rays emitted at 3° from a beryllium target inside the synchrotron. The spectrum contains a contamination of low energy bremsstrahlung photons produced in the wall of the synchrotron vacuum box.

The energy resolution and energy calibration were not required for angular distribution measurements, so were not directly measured. Both were inferred from spectra, and from the results obtained by others using this type of counter [6]), especially those of Cassels *et al.* [7]).

The absolute efficiency was required in order to obtain cross sections abso-

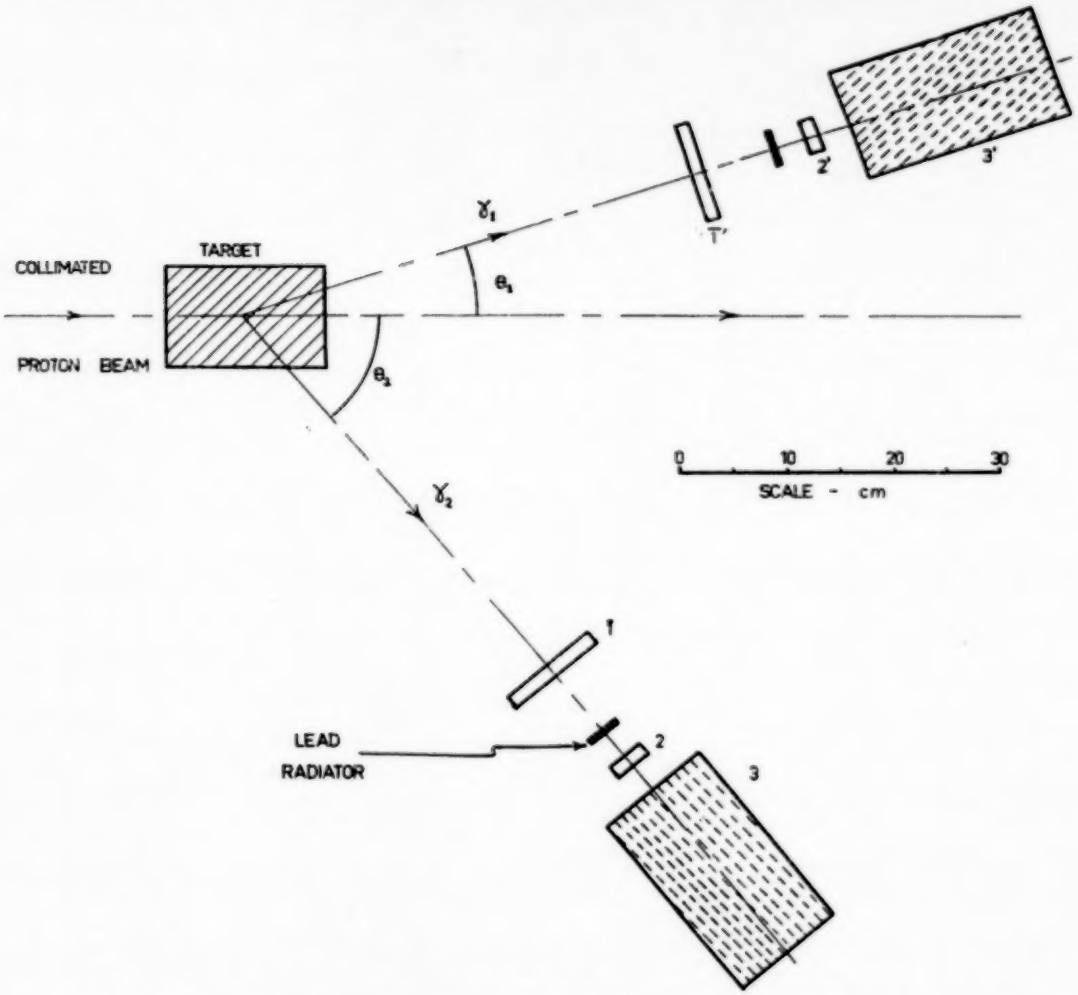

Fig. 1. Plan of the apparatus for the measurement of meson production in an external target.

lutely. The number of pairs produced in the radiator can be calculated from the known pair production cross section. The number of pairs lost due to scattering was estimated experimentally. The maximum efficiency was found to be 15 %, independent of energy for all but the lowest energies. The maximum occurred for a radiator thickness of 6 mm. This result agrees with similar measurements [8]).

At γ energies estimated to be 150 and 300 MeV, the absorption coefficients for lead were measured as 0.077 ± 0.013 cm$^2 \cdot$ g^{-1} and 0.097 ± 0.012 cm$^2 \cdot$ g^{-1}.

For work with targets external to the machine, the arrangement of target and

counters was as shown in fig. 1. Counting rates were much lower than those obtained with the internal target — about 0.1 counts per minute instead of 200 counts per minute. The background was high, particularly at small angles and at low pulse height, so it was found necessary to count under all four conditions:

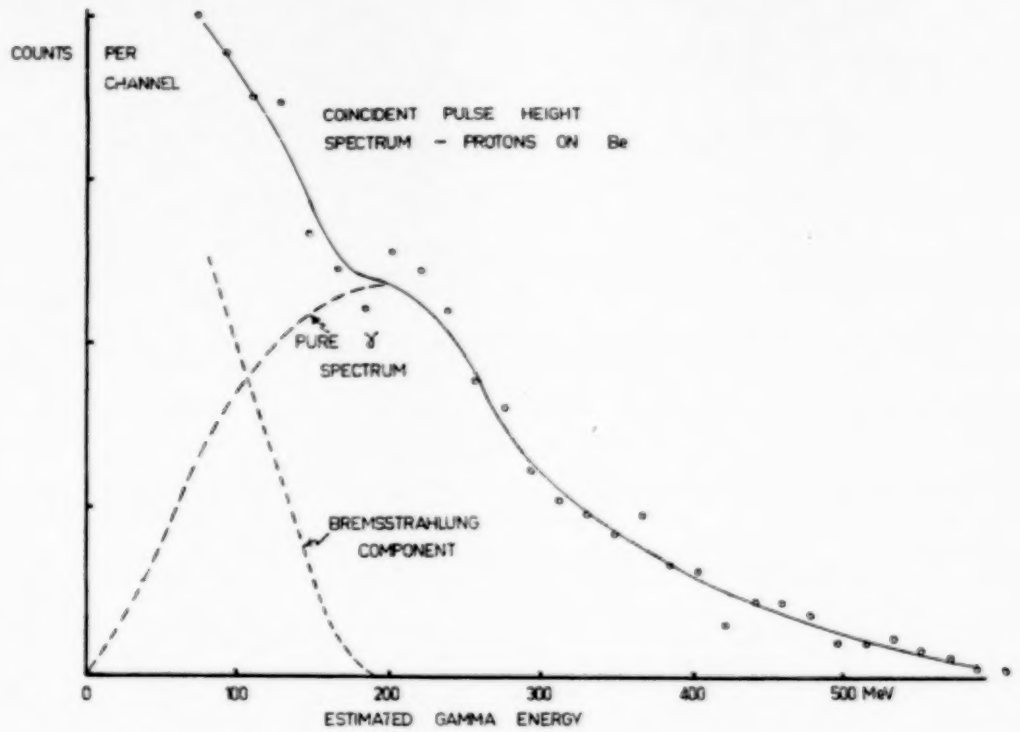

Fig. 2. Pulse height spectrum for gamma rays from an internal Be target. The gammas had to pass through the wall of the synchrotron vacuum box, and this converted about 30 % to electron pairs. The bremsstrahlung from the pairs accounts for most of the lower energy gamma rays.

	Target	Radiator
I	In	In
II	In	Out
III	Out	In
IV	Out	Out

The spectrum wanted, denoted A, is then

$$A = (I+IV)-(II+III).$$

Fig. 3 shows the A spectrum for the case of a carbon target, 930 MeV protons, and at 10° lab. It is compared with a spectrum obtained by Bayukov *et al.* [9]). Their spectrum has been shifted upward in energy, and has had our estimated counter resolution folded in. The fit is satisfactory within the low statistics of

the present measurements. A similar procedure has been used with all spectra in order to estimate total counts.

A rough measurement of the absorption coefficient for spectrum A, all energies, gave 0.05 ± 0.02 cm² per g of lead. The result verifies the fact that the telescope was selecting gamma rays.

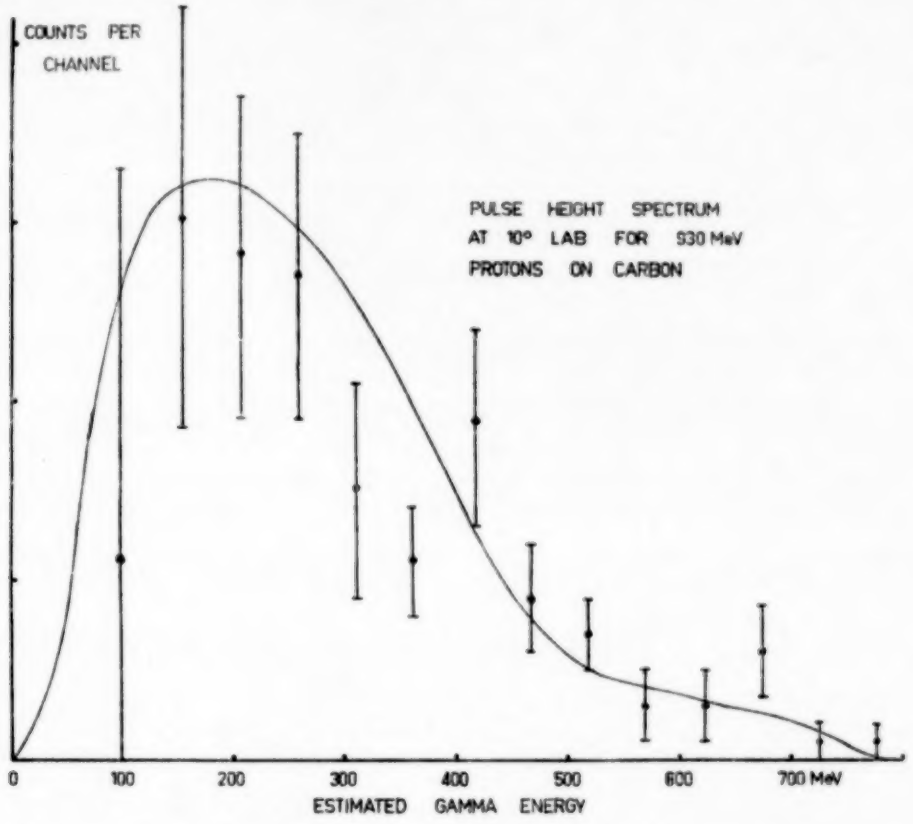

Fig. 3. Pulse height spectrum for gamma rays emitted at 10° from an external carbon target. The curve fitted to the points is derived from ref.[9]).

Normal beam monitoring was with a small counter placed in front of the target. The monitor was calibrated absolutely in one series of measurements by area scanning of tracks in an emulsion exposed normal to the beam. The calibration was checked by a counter method. The beam was well focussed and collimated to a size 5 cm by 3 cm, so could be estimated by scanning this area with a 0.5 cm by 0.5 cm scintillator. The beam duration and time structure were such that only a sample 0.25 cm² could be counted with acceptable counting loss on a 10 Mc/s scaler.

3. Results

3.1. TOTAL CROSS SECTIONS

The 660 MeV total cross section for π^0 production in p—C collisions was deduced from the 90° c. of m. differential cross section, using the angular

distribution obtained by Dunaitzev and Prokoshkin [4]). The result was 21 ± 9 mb which compares with the result 28 ± 3 mb obtained at Dubna. The result for the total cross section at 930 MeV was 69 ± 14 mb for carbon, and 66 ± 25 mb for aluminium. Our experimental angular distributions were used in obtaining these.

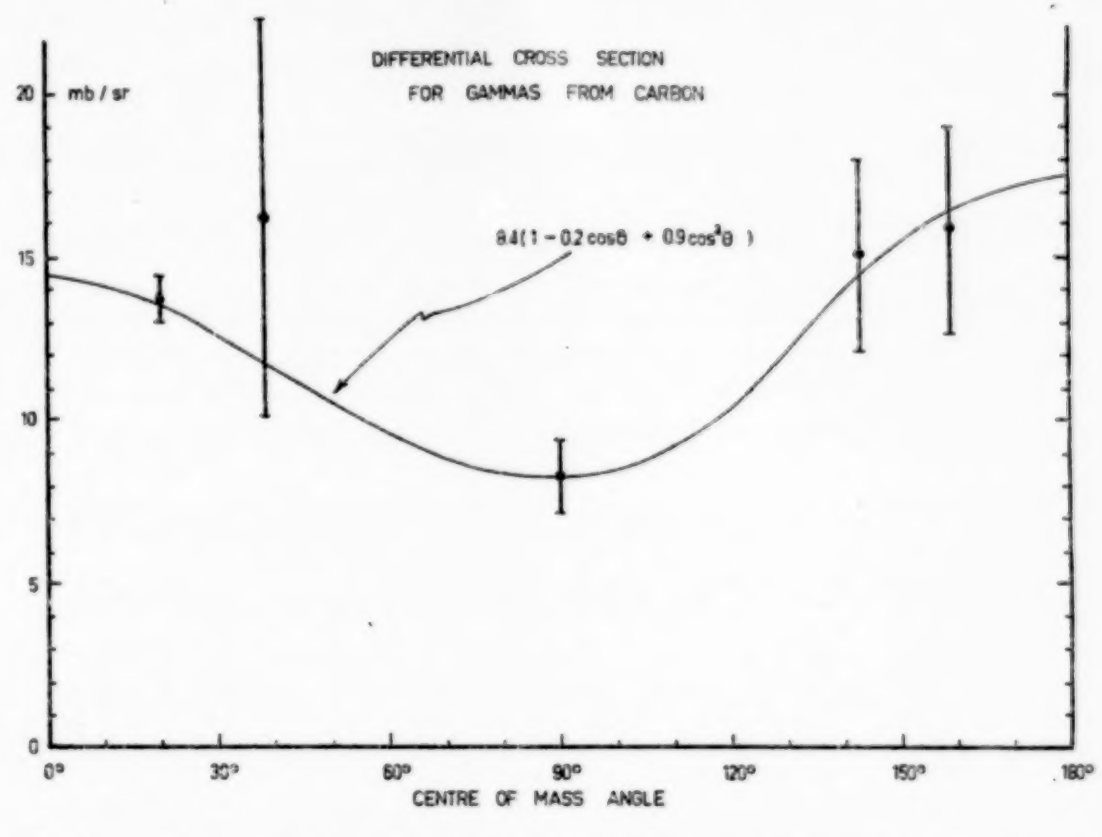

Fig. 4. Angular distribution of gamma rays from 930 MeV protons on carbon. The curve shown is the best fit to the experimental points.

The errors are mainly from counting statistics, and their size reflects the poor counting rate of about 0.1 count per minute. The cross sections ought to be proportional to the $\frac{2}{3}$ power of the atomic weight. This suggests that the aluminium cross section ought to be near the upper limit allowed by the error.

3.2. ANGULAR DISTRIBUTION AT 930 MeV

The analysis of the angular distribution was directed toward the deduction from it of the nucleon-nucleon angular distribution. This approach should provide useful information regarding the nucleon-nucleon interaction, and should show whether the complex nucleus production can be understood in a simple way in terms of the two-body production.

The results obtained, corrected for background, finite size of target, and absorption in target, and integrated over all γ energies, were as in table 1.

TABLE 1

Angular distribution results for γ rays from proton-carbon collisions at 930 MeV

Lab. angle	10°	20°	55°	115°	140°
Counts/10^4 monitor	73 ± 4	81 ± 30	28 ± 5	28 ± 5	25 ± 5

This angular distribution was converted to the c. of m. frame of the two interacting nucleons. Because of the Fermi energy of the struck nucleons, this frame is only an average c. of m. frame. The transformation velocity to be used depends on the excitation function for the reaction considered. If this is increasing with energy, for example, the transformation velocity will be less than that corresponding to a target nucleon at rest. The excitation function at 930 MeV is not known, but the results of Batson *et al.* [10]), and the calculations of Mandelstam [2]), suggest that it is varying only slowly with energy. The transformation velocity chosen was that for a target nucleon at rest. This choice may be slightly in error, but not so much as to affect conclusions made about the asymmetry about 90° of the angular distribution.

The best fit to the distribution, in the mean c. of m. system, was

$$W_\gamma(\theta) = 1-(0.2\pm0.3)\cos\theta+(0.9\pm0.3)\cos^2\theta.$$

To convert the gamma angular distribution to the meson angular distribution, an analysis similar to that given by Tyapkin [11]) was used. This shows that for an angular distribution of γ rays of the form

$$W_\gamma(\theta) = A+B\cos\theta+C\cos^2\theta,$$

the meson angular distribution is

$$W_\pi(\theta) = a+b\cos\theta+c\cos^2\theta$$

where

$$a = A+\frac{I_1-1}{3I_1-1}C, \qquad b = \frac{B}{I_2}, \qquad c = \frac{2C}{(3I_1-1)};$$

here, with

$$e_{\pi\,\mathrm{min}} = e_\gamma+\frac{1}{4e_\gamma},$$

we have put

$$I_1 = \int_0^\infty \mathrm{d}e_\gamma \int_{e_{\pi\,\min}}^\infty \frac{\left(e_\pi - \frac{1}{2e_\gamma}\right)^2 F(e_\pi)\mathrm{d}e_\pi}{(e_\pi^2-1)^{\frac{3}{2}}},$$

$$I_2 = \int_0^\infty \mathrm{d}e_\gamma \int_{e_{\pi\,\min}}^\infty \frac{\left(e_\pi - \frac{1}{2e_\gamma}\right) F(e_\pi)\mathrm{d}e_\pi}{(e_\pi^2-1)},$$

the normalization being such that

$$\int_0^\infty \mathrm{d}e_\gamma \int_{e_{\pi\,\min}}^\infty F(e_\pi)/\sqrt{e_\pi^2-1}\,\mathrm{d}e_\pi = 1.$$

Energies e are in units of the π^0 rest mass and $F(e_\pi)$ is the pion energy distribution, assumed independent of the angular distribution $W_\pi(\theta)$.

The function $F(e_\pi)$ is not known, but a reasonable form for it can be inferred from the measurements of Bayukov *et al.* [9]). In any case, the results for the coefficients a, b, c are not very sensitive to the form of the function. This was tested by trying a rectangular form for $F(e_\pi)$, which was found to give values of b and c different by about 20 %, still within the error of the present experiment. This lack of sensitivity to the shape of $F(e_\pi)$ justifies the assumption that the angle and energy distributions of the mesons may be considered independent.

The result for the meson angular distribution was

$$W_\pi(\theta) = 1-(0.4\pm0.6)\cos\theta+(3.0\pm1.5)\cos^2\theta.$$

A similar calculation from the results of Dunaitzev and Prokoshkin [4]) at 660 MeV gave

$$W_\pi(\theta) = 1-0.38\cos\theta+0.23\cos^2\theta.$$

The pion distribution we consider to be the product of the proton-nucleon pion distribution, and a function taking account of the absorption of the incident proton beam and of the outgoing mesons. Prokoshkin [1]) has calculated the latter function using a simple optical model. We have calculated the function for a model under the following assumptions:

(a) The nuclear density ρ is the function of radius suggested by the electron scattering measurements of Hofstadter [12]):

$$\rho = \rho_0(1+\tfrac{4}{3}r^2/a_0^2)\exp(-r^2/a_0^2), \quad a_0 = 1.635\times10^{-13}\ \mathrm{cm}.$$

(b) Production is incoherent. The cross section is obtained by summing contributions from all parts of the nucleus.

(c) The cross section for meson absorption was taken to be 200 mb, while the cross section for absorption of the nucleons was taken as a parameter.

We find the cross section σ_a for absorption of the incident protons, to be

$$\sigma_a = 43.6x\ \mathrm{mb},$$

where $(1+x)$ is the $(180°/0°)$ asymmetry.

In the c. of m. frame of the nucleons one expects an angular distribution of the approximate form

$$1-[0.5x/(1+0.2x)]\cos\theta+[0.3x/(1+0.2x)]\cos^2\theta.$$

The result for the meson distribution at 660 MeV corresponds to isotropic distribution in the proton-nucleon system, and to a proton-nucleon cross section of 39 ± 3 mb. This agrees very well with the proton-free nucleon cross section (mean of σ_{pp} and σ_{np}) of 38 mb, given by Hess [13]).

The free proton-nucleon cross section at 930 MeV is 43 mb (Law *et al.* [14])); one therefore expects a meson angular distribution, due to absorption effects alone, of the form

$$1-0.40\cos\theta+0.24\cos^2\theta.$$

From this and the experimental result, it follows that the angular distribution of mesons in free proton-nucleon collisions at 930 MeV is

$$1+(0.6\pm0.6)\cos\theta+(2.6\pm1.6)\cos^2\theta.$$

This expression is expected to be symmetrical about 90°, that is the coefficient of cos θ ought to be zero. This follows from the symmetry of p—p collisions, and for p—n collisions follows from an isobaric spin and angular momentum analysis such as that of Rosenfeld [15]).

4. Conclusions

The simple model in which meson production on nuclei is supposed to take place in isolated proton-nucleon interaction seems to account very well for the results reported by Dunaitzev and Prokoshkin [4]). Its application to our results at 930 MeV suggests that the angular distribution of pions in proton-nucleon production is strongly anisotropic.

Mandelstam's calculations predict that at 930 MeV the angular distribution should be isotropic, and the cross section lower than at 660 MeV. The result of Batson *et al.*, and of the present carbon experiment, suggests that the cross section is higher.

The higher cross section might be due to production in angular momentum states not considered by Mandelstam, such as those in which the isobar and the remaining nucleon are in a relative D state. The considerable anisotropy observed in the proton-nucleon angular distribution supports this conclusion.

The authors wish to thank Dr. G. W. Hutchinson for his valued assistance in supervising this work, Professor P. B. Moon for his encouragement, and Dr. L. Castillejo and Mr. G. P. Macauley for discussion.

A. M. S. thanks the Royal Society for his Rutherford Scholarship, and R. R. the Department of Scientific and Industrial Research for his Research Studentship.

References

1) Y. D. Prokoshkin, Proc. CERN Symposium **2** (1956) 385
2) S. Mandelstam, Proc. Roy. Soc. A **244** (1958) 491
3) S. J. Lindenbaum and R. M. Sternheimer, Phys. Rev. **105** (1957) 1874
4) A. F. Dunaitzev and Y. D. Prokoshkin, J.I.N.R. Report P-273 1959
5) Y. D. Prokoshkin and A. A. Tyapkin JETP **32** (1957) 750
6) J. V. Jelley, Čerenkov Radiation and its Applications (Pergamon Press, 1958)
7) J. M. Cassels, G. Fidecaro, A. M. Wetherell and J. R. Wormald, Proc. Phys. Soc. A **70** (1957) 405
8) L. J. Koester and F. E. Mills, Phys. Rev. **105** (1957) 1900
9) Y. D. Bayukov, M. S. Kozodayev, K. O. Oganesian, Y. D. Prokoshkin and A. A. Tyapkin, Nuclear Physics **4** (1957) 61
10) A. P. Batson, B. B. Culwick, J. G. Hill and L. Riddiford, Proc. Roy. Soc. A **251** (1959) 218; Also A. P. Batson, B. B. Culwick, H. B. Klepp and L. Riddiford, Proc. Roy. Soc. A **251** (1959) 233
11) A. A. Tyapkin, JETP **30** (1956) 1150
12) R. Hofstadter, Revs. Mod. Phys. **28** (1956) 214
13) W. N. Hess, Revs. Mod. Phys. **30** (1958) 368
14) M. E. Law, G. W. Hutchinson and D. H. White, Nuclear Physics **4** (1959) 600
15) A. H. Rosenfeld, Phys. Rev. **96** (1954) 139

2.L *Nuclear Physics* **14** (1959/60) 232—237; © *North-Holland Publishing Co., Amsterdam*

Not to be reproduced by photoprint or microfilm without written permission from the publisher

WIGNER's INEQUALITIES FOR RELATIVISTIC SCATTERING

P. MENOTTI

Istituto di Fisica della Università di Pisa

Received 26 July 1959

Abstract: Wigner's inequalities for the momentum derivatives of the scattering phases are extended to the relativistic scattering of particles of spin zero and one half by a central potential of finite range.

1. Introduction

Some years ago Wigner [1]) established a lower bound for the derivative $\mathrm{d}\eta_l/\mathrm{d}k$ of the scattering phase η_l (angular momentum l) with respect to the momentum k, for the non-relativistic scattering. In this case a simplified causality argument leads to the result that the momentum derivative of the phase must be greater than $-a$, a being the radius of the scattering centre, while the general properties of the R-matrix must be employed to derive a more accurate lower bound.

A simplified derivation of the inequalities for non-relativistic scattering of spin zero particles by a central potential of short range due to Corinaldesi and Zienau [2]) is essentially based on the remark that the probability of the particle being inside the region of interaction cannot be negative.

In this note Wigner's inequalities for relativistic potential scattering are obtained by a method similar to that of ref. [2]). The cases considered are those of particles of spin zero and one-half whose wave functions obey the Klein-Gordon and the Dirac equations respectively. The potential can be regarded either as a (Lorentz) scalar, denoted by $U(r)$, or as the fourth component of a four-vector, denoted by $V(r)$.

In the former case the Klein-Gordon equation differs from the Schroedinger equation only in the momentum dependence of the energy ($E = \sqrt{k^2+m^2}$ instead of $k^2/2m$, $\hbar = c = 1$). The derivation of the inequalities is then identical with that for non-relativistic scattering.

In the latter case the difference is deeper. Two solutions ψ_1 and ψ_2 of the Klein-Gordon equation corresponding to different energies E_1 and E_2, are not orthogonal in the usual sense. In fact their product is expressed by an integral involving the function E_1+E_2-2V as well as $\psi_1^*\psi_2$. When $E_1 = E_2 = E$ such an integral can be interpreted as the charge. It is positive for an arbitrary wave function only if $E-V > 0$. Therefore the method of

ref. [2]), based on the positive-definiteness of the partial normalization integral extended to the interaction region, can be employed only when the potential is attractive or, if repulsive, is everywhere smaller than E. On the other hand, in the case of the Dirac equation, integrals of the charge density $\psi^\dagger\psi$ are always positive definite and Wigner's inequalities can be established without any restriction on the potential.

2. Scattering of Particles of Spin $\frac{1}{2}$

If the potentials U and V are spherically symmetric, the Dirac equation reduces to the equations

$$\begin{aligned}(E-V+m+U)f-\left(\frac{\mathrm{d}g}{\mathrm{d}r}+(1+\kappa)\frac{g}{r}\right)&=0\\(E-V-m-U)g+\left(\frac{\mathrm{d}f}{\mathrm{d}r}+(1-\kappa)\frac{f}{r}\right)&=0\end{aligned}\qquad(1)$$

for the radial components $f(r)$ and $g(r)$ of the wave functions [3]).

The quantum number κ takes the values

$$\begin{aligned}\kappa&=-(j+\tfrac{1}{2})=-(l+1)\quad\text{if}\quad j=l+\tfrac{1}{2},\\\kappa&=(j+\tfrac{1}{2})=l\qquad\quad\text{if}\quad j=l-\tfrac{1}{2}.\end{aligned}$$

Introducing the new functions

$$F=rf,\quad G=rg,\quad \varphi=\begin{pmatrix}F\\G\end{pmatrix},$$

eq. (1) can be written in the form

$$\left\{i\sigma_2\frac{\partial}{\partial r}-(m+U)\sigma_3+\frac{\kappa}{r}\sigma_1+V(r)\right\}\varphi(E,r)=E\varphi(E,r)\qquad(2)$$

where σ_1, σ_2 and σ_3 are the familiar Pauli matrices.

Let us consider two solutions $\varphi(E_1,r)$ and $\varphi(E_2,r)$ corresponding to different energies E_1 and E_2 and to the same κ.

Multiplying by $\varphi(E_2,r)$ on the right the equation

$$\varphi^\dagger(E_1,r)\left\{-i\sigma_2\frac{\overleftarrow{\partial}}{\partial r}-(m+U)\sigma_3+\frac{\kappa}{r}\sigma_1+V(r)\right\}=E_1\varphi^\dagger(E_1,r)$$

and by $\varphi^\dagger(E_1,r)$ on the left the equation

$$\left\{i\sigma_2\frac{\partial}{\partial r}-(m+U)\sigma_3+\frac{\kappa}{r}\sigma_1+V(r)\right\}\varphi(E_2,r)=E_2\varphi(E_2,r)$$

and subtracting we obtain

$$i\frac{\partial}{\partial r}\left\{\varphi^\dagger(E_1,r)\sigma_2\varphi(E_2,r)\right\}=(E_2-E_1)\varphi^\dagger(E_1,r)\varphi(E_2,r).$$

Dividing both sides of this equation by E_2-E_1 and integrating with respect to r from 0 to a we get

$$\int_0^a \varphi^\dagger(E_1, r)\varphi(E_2, r)\mathrm{d}r = \frac{i}{E_2-E_1}[\varphi^\dagger(E_1, r)\sigma_2\varphi(E_2, r)]_{r=0}^{r=a}. \tag{3}$$

It is easy to show that $\varphi^\dagger(E_1, 0)\sigma_2\varphi(E_2, 0) = 0$ if the potentials are continuous for $r = 0$ together with their first and second derivatives. Therefore the right hand side of (3) reduces to

$$i(E_2-E_1)^{-1}[\varphi^\dagger(E_1, a)\sigma_2\varphi(E_2, a)].$$

In the limit $E_2 \to E_1$ eq. (3) gives

$$0 \leqq \int_0^a \varphi^\dagger(E_1, r)\varphi(E_1, r)\mathrm{d}r$$

$$= \lim_{E_2\to E_1} \frac{1}{E_2-E_1}[F^*(E_1, a)G(E_2, a)-F(E_2, a)G^*(E_1, a)].$$

Because of the restrictions on the potentials the integral is convergent and the limit must be finite. Therefore the expression $F^*(E_1, a)G(E_1, a)-$ $-F(E_1, a)G^*(E_1, a)$ must be zero. This can be used to show that

$$0 \leqq F^*(E, a)\frac{\partial G(E, a)}{\partial E} - G^*(E, a)\frac{\partial F(E, a)}{\partial E}. \tag{4}$$

In this inequality $F(E, a)$ and $G(E, a)$ can be expressed in terms of the scattering phase. In the region $r > a$ where the potentials U and V vanish, a scattering wave function has the form

$$\begin{pmatrix} F_\alpha \\ G_\alpha \end{pmatrix} + \mathrm{e}^{2i\eta}\begin{pmatrix} F_\beta \\ G_\beta \end{pmatrix}. \tag{5}$$

Here $\binom{F_\alpha}{G_\alpha}$ is the ingoing wave and $\binom{F_\beta}{G_\beta}$ the outgoing wave. The phase η depends on the quantum numbers E, l and κ characterizing the solution. The functions F_β and G_β are the complex conjugates of F_α and G_α.

The expressions for these functions are:

(i) $\kappa = j+\frac{1}{2} = l$

For $r > a$ eq. (2) reduces to

$$\begin{aligned} G' + \frac{l}{r}G &= (E+m)F, \\ -F' + \frac{l}{r}F &= (E-m)G. \end{aligned} \tag{6}$$

With the aid of the identities

$$\frac{\mathrm{d}}{\mathrm{d}\rho}j_l(\rho) = \frac{l}{\rho}j_l(\rho) - j_{l+1}(\rho), \quad \frac{\mathrm{d}}{\mathrm{d}\rho}j_l(\rho) = j_{l-1}(\rho) - \frac{l+1}{\rho}j_l(\rho)$$

for the spherical Bessel and Neumann functions $j_l(\rho)$ and $n_l(\rho)$ it can be shown that

$$\begin{aligned} F_\alpha &= \sqrt{E-m}kr\{-j_{l-1}(kr)+in_{l-1}(kr)\}, \\ G_\alpha &= \sqrt{E+m}kr\{-j_l(kr)+in_l(kr)\} \end{aligned} \tag{7}$$

are solutions of (6). They have the character of ingoing waves as it is easily shown by inserting the asymptotic expansions for $j_l(\rho)$ and $n_l(\rho)$ in (7). The solutions

$$\begin{pmatrix} F_\beta \\ G_\beta \end{pmatrix} = \begin{pmatrix} F_\alpha^* \\ G_\alpha^* \end{pmatrix}$$

describe outgoing waves.

(ii) $\kappa = -(j+\frac{1}{2}) = -(l+1)$

The radial wave functions for $r > a$ obey the equations

$$\begin{aligned} G' - \frac{l+1}{r} G &= (E+m)F, \\ -F' - \frac{l+1}{r} F &= (E-m)G, \end{aligned} \tag{6'}$$

whose ingoing solutions are

$$\begin{aligned} F_\alpha &= \sqrt{E-m}kr\{-j_{l+1}(kr)+in_{l+1}(kr)\}, \\ G_\alpha &= \sqrt{E+m}kr\{j_l(kr)-in_l(kr)\}. \end{aligned} \tag{7'}$$

Substituting (5) for the wave function in the inequality (4) we have

$$\begin{aligned} 0 \leqq\ & 2i\dot{\eta}(F_\alpha G_\beta - G_\alpha F_\beta) + (F_\alpha \hat{G}_\beta + F_\beta \hat{G}_\alpha - \hat{F}_\alpha G_\beta - \hat{F}_\beta G_\alpha) \\ & + (F_\beta \hat{G}_\beta - \hat{F}_\beta G_\beta)e^{2i\eta} + (F_\alpha \hat{G}_\alpha - \hat{F}_\alpha G_\alpha)e^{-2i\eta} \end{aligned} \tag{8}$$

where the dot indicates derivation with respect to E.

Using the relations $2i(F_\alpha G_\beta - G_\alpha F_\beta) = 4k$, which follow from (7) and (7') and from the properties of the Bessel and the Neumann functions, we obtain the general inequality for particles of spin $\frac{1}{2}$

$$\begin{aligned} \dot{\eta} \geqq \frac{1}{4k}[& (\hat{F}_\alpha G_\beta + \hat{F}_\beta G_\alpha - F_\alpha \hat{G}_\beta - F_\beta \hat{G}_\alpha) + (\hat{F}_\beta G_\beta - F_\beta \hat{G}_\beta)e^{2i\eta} \\ & + (\hat{F}_\alpha G_\alpha - F_\alpha \hat{G}_\alpha)^{-2i\eta}]_{r=a}. \end{aligned} \tag{9}$$

The following cases are particularly interesting.

a) $\kappa = -1,\ l = 0,\ j = \frac{1}{2}$

The free wave functions F_α and G_α are

$$\begin{aligned} F_\alpha = F_\beta^* &= \sqrt{E-m}\left\{\cos kr - \frac{\sin kr}{kr} - i\left(\frac{\cos kr}{kr} + \sin kr\right)\right\}, \\ G_\alpha = G_\beta^* &= \sqrt{E+m}\{\sin kr + i\cos kr\}. \end{aligned}$$

Substituting them in (9) this becomes

$$\frac{d\eta}{dk} \geqq -a + \frac{m}{2Ek}\sin[2(ka+\eta)] + \frac{1}{2aE(E+m)}\{1-\cos[2(ka+\eta)]\},$$

which in the limit $k \to 0$ reduces to the Wigner non-relativistic inequality for s-waves.

b) $\kappa = 1, \quad l = 1, \quad j = \frac{1}{2}$

With the free wave functions

$$F_\alpha = F_\beta^* = \sqrt{E-m}\{-\sin kr - i\cos kr\},$$

$$G_\alpha = G_\beta^* = \sqrt{E+m}\left\{\cos kr - \frac{\sin kr}{kr} - i\left(\frac{\cos kr}{kr} + \sin kr\right)\right\},$$

eq. (9) reads

$$\frac{d\eta}{dk} \geqq -a + \frac{E+m}{2aEk^2}\{1-\cos[2(ka+\eta)]\} - \frac{m}{2Ek}\sin[2(ka+\eta)].$$

As $k \to 0$ this tends to the non-relativistic inequality for p-waves.

3. Scattering of Spin Zero Particles

If the potentials are central, the radial part R of the wave function of angular momentum l and energy E obeys the Klein-Gordon equation

$$\left[-\frac{1}{r^2}\frac{d}{dr}\left(r^2\frac{d}{dr}\right) + \frac{l(l+1)}{r^2}\right] R = [(E-V)^2 - m^2 + U]R.$$

The corresponding equation for $\varphi = rR$ is

$$-\varphi''(E,r) + \frac{l(l+1)}{r^2}\varphi(E,r) = [k^2 - 2EV + V^2 + U]\varphi(E,r)$$

where $E = \sqrt{k^2+m^2}$. As before we consider two solutions $\varphi(E_1, r)$ and $\varphi(E_2, r)$ corresponding to the energies E_1 and E_2 and to the same angular momentum and with the same technique we obtain the equation

$$\frac{d}{dr}\{\varphi^{*\prime}(E_2,r)\varphi(E_1,r) - \varphi'(E_1,r)\varphi^*(E_2,r)\}$$
$$= [k_1^2 - k_2^2 - 2V(E_2-E_1)]\varphi^*(E_2,r)\varphi(E_1,r).$$

Integrating over r from 0 to a we have

$$\int_0^a \left[1 - \frac{2V(E_1-E_2)}{k_1^2-k_2^2}\right]\varphi^*(E_2,r)\varphi(E_1,r)\,dr$$
$$= \frac{1}{k_1^2-k_2^2}[\varphi^{*\prime}(E_2,r)\varphi(E_1,r) - \varphi'(E_1,r)\varphi^*(E_2,r)]_{r=0}^{r=a}. \quad (10)$$

If the potentials are such that $\lim_{r\to 0} rV = 0$ and $\lim_{r\to 0} r^2 U = 0$ eq. (10) gives in the limit $k_1 \to k_2$

$$\int_0^a \left(1 - \frac{V}{E}\right) \varphi^*(E_1, r)\varphi(E_1, r)\mathrm{d}r$$

$$= -\frac{1}{2k}\left(\varphi(E_1, r)\frac{\partial^2 \varphi^*(E_1, r)}{\partial k \partial r} - \frac{\partial \varphi(E_1, r)}{\partial r}\frac{\partial \varphi^*(E_1, r)}{\partial k}\right)_{r=a}.$$

The right hand side is identical with its non-relativistic counterpart. The left hand side is certainly greater than zero if $V < E$. In such a case the non-relativistic inequalities

$$\frac{\mathrm{d}\eta}{\mathrm{d}k} \geqq \frac{1}{4k}\left[(\alpha + \beta \mathrm{e}^{2i\eta})\left(\frac{\partial^2 \alpha^*}{\partial r\, \partial k} + \frac{\partial^2 \beta^*}{\partial r\, \partial k}\mathrm{e}^{-2i\eta}\right)\right.$$

$$\left. - \left(\frac{\partial \alpha}{\partial r} + \frac{\partial \beta}{\partial r}\mathrm{e}^{2i\eta}\right)\left(\frac{\partial \alpha^*}{\partial k} + \frac{\partial \beta^*}{\partial k}\mathrm{e}^{-2i\eta}\right)\right]_{r=a}$$

with

$$\alpha = F(k, r) = \frac{1}{i^{l+1}}\sqrt{\tfrac{1}{2}\pi k r}\, H^{(2)}_{l+\frac{1}{2}}(kr) \quad \text{and} \quad \beta = (-1)^{l+1} F(-k, r)$$

are valid also for relativistic scattering of spin zero particles.

The author is indebted to Prof. L. A. Radicati for his interest in this work, which has been suggested and supervised by Dr. E. Corinaldesi.

References

1) E. P. Wigner, Phys. Rev. **98** (1955) 145
2) E. Corinaldesi and S. Zienau, Proc. Camb. Phil. Soc. **52** (1956) 599
3) H. A. Bethe, Handb. der Physik **24/1** (1933) 312

6.A:7.C *Nuclear Physics* **14** (1959/60) 238—242; © *North-Holland Publishing Co., Amsterdam*
Not to be reproduced by photoprint or microfilm without written permission from the publisher

COUPLED ERRORS ON SCATTERING PHASE SHIFTS

DOUGLAS MILLER
Cyclotron Laboratory, Harvard University, Cambridge, Mass. †

Received 25 August 1959

Abstract: During a least squares analysis of scattering data, a hypothetical energy dependence for the phase shifts often reduces the errors considerably. The mechanism of this error reduction becomes explicit only when the grid method of searching for a best fit is employed. Our illustration is drawn from low energy counter measurements on the pion nucleon system.

1. Introduction

When the interaction region is well-defined, the scattering phase shifts at low energies may be expected to vary with the $(2L+1)$ st power of the barycentric momentum [1]). This energy dependence is extremely fruitful for analyzing pion-nucleon scattering [2]). In particular, the errors on the phase shifts (originally obtained from data at one energy) are reduced remarkably by subjecting the analysis to the familiar energy dependence and including data at another energy. But these reduced errors now rely heavily on the energy dependence suggested by theory.

TABLE 1
Data selected for the $T = \frac{3}{2}$ analysis

Incident energy (MeV)	Scattering angle	Differential cross-section (mb/sr)	Standard deviation (mb/sr)
41.5	53.0°	0.252	0.020
	69.1	0.360	0.025
	100.4	0.777	0.038
	128.0	1.145	0.067
	141.7	1.495	0.084
	163.5	1.750	0.106
24.8	66.0°	0.286	0.028
	92.0	0.458	0.042
	163.5	0.993	0.122

† This work was partially supported by the joint program of the U. S. Office of Naval Research and the U. S. Atomic Energy Commission.

Several questions arise in a natural fashion.

1) What types of errors were removed by analyzing data at more than one energy?

2) With what accuracy can it be stated that the data failed to disprove the hypothetical energy dependence?

3) Can some portion of this increased precision be traced to the added data, or must it be regarded as due entirely to the assumed energy dependence?

4) Does the error situation suggest design criteria for new experiments?

We have found that the grid method of searching illuminates these questions. In order to illustrate the method, we selected data on the process $\pi^+ + p \to \pi^+ + p$: the very accurate data at 41.5 MeV [3]) and the lowest energy counter data at 24.8 MeV [4]). These data are displayed in table 1.

2. The Method of Study

In order to provide a criterion for fit, we calculated the fitting parameter [5])

$$\chi^2 = \sum_{i=1}^{N} \frac{1}{\Delta_i^2} [E_i - D_i]^2.$$

Here $E_i(\theta)$ denotes an experimental value of the differential cross-section and $\Delta_i(\theta)$ denotes its standard deviation; $D_i(\theta)$ represents a value for the same differential cross-section calculated from a set of phase shifts which we wish to compare with the data. Note that the sum runs over N measurements in which the errors are independent and statistical.

The grid method recommends itself for this problem because the computing machine can work with an expression for the differential cross-section which is concise:

$$D(\theta) = \lambda\!\!\!^{-2} \left\{ \left| \frac{-n}{1-\omega} + a_3\eta + (2a_{33} + a_{31})\eta^3\omega \right|^2 + (a_{33} - a_{31})^2 \eta^6 (1-\omega^2) \right\};$$

$\lambda\!\!\!^{-}$ represents the reduced wave length and η denotes the relative momentum (in units of $m_\pi c$) in the barycentric system; $\omega \equiv \cos\theta$ and the Coulomb parameter $n = e^2/\hbar v$, where v is the relative velocity of the two particles. In addition, the phase shifts are written in terms of scattering lengths: $a_3 \equiv \alpha_3/\eta$ for the $L = 0$ interaction, as well as $a_{33} \equiv \alpha_{33}/\eta^3$ and $a_{31} \equiv \alpha_{31}/\eta^3$ for the $J = \frac{3}{2}$ and $J = \frac{1}{2}$ P-wave interactions, respectively [2]).

Two approximations were suggested by the low energy. No partial waves above $L = 1$ were admitted. Also, $e^{2i\alpha_i} - 1$ was approximated by $2i\alpha_i$. Our approximate treatment of Coulomb scattering is due to Van Hove [6]). Relativistic improvements contributed by Solmitz [7]) are extremely small.

The Coulomb scattering amplitude was treated in Born approximation. In effect, we neglected the Coulomb interaction inside the range of the nuclear

interaction. As that value of the separation within which the interaction may be approximated as purely nuclear, we selected the Compton wave length of the pion and corrected the scattering lengths to first order in η. The effect of this correction was to isolate the nuclear portion of each scattering length.

Starting with the 41.5 MeV data, we searched the region of the Fermi type solution [8]) in intervals of 0.05 radians in each of the three scattering lengths. In the space whose axes measure a_3, a_{33} and a_{31}, the minimum of χ^2 locates our best fit and corresponds to the set $\hat{a}_3$, $\hat{a}_{33}$, $\hat{a}_{31}$. Nearby we find ellipsoidal contours for χ^2 corresponding to $\chi^2_{\min}+1$, $\chi^2_{\min}+2$, $\chi^2_{\min}+3$, etc. Since $\chi^2-\chi^2_{\min}$ depends quadratically on the deviations $d_1 \equiv a_3-\hat{a}_3$, $d_2 \equiv a_{33}-\hat{a}_{33}$ and $d_3 \equiv a_{31}-\hat{a}_{31}$, we define the G matrix by $\chi^2-\chi^2_{\min} = \sum_{i,j=1}^{3} G_{ij}d_i d_j$. [9])

Elements of the G matrix were found by graphical means from the grid. The reciprocal of the G matrix is the moment matrix [10]) Diagonal elements of the moment matrix provide the variances in a_3, a_{33} and a_{31} and off-diagonal elements reveal the correlation between the errors on two scattering lengths.

3. Discussion of the Results

Our analysis of the 41.5 MeV data yielded the phase shifts $\alpha_3 = -(0.098 \pm 0.013)\eta$ $\alpha_{33} = (0.237 \pm 0.016)\eta^3$ $\alpha_{31} = -(0.054 \pm 0.007)\eta^3$. For six independent pieces of data and three parameters, the most likely value of $\chi^2_{\min}$ is three [10]). Our result is $\chi^2_{\min} = 2.50$.

The error on a_{31} is small enough to be noteworthy. This small uncertainty can be traced to the fact that a_{31} is only weakly coupled to the other scattering lengths. However, the errors on a_3 and a_{33} are significantly larger. Strong coupling between these scattering lengths increased the uncertainty of both a_3 and a_{33}. The grid method of searching affords a picture of this coupling. In fig. 1 we project the $\chi^2_{\min}+1$ ellipsoid on the $a_{31} = -0.054$ plane. If either scattering length is changed, the corresponding change which must be made in the other scattering length is well determined by the correlation.

At 41.5 MeV, the a_{31} correlations were broken down by measuring the cross-section at a number of angles. The persistence of the strong correlation between a_3 and a_{33} can be traced to the theoretical expression for the cross-section in terms of phase shifts.

In the effort to break down this strong correlation between a_3 and a_{33}, the 24.8 MeV counter measurements are helpful. The decrease in energy from 41.5 MeV causes α_{33} to become smaller than α_3. Moreover, the three angles at 24.8 MeV were selected in order to focus the measurement on α_3. The angle of 66° is that at which the cross-section is most sensitive to the value of α_3 because of the strong interference between Coulomb and nuclear scattering. A 90° measurement isolates the $L = 0$ interference from the $L = 1$ interference. The 163° measurement depends only on the scattering amplitude without spin flip.

The 24.8 MeV data suggested a similar analysis. The decrease in energy improved the knowledge of a_3 at the expense of a_{33} and a_{31}. This can be seen in fig. 1 where the correlation between a_3 and a_{33} for the 24.8 MeV data is displayed. Notice how the difference in energy tilts one ellipse with respect to the other.

Data at these two energies can be related only if some hypothesis is made about the energy dependence of the phase shifts. We have tested the aforementioned hypothesis by performing the χ^2 sum over all measurements at the

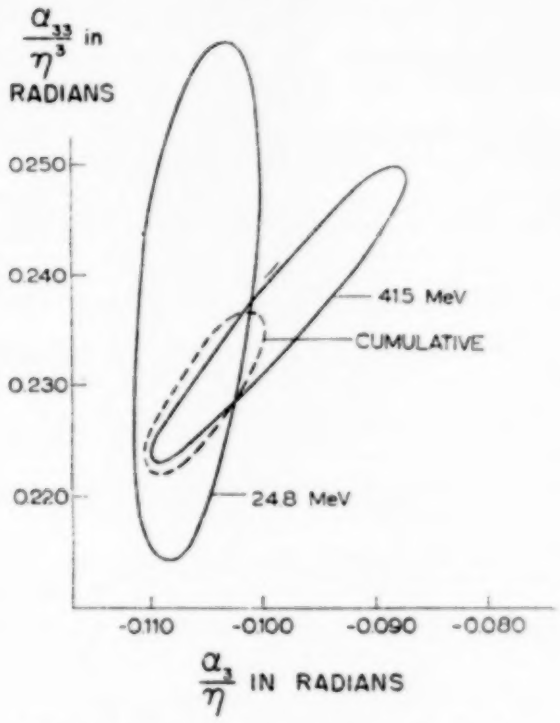

Fig. 1. The correlation between a_3 and a_{33}.

two energies. As the three new pieces of data were added (we now have 9 pieces of data and 3 parameters), $\chi^2_{\min}$ increased from 2.50 to 3.20. A comparison of this increase with the statistical expectation [10]) shows that all the data are consistent with the hypothesis.

Some correlation between a_3 and a_{33} still exists. In fig. 1, the dotted ellipse for the cumulative analysis affords a picture of the extent of this correlation. The ellipse is not small because the area common to the two $\chi^2_{\min}+1$ ellipses is small. Rather it is small because the width of the 41.5 MeV ellipse limits its vertical extent and the width of the 24.8 MeV ellipse limits its horizontal extent. Our cumulative ellipse would possess the same size and shape no matter whether the overlap were large or small. The degree of overlap affects only $\chi^2_{\min}$. For this reason, it measures the validity of the energy dependence hypothesis and does not affect the errors on the scattering lengths.

The error analysis for all the 41.5 MeV and 24.8 MeV data on positive pions

resulted in the values

$$\alpha_3 = -(0.106 \pm 0.006)\eta, \quad \alpha_{33} = (0.229 \pm 0.008)\eta^3, \quad \alpha_{31} = -(0.054 \pm 0.008)\eta^3.$$

The errors depend on the energy dependence hypothesis. However, the errors on these $T = \frac{3}{2}$ phase shifts do not rely on the validity of charge independence. Rather they are available to contribute to a quantitative statement of the accuracy of the charge independence hypothesis [11]).

References

1) L. I. Schiff, Quantum Mechanics (McGraw-Hill, New York, 1949)
2) Jay Orear, Phys. Rev. **96** (1954) 176
3) S. W. Barnes, B. Rose *et al.* Proceedings of Seventh Rochester Conference (1957)
4) D. Miller and J. Ring, Ph. D. Theses, Univ. of Rochester (1958)
5) E. Fermi and N. Metropolis, Los Alamos Report 1492 (1952)
6) L. Van Hove, Phys. Rev. **88** (1952) 1358
7) F. J. Solmitz, Phys. Rev. **98** (1954) 1799
8) H. A. Bethe and F. de Hoffmann, Mesons and Fields, vol. II (Row, Peterson and Co., White Plains, N. Y. 1955)
9) H. L. Anderson, W. C. Davidon, M. Glicksman and U. E. Kruse, Phys. Rev. **100** (1955) 279
10) Harald Cramer, Mathematical Methods of Statistics (Almquist and Wiksell, Uppsala, 1954)
11) A. Stanghellini, Nuovo Cimento **10** (1958) 398

1.E.4:
2.C:3.A

Nuclear Physics **14** (1959/60) 243—247; © *North-Holland Publishing Co., Amsterdam*
Not to be reproduced by photoprint or microfilm without written permission from the publisher

LIFETIME OF THE 3.56-MeV STATE OF Li^6

LESLIE COHEN and RALPH A. TOBIN

Nucleonics Division, United States Naval Research Laboratory, Washington 25, D. C.

Received 10 August 1959

Abstract: The bremsstrahlung beam from the U. S. Naval Research Laboratory 25-MeV betatron was used to excite the 3.56-MeV state in Li^6. The gamma radiation resulting from the de-excitation of these nuclei was observed with and without a Li^6 absorber inserted in the primary beam. Assuming a spin assignment $J = 0$ for the excited state, and using a calculated Doppler with of 11.3 eV for enriched lithium metal, an analysis of the data yields a mean lifetime of $(7.2^{+1.3}_{-1.3}) \times 10^{-17}$ sec.

1. Introduction

The present study is part of the continuing program of nuclear resonance fluorescence initiated in the Betatron Section at the U. S. Naval Research Laboratory. Excited states of nuclei are produced by irradiating scatterers containing the nuclei with the X-rays from the betatron. The gamma rays accompanying the de-excitation of these states are then observed, and measurements are made from which resonance parameters of these states can be determined. The 3.56-MeV state of Li^6 has been produced and studied in this manner. A preliminary report of this work was made at the 1959 meeting of the American Physical Society in Cambridge, Massachusetts [1]).

2. Experimental Procedure

The experimental arrangement was essentially the same as that described in a previous article [2]). The X-ray beam was collimated to a 4-in. diameter at the scatterer position. The shielded NaI(Tl) detector (4-in. diam × 4 in.) was placed at an angle of about 130° to the beam. A gated 20-channel pulse-height analyzer was used to examine the pulse-height spectrum from the crystal-phototube-amplifier system. In the initial phase of this work, a natural-lithium target was used. It was found that the betatron could be operated to energies as high as 6.5 MeV with no noticeable neutron background. This energy was therefore used. An analysis of the scattered beam showed a gamma ray with an energy of about 3.5 MeV as the sole nuclear radiation. This radiation was observed at all betatron energies above 3.5 MeV. Because this energy is close to that of the second excited state of Li^6, metallic lithium enriched to 96 % Li^6

was obtained. With the aid of a hydraulic press, two uniformly thick discs were formed. The scatterer is 6 in. in diameter and 0.347 g/cm² thick; the absorber, 3 in. and 0.314 g/cm². As expected, the yield from the enriched scatterer was greatly enhanced. A histogram of the pulse-height distribution is shown in fig. 1; the distribution for the 4.43-MeV gamma ray from a polonium-beryllium source is given for comparison.

With the system of Li^6 scatterer and NaI(Tl) scintillator acting as a detector of 3.56-MeV photons in the bremsstrahlung beam, the second disc of Li^6 (the absorber) was placed in the primary beam. Twenty-five pairs of 15-minute

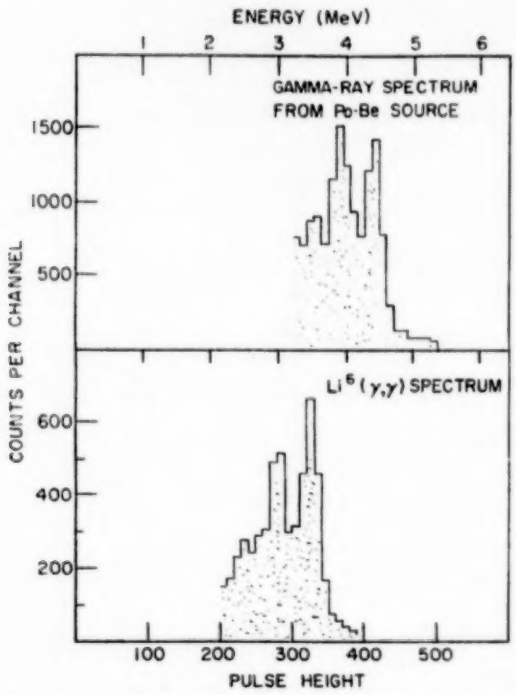

Fig. 1. The pulse-height distribution from the NaI crystal of the gamma rays scattered by Li^6 metal. The pulse-height distribution of the 4.43-MeV gamma ray is given by the histogram on top for energy calibration.

runs were made this way, i.e., with the absorber alternately in and out of the primary beam. From these measurements and from background measurements with no scatterer, the transmission of 3.56-MeV radiation through the absorber was determined to be 0.626 ± 0.018.

3. Analysis of the Data

The transmission that is measured in this experiment is a function of many variables: the resonance parameters of the nuclear state that is observed; the cross sections for the various electronic processes at the resonant energy; and the composition of scatterer and absorber. The cross section for the resonance absorption of gamma rays by a stationary nucleus is given by the single-level

Breit-Wigner formula. However, this formula must be modified to take into account the thermal motion of the nuclei in the material used. The resultant Doppler-broadened nuclear resonance cross section is expressed by [3])

$$\sigma_n(E) = \sigma_0 \psi(\xi, x)$$

where σ_0 is the peak cross section obtained from the Breit-Wigner formula; ξ is the ratio of natural width Γ to Doppler width Δ; x is the energy off of resonance in units of half-widths, i.e., $x = (E-E_0)/\frac{1}{2}\Gamma$, and $\psi(\xi, x)$ is a tabulated function [4]). Using these definitions, the expression for the transmission is

$$\frac{\int \frac{\sigma_n(E)}{\sigma_n(E)+2\sigma'_e} e^{-[\sigma_n(E)+\sigma'_e]N\tau} \left[1-\exp\left(-[\sigma_n(E)+2\sigma'_e]\frac{Nt}{\cos\alpha}\right)\right] dE}{\int \frac{\sigma_n(E)}{\sigma_n(E)+2\sigma'_e} \left[1-\exp\left(-[\sigma_n(E)+2\sigma'_e]\frac{Nt}{\cos\alpha}\right)\right] dE}$$

In this expression, $N\tau$ and Nt are the numbers of Li^6 nuclei per cm^2 in absorber and scatterer, respectively; the angle α is the angle of both incidence and scattering; and σ'_e is the total electronic absorption cross-section of a lithium atom at 3.56 MeV divided by the fraction of atoms that is Li^6. These numbers are readily calculated, leaving the transmission a function of only two parameters, σ_0 and ξ. In principle, if one is known, the other is determined by a transmission measurement. In this case, σ_0 is assumed to be known from what follows.

From the Breit-Wigner formula, σ_0 is given by the expression

$$\sigma_0 = 4\pi\lambda^2 \frac{2J+1}{2(2I+1)} \frac{\Gamma_\gamma}{\Gamma},$$

where J and I are the spins of the excited state and ground state, respectively, and Γ_γ/Γ is the branching ratio for the decay of the state by an electromagnetic transition to the ground state. No stop-over radiation to the first excited state has been observed; and, since the state does not break up into He^4+d, which is energetically possible, the branching ratio is assumed to be unity [5]). The ground state is known to have spin $I = 1$. Knowledge of the spin of the excited state would therefore determine the value of σ_0. The 3.56-MeV level of Li^6 has been studied by many workers. Mackin [6]) observed the $Be^9(p, \alpha)Li^{6*}(\gamma)Li^6$ reaction. He found the internal pair spectrum to be consistent only with an M1 or E2 assignment to the gamma transition, thus establishing the even parity of the state. The upper limits for the lifetime obtained from Doppler shift measurements [7]) are consistent with M1 radiation but not E2, establishing the state as 0^+, 1^+, or 2^+. The fact that the state does not break up into He^4+d is attributable to an assignment of $J = 0^+$, or $T = 1$, or both. The inability to excite this state by the inelastic scattering of deuterons [8]) indicates that $T = 1$.

From this probable $T = 1$ assignment and from energy considerations, the state is most probably the analogue of the ground state of He^6 which has $J = 0^+$. In addition, the (p, γ) and the (p, $\alpha\gamma$) angular correlations in the reaction $Be^9(p, \alpha)Li^{6*}(\gamma)Li^6$ have been observed [9]) and both have been found to be isotropic. These results are also consistent with a spin assignment of $J = 0$ to the 3.56-MeV state. It is therefore assumed that $J = 0$ for the second excited state of Li^6. Using this value, σ_0 is calculated to be 64.3 b.

The expression for the transmission, a function of ξ only, has been evaluated by numerical integration for several values of ξ. The results are plotted as the

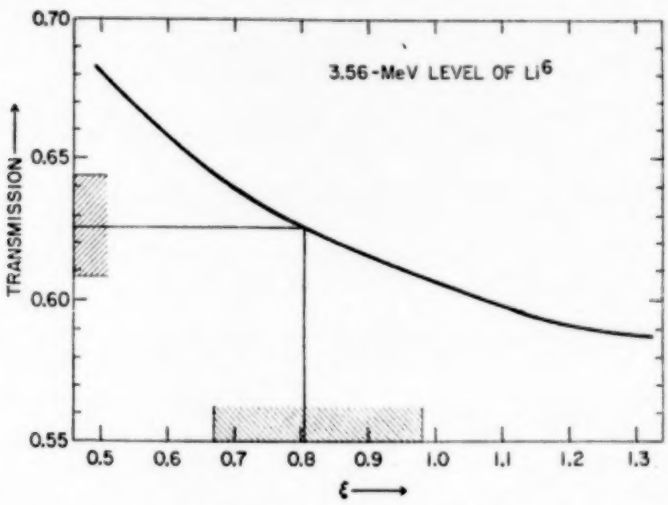

Fig. 2. The transmission as a function of ξ. The uncertainties are indicated by the shading.

solid curve in fig. 2. The observed transmission and associated uncertainties are indicated by the shading on the ordinate. The corresponding values of ξ, as indicated by the shading on the abscissa, are $\xi = 0.80^{+0.18}_{-0.13}$. To obtain Γ, we must know Δ, since $\xi = \Gamma/\Delta$. The Doppler width is given by

$$\Delta = \sqrt{\frac{2E_0^2 kT_{eff}}{Mc^2}}$$

where k is the Boltzmann constant and M is the mass of the target nucleus. The effective temperature is given by [10])

$$T_{eff} = T\left[3(T/\theta)^3 \int_0^{\theta/T} t^3 \left(\frac{1}{e^t - 1}\right) dt\right]$$

where T is the room temperature and θ is the Debye temperature for the scatterer and absorber material. This expression can be simplified to

$$T_{eff} = T\left[\frac{C_V(\theta/T)}{24} + \frac{3\theta/T}{4[e^{(\theta/T)} - 1]} + \frac{3\theta/T}{8}\right]$$

where $C_V(\theta/T)$ is the specific heat in calories per mole at the absolute temperature T. The measured Debye temperature for natural-lithium metal [11]) is 430°. If this value is corrected for the square roots of the effective masses in natural lithium and in the enriched lithium, one obtains 461° as the Debye temperature for the enriched material. This correction makes a change of less than 1 % in the Doppler width. The corrected value is 11.3 eV. Using this value, one then obtains $\Gamma = (9.1^{+2.0}_{-1.5})$ eV, or the mean lifetime $\tau = \hbar/\Gamma$ is $(7.2^{+1.5}_{-1.3}) \times 10^{-17}$ sec.

Kurath [12]) has made calculations with intermediate coupling wave functions and has found that the width is quite insensitive to the strength of the spin-orbit coupling. For the M1 transition, he obtained a value of 8.35 eV at the LS limit, 8.7 eV in the region where the energy spectrum matches the experimental one, and 8.8 eV for as large a spin-orbit coupling as is reasonable at the upper end of the 1p shell. Experimental and theoretical work are thus in agreement.

References

1) Leslie Cohen and Ralph Tobin, Bull. Am. Phys. Soc. **4** (1959) 151
2) L. Cohen, R. A. Tobin and J. McElhinney, Phys. Rev. **114** (1959) 590
3) H. A. Bethe, Revs. Mod. Phys. **9** (1937) 71
4) Rose, Miranker, Leak, Rosenthal and Hendrickson, Westinghouse Atomic Power Division (Pittsburgh, Pa.) Report SR-506, Vols. I and II (October 1954)
5) F. Ajzenberg and T. Lauritsen, Revs. Mod. Phys. **27** (1955) 77
6) R. J. Mackin, Phys. Rev. **94** (1954) 648
7) H. J. Rose and E. K. Warburton, Phil. Mag. Ser. 8 **2** (1957) 1468;
   R. A. J. Levesque and S. M. Shafroth, Phys. Rev. Letters **2** (1959) 485
8) C. P. Browne and C. K. Bockelman, Phys. Rev. **105** (1957) 1301
9) J. Stoltzfus, J. Friichtenicht and E. B. Nelson, Bull. Am. Phys. Soc. **1** (1956) 329
10) W. E. Lamb, Phys. Rev. **55** (1939) 190
11) M. Blackman in Handbuch der Physik, Vol. **7**, Part 1 (Springer-Verlag, 1955) pp. 325–382
12) D. Kurath, private communication

1.E.3:
1.E.5

Nuclear Physics **14** (1959/60) 248—255; © *North-Holland Publishing Co., Amsterdam*
Not to be reproduced by photoprint or microfilm without written permission from the publisher

ISOTOPE SHIFT FROM NON-UNIFORM NUCLEAR CHARGE DISTRIBUTIONS

A. S. MELIGY

Faculty of Science, University of Alexandria, Egypt

Received 7 August 1959

Abstract: The isotope shift is derived by solving Dirac's equations for an electron in the static field of a nuclear charge distribution of trapezoidal shape. The values of the parameters identifying this distribution are obtained from the analysis of the electron-nucleus scattering experiments. The magnitude of the derived isotope shift is found to be very nearly half the value previously predicted by a uniformly charged nucleus with radius $1.5\times10^{-13}A^{\frac{1}{3}}$ cm. Remarkable agreement is thus achieved between the isotope shift predicted by the present theory and the experimental results.

1. Introduction

The theory of isotope shift has been recently reviewed by Breit [1]). On the usual assumption of uniform nuclear charge distribution with radius $1.5\times10^{-13}A^{\frac{1}{3}}$ cm Crawford and Schawlow [2]) found that the predicted isotope shift is about twice the observed magnitude. Brix and Kopfermann [3]) and Humbach [4]) have reached the same conclusion. Wilets, Hill and Ford [5]) tried to minimize this discrepancy by assuming the compressibility of nuclear matter.

The usual way of evaluating the isotope shift is by means of the perturbation method using the electron wave function for a point nucleus. The results predicted by such calculations require corrections for the distortion of the wave function by the extended nuclear charge distribution. A derivation of the isotope shift which avoids perturbation theory and at same time takes account of the wave function distortion has been reported by Bodmer [6]).

In the present work the above mentioned isotope shift discrepancy is carefully treated by taking into account the detailed shape of the nuclear charge distribution as obtained from the analysis of electron-nucleus scattering experiments. The derivation of the isotope shift is made by solving Dirac's equations for an electron in the field of an extended nucleus.

2. The Electron-Nucleus Potential

The Stanford electron scattering experiments have demonstrated clearly the non-uniformity of nuclear charge distributions [7]). For heavy nuclei, the charge

density has been described by three different functional forms which fit the scattering data equally well. For mathematical convenience, we take for the charge density, the trapezoidal shape defined by [8])

$$\begin{aligned} \rho(r) &= \rho(0), && 0 < r < c-z, \\ &= \rho(0)(c+z-r)/2z, && c-z < r < c+z, \\ &= 0, && r > c+z, \end{aligned} \tag{1}$$

where c is the half-way density radius, $t = 1.60z$ is the surface thickness and $\rho(0)$ is the central charge density given by

$$\rho(0) = \frac{3Ze}{4\pi c^3}\left[1+\frac{z^2}{c^2}\right]^{-1}. \tag{2}$$

In terms of this shape of the charge density, the analysis of scattering experiments give the values

$$\begin{aligned} c &= 1.05\times 10^{-13} A^{\frac{1}{3}} \text{ cm} \\ z &= 1.53\times 10^{-13} \text{ cm}. \end{aligned} \tag{3}$$

These values have been obtained from those determined by the Fermi shape by multiplying the latter by the appropriate converting factors.

The electron potential energy in the static field of the charge distribution (1) is given by

$$\begin{aligned} V^{(1)} &= -\frac{2\pi}{3} e\rho(0) c^2 \left[3+\frac{z^2}{c^2}-\frac{r^2}{c^2}\right], && 0 < r < c-z, \\ V^{(2)} &= -\frac{\pi e}{6z}\rho(0)\left[r^3-2(c+z)r^2-\frac{(c-z)^4}{r}+2(c+z)^3\right], && c-z < r < c+z, \\ V^{(3)} &= -Ze^2/r, && r > c+z. \end{aligned} \tag{4}$$

3. The Electron Wave Functions

On Dirac's theory, an electron moving in a central field with potential energy V has radial wave functions f/r and g/r satisfying the equations

$$\begin{aligned} (E+m_0c^2-V)f - c\hbar\left(\frac{\mathrm{d}}{\mathrm{d}r}+\frac{j}{r}\right)g = 0, \\ (E-m_0c^2-V)g + c\hbar\left(\frac{\mathrm{d}}{\mathrm{d}r}-\frac{j}{r}\right)f = 0, \end{aligned} \tag{5}$$

where j is a quantum number of eigenvalues $-1, +1, -2, +2, \ldots$ corresponding to the s, $p_{\frac{1}{2}}$, $p_{\frac{3}{2}}$, $d_{\frac{3}{2}}, \ldots$ states respectively. The solutions of these equations for the three parts of the potential function (4) are derived in the following.

3.1. INSIDE THE NUCLEUS

In the whole of the nuclear domain, $0 < r < c+z$, a satisfactory approximation of the expansions representing the wave functions is obtained by neglecting powers of Zc/a_H (a_H being the Bohr radius for hydrogen) which is negligibly small. This approximation can be effected by putting $E = m_0c^2 = 0$ in eqs. (5). The equations for f and g, for the state $j = -1$, then are

$$\begin{aligned} \frac{dg}{dr} - \frac{g}{r} + \frac{V}{c\hbar} f = 0, \\ \frac{df}{dr} + \frac{f}{r} - \frac{V}{c\hbar} g = 0. \end{aligned} \tag{6}$$

Only the case $j = -1$ is considered because the principal effects of nuclear structure appear in the energy levels of the s electrons.

On solving eqs. (6) for the first part $V^{(1)}$ of the potential function and neglecting powers of α^2 (α being the fine structure constant) we obtain the following regular solutions for $0 < r < c-z$

$$\begin{aligned} f^{(1)}(r) &= -\frac{\varepsilon}{2c}\left(1+\frac{z^2}{c^2}\right)^{-1} r^2\left[1+\frac{z^2}{3c^2}-\frac{r^2}{5c^2}\right], \\ g^{(1)}(r) &= r, \end{aligned} \tag{7}$$

where

$$\varepsilon = Z\alpha \tag{8}$$

In solving eqs. (6) for the second part $V^{(2)}$ of the potential function, one first makes the substitution

$$r = c-z+x. \tag{9}$$

Then assuming the power series solutions

$$f = \sum_{n=0}^{\infty} a_n x^{n+\lambda}, \quad g = \sum_{n=0}^{\infty} b_n x^{n+\lambda}$$

it is found that $\lambda = 0$, and it follows from the continuity of both f and g at $r = c-z$ or $x = 0$, that $a_0 = f^{(1)}(c-z)$, $b_0 = g^{(1)}(c-z)$. Thus we obtain the following solutions for $c-z < r < c+z$.

$$\begin{aligned} f^{(2)}(r) &= -\tfrac{2}{5}\varepsilon c\left(1+\frac{z^2}{c^2}\right)^{-1}\left[1-\tfrac{3}{2}\frac{z}{c}+\tfrac{1}{6}\frac{z^2}{c^2}+\tfrac{1}{6}\frac{z^3}{c^3}+\tfrac{1}{6}\frac{z^4}{c^4}\right. \\ &\quad +\left(1+\tfrac{1}{3}\frac{z}{c}-\tfrac{13}{9}\frac{z^2}{c^2}+\tfrac{1}{9}\frac{z^3}{c^3}\right)\frac{3x}{2c}-\left(1-12\frac{z}{c}+\tfrac{13}{3}\frac{z^2}{c^2}\right)\frac{x^2}{4c^2} \\ &\quad \left.-\left(1-\frac{z}{c}\right)\frac{x^3}{c^3}+\left(1-\tfrac{13}{5}\frac{z}{c}\right)\frac{5x^4}{32zc^3}+\frac{x^5}{32zc^4}+\frac{(c-z+x)^{-1}x^6}{48zc^4}\right], \\ g^{(2)}(r) &= r, \end{aligned} \tag{10}$$

where x is given by (9). At $r = c+z$ the following ratio is given by

$$K = f^{(2)}(c+z)/g^2(c+z)$$
$$= -\tfrac{2}{5}\varepsilon\left(1+\frac{z^2}{c^2}\right)^{-1}\left(1+\frac{z}{c}\right)^{-1}\left[1+\tfrac{3}{2}\frac{z}{c}+\tfrac{1}{6}\frac{z^2}{c^2}+\frac{z^3}{c^3}\left(\tfrac{7}{3}+\frac{z}{c}\right)\left(1+\frac{z}{c}\right)^{-1}\right]. \quad (11)$$

3.2. OUTSIDE THE NUCLEUS

For the electron outside the nucleus we substitute in eqs. (5), $V = -Ze^2/r$ and then put

$$E = m_0c^2\left(1+\frac{\varepsilon^2}{k^2}\right)^{-\frac{1}{2}}, \quad \zeta = \frac{2Zr}{a_H\sqrt{k^2+\varepsilon^2}}. \quad (12)$$

By solving the resulting equations in power series near $\zeta = 0$, we find a pair of regular solutions which, apart from a common multiplicative constant, can be expressed as follows

$$f_\sigma = \varepsilon[(\mu-\sigma-j)I_{k,\sigma-\frac{1}{2}}(\zeta)+(\mu+\sigma-j)(k-\sigma)I_{k,\sigma+\frac{1}{2}}(\zeta)]$$
$$g_\sigma = \mu[(\nu-\sigma+j)I_{k,\sigma-\frac{1}{2}}(\zeta)+(\nu+\sigma+j)(k-\sigma)I_{k,\sigma+\frac{1}{2}}(\zeta)], \quad (13)$$

and an irregular pair of solutions which, apart from another common factor, is represented by the functions $f_{-\sigma}$, $g_{-\sigma}$ where

$$\mu = k+\sqrt{k^2+\varepsilon^2}, \quad \nu = k-\sqrt{k^2+\varepsilon^2}, \quad \sigma = \sqrt{j^2-\varepsilon^2} \quad (14)$$

and $I_{k,m}(\zeta)$ is the confluent hypergeometric function [9]).

Now, if the law $1/r$ for the potential holds down to $r = 0$, only the regular functions f_σ, g_σ would be needed and they should be conditioned by $k = \sigma$, $\sigma+1, \ldots$ in order that they remain finite at infinity. However, the law of potential changes inside the nucleus and the values of $k-\sigma$ will no longer be integral. In this case, the above solutions, regular or irregular, will tend to infinity as $\zeta \to \infty$. But, since for an atomic electron the wave functions should tend to zero as $\zeta \to \infty$, one has to construct solutions satisfying this requirement. This is achieved when the above regular functions f_σ, g_σ and irregular functions $f_{-\sigma}$, $g_{-\sigma}$ are combined in the following way

$$f^{(3)} = \frac{1}{\sin 2\pi\sigma}[\Gamma(k+\sigma+1)\sin\pi(k+\sigma)f_\sigma+\Gamma(k-\sigma+1)\sin\pi(k-\sigma)f_{-\sigma}]$$

$$g^{(3)} = \frac{1}{\sin 2\pi\sigma}[\Gamma(k+\sigma+1)\sin\pi(k+\sigma)g_\sigma+\Gamma(k-\sigma+1)\sin\pi(k-\sigma)g_{-\sigma}].$$

These functions can be expressed in terms of Whittaker's function [9]) $W_{k,m}(\zeta)$ as follows

$$f^{(3)} = \varepsilon[(\mu-\sigma-j)(k+\sigma)W_{k,\sigma-\frac{1}{2}}(\zeta)-(\mu+\sigma-j)(k-\sigma)W_{k,\sigma+\frac{1}{2}}(\zeta)]$$
$$g^{(3)} = \mu[(\nu-\sigma+j)(k+\sigma)W_{k,\sigma-\frac{1}{2}}(\zeta)-(\nu+\sigma+j)(k-\sigma)W_{k,\sigma+\frac{1}{2}}(\zeta)]. \quad (15)$$

When ζ is real, the function $W_{k,m}(\zeta) \to 0$ as $\zeta \to \infty$. It follows that $f^{(3)}$ and $g^{(3)}$ represent the appropriate wave functions of the electron in the pure Coulomb field outside the nucleus.

4. The Energy Displacement

In order to determine the effect of the finite nuclear size on the electronic energy levels, that is the energy displacement, one has first to obtain the corresponding effect on the quantum number k. This is obtained by satisfying, at $r = c+z$, the continuity condition

$$f^{(3)}|g^{(3)} = f^{(2)}|g^{(2)}. \tag{16}$$

Since at the nuclear boundary, ζ is small it is quite adequate to retain only the lowest power of ζ in each series involved in the expansions of the functions $f^{(3)}$ and $g^{(3)}$.

Now, the function $W_{k,m}(\zeta)$ can be represented as follows [9]);

$$W_{k,m}(\zeta) = \Gamma(k+m+\tfrac{1}{2}) \cos \pi(k-m-\tfrac{1}{2}) I_{k,m}(\zeta) + \Gamma(k-m+\tfrac{1}{2}) \sin \pi(k-m-\tfrac{1}{2}) N_{k,m}(\zeta).$$

For small values of ζ

$$I_{k,m}(\zeta) = \zeta^{\frac{1}{2}+m}/\Gamma(2m+1), \quad N_{k,m}(\zeta) = -\frac{1}{\pi}\Gamma(2m)\zeta^{\frac{1}{2}-m}$$

and accordingly

$$W_{k,m}(\zeta) = \frac{\Gamma(\frac{1}{2}+m+k)}{\Gamma(2m+1)} \cos \pi(k-m-\tfrac{1}{2})\zeta^{\frac{1}{2}+m} - \frac{1}{\pi}\Gamma(k-m+\tfrac{1}{2})\Gamma(2m) \sin \pi(k-m-\tfrac{1}{2})\zeta^{\frac{1}{2}-m}.$$

It follows from (15) that the functions $f^{(3)}$ and $g^{(3)}$ near $r = c+z$ can be approximately represented by

$$\begin{aligned} f^{(3)} &= \varepsilon \frac{\Gamma(k+\sigma+1)}{\Gamma(2\sigma)} (\mu-j-\sigma) \cos \pi(k-\sigma)\zeta^{\sigma} - \frac{\varepsilon}{\pi}\Gamma(k-\sigma+1)\Gamma(2\sigma+1)(\mu-j+\sigma) \sin \pi(k-\sigma)\zeta^{-\sigma}, \\ g^{(3)} &= \mu \frac{\Gamma(k+\sigma+1)}{\Gamma(2\sigma)} (\nu+j-\sigma) \cos \pi(k-\sigma)\zeta^{\sigma} - \frac{\mu}{\pi}\Gamma(k-\sigma+1)\Gamma(2\sigma+1)(\nu+j+\sigma) \sin \pi(k-\sigma)\zeta^{-\sigma}. \end{aligned} \tag{17}$$

Substitution of these values in (16) gives

$$\tan \pi(k-\sigma) = \frac{\pi\Gamma(k+\sigma+1)(\mu-j-\sigma)\zeta_0^{2\sigma}(\varepsilon-(j-\sigma)K)}{\Gamma(2\sigma)\Gamma(2\sigma+1)\Gamma(k-\sigma+1)(\mu-j+\sigma)(\varepsilon-(j+\sigma)K)}, \tag{18}$$

where ζ_0 is the value of ζ at $r = c+z$, and $K = f^{(2)}/g^{(2)}$. Notice that in (18), ν is absent since we have replaced the factor

$$(\nu+j+\sigma)/(\nu+j-\sigma) \quad \text{by} \quad (j+\sigma)(\mu-j+\sigma)/(j-\sigma)(\mu-j-\sigma).$$

Solving (18) for k, we obtain

$$k = n-|j|+\sigma + \frac{\Gamma(n-|j|+2\sigma+1)(\mu-j-\sigma)y_0^{2\sigma}(\varepsilon-(j-\sigma)K)}{\Gamma(2\sigma)\Gamma(2\sigma+1)\Gamma(n-|j|+1)\left[(n-|j|+\sigma)^2+\varepsilon^2\right]^{\sigma}(\mu-j+\sigma)(\varepsilon-(j+\sigma)K)}, \quad (19)$$

where

$$y_0 = \frac{2Z}{a_H}(c+z) \quad (20)$$

and μ becomes as

$$\mu = n-|j|+\sigma+\sqrt{(n-|j|+\sigma)^2+\varepsilon^2},$$

n being the principal quantum number. The values of k given by (19) contain the term $n-|j|+\sigma$ which is the eigenvalue of k when the nucleus is considered as a point charge. The additional term must then express the finite nuclear size effect. It follows from (12) that the corresponding energy displacement is

$$\Delta E = \frac{RZ^2\Gamma(n-|j|+2\sigma+1)(\mu-j-\sigma)y_0^{2\sigma}(\varepsilon-(j-\sigma)K)}{\sigma\Gamma^2(2\sigma)\Gamma(n-|j|+1)\left[(n-|j|+\sigma)^2+\varepsilon^2\right]^{\sigma+\frac{1}{2}}(\mu-j+\sigma)(\varepsilon-(j+\sigma)K)}\ \mathrm{cm}^{-1} \quad (21)$$

where R is Rydberg's constant.

The formula (21) is valid for all states and can be generally used for arbitrary charge distributions whose effect appears in the quantity K. For the present model described by eq. (1), with K given by eq. (11), the energy displacement for an s electron is sufficiently accurately represented by

$$(\Delta E)_z = \frac{RZ^2(3-2\sigma)}{\sigma\Gamma^2(2\sigma)n^3(3+2\sigma)}\left(\frac{2Z}{a_H}(c+z)\right)^{2\sigma} \times\left[1-\frac{10\sigma}{(9-4\sigma^2)}\left(\frac{z}{c}\right)\left(1+\frac{z}{c}\right)^{-2}\left(1+\frac{z^2}{c^2}\right)^{-1}\left(1-\frac{2}{3}\frac{z}{c}+\frac{z^2}{c^2}\right)\right]\mathrm{cm}^{-1}, \quad (22)$$

with $\sigma = \sqrt{1-\varepsilon^2}$. The present displacement is written as $(\Delta E)_z$ to emphasize the presence of the surface parameter z and to distinguish it from the displacement $(\Delta E)_0$ predicted by a uniform charge distribution (zero surface thickness) with radius given by the empirical formula

$$a = 1.5\times10^{-13}A^{\frac{1}{3}}\ \mathrm{cm}. \quad (23)$$

The latter displacement is obtained from (22) by putting $z = 0$ and replacing c by a, viz.

$$(\Delta E)_0 = \frac{RZ^2(3-2\sigma)}{\sigma\Gamma^2(2\sigma)n^3(3+2\sigma)}\left(\frac{2Za}{a_H}\right)^{2\sigma}. \quad (24)$$

It is convenient to compare the displacements in the two models. The relevant ratio is

$$\gamma = (\Delta E)_z/(\Delta E)_0$$
$$= \left(\frac{c+z}{a}\right)^{2\sigma}\left[1-\frac{10\sigma}{(9-4\sigma^2)}\left(\frac{z}{c}\right)\left(1+\frac{z}{c}\right)^{-2}\left(1+\frac{z^2}{c^2}\right)^{-1}\left(1-\tfrac{2}{3}\frac{z}{c}+\frac{z^2}{c^2}\right)\right]. \quad (25)$$

5. The Isotope Shift

The isotope shift $(\delta\Delta E)_z$, which is the difference in $(\Delta E)_z$ between two isotopes of the same element having nuclear radial parameters c and $c+\delta c$ (z is constant) is given from eq. (22) as

$$(\delta\Delta E)_z = 2\sigma(\Delta E)_z\frac{\delta c}{c}\left(1+\frac{z}{c}\right)^{-1}$$
$$\times\left[1+\frac{5\left(\frac{z}{c}\right)\left(1-\frac{z}{c}\right)^3\left(1+\frac{z}{c}\right)^{-2}\left(1+\frac{z^2}{c^2}\right)^{-2}\left(1+\tfrac{2}{3}\frac{z}{c}+\frac{z^2}{c^2}\right)}{9-4\sigma^2-10\sigma\left(\frac{z}{c}\right)\left(1+\frac{z}{c}\right)^{-2}\left(1+\frac{z^2}{c^2}\right)^{-1}\left(1-\tfrac{2}{3}\frac{z}{c}+\frac{z^2}{c^2}\right)}\right]. \quad (26)$$

For the constant density model, we have

$$(\delta\Delta E)_0 = 2\sigma(\Delta E)_0\frac{\delta a}{a}. \quad (27)$$

In an actual evaluation of the isotope shift, screening effects have to be considered. The effect of screening of the nuclear charge by inner electron shells is obtained in the same way as for the doublet fine structure by multiplying the shifts given by (26) and (27) by the factor

$$\frac{n^3 Z_0^2}{n_0^3 Z^2}\left(1-\frac{\mathrm{d}\Delta}{\mathrm{d}n}\right)$$

where $Z_0 e$ is the external effective nuclear charge, n_0 is the effective principal quantum number and Δ is the quantum defect, $\Delta = n - n_0$. The effect of screening of inner electron shells by the valence electron must also be considered. Crawford and Schawlow [2]) found that this effect reduces the shifts by about 20 percent.

As previously pointed out [2, 3, 4]), the shift $(\delta\Delta E)_0$ predicted by the constant density model and using the radius given by (23), when corrected for screening, gives values very nearly twice the observed size. It is therefore sufficient, for the purpose of comparison of the present shift $(\delta\Delta E)_z$ with experiment, to evaluate the ratio $(\delta\Delta E)_z/(\delta\Delta E)_0$. Since both c and a vary as $A^{\frac{1}{3}}$, then

$\delta c/c = \delta a/a$. It follows from (26) and (27) that the relative size of the isotope shifts in the two models is given by

$$\eta = (\delta \Delta E)_z/(\delta \Delta E)_0$$
$$= \gamma(1+z/c)^{-1} \qquad (28)$$
$$+ \frac{5}{(9-4\sigma^2)} \left(\frac{c+z}{a}\right)^{2\sigma} \left(\frac{z}{c}\right)\left(1+\frac{z}{c}\right)^{-3} \left(1+\frac{z^2}{c^2}\right)^{-2} \left(1-\frac{z}{c}\right)^{3} \left(1+\tfrac{2}{3}\frac{z}{c}+\frac{z^2}{c^2}\right),$$

where γ is given by (25), c and z by (3) and a by (23).

Values of γ and η for elements widely spread in the periodic table are listed in table 1.

TABLE 1

Element	Z	A	γ	η
Cr	24	50	0.67	0.51
Ru	44	100	0.64	0.52
Sm	62	150	0.64	0.54
Pb	82	208	0.67	0.56

It is obvious from this table that the ratios γ and η are very nearly constant. The result that $\gamma > \eta$ means that the energy displacements are less sensitive to the details of the charge distribution near the nuclear surface than the isotope shifts. The fact that $\eta \approx 0.5$ is a significant evidence for the success of the present treatment as it leads to remarkable agreement between the theoretical and experimental isotope shifts.

The author is indebted to Professor L. Rosenfeld for the critical reading of the manuscript.

References

1) G. Breit, Revs. Mod. Phys. **30** (1958) 507
2) M. F. Crawford and A. L. Schawlow, Phys. Rev. **76** (1949) 1310
3) P. Brix and H. Kopfermann, Z. Physik **126** (1949) 344
4) W. Humbach, Z. Physik **133** (1952) 589
5) L. Wilets, D. L. Hill and K. W. Ford, Phys. Rev. **91** (1953) 1488
6) A. R. Bodmer, Proc. Phys. Soc. A **66** (1953) 1041;
A. R. Bodmer, Nuclear Physics **9** (1958) 371
7) R. Hofstadter, Revs. Mod. Phys. **28** (1956) 214;
D. G. Ravenhall, Revs. Mod. Phys. **30** (1958) 430
8) B. Hahn, D. G. Ravenhall and R. Hofstadter, Phys. Rev. **101** (1956) 1131
9) A. S. Meligy, Nuclear Physics **1** (1956) 610

1.D.1:
3.A

Nuclear Physics **14** (1959/60) 256—262; © *North-Holland Publishing Co., Amsterdam*
Not to be reproduced by photoprint or microfilm without written permission from the publisher

QUADRUPOLE ENHANCEMENT IN O^{17} AND F^{17}

G. BARTON †, D. M. BRINK and L. M. DELVES
Clarendon Laboratory, Oxford

Received 3 August 1959

Abstract: A previous calculation of E2 enhancement is improved, first by refining the single-particle functions, and then by using Brillouin-Wigner in place of Rayleigh-Schroedinger perturbation theory. The higher order correlations thus introduced enable one to bring the theory into agreement with the data on both O^{17} and F^{17}. Finally, we present some considerations on the extension of the theory to heavier nuclei.

1. Introduction

In an earlier paper [1]), referred to below as I, an attempt was made to calculate for the odd-proton nucleus F^{17} the enhancement of the $2s_{\frac{1}{2}}$ to $1d_{\frac{5}{2}}$ E2 transition due to the residual interaction $V-U$ between the odd particle and the core protons. The observed reduced matrix element lies between the limits

$$8.45f^2 \leqq |\langle||Q||\rangle| \leqq 11f^2, \quad (f = 10^{-13}\,\text{cm}). \tag{1}$$

Taking the polarizability (denoted by B/E) of the core from the O^{17} data we found a core contribution of $-1.1f^2$ to first order in $V-U$. The single proton matrix element was insensitive to the change from oscillator to finite square well wave functions and gave a contribution of $-4f^2$, making a total well outside the experimental limits. Furthermore the value of B/E needed to fit the O^{17} data was higher by a factor of roughly 1.4 than the theoretical predictions.

In the appendix we report an improved calculation of the single proton radial wave functions for the $2s_{\frac{1}{2}}$ and $1d_{\frac{5}{2}}$ states. Rather surprisingly these give an increase in the radial integral $|\int R_{s_{\frac{1}{2}}} R_{d_{\frac{5}{2}}} r^4 dr|$ from $9.9f^2$ to $17.3f^2$. If we accept for the moment the previously evaluated core contribution, which is not sensitive to the change in the single particle functions, this makes a total of $-8.1f^2$ for the reduced matrix element, so near the experimental value that the remaining discrepancy can hardly be significant. (In fact an independent measurement of the F^{17} mean life [2]) gives a lower limit on the matrix element in good accord with this value.)

The difficulty that the calculated core polarizability is too low still remains. It has been suggested, notably by Eden [3]), that the Rayleigh-Schroedinger expression to first order in $V-U$ may embrace less of the total effect than

† Now at the Institute for Advanced Study, Princeton.

would normally be suspected. It is possible for instance that those higher order terms which simulate a static core distortion combine to give an enhancement comparable to that due to the leading (first order) term, even though the effect of other higher order terms is small.

It is a feature of the first order calculation in I that the contribution coming from core polarization is smaller for the proton than for the neutron by a factor of between 2 and 4 depending on the exchange mixture in the nucleon-nucleon force. An attempt to improve the calculation by including some higher order effects raises the question whether the improved calculation maintains the difference between the odd-proton and neutron enhancements or equalises them. Here we attempt to answer this problem.

Before presenting further arguments we recall that the unconventional first order result rests on only two conditions:

(i) The space-direct and space-exchange orbital integrals are approximately equal.

(ii) The core protons are spin saturated.

Now, in a heavy nucleus, where the internucleon potential can adequately be dealt with in the zero-range approximation, condition (i) is satisfied more closely even than in O^{16}, though for rather different reasons. Condition (ii) of course ceases to apply exactly as we pass from LS to jj coupling, but one would expect that it can be retained as a relevant first approximation. Then the result about the proton-neutron enhancement ratio should be approximately valid for such nuclei.

We return now to the effects of higher order terms on the core polarization. The most straightforward and intuitively the most illuminating way of including at least some of these is to rearrange the Rayleigh-Schroedinger series into a Brillouin-Wigner expansion [4]). In the present context this amounts to including the diagonal matrix elements of the perturbation into the zero-order Hamiltonian. Again neglecting normalization terms eq. (3) of I is then replaced by

$$1\rangle_J = |0J\rangle + \sum_{n\neq 0J} |n\rangle \frac{\langle n|V-U|0J\rangle}{E_J+\langle 0J|V-U|0J\rangle - E_n - \langle n|V-U|n\rangle},$$

where E_J, E_n denote the energy eigenvalues of the O^{16} ground-state Hartree-Fock equation as discussed in I. The calculation then proceeds as before; but whereas previously each excited core configuration appeared with only a single energy denominator we must now allow for the splitting up of these configurations by the perturbation.

The *overall* effect is clearly a lowering of the mean energy denominator E. In the special case of the $A = 17$ nuclei, the expressions $\langle n|V-U|n\rangle$ refer of course to 17-body states of the type enumerated in I, but we can estimate their magnitude empirically from the effects that similar matrix elements are

known to have in the neighbouring O^{16}. Since that nucleus has even parity excited states as low as 6 MeV, it is clear that the drop to be expected in E is quite sufficient to bring the polarizability B/E into agreement with the $A = 17$ data.

It is interesting to note here that this lowering of E is caused by the appearance in the denominator of terms $\langle n|V-U|n\rangle$, which in the context of the Rayleigh-Schroedinger series embody typical two-particle correlation effects (configuration splitting). Nevertheless it follows from the considerations of I that by completing the calculations as before we include in the final result only those effects of such interparticle correlations which simulate the static distortion of the core.

2. The Induced Charge on the Odd Nucleon

We now turn to the question of the relative magnitudes of the induced charges of the odd neutron and odd proton in O^{17} and F^{17}. Here we split the electric quadrupole operator Q into parts with definite isobaric spin $T = 0$, $T = 1$:

$$\begin{aligned} Q &= \tfrac{1}{2}(Q_0+Q_1), \\ Q_0 &= \sum_i r_i^2 Y_{20}(\Omega_i), \\ Q_1 &= \sum_i \tau_3(i) r_i^2 Y_{20}(\Omega_i). \end{aligned} \tag{2}$$

The calculation is similar to that in I, and the contribution to a quadrupole matrix element from core polarization is

$$\begin{aligned} \delta\langle J|Q_{0,1}|J'\rangle = \sum_n \frac{1}{E_n} \{&\langle 0J|Q_{0,1}|n\rangle\langle n|V-U|0J'\rangle \\ &+\langle 0J|V-U|n\rangle\langle n|Q_{0,1}|0J'\rangle\}, \end{aligned} \tag{3}$$

which reduces to

$$\delta\langle J|Q_{0,1}|J'\rangle = \frac{1}{E_{0,1}} \{\langle 0J|(V-U)Q_{0,1}|0J'\rangle+\langle 0J|Q_{0,1}(V-U)|0J'\rangle\} \tag{4}$$

on making the closure approximation. The improvement in the present calculation lies hidden in the energy denominators in eq. (3) and the mean energy denominators $E_{0,1}$ in eq. (4). In the first order calculation these depended only on the zero order energies while now the energy denominators are those of Brillouin-Wigner perturbation theory and already contain some higher order effects of the two-body forces as discussed in section (1).

With $Q = Q_0$ the intermediate states $|n\rangle$ in eq. (3) are those whose parents contain excitations of the O^{16} core with isobaric spin $T = 0$, while with $Q = Q_1$ the states $|n\rangle$ contain $T = 1$ core excitations. Empirically all the observed low

excited states of O^{16} are $T = 0$ states; hence the mean energy in eq. (4) should be lower for calculating the core contribution to the matrix element of Q_0 than for Q_1.

In I the quadrupole enhancements for the odd nucleon are given in terms of the mean energy E, some function of the radial matrix elements (denoted here by M) and parameters C_n and C_p for the proton and neutron respectively. For the present purpose we require the $T = 0$ and $T = 1$ components of C_p and C_n,

$$C_0 = \tfrac{1}{2}(C_p + C_n), \quad C_1 = \tfrac{1}{2}(C_p - C_n).$$

In terms of these parameters the contribution to the matrix elements of Q_0 and Q_1 from core polarization are

$$\langle J|Q_0|J'\rangle = MC_0/E_0,$$
$$\langle J|Q_1|J'\rangle = MC_1/E_1,$$

and the enhancements for the odd proton in F^{17} and the odd neutron in O^{17} are

$$\delta\langle Q_p\rangle = M\left\{\frac{C_0}{E_0} - \frac{C_1}{E_1}\right\},$$

$$\delta\langle Q_n\rangle = M\left\{\frac{C_0}{E_0} + \frac{C_1}{E_1}\right\}.$$

The $T = 0$ part gives the same contribution to the neutron and proton matrix elements, while the $T = 1$ part gives opposite contributions. If $E_0 = E_1$ the original result of paper I stands, while, if $E_0 \ll E_1$ we have

$$\delta\langle Q_p\rangle \approx \delta\langle Q_n\rangle,$$

i.e. the conventional result of Raz holds, which means that the core polarization contributes equally in the odd neutron and odd proton cases.

The physical reason for the result is clear: The neutrons and protons move in phase in a $T = 0$ excitation of the O^{16} core and in antiphase in a $T = 1$ excitation. The first order calculation shows that the odd neutron polarizes the protons of the core more effectively than the odd proton, and if $T = 0$ and $T = 1$ excitations lie at the same mean energy, this effect predominates and the neutrons carry a greater induced charge. On the other hand, if the relevant $T = 0$ states lie much lower than the $T = 1$ states, the core protons and neutrons prefer to move in phase rather than out of phase. This washes out the other effect. It is interesting to note that manifestly collective effects appear simply in the energy denominators and do not have to be included in the wave functions.

If the core polarizability is to be large enough to explain the observed quadrupole moment of O^{17}, at least one of the mean excitation energies E_0, E_1 in eq. (4) must be small, i.e. of the order of 14 MeV. The intermediate states $|n\rangle$ in (3) consist of an odd nucleon coupled to parent core excitations. The parent

states which give an appreciable contribution to the sum in eq. (3) should resemble those $I = 2$ even parity states in O^{16} that have large ground state quadrupole matrix elements. Of the $I = 2$ states below 13 MeV, the 6.91 MeV state has a ground state matrix element which is near the single particle value, the ground state matrix element of the 11.51 MeV state may be larger [5]), while that of the 9.84 MeV state is much smaller [5]). Apparently there are no states known between 13 and 20 MeV that have matrix elements appreciably larger than the single particle values. If the ground state quadrupole matrix element of the 11.51 MeV state turns out to be several times larger than the single particle value, it must contribute a considerable part of the sum (3) and the $T = 0$ mean energy E_0 may be near 12 MeV, thus explaining the quadrupole moment of O^{17}. If on the other hand this is not the case no definite statement can be made.

3. Application to Heavy Nuclei

Recent work by Elliott [6]) and Mottelson [7]) has shown that it is possible to devise particle coupling schemes based on the shell model which contain collective effects. Elliott's results have application to rotational states in light nuclei, $20 < A < 28$, while the work of Mottelson may help in understanding vibrational states in heavy nuclei. Both these calculations have an element in common: they lump the closed shells together as a "core" and aim to treat the interaction of the nucleons outside closed shells more or less exactly. The interaction between particles outside closed shells and the core can be treated in perturbation theory and has the effect of modifying the particle-particle interaction for particles in the unfilled shells and of giving these particles induced charges in addition to their normal charge. The enhancement of E2 transition probabilities comes partly from the coupling scheme and partly from core polarization. The value of the induced charge required to fit observed transition rates is about one electronic charge. A difficulty arises at this point. If both neutron and proton have equal induced charges, as they have according to conventional theory, the effective charge of a proton is made up of its own charge e plus the induced charge e yielding a total effective charge $2e$. The neutron has only its induced charge e. Thus nuclei with mostly protons in unfilled shells would have larger E2 transition rates than nuclei with mainly neutrons in unfilled shells, while present evidence suggests the contrary, vis. that protons and neutrons carry roughly equal effective charges.

The result found in paper I and developed further here, that in certain cases the induced charge on protons can be less than that on neutrons, may provide a solution to this dilemma.

Appendix

The computation of the radial wave-functions was carried out on the Ferranti Mercury computer at the Oxford University Computing Laboratory. The machine was programmed to calculate eigenfunctions of the Schroedinger equation with a potential [8])

$$\frac{-V_0}{1+\exp[\alpha(r-r_0)]} - \frac{\lambda\hbar^2 V_0}{4m^2c^2}\,\frac{\exp[\alpha(r-r_0)]}{(1+\exp[\alpha(r-r_0)])^2}\mathbf{L}\cdot\mathbf{S}+V_c(r)$$

where $V_c(r)$ is the Coulomb potential due to a charge density of the form

$$\rho(r) = \frac{\rho_0\left(\dfrac{1+\omega r^2}{r_{0c}^2}\right)}{1+\exp[\alpha_c(r-r_{0c})]}.$$

The machine varied the well depth V_0 to give an eigenfunction of the required principal quantum number n, L, J, and binding energy, and printed out the normalised wave-function at specified intervals in r. The matrix elements were then computed by hand. A range of parameters was used. The set

$$\alpha = 1.4f^{-1},\quad r_0 = 1.19A^{\frac{1}{3}}f,\quad \lambda = 39.5f^{-2},$$

$$\alpha_c = \infty,\qquad \omega = 0,\qquad r_{0c} = 0.86r_0,$$

which agrees well with shell model assignments, gave the following well depths for the states, with binding energies shown:

	Binding energy (MeV)	V_0 (MeV)
$1d_{\frac{5}{2}}$	0.6	49.15
$2s_{\frac{1}{2}}$	0.1	51.95

The corresponding radial matrix element $\int R_s R_d r^4 dr = -17.28$. This compares with the values -9.9 and -10.0 found previously [1]) for an oscillator well and for a square well with the Coulomb field included outside the well, but neglected inside. Since, owing to the weighting factor r^2, most of the contribution to the matrix element comes from outside the potential well, in the tail of the wave-functions, this increase by 80 % in the matrix element over that given by the wave-functions for a square well plus external Coulomb potential arises from an increase in the amplitude of the tails of the individual wave-functions by about 40 %. Of this, about 20 % is contributed by the inclusion of the Coulomb potential inside the well; this tends to uncrease the tail of the wave-function. Most of the other 20 % arises from rounding off the well edge, which allows the wave-function to leak through the edge more readily than if it were square.

Inclusion of the spin-orbit force raises the matrix element by about 3 %; the results are wholly insensitive to the shape of the charge distribution.

These results disagree with the usual expectation that a rounded well will give numbers intermediate between a square well and an oscillator well. However, this customary argument is incomplete. The shape of the wave-function inside the potential is not sensitive to the potential form, and calculations for which the main contribution comes from this region can be correlated in this way. Examples are energy level sequences and overlap integrals $\int R_1 R_2 r^2 \mathrm{d}r$. The latter are in fact > 98 % even between oscillator and square well functions. The tails of the wave-functions, however, depend rather strongly on the details of the potential, and no general rule can be formulated for calculations which are sensitive to the wave-functions at large distances.

References

1) G. Barton, Nuclear Physics **11** (1959) 466
2) Holland, Lynch and Hanna, Phys. Rev. **112** (1958) 903
3) R. J. Eden, private communication
4) See for instance Mott and Sneddon, Wave Mechanics and its Applications (Oxford, 1948)
5) R. E. Meads, private communication
6) J. P. Elliott, Proc. Roy. Soc. A **245** (1958) 128, 568
7) B. R. Mottelson, in The Many Body Problem, Vol. 1 (Dunod, Paris, 1959)
8) H. Feshbach, Annual Review of Nuclear Science (1958)

7.A *Nuclear Physics* **14** (1959/60) 263—269; © *North-Holland Publishing Co., Amsterdam*

Not to be reproduced by photoprint or microfilm without written permission from the publisher

AN ASYMPTOTIC CAUSALITY REQUIREMENT FOR SYSTEMS WITH CONSTRAINED INPUTS

J. SUCHER

Department of Physics, University of Maryland, College Park, Maryland †

Received 8 August 1959

Abstract: The usual formulation of causality for simple linear systems: "no output before input", may fail to imply that the system kernel $K(\tau)$ is a causal function of the time delay τ, because the class of physically admissible input functions may not contain a complete set of causal signals. An attempt is made to formulate a causality requirement, asymptotic in nature, which overcomes this difficulty. It is found, rather generally, that systems which satisfy this requirement cannot have a finitely acausal kernel. If it could be shown that the kernel cannot be infinitely acausal, the validity of the usual dispersion relations for such systems would be ensured.

1. Introduction

Consider a physical system, for example a four-terminal electrical network, which transforms an input signal, say $f(t)$, into an output signal, say $g(t)$, in a reproducible way. Let $\mathscr{I}$ denote the class of all admissible (physically possible) input signals. If the system is linear and if its properties do not vary with time ††, the relation between input and output may be written in the form [1])

$$g(t) = \int_{-\infty}^{\infty} K(t-t')f(t')\mathrm{d}t', \quad f \in \mathscr{I}, \tag{1}$$

where the kernel $K(t-t') = K(\tau)$ is a function which characterizes the system.

The usual formulation of the causality requirement for such systems is most readily given in terms of the concept of a *causal* function: $h(t)$ is causal if

$$h(t) = 0 \quad \text{for } t < 0. \tag{2}$$

The causality statement then takes the form:

To a causal input $f(t)$ there corresponds an output $g(t)$ which is also causal. (A)

This requirement immediately leads to the condition that

$$\int_{-\infty}^{\infty} K(t-t')\, f(t')\mathrm{d}t' = 0 \qquad (t < 0), \tag{3}$$

for all admissible causal inputs $f(t)$.

† This research was supported in part by the U. S. Air Force through the Air Force Office of Scientific Research of the Air Research and Development Command.

†† It is then assumed that the set $\mathscr{I}$ is invariant under translations of the origin of time.

It follows from eq. (3) that if the set of causal admissible input functions (we denote this subset of $\mathscr{I}$ by $\mathscr{I}_C$ hereafter) is a *complete* set, in the interval $0 \leqq t \leqq \infty$, then $K(t-t')$ vanishes for $t < 0$ and $t' > 0$, so that $K(\tau)$ is a causal function of τ. But the causal nature of $K(\tau)$ implies in turn that the Fourier transform of $K(\tau)$, the generalized impedance or S-matrix for the system, will have analyticity properties which will lead to dispersion relations for the system †.

We may now remark that there exist situations of physical interest in which the set $\mathscr{I}_C$ of admissible causal input functions is *not* complete. In fact, in the examples we have in mind the set $\mathscr{I}_C$ is empty. In this case, therefore, the causality condition (A) leads to no consequences whatsoever regarding the properties of the system.

Illustrations of such a situation are provided by the non-relativistic, single particle Schrödinger equation and by the Klein-Gordon equation, in the absence of external fields. The usual physical interpretation of these equations requires that the time-Fourier transform of the wave function at a given point in space vanish, respectively, for $\omega < 0$ and for $-m < \omega < m$. (Here ω is the variable reciprocal to t and m is the particle mass.) It follows that, in either case, the wave function at a given point in space cannot be a causal function of the time ††. This circumstance led Van Kampen [2]), in his work on the Schrödinger equation, to the introduction of a new causality condition involving probabilities; it led Knight and Toll [3]), in their work on the Klein-Gordon equation, to the introduction of the concept of "the scattering of a bound state of the source".

With these examples in mind, it seemed worthwhile to examine the analogous problem for the less complicated situation provided by simple linear systems, characterized by eq. (1). In particular, we consider the problem of the formulation of a non-trivial (non-empty) causality condition for systems for which the class $\mathscr{I}_C$ of admissible causal inputs may not be complete, that is, for systems with *constrained* inputs. It may be hoped that this will lead to some insight regarding the application of causality to quantum mechanics †††.

One might like such a formulation to satisfy some or all of the following requirements:

(a) The formulation should have some intuitive basis, i.e. have some discernable connection with an intuitive meaning of causality.

(b) The formulation should be applicable to, and have some implications

† For a comprehensive analysis, see ref. [1]).

†† For an elegant proof see ref. [2]), footnote **3**.

††† Alternatively, one may regard such an investigation as an attempt to answer the following problem: Observers A and B can perform experiments on identical "black boxes". Their detection equipment is identical but observer B has, in contrast to A, only a limited number of causal input signals available. (For example, B may not be able to generate frequencies ω between ω_1 and ω_2.) By repeated experiment, A determines that the system is described by a causal kernel. Could B have predicted this by experiment on his copy? Each observer is idealized to the extent that an infinite time is allowed for each experiment.

for a wide variety of constrained input systems, including systems for which $\mathscr{I}_C$ is empty.

(c) The formulation should be powerful enough to permit inferences to be drawn concerning the analytic properties of the S-matrix for such systems.

In section 2, a causality requirement, asymptotic in nature, is formulated which satisfies conditions (a) and (b). Some consequences of this requirement are obtained in section 3. The results, and the possibility of satisfying condition (c), are discussed in section 4.

2. An Asymptotic Causality Requirement

We would like to formulate a causality requirement for a simple linear system with constrained inputs. In particular, we do not wish to assume that the system admits inputs which are causal functions of time. With no causal signals, or only a few, available to "test" causality, we assume that the system admits as input signals functions $f(t)$ which we shall call "quasi-causal" and which are asymptotically zero in the following sense:

(i) $f(-\infty) = 0$;

(ii) there exists a time $t_{(f)}$ such that for $t \leqq t_{(f)}$, $|f(t)|$ is a non-decreasing (4) function of t, not equal to zero.

An example of a quasi-causal signal is the function $e^{-|t|}$, with $t_{(f)}$ any negative number.

What would one expect for the behaviour of the output $g(t)$ generated by a quasi-causal input $f(t)$? If the system is to be causal in some sense, one might expect that the amplification factor $\rho(t)$, defined as the ratio of $g(t)$ to $f(t)$, does not become arbitrarily large as $t \to -\infty$ †. We formulate this expectation that $\rho(t) = g(t)/f(t)$ is bounded in the neighbourhood of $t = -\infty$, or equivalently, that $g(t) = O[f(t)]$ as $t \to -\infty$, as an asymptotic causality requirement:

To a quasi-causal input $f(t)$ there corresponds an output $g(t)$ such that $g(t) = O[f(t)]$ as $t \to -\infty$. (B)

As support for the imposition of condition (B) as a causality requirement for simple linear systems is the fact that (B) is indeed satisfied by a system which satisfies (A) and admits a complete set of causal signals. For we have the theorem,

Theorem 1. If a system has a causal kernel, it satisfies condition (B).

The proof is immediate, since for causal $K(\tau)$ and quasi-causal $f(t)$ it follows that for $t \leqq t_{(f)}$ (see eq. (4)),

† An acausal system could easily violate this requirement by collecting more and more contributions to $g(t)$ from the "future", as $t \to -\infty$.

$$|g(t)| \leqq \int_{-\infty}^{t} |K(t-t')||f(t')|\mathrm{d}t' \leqq |f(t)| \int_{-\infty}^{t} |K(t-t')|\mathrm{d}t',$$

so that $\rho(t)$ is bounded by † $\int_0^\infty |K(\tau)|\mathrm{d}\tau$ for $t \leqq t_{(f)}$.

We can therefore ask the more interesting question: what restrictions does the asymptotic causality requirement (B) impose on the kernel $K(\tau)$? The answer will of course depend, as in the case for condition (A), on the class $\mathscr{I}$ of physically admissible input functions. Some results in this direction are obtained in the next section.

3. Some Consequences of Requirement (B)

To facilitate discussion, we introduce some definitions: $K(\tau)$ will be called acausal if it is not a causal function; if $K(\tau)$ is acausal but for some $T < 0$, $K(\tau) = 0$ for $\tau < T$, $K(\tau)$ will be called finitely acausal; if $K(\tau)$ is acausal, but not finitely so, $K(\tau)$ will be called infinitely acausal. We shall also restrict the discussion to those systems for which $K(\tau)$ is known to be Lebesgue-integrable in the interval $(-\infty, \infty)$. We then have

Theorem 2. If a system satisfies (B) and admits, for some $\delta > 0$, an input of the form $\mathrm{e}^{-\delta t}$, the kernel $K(\tau)$ cannot be finitely acausal.

For proof, it is sufficient to consider the case $\delta = 1$. If $g(t)$ is the output corresponding to the quasi-causal input

$$f(t) = \mathrm{e}^{-t^2}, \tag{5}$$

it is readily seen from eq. (1), on letting $t' \to t'+t$, that

$$\rho(t) = g(t)/f(t) = \int_{-\infty}^{0} K(-t')\mathrm{e}^{-(t'^2+2t't)}\mathrm{d}t' + \eta(t), \tag{6}$$

where $\eta(t)$ is defined by

$$\eta(t) = \int_0^\infty K(-t')\,\mathrm{e}^{-(t'^2+2t't)}\mathrm{d}t'. \tag{7}$$

Now, the first term on the right hand side of eq. (6) is certainly bounded for $t < 0$, as is easily seen. The requirement that the system satisfy (B) and admit e^{-t^2} as an input signal therefore leads to the condition that $\eta(t)$, defined by eq. (7), is a bounded function of t in the inverval $(-\infty, 0)$.

Because of the growing exponential factor $\mathrm{e}^{-2t't}$ in the integrand of eq. (7), it seems plausible that $\eta(t)$ cannot be bounded unless $K(-t')$ vanishes for $t' > 0$. A proof that $K(\tau)$ vanishes for $\tau < 0$ if $\eta(t)$ is bounded for $t < 0$ may be obtained if it is assumed, a priori, that $K(\tau)$ is at worst finitely acausal. To this end, we note that $\eta(t)$ may be extended into the complex plane, as a function of a complex variable $z = t+iy$, with

$$\eta(z) \equiv \int_0^\infty K(-t')\mathrm{e}^{-(t'^2+2t'z)}\mathrm{d}t', \tag{8}$$

† We thereby exclude systems for which $\int_0^\infty |K(\tau)|\mathrm{d}\tau$ diverges, corresponding to the restriction imposed on $K(\tau)$ in section 3.

and that $\eta(z)$ so defined is an *entire* function of z. If now $K(\tau)$ is zero for $\tau < T < 0$, so that the integration in eq. (8) extends over only a finite interval, it can be shown that $\eta(z)$ is a bounded function of z. This follows from the lemma, proved in the appendix,

Lemma: Let $k(t')$ be integrable in the inverval $(0, b)$. Then the entire function $u_a(z)$, defined for any $a \in (0, b)$ by

$$u_a(z) = \int_0^a k(t')\mathrm{e}^{-t'z}\mathrm{d}t', \tag{9}$$

is bounded everywhere, if it is bounded for real negative z.

Since a bounded, entire function is a constant it follows that $u_a(z)$ is a constant. But the condition $\mathrm{d}u/\mathrm{d}z = 0$ and the theorem on the uniqueness of the inverse Laplace transform then imply that $k(t')$ vanishes in the interval $(0, a)$. The same argument, applied to eq. (8), shows that $K(\tau)$ vanishes in the interval $(T, 0)$, so that $K(\tau)$ is a causal function.

Theorem 2 may be restated in the form: If $K(\tau)$ vanishes in some neighborhood of $\tau = -\infty$, then if the system satisfies (B) and admits an input of the form $\mathrm{e}^{-\delta t^2}$, $K(\tau)$ vanishes for all $\tau < 0$, i.e. $K(\tau)$ is a causal function. A somewhat more powerful result [4]) may be obtained by using methods similar to those used in the appendix:

Theorem 3. If $K(\tau) = \mathrm{O}[\mathrm{e}^{-\beta|\tau|^{2+\varepsilon}}]$ for some positive β and ε, as $\tau \to -\infty$, then if the system satisfies (B) and admits an input of the form $\mathrm{e}^{-\delta t^2}$, $K(\tau)$ is a causal function.

4. Discussion

The results obtained in the preceding section may be summarized by stating that the imposition of the causality requirement (B) on a simple linear system with an integrable kernel $K(\tau)$ implies, with some additional assumptions, that $K(\tau)$ is a causal function. The additional assumptions were:

(i) The system admits an input of the form $\mathrm{e}^{-\delta t^2}$ for some $\delta > 0$.

(ii) The kernel $K(\tau)$ vanishes "sufficiently rapidly" as $\tau \to -\infty$.

In theorem 2, "sufficiently rapid" is taken to mean that $K(\tau)$ is identically zero in some neighbourhood of $\tau = -\infty$. Theorem 3 shows that it is sufficient to assume that as $\tau \to -\infty$, $K(\tau) = \mathrm{O}[\mathrm{e}^{-\beta|\tau|^{2+\varepsilon}}]$.

Whether assumption (ii) is in fact necessary has not been determined. It should be noted that the requirement that $K(\tau)$ be integrable in $(-\infty, \infty)$ already implies [5]) that $K(\tau)$ vanishes at a certain rate as $\tau \to -\infty$. The integrability of $K(\tau)$ may therefore be sufficient to make an assumption of the type (ii) superfluous, at least if assumption (i) is broadened. It is tempting to speculate that this is in fact the case, and that, more generally, a single assumption of the type

(i') the system admits a "sufficiently large" class of quasi-causal input functions,

is sufficient to ensure that if the system satisfies condition (B) its kernel is a causal function. It could then be asserted that the causality requirement (B) also satisfies condition (c), stated at the end of section I, since the Fourier transform of a causal function is analytic in the upper half of the complex plane. Furthermore, for the class of systems satisfying (i'), the requirement (B) would ensure that both the ordinary causality requirement (A) as well as the usual dispersion relations are valid. What is meant by "sufficiently large" in this context, remains to be discovered. If it should turn out, in particular, that systems for which the admissible input signals have Fourier transforms which vanish in some interval are included † in the class of systems in question, applications of (B) to quantal systems might be possible.

I am indebted to Professor Marcel Riesz and to Dr. Khosrow Chadan for their help with mathematical problems. I would like to thank Dr. John G. Taylor and Dr. John S. Toll for discussions of this subject.

Appendix ††

Suppose that $u_a(z)$ is bounded for real z, in the inverval $(-\infty, 0)$. It follows from eq. (9) alone that $u_a(z)$ is also bounded both in the interval $(0, \infty)$ and on the imaginary axis. Thus $u_a(z)$ is bounded along each of the four coordinate-rays. Now eq. (9) also implies that

$$|u_a(z)| \leqq G e^{a|z|}$$

where $G = \int_0^a |k(t')| dt'$. It is now possible to apply a theorem of the Phragmén-Lindelöf type which states that if $v(z)$ is analytic in a sector of angular width less than π, is bounded along the two rays which define the sector, and satisfies an inequality of the form

$$|v(z)| \leqq G_1 e^{C_2|z|},$$

where the G_j are constants, then $v(z)$ is a bounded function in the sector [6]). Applied to each of the four quadrants of the complex plane in turn, this theorem implies that $u_a(z)$ is bounded in each quadrant. Hence, $u_a(z)$ is a bounded function of z.

In the proof of theorem 3 a similar theorem of the Phragmén-Lindelöf type is utilized to show that $\eta(z)$ (eq. (8)) is [4]) a bounded function of z. From this, the vanishing of $K(\tau)$ for $\tau < 0$ follows as in the proof of theorem 2.

† A simple example of a quasi-causal signal whose Fourier transform vanishes in an interval is provided by the function $(1-it)^{-1}e^{-it}$ (the interval being $(-\infty, 1)$ in this case). This remark shows that the causality requirement (B) will certainly have *some* content for systems of this type.

†† The proof given in this appendix is due to M. Riesz (private communication).

References

1) See, for example, J. S. Toll, Phys. Rev. **104** (1957) 1760
2) N. G. van Kampen, Phys. Rev. **91** (1953) 1267
3) J. Knight and J. S. Toll, Ann. Phys. **3** (1958) 49
4) Kh. Chadan, private communication
5) See, e.g., G. Valiron, Théorie des Fonctions (Masson, Paris, 1948) p. 113
6) G. Pólya and G. Szegő, Aufgaben und Lehrsätze aus der Analysis, Vol. I (Springer-Verlag, Berlin, 1954) p. 145

2.C *Nuclear Physics* **14** (1959/60) 270—276; © *North-Holland Publishing Co., Amsterdam*
Not to be reproduced by photoprint or microfilm without written permission from the publisher

THE DISINTEGRATION OF Ne^{20} BY FAST NEUTRONS

R. J. BELL †, T. W. BONNER and F. GABBARD ††
The Rice Institute, Houston, Texas †††

Received 17 August 1959

Abstract: The cross section for the $Ne^{20}(n, \alpha)O^{17}$ reaction was measured for neutron energies between 2.8 and 7.3 MeV. The (n, α) disintegrations were detected in a grid-type ionization chamber filled with neon. The cross section for this reaction varies between 10 and 270 millibarns in this energy range and shows many narrow resonances. Disintegrations were observed leaving O^{17} in the ground state and in the first three excited states.

1. Introduction

The disintegration of neon by fast neutrons has been studied by Johnson, Bockelman and Barschall [1]) with neutrons of energies up to 3.3 MeV. The purpose of the present experiments was to extend the measurement to higher energies. Recent experiments on the disintegration of N^{14} by neutrons [2]) have shown unexpectedly large cross sections for the (n, α) process and so it is of especial interest to study the (n, α) cross sections in a number of other light elements over a wide range of neutron energies. Below a neutron energy of 7.5 MeV the only reaction (excluding elastic and inelastic scattering) expected by the bombardment of Ne^{20} with fast neutrons is $Ne^{20}(n, \alpha)O^{17}$. The energetics of this and other possible competing reactions are as follows:

$$\begin{aligned} N^{20}+n &\rightarrow O^{17}+\alpha-0.603 \text{ MeV}. \\ &\rightarrow F^{20}+p-6.19 \text{ MeV}. \end{aligned} \qquad (1)$$

Although proton emission is possible above 6.5 MeV, the Coulomb barrier prevents this reaction from occurring to a measurable extent. Natural neon, which was used in this experiment contains 80.8 % Ne^{20}, 8.9 % Ne^{22} and 0.26 % Ne^{21}. The Q-values for the (n, α) reactions in the less abundant isotopes are −5.70 MeV and 0.704 MeV respectively. The only other charged particle reaction energetically possible is $Ne^{21}(n, p)F^{21}$ with a Q-value of −5.7 MeV. These reactions were not observed in this experiment even though the chamber resolution was sufficient to have resolved them from other particle groups if they had been present to an appreciable extent.

† Now at Virginia Polytechnic Institute, Blacksburg, Va.
†† Now at the University of Kentucky, Lexington, Ky.
††† Supported in part by the U. S. Atomic Energy Commission.

Addition of a neutron to a Ne^{20} nucleus forms Ne^{21} with an excitation energy of 6.756 MeV [3]). Energy levels of the compound nucleus above about 9 MeV may be studied by the (n, α) reaction since the Coulomb barrier strongly inhibits the emission of alpha particles having energy of less than ≈ 2 MeV.

2. Experimental Method

The apparatus used for detecting the (n, α) events was a grid-type ionization chamber utilizing electron collection. A description of this chamber has been given previously [2]). Monoenergetic neutrons were obtained from the T(p, n)He^3 and D(d, n)He^3 reactions with the Rice Institute 5.5 MeV Van de Graaff accelerator. A thin Zr-T target which was 30 keV thick for 1 MeV protons was used to produce neutrons of energies from 2.8 to 4.4 MeV and a deuterium gas target was used for higher neutron energies. Neutrons emitted in a small solid angle about 0° with respect to the accelerated beam were used in the measurements. The half angle intercepted by the sensitive volume was $\pm 8°$ when the chamber was at a distance of 30 cm from the target. Neutron energies were obtained from published tables [4]) for the charged particle energies corrected for energy loss in the foils and in the target material.

For the experiments, the ionization chamber was filled to a pressure of 4 atmospheres with natural neon of spectroscopic grade. The chamber filled with neon was placed at a distance of 30 or 40 cm from the neutron source at 0° to the accelerator beam such that the mean direction of the incident neutrons was perpendicular to the chamber axis and centered vertically between the top plate and grid. The neutron flux was monitored by a long-counter which was placed directly behind the ionization chamber at one meter from the target.

The pulses produced in the ion chamber by the neutron induced alpha disintegrations were amplified [2]) and displayed on a 20-channel analyzer. Pulse-height distributions obtained at neutron energies of 4.1 and 7.3 MeV are shown in fig. 1. In the spectrum taken at 4.1 MeV, the peak near channel 26 corresponds to alpha disintegrations leading to the ground state of O^{17} and the lower peak to alpha emission leaving O^{17} in its first excited state at 0.870 MeV. The tail below the peaks is produced by wall-effects and by disintegrations occurring between the grid and collecting plate which give a continuous distribution in pulse size. The pulse-height resolution did not vary appreciably from the value of 8 % at 4.1 MeV for neutron energies between 2.8 and 4.4 MeV. The lower part of fig. 1 shows the pulse-height distribution obtained at 7.3 MeV. The higher energy peak results from unresolved alpha groups going to the ground state and first excited state of O^{17} and the lower peak is produced by groups going to the 3.06 and 3.85-MeV states in O^{17}. As is evident from the figure, the pulse-height resolution is much poorer at 7.3 MeV than at 4.1 MeV. This difference in resolution is accounted for by the difference in purity of the

gas in the chamber in the two instances. The spectrum shown for 4.1 MeV was taken shortly after the chamber was filled while the 7.3-MeV spectrum was taken after the gas had stood in the chamber for a period of two weeks. Electron attachment by electro-negative impurities outgassing from the chamber walls produced the observed broadening. Pulse-height resolution for neutron energies between 4.4 and 7.3 MeV was about constant at 20 % as shown in the example of fig. 1. A more complete discussion of the factors which influence chamber resolution is given in ref.[2]).

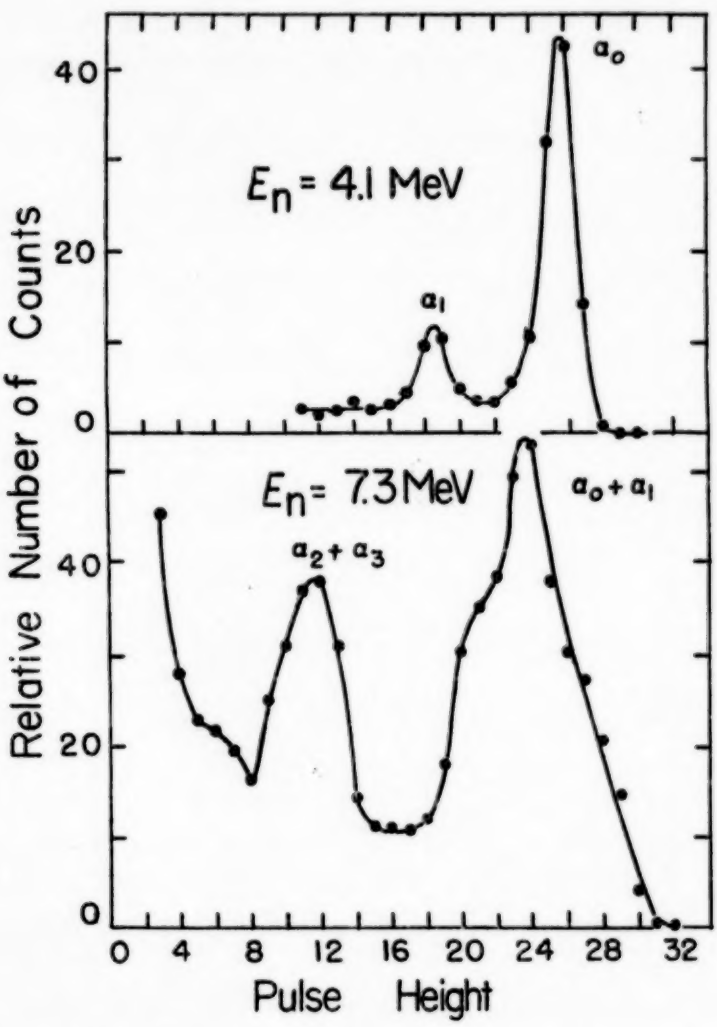

Fig. 1. Pulse-height distributions from $Ne^{20}(n, \alpha)O^{17}$ at neutron energies of 4.1 and 7.3 MeV. The difference in resolution in the two cases was caused by electron attachment.

The energy resolution of the neutrons was limited by the target thickness and the angular spread across the sensitive volume of the ionization chamber. The energy spread for the T^3 target was 23 keV in the energy range where this target was used. The energy resolution of the neutrons from the deuterium source was estimated to be approximately 100 keV.

3. Analysis of Data

The number of (n, α) events associated with each group was calculated from the pulse distributions such as fig. 1. This number was corrected for wall-loss by dividing by $(1-\rho)$ where ρ is the fraction of the alpha particles lost by wall-effect. The method of determining ρ has been previously discussed [2]). The maximum correction for wall-loss in this experiment was 29 %. The absolute long-counter efficiency in counts per neutron/cm² was determined by counting a standard Ra-Be source placed one meter from the counter. A correction to the number of counts for the relative efficiency as a function of neutron energy was made using the data of Allen and Ferguson [5, 6]), and Perry *et al.* [6]).

4. Results

The cross sections for the $Ne^{20}(n, \alpha)O^{17}$ and $Ne^{20}(n, \alpha)O^{17*}$ reactions are plotted in figs. 2 and 3. For neutron energies between 2.8 and 4.4 MeV, obtained with the T+p reaction, the cross sections for disintegration to the ground state and the first excited state of O^{17} are plotted separately. Between 4.4 and 7.3 MeV, where the D+d source was used, only the sum of these two cross sections

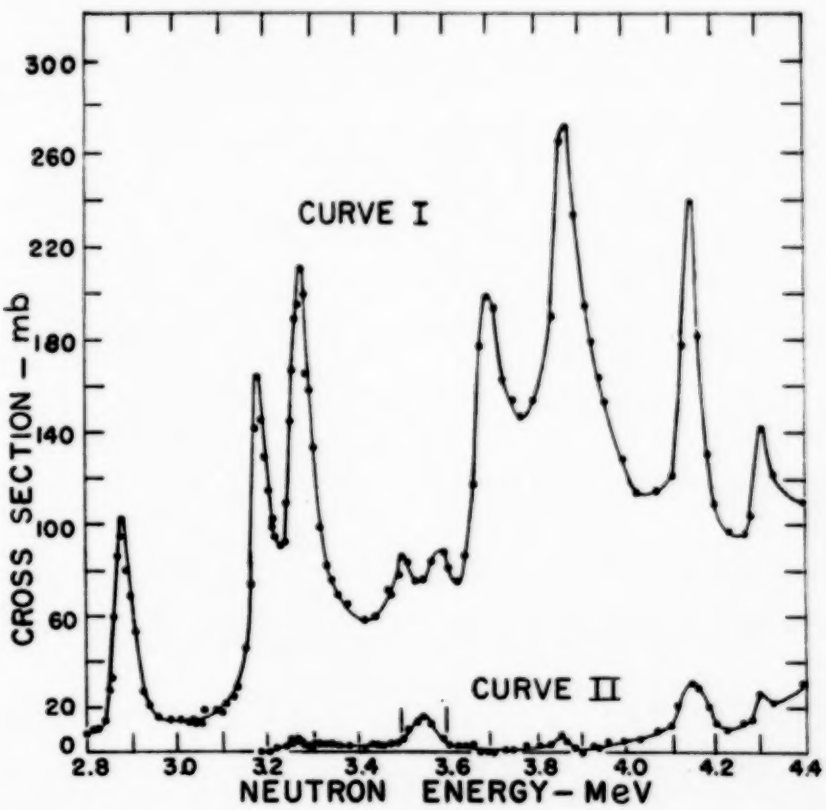

Fig. 2. Cross section for the $Ne^{20}(n\,\alpha)O^{17}$ reaction as a function of neutron energy. Curves I and II show the cross sections for alpha disintegration to the ground state and the first excited state of O^{17} respectively. Neutron energy resolution for the Zr-T target used was 23 keV.

is given since the two alpha groups were poorly resolved in this energy range. Above 6.5 MeV, the sum of the (n, α) cross sections for disintegrations leaving O^{17} in excited states at 3.06 and 3.85 MeV has been plotted.

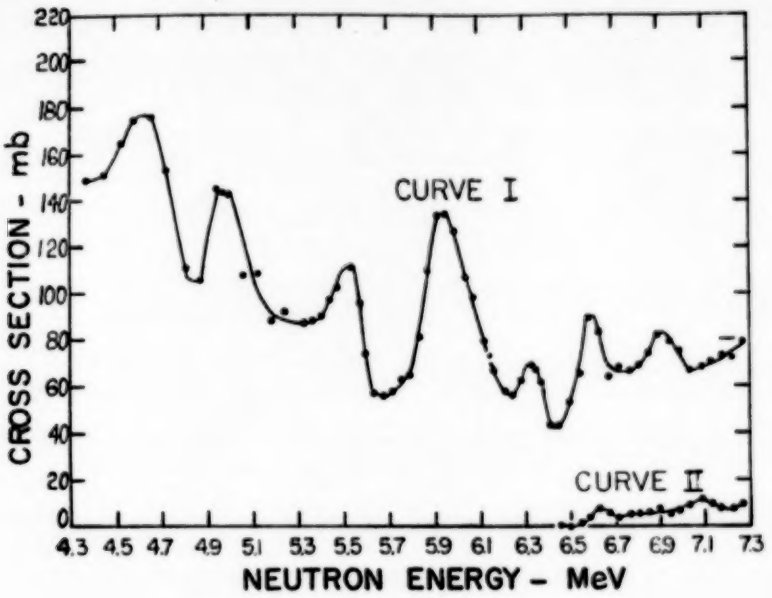

Fig. 3. Cross section for the $Ne^{20}(n, \alpha)O^{17}$ reaction from 4.3 to 7.3 MeV. Curve I shows the sums of the cross sections for alpha disintegration to the ground state and first excited state of O^{17}. Curve II is the sum of the partial cross sections for disintegration to the 3.06 and 3.85 MeV states in O^{17}. Neutron energy resolution for the deuterium gas target used was $\approx$ 100 keV.

TABLE 1

Resonances in the $Ne^{20}(n, \alpha)O^{17}$ reaction

Resonant energy (MeV)	Excitation energy in Ne^{21} (MeV)	Level width Γ (keV)	$\sigma(n, \alpha)$ total (mb)
2.89	9.50	40	100
3.19	9.79	40	163
3.29	9.88	45	213
3.52	10.11	35	89
3.60	10.18	40	93
3.70	10.28	65	197
3.87	10.44	85	277
4.15	10.71	30	265
4.31	10.86	40	167
4.63	11.16	300	178
4.98	11.49	100	145
5.52	12.01	120	112
5.93	12.40	240	138
6.33	12.78	125	68
6.60	13.04	$<$100	97
6.93	13.35	220	89

Sixteen resonances were observed between neutron energies of 2.8 and 7.3 MeV. The energy levels in Ne^{21} corresponding to these resonances lie between excitation energies of 9.4 and 13.6 MeV. The observed resonance energies with widths, neutron energy resolution, and peak cross sections are listed in table 1. From 2.8 to 4.4 MeV, the total neutron energy spread is about 23 keV so that only very weak resonances would be missed. Above 4.4 MeV, the spread in energy of the neutrons is much greater and so closely spaced resonances would not be resolved. Because of this poorer resolution, the apparent change in the average observed width of the resonances in going from the tritium to the deuterium target is probably not real.

Johnson *et al.*[1]) have measured the (n, α) cross section for neutron energies below 3.3 MeV using a proportional counter as a detector. These authors give a cross section of 130 mb at a neutron energy of 2.9 MeV which is 30 % higher than the data reported here; nevertheless, the agreement is within experimental error. The 3.19 and 3.29 MeV resonances were not resolved in Johnson's measurements. Flack and Warren [7]) gave a preliminary report of resonances in Ne^{20} observed by the (n, α) reaction for neutron energies from 3 to 5.2 MeV. The total neutron cross section for Ne^{20} has been measured by Sikkema [8]) between 1.9 and 3.5 MeV neutron energy. These data were taken with poorer resolution than the corresponding (n, α) data presented here.

The errors in the absolute values of the cross section are estimated as follows. (1) Uncertainty in the neutron flux, ± 15 %. Factors included in this error estimate are the uncertainty in the attenuation of the neutrons by the pressure vessel of the ion chamber, the error in the calibration of the neutron source, and the error in the relative long counter efficiency. (2) Error in the number of Ne^{20} nuclei in the sensitive volume of the ion chamber, ± 5 %. (3) Errors in the number of (n, α) counts as obtained from the pulse-height distribution, ± 15 %. These errors include the error in the integration of the alpha peaks and the errors in the corrections for the wall-loss. Based on these estimates, the absolute cross sections for the Ne^{20}(n, α)O^{17} reaction should be accurate to ± 25 %. The error in the relative cross section is somewhat less.

The (n, α) cross section in Ne^{20} accounts for approximately 25 % of the total cross section at the 2.9 MeV resonance (see fig. 2) and remains relatively large above this neutron energy. This large cross section for alpha emission indicates, as in the N^{14}(n, α)B^{11} reaction [2]), that alpha particles are emitted by certain light nuclei in a much larger fraction of the disintegrations than is expected on the basis of the shell model.

Since the angular momenta and parities of the levels in Ne^{21} corresponding to the resonances of figs. 2 and 3 are not known, the partial reduced widths for the neutron and alpha-particle channels for a representative resonance were calculated for various assumed values of J^{π} in order that a more quantitative argument about the alpha emission probability relative to that for the neutrons

could be made. This calculation was made for the 3.29 MeV resonance assuming angular momenta of $\frac{1}{2}$, $\frac{3}{2}$ and $\frac{5}{2}$ and using both parities for each spin assumption. The channel radii used for the neutron and alpha channels were 5.2×10^{-13} cm and 5.8×10^{-13} cm respectively. For all assumed spin and parity values except $\frac{5}{2}^-$, the ratio of the reduced width to the Wigner limit for the alpha channel was greater than the corresponding ratio for the neutron channel and the two ratios were equal for the $\frac{5}{2}^-$ assumption. At the 2.89 and 3.19 MeV resonances the (n, α) cross section comprises a larger fraction of the total cross section than at the 3.29 MeV resonance; therefore, for the same angular momentum and parity assumed for the compound state, the reduced widths for the alpha channel relative to the neutron channel would be even larger.

These results support the suggestion made previously in connection with the $N^{14}(n, \alpha)B^{11}$ reaction [2]) that the nucleons composing these excited states of the compound system form strongly bound groups such as alpha particles which move collectively about the other nucleons or nucleon groups.

References

1) Johnson, Bockelman and Barschall, Phys. Rev. **82** (1951) 117
2) Gabbard, Bichsel and Bonner, Nuclear Physics **14** (1959/60) 277
3) F. Ajzenberg and T. Lauritsen, Revs. Mod. Phys. **27** (1955) 77
4) See, e. g., J. L. Fowler and J. E. Brolly, Jr., Revs. Mod. Phys. **28** (1956) 103
5) W. D. Allen and A. T. G. Ferguson, Proc. Phys. Soc. A **70** (1957) 639
6) Perry, Haddad and Smith, Progress in Nuclear Energy, Ser. 1, Vol. II, Chapter by W. D. Allen and R. L. Henkel (Pergamon Press, New York, 1958)
7) F. C. Flack and J. B. Warren, Proc. Roy. Soc. Canada **47** (1953) 131(A)
8) C. P. Sikkema, Nuclear Physics **3** (1957) 375

2.C *Nuclear Physics* **14** (1959/60) 277—294; © *North-Holland Publishing Co., Amsterdam*
Not to be reproduced by photoprint or microfilm without written permission from the publisher

THE DISINTEGRATION OF NITROGEN BY FAST NEUTRONS

FLETCHER GABBARD †, H. BICHSEL †† and T. W. BONNER
The Rice Institute, Houston, Texas †††

Received 17 August 1959

Abstract: The disintegration of nitrogen by fast neutrons has been studied using a grid-type ionization chamber filled with nitrogen or a nitrogen-argon mixture. Monoenergetic neutrons for studying the reactions from a neutron energy of 1.3 to 8.2 MeV were produced by the $T^3(p, n)He^3$ and $D(d, n)He^3$ reactions. One group of protons, three alpha particle groups, and a group of tritons were observed as disintegration products of the neutron reactions in nitrogen. The $N^{14}(n, p)C^{14}$ reaction leaving C^{14} in its ground state was studied from 1.3 to 4.3 MeV and the maximum cross section observed was 230 mb. Four groups of α-particles leading to the ground, 2.14, 4.46, and 5.03 MeV levels in B^{11} were observed in the experiment. The cross section for the α-particle group leading to the ground state of B^{11} varied from 5 mb at a neutron energy of 1.3 MeV to 390 mb at 4.2 MeV and decreased for higher neutron energies. Triton emission leading to the ground state of C^{12} was observed above a neutron energy of 5.6 MeV.

Above 7 MeV, the cross sections for disintegration by emission of each of the alpha groups and by triton emission were about equal and were approximately 40 mb. The cross sections show many narrow resonances in the neutron energy range studied. The data show that alpha emission relative to proton and neutron emission from these highly excited states of N^{15} is much more probable than expected on shell model considerations.

1. Introduction

The disintegration of nitrogen by fast neutrons was first observed in a cloud chamber by Feather in 1932 [1]). Since that time neutron reactions in nitrogen have been studied by many investigators using various techniques for observing the disintegration products. Neutron reactions in nitrogen leading to the emission of charged particles which are energetically possible below a neutron energy of 10 MeV are the following [2]):

$$\begin{aligned} N^{14} + n &\rightarrow C^{14} + p + 0.627 \text{ MeV} \\ &\rightarrow B^{11} + \alpha - 0.154 \text{ MeV} \\ &\rightarrow C^{12} + t - 4.007 \text{ MeV} \\ &\rightarrow C^{13} + d - 5.316 \text{ MeV}. \end{aligned}$$

† Now at the University of Kentucky, Lexington, Ky.
†† Now at the University of Washington, Seattle, Wash.
††† Supported in part by the U. S. Atomic Energy Commission. A preliminary report of this work has been given in ref. [34]).

Johnson and Barschall [3]) have measured (with $\approx$ 20 keV resolution) the cross sections for (n, p) and (n, α) reactions in the neutron energy range from 0.2 to 2 MeV using a proportional counter as a detector. These two reactions in N^{14} have been studied with poorer energy resolution between 2 and 3.6 MeV by Bollman and Zünti [4]). The (n, α) reaction has been investigated with continuous neutron sources by a number of authors [5–7]). The above investigators did not detect α-particle emission below 1 MeV. Above this energy the cross section for α-emission rises rapidly. It seemed desirable to extend the measurements of the (n, α) and (n, p) cross sections with good energy resolution to higher neutron energies to study the ratio of the (n, α) and (n, p) cross sections.

The (n, d) reaction has never been identified although the measurements made to date do not exclude its presence in the neutron reactions with N^{14}. Lillie [8]) has studied the disintegration of nitrogen by 14.1 MeV neutrons in a cloud chamber. He reports that the sum of the (n, p), (n, t) and (n, d) reactions is 100 mb at this energy. No groups which could be identified with the (n, d) reaction were observed in the present work. Observation of the (n, d) reaction in an ionization chamber is complicated by the fact that the Q-values for the (n, α_3), (n, p_1) and (n, d) reactions are very nearly the same (i.e. -5.18, -5.36 and -5.32 MeV respectively).

The (n, t) reaction has not been definitely observed prior to the present work. Triton emission to only the ground state of C^{12} is energetically possible in the energy range of this experiment.

The reactions which are the inverse of the (n, p) and (n, α) processes have been studied over a portion of the energy range covered in the present experiment. The yield of neutrons from the C^{14}(p, n)N^{14} reaction has been studied up to a proton energy of 2.5 MeV, and the angular distributions of the neutrons have been observed at a few resonances [9–12]). Total cross-section measurements for the (p, n) reaction have been made by Gibbons and Macklin [13]) and by Sanders [11]) for the proton-energy range 0.6 to 3 MeV. The B^{11}(α, n)N^{14} reaction has been observed by a number of investigators [14–17]). The Los Alamos group[17]) has measured the total cross section for this reaction up to an alpha energy of 6 MeV. Comparison of the total cross sections for the N^{14}(n, α)B^{11} and N^{14}(n, p)C^{14} reactions to the cross section for these inverse reactions will provide an additional check on the principle of detailed balance.

2. Experimental Method

The apparatus used for detecting the disintegrations in the present investigation was a grid-type ionization chamber utilizing electron collection. A schematic diagram of the chamber showing dimensions and the relative positions of the various electrodes is given in fig. 1. The purpose of the grid is to screen the electron collector from the motion of the positive ions, thus making

the electron pulse size independent (except for secondary effects) of the position at which the ionizing event occurred within the volume lying above the grid and within the radius of the collecting plate. A grid was first used in an ionization chamber by Alfvén [18]) and the application of the grid as used here was first suggested by Frisch. A theoretical analysis of the operation of such an ionization chamber has been made by Buneman *et al.* [19]).

The neutron sources which were used in the experiments were $Li^7(p, n)Be^7$, $T(p, n)He^3$ and the $D(d, n)He^3$ reactions. The lithium target was natural lithium evaporated on a 20-mil Ta backing and was 10-keV thick to 2.0-MeV protons. This target was used for the neutron-energy range $1.3 < E_n < 1.8$ MeV. A thin Zr-T target was used to produce neutrons of energies from 1.3 to 5.0 MeV, and a deuterium gas target was used for higher neutron energies. The

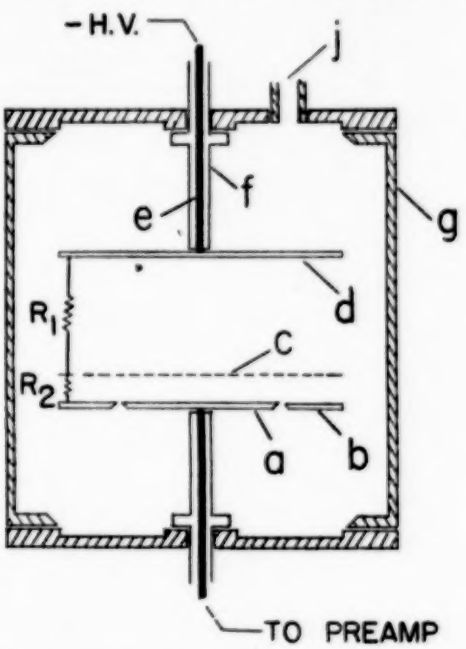

Fig. 1. Schematic diagram of the ionization chamber.
(a) collecting plate, (b) guard ring, (c) grid; 0.005 stainless wire 0.09 cm. apart, (d) high voltage plate, (e) conductor, (f) teflon insulator, (g) stainless pressure vessel; $\frac{1}{8}$-inch wall, (j) port for filling, R_1-80 megohm, R_2-40 megohm, dimensions: radius of (a)-4.5 cm; (a) to (c)-1.55 cm; (c) to (d)-6.42 cm.

Zr-T target was 30 keV thick to 1 MeV protons and was supported on a gold backing 40 mil thick. The deuterium target consisted of a thin walled platinum chamber, 1.5 inches long, with a 0.77 mg/cm^2 nickel foil between the deuterium gas and the vacuum system. This gas chamber was filled to a pressure of one-quarter atmosphere with deuterium. The targets were cooled by an air jet. The charged particles were accelerated by the Rice Institute 5.5 MeV Van de Graaff accelerator.

The neutron energy resolution in the experiments was limited by the target thickness and the energy spread across the ion chamber due to the energy

variation with angle. Secondary effects influencing the resolution are scattering of neutrons in the pressure vessel of the ion chamber and multiple scattering in entrance foils to the gas targets. Scattering in the iron is estimated to be ≈ 2 % and has been neglected. Calculations based on the theory of Molière [20]) have been made for multiple scattering of deuterons in the nickel foil and show that this effect could account for less than 10 keV in the neutron energy spread if one assumes that the foil is of uniform thickness. The neutron energy resolution for the lithium and Zr-T targets was 15 ± 3 keV and 25 ± 5 keV respectively, except for neutron energies between 2.4 and 2.6 MeV where it was ≈ 20 keV. The resolution for the (d—d) neutrons, including energy loss in the deuterium and the angular spread across the chamber, varies from 90 keV at 4.2 MeV to 55 keV at 8.2 MeV.

For the experiments the ionization chamber was filled with pure nitrogen or a mixture of nitrogen and argon. After filling, the chamber was placed at a distance of 30 or 40 cm from the neutron source at 0° to the accelerator beam such that the mean direction of the incident neutrons was perpendicular to the cylinder axis and centered vertically between the top plate and grid (see fig. 1). No attempt was made to collimate the neutrons. Directly behind the ionization chamber at one meter from the target, a long counter was positioned for the purpose of monitoring the neutron flux. The long counter was constructed according to the Hanson and McKibben [21]) recipe, except that the BF_3counter used was of thin walled copper 1 inch in diameter with a sensitive volume 12 inches long without Ceresin around it.

Experiments were carried out with a number of different fillings of nitrogen and a nitrogen-argon mixture. Two runs, one covering the neutron-energy range 1.3 to 4.2 MeV and one covering the range 4.2 to 8.2 MeV, were made with the chamber filled to 6 atmospheres with spectroscopic nitrogen. One run for observing only the (n, α) reaction was made with 2 atmospheres of high purity commercial nitrogen in the chamber and covering the neutron energy range 1.8 to 5 MeV. Data were taken between 1.3 and 1.8 MeV with a $Li^7(p, n)Be^7$ source and a chamber filling of 2 atmospheres of nitrogen and 4 atmospheres of argon. The threshold for the neutron disintegration of argon is 2.6 MeV [22]) and so the argon gave no contribution. Experiments with this nitrogen and argon mixture were also carried out at a neutron energy of 7.2 MeV. The neutron reaction cross section in argon is about 100 times less than for nitrogen at this energy.

The pulses produced in the ion chamber by the neutron induced disintegrations were fed into a "cascode" preamplifier [23]) which consisted of a negative feedback ring of three 6AK5 electron tubes with a cathode follower output. This amplifier had a gain of about 50. The preamplifier output was further amplified by a linear amplifier with a 0.5 megacycle bandwidth. The pulses as seen on the output of this amplifier had a rise time of 3 μs. The total gain of the

system was about 10^5. The pulse-height spectrum was displayed on either a 20-channel analyzer or a 256-channel analyzer.

A pulse-height spectrum obtained at a neutron energy of 1.5 MeV is given in fig. 2. The chamber filling was the nitrogen and argon mixture, and the pressure was 7.3 atmospheres. The group observed near channel 22 corresponds to protons from the disintegrations of N^{14} leading to the ground state of C^{14} and the lower group (channel 15) to alpha emission leaving B^{11} in its ground state. The tail below the peaks is caused by disintegrations occurring between the grid and collecting plate, which give a continuous distribution in pulse size, and by the wall effects to be discussed later. The pulse-height resolution for this example

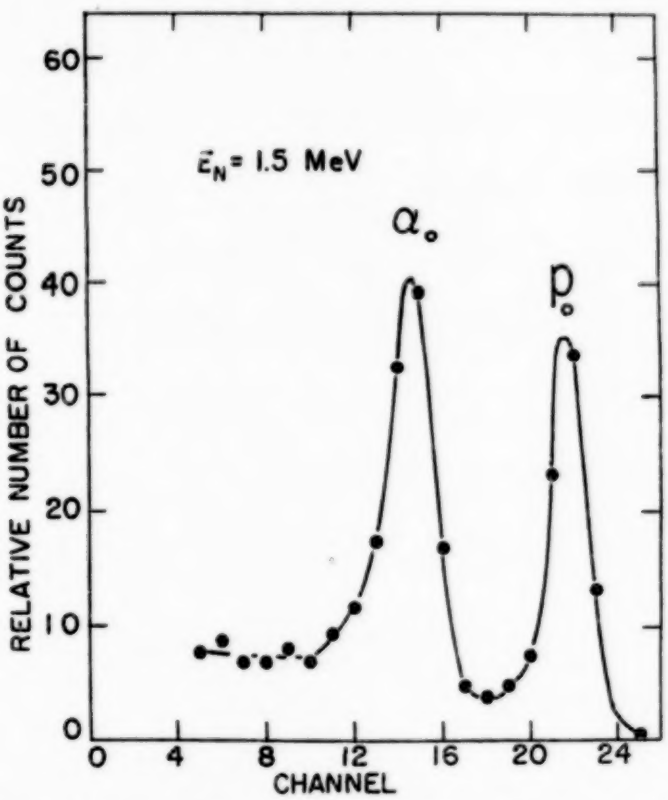

Fig. 2. Pulse-height spectrum from the disintegration of nitrogen by 1.5-MeV neutrons.

(fig. 2) was 9 % for the proton-group and 16 % for the alpha-group. The poorer resolution with alpha particles is thought to be caused by the larger columnar recombination along the more dense alpha track. The resolution for the alpha group improves rapidly with decreasing pressure.

Fig. 3 shows a pulse-height distribution taken at a neutron energy of 7.2 MeV with a nitrogen and argon filling and a total pressure of 5 atmospheres. The resolution is about 10 %. The peaks in the figure are labeled α_0, α_1, α_2 and α_3 to denote alpha disintegrations leading to the ground state and first three excited of B^{11} and the peak labeled T_0 corresponds to the group of tritons leading to the ground state of C^{12}. The sharp rise in the number of counts just

below channel 50 and at channel 20 is produced by the nitrogen and argon recoils respectively.

The peak in fig. 3 attributed to α_3 corresponds to about the same pulse size as would be expected from the group of protons leaving C^{14} in its first excited state or from the (n, d) reaction producing C^{13} in the ground state. In order to determine the composition of this peak, the change in the pulse-height spectrum obtained with 8.0-MeV neutrons was observed as a function of the gas pressure in the chamber. The pressure was varied so as to produce a change of 50 %, 45 % and 7 % respectively for the wall-loss of protons, deuterons, and the third group of alpha particles. This experiment showed that the sum of cross

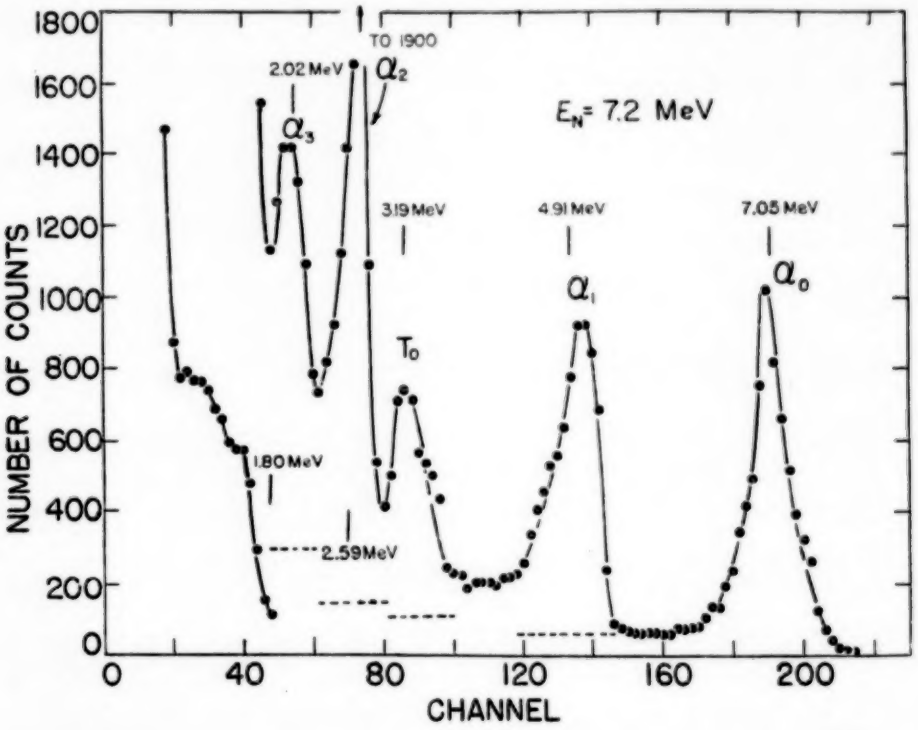

Fig. 3. Pulse-height spectrum from the disintegration of nitrogen by 7.2-MeV neutrons. The dotted lines are the backgrounds subtracted from the groups under which they are drawn.

sections for (n, p_1) and (n, d) for 8.0-MeV neutrons was less than 15 mb to be compared with 50 mb for the (n, α_3) cross section.

Factors which distort the pulse-height spectra and therefore influence the pulse-height resolution are: (1) electron attachment, (2) columnar recombination, and (3) electronic noise. Electron attachment, as the term implies, occurs when the primary electrons attach themselves to neutral gas molecules forming heavy negative ions which migrate very slowly in the collecting field. The loss in the size of the electron pulse produced by this effect depends upon the migration distance of the electrons before collection. Since the ionizing events are uniformly distributed throughout the chamber volume, attachment adver-

sely affects pulse-height resolution. Since nitrogen attaches electrons to a very small extent, the impurities (e.g. O_2 and H_2O) which the gas picks up during filling and which outgas from the chamber walls are responsible for electron attachment. To avoid contaminating gases in the nitrogen, the chamber was filled through a liquid air trap after the chamber had been pumped to a vacuum of 10^{-6} cm of Hg for several hours. In spite of these precautions the pulse-height resolution deteriorated steadily after filling, going from 6 % to 20 % in a period of two weeks. Presumably, this deterioration was caused by outgassing of the walls of the chamber. It was found that the best procedure for obtaining good pulse-height resolution was to fill the chamber with a fresh supply of high purity gas just before each run of duration from one to three days.

Columnar recombination (i.e. recombination of positive and negative ions along the charged particle track) increases as the density of ionization in the ion track increases. Because of this, the effect is more serious for high pressures of counting gas and for very densely ionizing particles. Recombination is more probable when the tracks are parallel to the collecting field than when they are perpendicular. Measurements of the line broadening produced by columnar recombination were made for a mixture of nitrogen and argon. Increasing the chamber pressure from 3 atmospheres to 7 atmospheres increased the line width of a 1.5-MeV alpha group by 10 % (see fig. 2). Further increase of pressure to 10 atmospheres produced a 50 % increase in line width. This effect could be definitely attributed to recombination because the proton line width did not increase nearly as much with pressure. If electron attachment had been responsible for the observed broadening of the alpha group, then the proton group would have been broadened the same amount.

The pulse size produced by electronic noise was about 10 % of the alpha pulse size in the worst case (i.e. at 1.3-MeV neutron energy).

The "wall-effect" is produced by particles whose tracks cross the boundary of the sensitive volume of the chamber or strike the high voltage electrode. Pulses corresponding to such tracks will not be counted in the energy group to which they belong and therefore represent a loss of counts, for which a correction must be made for computation of the cross section from the integral of the counts under the peaks. The fraction of the disintegrations lost in this way increases with the track length of the particles. For track lengths short compared to the dimensions of the sensitive volume of the chamber, the probability that a track will cross the boundary is approximately

$$\rho = \frac{r_0}{2}\left(\frac{1}{R} + \frac{1}{h_1}\right) \tag{1}$$

where r_0 is the track length, R is the radius of the sensitive volume, and h_1 is the height. For particle ranges greater than 1.4 cm, the wall-effect was measured experimentally by observing the protons from the $N^{14}(n, p)C^{14}$

reaction at several different pressures. This experiment was carried out at a neutron energy of 1.5 MeV. The amount of nitrogen in the chamber was kept constant at 1.3 atmospheres, and the pressure was increased successively by adding argon in 10-pound steps until a pressure of 10.7 atmospheres was reached.

Results for the wall-loss ρ versus track length, are given in fig. 4. The portion of the curve below a track length of 1.4 cm was calculated from eq. (1). To obtain

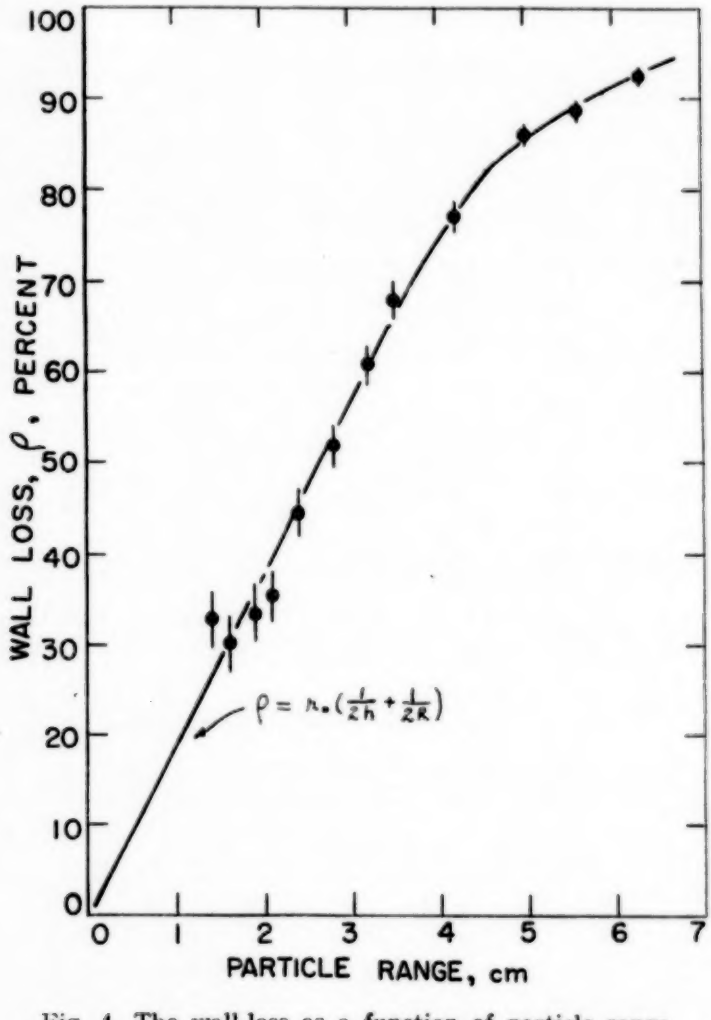

Fig. 4. The wall-loss as a function of particle range.

the correct number of disintegrations in each group for each neutron energy, the integrals of the peaks were divided by their respective efficiencies $(1-\rho)$ taken from fig. 4.

The scattering and absorption of neutrons by the chamber was measured by experiment. With the long counter at 0° to the accelerator beam and directly behind the chamber position and 1 metre from the target, the number of counts was 12 % less with the chamber in place than when the chamber was removed. This "attenuation" of the neutron flux was constant to within 2 % throughout

the range of energies covered in the experiments. It was assumed that half (6 %) of the flux attenuation occurred in the steel wall of the chamber pressure vessel nearest the neutron source. Therefore, the counts recorded in the long counter were increased by 6 % for the determination of the absolute cross section.

3. Data Analysis and Results

The number of disintegrations associated with each particle group was calculated from the pulse-height distributions similar to those shown in figs. 2 and 3. The integral of each peak was corrected for the background produced by particle groups of larger pulse size (see fig. 3). The correction to the data for the wall-loss was taken from fig. 4. The maximum wall-loss in the experiment was 72 % for 4.2 MeV protons in 6 atmospheres of nitrogen. Wall-losses of alpha particles never exceeded 29 %. The absolute neutron flux was determined by comparison of the number of counts obtained at each neutron energy with that observed when a Ra-Be source was placed one metre from a long counter. The number of counts was corrected for the relative efficiency of the long counter as a function of neutron energy, using the data of Allen and Ferguson [24]), and Perry *et al.* [25]). A correction of 6 % was made to allow for the attenuation of neutrons scattered by the ion-chamber pressure vessel.

Since the Li^7(p, n)Be^7 neutron source is not monoenergetic above a neutron energy of about 650 keV, a small correction for the second group of neutrons was made for the run made with this source ($1.3 < E_n < 1.8$ MeV). The second group of neutrons is 10 % as large as the main group in this energy range [26]).

The excitation function for the (n, p) reaction was not measured above a neutron energy of 4.2 MeV because of the large wall-loss above this energy. Wall-loss corrections for the protons ranged from 30 % to 72 % between 1.3 and 4.2 MeV, while the corresponding corrections for the most energetic alpha group did not exceed 29 % up to a neutron energy of 8.2 MeV.

Alpha disintegrations leaving B^{11} in its first three excited states at 2.14, 4.46 and 5.03 MeV were observed at the higher neutron energies. The cross section for each of these reactions is comparable to that for disintegration to the ground state of B^{11} above a neutron energy of 7 MeV. The reaction N^{14}(n, t)C^{12}, becomes energetically possible above 4.3 MeV and was observed in the experiment above a neutron energy of 5.6 MeV.

The cross sections for the disintegration of N^{14} leading to the emission of charged particles are plotted in figs. 5 and 6. Neutron energy resolution is indicated by the triangles.

The excitation function of the various modes of decay show many resonances with varying widths. Bonner *et al.* [16]) have studied the inverse reaction $B^{11}(\alpha,$

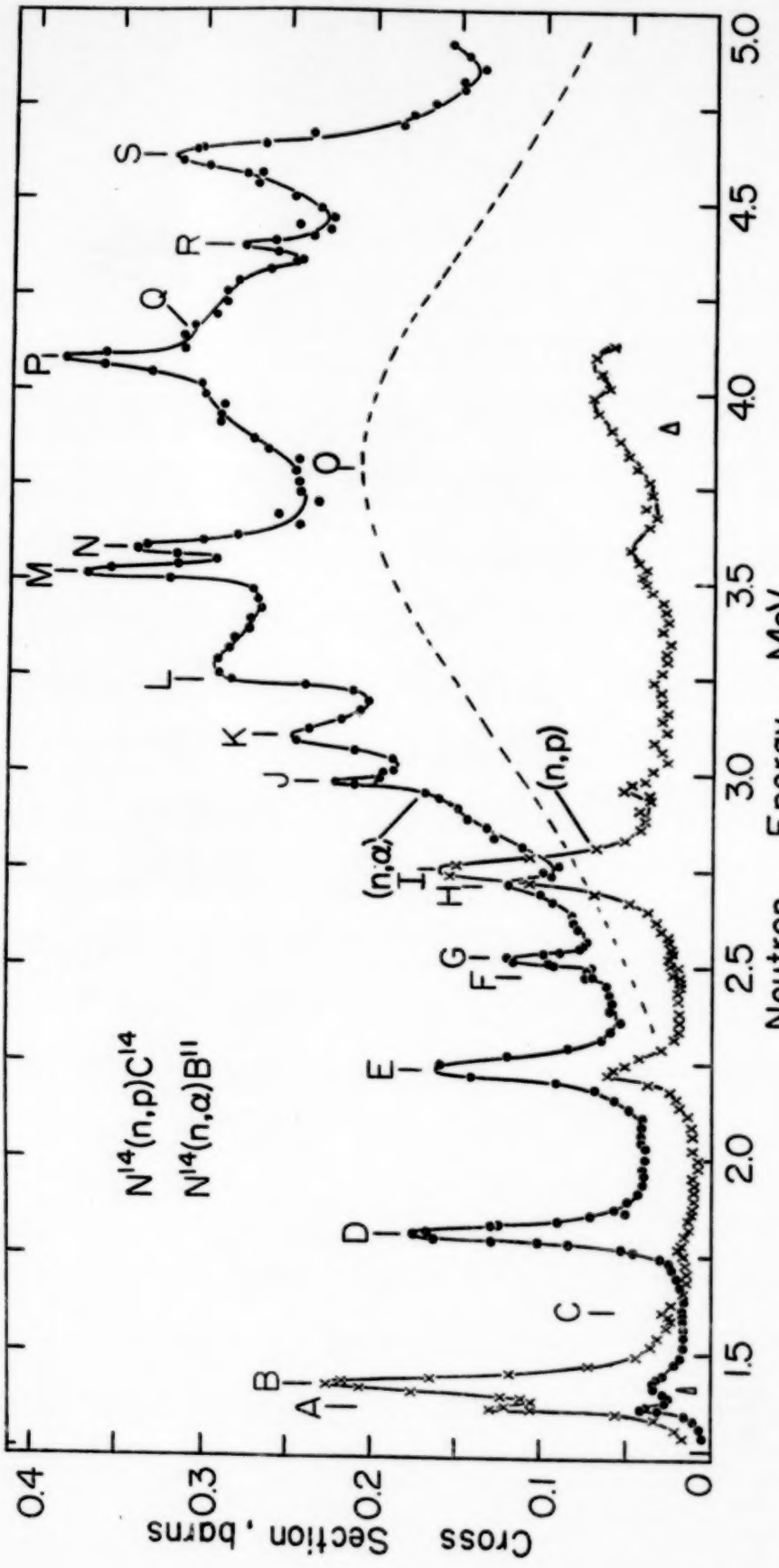

Fig. 5. Cross section for the (n, p) and (n, α) disintegrations of nitrogen leading to the ground states of C^{14} and B^{11} respectively.

n)N^{14} from just below the resonance marked D in fig. 5 through resonance P and have observed the same resonances which we observed in this energy region. These authors studied the resonances designated F and G with an alpha-energy resolution of approximately 3 keV and found that these resonances have widths of < 3 and ≈ 7 keV respectively. The broad change in the cross section which

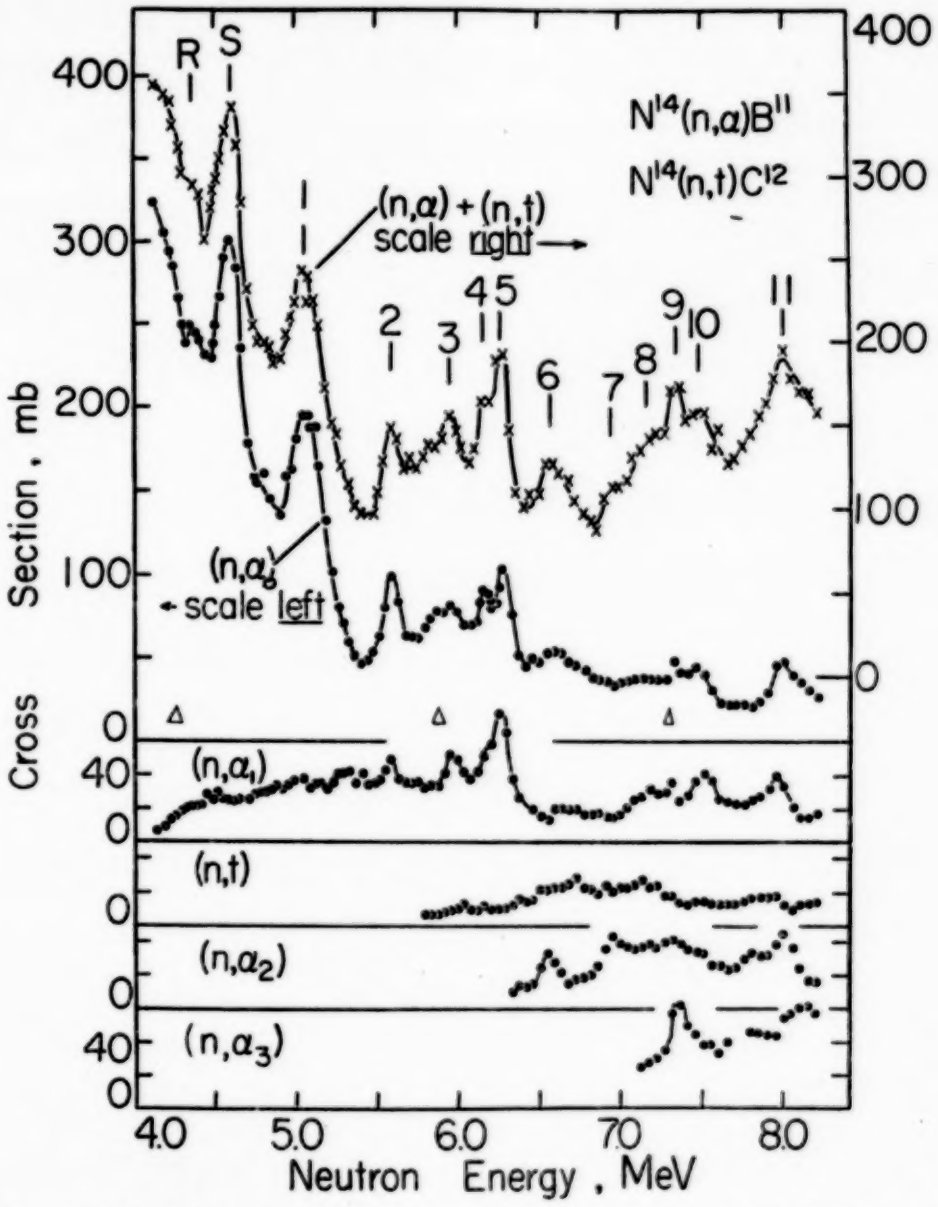

Fig. 6. Cross sections for the (n, α) and (n, t) disintegrations of nitrogen. The (n, α_3) cross section includes any (n, d) or (n, p) reactions which occur.

we have attributed to a resonance centered at approximately 3.8 MeV and labeled O in fig. 5 was also seen by these investigators.

The peaks designated by H and I in fig. 5 have experimental half widths of 40 keV and 95 keV respectively; they appear to correspond to different reson-

ances, one of which is shown much more strongly in the (n, p) reaction while the other is stronger in the (n, α) reaction. This view is substantiated by the data of Bonner *et al.* [16]) who measured the width of the resonance H in the inverse reaction $B^{11}(\alpha, n)N^{14}$ and found it to be 25 keV which is about $\frac{1}{3}$ as wide as the resonance I of fig. 5. Lee and Schiffer [27]) have also observed the resonances corresponding to H and I in the reaction $B^{11}(\alpha, p)C^{14}$.

TABLE 1

Resonances in the reactions $N^{14}(n, \alpha)B^{11}$ and $N^{14}(n, p)C^{14}$; 1.3 to 5.0 MeV

Resonance	Neutron energy (MeV)	σ_{α_0} [c]) (mb)	σ_{p_0} (mb)	N^{15*} (MeV)	Γ (keV)	Angular momentum and parity
A	1.35	41	75	12.10	20	$\frac{5}{2}^{\pm}$ [a])
B	1.41	35	220	12.15	56	$\frac{3}{2}^{\pm}$ [a])
C	1.61	<4	13	12.34	23	$\frac{1}{2}^{\pm}$ [a])
D	1.80	174	<5	12.51	50	$\frac{5}{2}^{+}$ [a, b])
E	2.23	139	61	12.92	70	$\frac{3}{2}^{-}$ [a, b])
F	2.47	20	<4	13.14	<3 [d])	
G	2.52	63	<4	13.18	≈7 [d])	
H	2.71	46	<10	13.35	40	$\frac{3}{2}^{-}$ [b])
I	2.74	<10	149	13.40	95	$\frac{5}{2}^{+}$ [b])
J	2.97	80	30	13.61	≈20	$(\frac{5}{2}^{-})$ [b])
K	3.09	85	15	13.72	60	
L	3.23	≈110	15	13.84	≈70	
M	3.51	120	24	14.11	≈20	
N	3.58	100	24	14.17	35	
O	≈3.8	200	40	14.37	≈2000	
P	4.08	87	23	14.64	50	
Q	≈4.1	75	30	14.66	≈300	
R	4.38	59	—	14.92	40	
S	4.61	140	—	15.13	complex	

[a]) These are the assignments of refs. [12]) and [28]).

[b]) These data from ref. [27]) whose data indicate that the 12.92 level is a doublet (see text). Parentheses indicate tentative assignments.

[c]) These σ's are the total reaction cross sections which proceed through the channel indicated by the subscripts. The σ given for each resonance is the change in the cross section due to resonance or the resonant cross section.

[d]) Widths from ref. [16]).

Interference between the broad level at 3.8 MeV and the resonance at a neutron energy of 3.23 MeV is indicated by the shape of the (n, α) excitation curve. The data of Bonner *et al.* [16]) from the $B^{11}(\alpha, n)N^{14}$ reaction clearly show this interference.

The work of Haddad *et al.* [17]) on the $B^{11}(\alpha, n)N^{14}$ differential cross section at 0° shows that resonance S at 4.6 MeV is made up of two narrow resonances at 4.5 and 4.6 MeV.

The $N^{14}(n, t)C^{12}$ reaction cross section is about as large as the cross section for any one of the alpha groups above a neutron energy of 6 MeV. The (n, t)

excitation curve does not show a resonant structure to as marked an extent as do the (n, α) excitation curves. This behavior is suggestive of a direct interaction process as an explanation for the triton emission, but the accuracy of the data is not sufficient to allow definite conclusions in this regard.

The positions, widths, and peak cross sections of the resonances observed in the disintegration of N^{14} by neutrons are listed in the tables 1 and 2. Resonance

TABLE 2

Resonances in the reaction $N^{14}(n, \alpha)B^{11}$; 4.8 to 8.2 MeV

Resonance	Neutron energy (MeV)	σ_{tot} [a] (mb)	σ_{α_0} (mb)	σ_{α_1} (mb)	σ_{τ_0} (mb)	σ_{α_2} (mb)	σ_{α_3} (mb)	N^{15*} (MeV)	Γ (keV)
1	5.06	110	100	$\approx$10	—	—	—	15.55	complex
2	5.60	60	50	18	—	—	—	16.06	100
3	5.95	40	25	20	$\approx$5	—	—	16.38	complex
4	6.17	50	30	20	—	—	—	16.59	75
5	6.26	120	70	70	—	—	—	16.67	100
6	6.57	50	22	$\approx$10	$\approx$10	25	—	16.95	complex
7	6.94	$\approx$30	—	—	—	$\approx$30	—	17.31	—
8	7.16	$\approx$40	$\approx$10	$\approx$20	$\approx$10	$\approx$10	—	17.51	—
9	7.34	$\approx$50	$\approx$10	$\approx$10	—	$\approx$10	40	17.68	120
10	7.48	$\approx$40	$\approx$30	$\approx$30	$\approx$5	$<$10	$<$20	17.81	180
11	8.00	80	30	30	$\approx$10	40	—	18.30	250

[a] σ_{tot} is the sum of the cross sections for (n, α) and (n, t) reactions. The other σ's are the total cross sections for the charged particle channels indicated by the subscripts.

widths vary from less than 3 keV to 2 MeV. The spins and parities given in table 1 for the N^{15} levels are the assignments of Fowler and Johnson [28]), Bartholomew *et al.* [12]) and Lee and Schiffer [27]). Preliminary data of the latter authors from the study of the proton angular distributions from the $B^{11}(\alpha, p)C^{14}$ reaction, indicate that the 12.92-MeV level, E in fig. 5, is a doublet, one component of which has $J^\pi = \frac{3}{2}^-$ and the other $\frac{7}{2}^-$. Fowler and Johnson [28]) and Bartholomew *et al.* [12]) have made conflicting assignments of the parities to the first three levels listed in table 1 and these parities have been left indefinite in the tabulation.

There are a number of operations and corrections which contribute to the errors in the determination of the cross sections. These are: (1) the integration of each of the particle groups in the pulse-height distribution at each neutron energy, (2) the correction for the wall effects (3) measurement of the gas pressure in the ion chamber, (4) measurement of distances of the ion chamber and the long counter monitor from the source, (5) calibration of the long counter with the standard source and correction for the relative efficiency of the long counter as a function of energy, and (6) counting statistics. Of these sources of errors, (1), (2) and (5) are most important. While integration of the particle groups does not introduce appreciable inaccuracy for the p, α_0 and α_1 groups,

it becomes the major source of error in the T_0, α_2 and α_3 particle groups because of the necessity for subtracting large backgrounds produced by the higher energy groups as shown in fig. 3. It is estimated that the error in integration of these (T_0, α_2, α_3) groups is about ± 40 %. Because this error is large compared to the wall-effect for these particles, the wall-effect correction was not made to the T_0, α_2 and α_3 data.

Wall-effect corrections to the p, α_0 and α_1 groups were made assuming that the particle emission was isotropic in the center of mass. Errors in the particle track-length in the gas due to this approximation can be as large as 4 % for alpha particles whose angular distribution is strongly peaked backward or forward. This error will be less for protons. The absolute error in the correction for the wall-effect is about ± 20 %. The effect of this error on the cross sections depends upon the size of the correction.

The calibration of the long counter was made with a standard Ra-Be source † (± 4 %) using the data of Allen and Ferguson [24]) for the efficiency of the counter for Ra-Be neutrons. The relative long-counter efficiency [24, 25]) and the absolute calibration should be accurate to ± 15 %.

In addition to the other runs, three independent determinations of the absolute cross section for the (n, α) reaction were made at the resonance at a neutron energy of 1.8 MeV. The precision of these determinations was ± 2 %; however, this does not reflect the errors due to items (1), (2), and (5) listed above.

Based upon the above considerations, estimates of the probable errors in the excitation functions of figs. 5 and 6 are as follows. The error in the (n, α) cross section below 5 MeV is ± 20 %. The error in the (n, p) cross section increases from ± 20 % to ± 30 % between 1.3 and 4.2 MeV. The accuracy of the total reaction cross section leading to particle emission between neutron energies of 4.0. and 8.2 MeV is ± 30 %. In this same energy range the (n, α_0) and (n, α_1) cross sections for the T_0, α_2 and α_3 groups are accurate to about $\pm$ 40 %. Relative errors in the data are somewhat less than these absolute error estimates.

5. Discussion of Results

The excitation functions for the C^{14}(p, n)B^{11} and the B^{11}(a, n)N^{15} reactions were calculated from the data obtained in the present experiment by the principle of detailed balance. Results of this calculation for the(p, n) reaction are shown in fig. 7 together with the direct measurements of Gibbons and Macklin [13]). The agreement between the measured and calculated values is seen to be good over the entire energy range. Fig. 8 shows the calculated excitation

† *Note added in proof:* Calibration of the long counter with a standard Pu—Be source indicates an efficiency that is 19 % greater, and cross sections which are larger by this same amount.

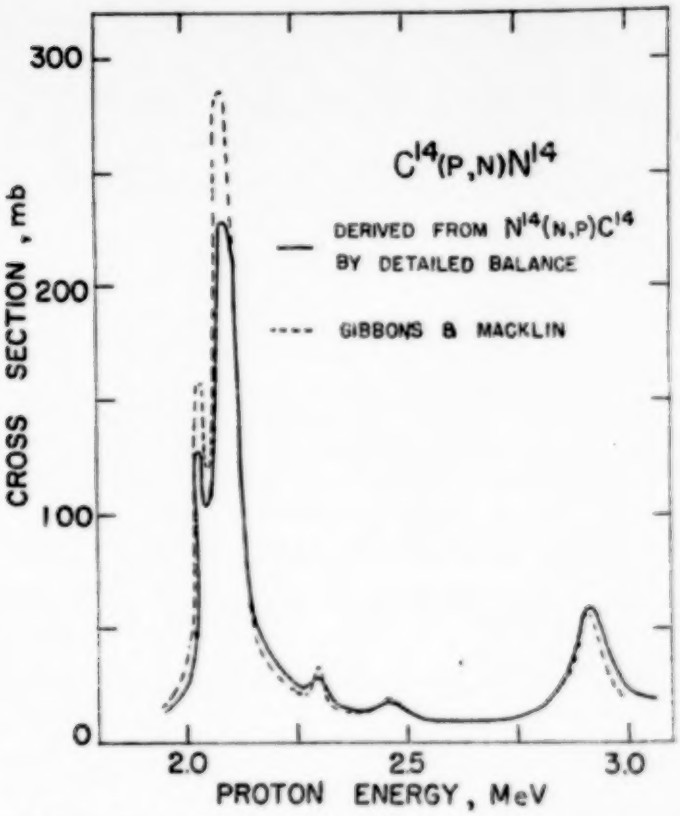

Fig. 7. Comparison of the $C^{14}(p, n)N^{14}$ cross section calculated from detailed balance with direct measurements.

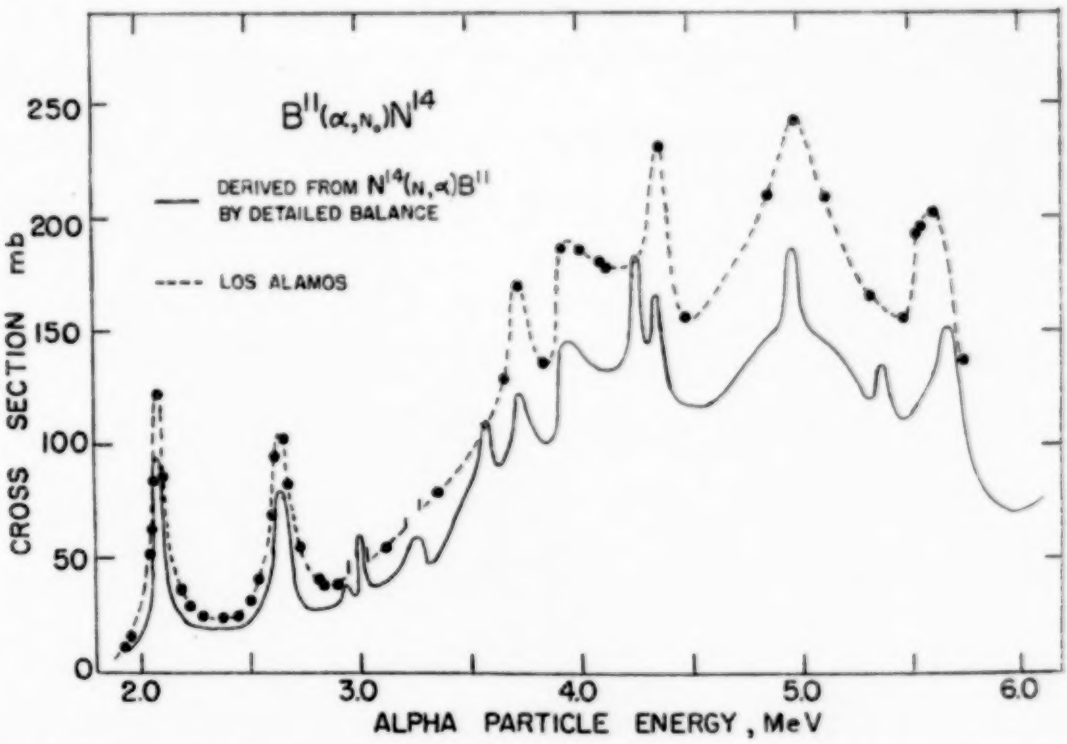

Fig. 8. Comparison of the $B^{11}(\alpha, n)N^{14}$ cross section calculated from detailed balance with direct measurements.

curve of $B^{11}(\alpha, n)N^{14}$ for the group of neutrons leaving N^{14} in the ground state, plotted with the experimental measurements of the Los Alamos group [17]) for this reaction. The cross section of the (α, n) reaction as calculated by detailed balance is generally about 25 % lower than the direct measurements. This difference is within the estimated error of the experiments.

The excitation curves of figs. 5 and 6 exhibit some rather interesting features: the general predominance of the cross section for alpha emission over that for proton emission from the N^{15} compound system and the relatively large cross section observed for the (n, t) process above the threshold for this reaction.

There are no selection rules which prohibit the disintegration of the compound nucleus, N^{15}, into either $C^{14}+p$ or $B^{11}+\alpha$. Since the energy of the protons is 0.75 MeV greater than that of the alpha particles, and the spins of the residual nuclei differ by only one unit, competition between the two modes of disintegration is expected for all levels of N^{15} observed in this experiment. Furthermore, the shell model [29]) would predict that proton emission should be an order of magnitude more probable than alpha emission since the N^{15} nucleus contains many protons and only an occasional alpha particle would appear at the nuclear surface.

The experimental data are in definite disagreement with shell-model expectations. The (n, α) cross section exceeds the (n, p_0) cross section at eleven of the fifteen resonances observed in the cross sections between 1.3 and 4.2 MeV. At three of these resonances corresponding to excitation energies of 12.51, 13.14 and 13.18 MeV in N^{15}, alpha emission is at least twenty times more probable than proton emission. At the broad resonance near 3.8 MeV the emission of alpha particles is about five times more probable than proton emission.

The partial widths and partial reduced widths, $\gamma^2 = \Gamma/2P_l$, for neutron, proton, and alpha emission for seven of the states in N^{15} were calculated and are given in table 3. Spins and parities, which are needed for the reduced width calculations, are not known for the remaining levels of N^{15} observed in this experiment. The neutron elastic scattering cross sections were obtained by subtracting the sum of the (n, α) and (n, p) cross sections observed in the experiment from the total neutron cross section. Inelastic neutron scattering is not energetically possible below 2.5 MeV, and its cross section is about two orders of magnitude less than the elastic scattering cross section below 4.0 MeV [30, 31]). Total neutron cross sections for the resonances below a neutron energy of 1.8 MeV were taken from the work of Hinchey *et al.* [32]). Less accurate data for the total cross section at the other resonances were obtained from BNL 325 (1958). The spin and parity assumed for each resonance is given in the table. Calculations of the reduced widths for the broad 3.8-MeV level are given for several different J^π assignments. The reaction radius R assumed for the neutron and proton channels was 4.8×10^{-13} cm, and that for the alpha channel was 5.3×10^{-13} cm. Penetrabilities $P_l = \rho/A_l^2$ were obtained from published

tables and graphs. The θ's are the ratios of the reduced widths to the Wigner limit, $\gamma_W^2 = \frac{3}{2}\hbar^2/\mu R^2$, for each channel. The Wigner limit is 2.90 MeV for the neutron and proton channels and 0.75 MeV for the alpha channel. With two exceptions, the value of the ratio θ for the alpha channel is greater than for the neutron or proton channels, regardless of the parity assumed for the first three levels.

These results show that these highly excited states of N^{15} definitely cannot be described by the shell model or, in fact, by any model in which the *individual*

TABLE 3

Resonance parameters for some excited states in N^{15}

E_n (MeV)	N^{15*} (MeV)	Assumed J	Γ_n (keV)	Γ_p (keV)	Γ_α (keV)	γ_n^2 (keV)	γ_p^2 (keV)	γ_α^2 (keV)	θ_n	θ_p	θ_α
1.35	12.10	$\frac{5}{2}^-$	19	0.8	0.4	15 [c]	57 [c]	50 [d]	0.005	0.020	0.067
		$\frac{5}{2}^+$				75	4.5	10	0.026	0.002	0.013
1.41	12.15	$\frac{3}{2}^-$	40	11	1.8	29	12	22	0.010	0.004	0.030
		$\frac{3}{2}^+$				17	55	45	0.006	0.019	0.060
1.61	12.34	$\frac{3}{2}^-$	21	0.2	<0.1	14	7	<3	0.005	0.002	<0.004
		$\frac{3}{2}^+$				55	0.8	<2	0.019	0.0003	<0.003
1.80	12.51	$\frac{5}{2}^+$	37	0.5	9.0	82	1.5	45	0.028	0.0005	0.060
2.23 [b]	12.92	$\frac{3}{2}^-$	39	7.8	18	20	5	19	0.007	0.002	0.025
2.97	13.61	$\frac{5}{2}^-$	16	1.1	3.2	7	8	4	0.002	0.003	0.006
3.8	14.4	$\frac{1}{2}^-$	1×10^3	2×10^2	1×10^3	310	83	580	0.11	0.03	0.78
		$\frac{3}{2}^-$				310	83	290	0.11	0.03	0.39
		$\frac{5}{2}^+$				550	160	360	0.19	0.06	0.49

[a]) Explanation of the symbols: The Γ's are the partial widths for each channel in the centre-of-mass system; $\gamma^2 = \Gamma/2P_l$ is the reduced width where P_l is the penetration factor defined by $\rho/(F_l^2+G_l^2)$; the ratio of γ^2 to the Wigner limit is designated by θ.

[b]) This level may be a doublet; see footnote [b]), table 1.

[c]) The interaction radius assumed for the neutron and proton channels was 4.8×10^{-13} cm.

[d]) The interaction radius assumed for the α channel was 5.3×10^{-13} cm.

nucleons are pictured as moving about each other in some fashion. They suggest rather that the nucleons composing the levels tend to form rather strongly bound groups of nucleons (e.g. alpha particles or tritons) which then share the excitation energy of the compound nucleus. This conclusion is supported by the relatively high cross section observed for triton emission above the threshold for this reaction.

Another example where the (n, α) cross section is greater than the (n, p) cross section has been found in this laboratory by Marion and Brugger [33]). They found that the F^{19}(n, α) cross section is greater than the (n, p) cross section by a factor of 2 or 3 over a neutron energy region of 6.5 to 8 MeV.

One of us (F. G.) wishes to thank the Texas Company for the grant of a fellowship during the progress of this work.

References

1) N. Feather, Proc. Roy. Soc. A **136** (1932) 709; **142** (1933) 689
2) F. Ajzenberg and T. Lauritsen, Revs. Mod. Phys. **27** (1955) 77
3) C. H. Johnson and H. H. Barschall, Phys. Rev. **80** (1950) 818
4) W. Bollman and W. Zünti, Helv. Phys. Acta. **24** (1951) 517
5) A. Stebler and P. Huber, Helv. Phys. Acta. **21** (1948) 59
6) W. Stetter and W. Bothe, Z. Naturforschg. **6a** (1951) 61
7) G. von Gierke, Z. Naturforschg. **8a** (1953) 567
8) A. B. Lillie, Phys. Rev. **87** (1952) 716
9) Roseborough, McCue, Preston and Goodman, Phys. Rev. **83** (1951) 1133
10) Shoupp, Jennings and Sun, Phys. Rev. **75** (1949) 1
11) R. M. Sanders, Phys. Rev. **104** (1956) 1434
12) Bartholomew, Brown, Gove, Litherland and Paul, Can. J. Phys. **33** (1955) 441
13) J. H. Gibbons and R. L. Macklin (to be published)
14) Hornyak, Lauritsen, Morrison and Fowler, Revs. Mod. Phys. **22** (1950) 291
15) R. E. Trumble, Phys. Rev. **94** (1954) 748A
16) Bonner, Kraus, Marion and Schiffer, Phys. Rev. **102** (1956) 1348
17) E. Haddad, Los Alamos, private communication
18) H. Alfvén, Nature **136** (1935) 70, 394
19) Buneman, Cranshaw and Harvey, Can. J. Phys. A **27** (1949) 191
20) E. Segrè, Experimental Nuclear Physics. (John Wiley & Sons, Inc., Vol. 1, New York, 1952) p. 287
21) A. O. Hanson and J. L. McKibben, Phys. Rev. **72** (1947) 673
22) E. H. Bellamy and F. C. Flack, Phil. Mag. **46** (1955) 341
23) Harvey, Jackson, Eastwood and Hanna, Can. J. Phys. **35** (1957) 258
24) W. D. Allen and A. T. G. Ferguson, Proc. Phys. Soc. A **70** (1957) 639
25) Perry, Haddad and Smith, Published in Progress in Nuclear Energy, Series I, Vol. II, chapter by W. D. Allen and R. L. Henkel (Pergamon Press, New York, 1958)
26) L. Cranberg, Private communication
27) L. L. Lee and J. P. Schiffer, Phys. Rev. **115** (1959) 160
28) J. L. Fowler and C. H. Johnson, Phys. Rev. **98** (1955) 728
29) J. H. D. Jensen and M. Goeppert-Mayer, The Elementary Theory of Nuclear Shell Model (John Wiley & Sons, Inc., New York, 1955)
30) Hugh E. Hall and T. W. Bonner, Nuclear Physics **14** (1959/60) 295
31) R. B. Day, Phys. Rev. **102** (1956) 767
32) Hinchey, Stelson and Preston, Phys. Rev. **86** (1952) 483
33) J. B. Marion and R. M. Brugger, Phys. Rev. **100** (1955) 69
34) F. Gabbard, H. Bichsel and T. W. Bonner, Comptes Rendus du Congrès International de Physique Nucléaire; Interactions Nucléaires aux Basses Energies et Structure des Noyaux (Dunod, Paris, 1959) p. 406

2.C *Nuclear Physics* **14** (1959/60) 295—313; © *North-Holland Publishing Co., Amsterdam*
Not to be reproduced by photoprint or microfilm without written permission from the publisher

GAMMA RADIATIONS FROM INELASTIC SCATTERING OF FAST NEUTRONS IN C^{12}, N^{14} AND O^{16}

H. E. HALL and T. W. BONNER
The Rice Institute, Houston, Texas †

Received 17 August 1959

Abstract: Measurements have been made of the cross section for the production of 4.43-MeV γ-radiation by the inelastic scattering of neutrons by C^{12}. The experiments have been carried out using monoenergetic neutrons with energies of from 4.6 to 9.8 MeV. Ten resonances were observed in this energy range and the maximum cross section of 45 mb/sr was obtained at a neutron-energy of 8.1 MeV. Measurements made with an O^{16} scatterer also showed many resonances for the production of γ-radiation with energies of 6.14, 6.91 and 7.12 MeV. The maximum cross section for γ-emission was obtained with 9.1-MeV neutrons and amounted to 30 mb/sr. Population of the 6.06-MeV pair emitting state in O^{16} was not observed and an upper limit on the probability of exciting this state was less than 10 % of that for the excitation of the γ emitting states. Gamma radiations from the interaction of fast neutrons in N^{14} were observed with neutrons of energies from 4.7 to 8.1 MeV. Gamma radiations with energies of 1.64, 2.14, 2.31, 4.46 and 5.06 MeV were observed. Approximately half of the cross section for the production of γ-radiation is from the $N^{14}(n, \alpha)B^{11*}$ reaction and the rest is from inelastic scattering in N^{14}. At a neutron energy of 7.3 MeV the cross section for the $N^{14}(n, n'\gamma)N^{14}$ reaction, including cascades, is 16.2 mb/sr and the cross section of the $N^{14}(n, \alpha)B^{11*}$ reaction leading to the first three excited states is 10.7 mb/sr.

1. Introduction

Gamma radiation from the inelastic scattering of neutrons in C^{12} and O^{16} has been observed by Thompson and Risser [1]) using 14-MeV neutrons. Battat and Graves [2]) have measured the cross section for the production of 4.43-MeV gamma radiation from inelastic scattering of 14-MeV neutrons in C^{12} using a three crystal spectrometer. Day [3]) has measured the cross section for the production of gamma radiation from C^{12} using 6.58-MeV neutrons, from O^{16} using 7.06-MeV neutrons, and from N^{14} using 3.95-MeV neutrons. The purpose of the present experiment was to measure the cross section for the production of gamma radiation from C^{12}, N^{14} and O^{16} as a function of neutron energy from threshold to a neutron energy of 10 MeV for C^{12} and O^{16}, and to 8 MeV for N^{14}. Since narrow resonances have been observed in the cross section for neutron scattering in this energy range, neutrons with a relatively small spread in energy are needed to obtain the true excitation curve.

† Supported in part by the U. S. Atomic Energy Commission; Preliminary reports of these experiments given in refs. [17]).

2. Experimental Procedure

The experimental arrangement for measuring the gamma radiation produced by neutron inelastic scattering made use of a ring scatterer and a NaI detector placed behind a shadow cone. A diagram of the apparatus is shown in fig. 1.

Neutrons inelastically scattered in the annular scatterer produce γ-radiations which, in the C^{12} and O^{16} experiment, were measured by a 1 inch $\times$ 1 inch NaI(Tl) crystal which had a resolution of less than 9 % for the 662-keV γ-radiation from Cs^{137}. In the N^{14} experiment, most of the data were taken using a 1 inch $\times$ 1 inch CsI crystal having approximately the same energy resolution. The pulses were then analyzed using a multichannel pulseheight analyzer. Neutrons in the energy range from 4.5 to 9.3 MeV were obtained from

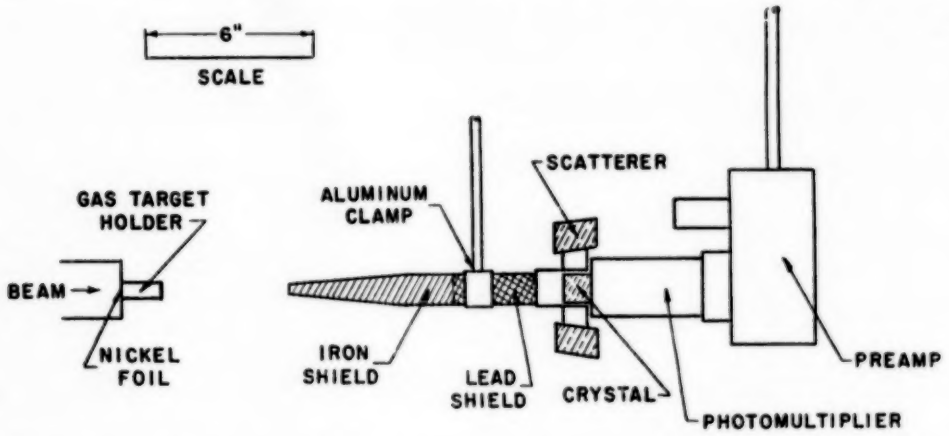

Fig. 1. Experimental arrangement for the measurement of γ-radiation from inelastic scattering.

the $H^2(d, n)He^3$ reaction using the deuteron beam from the 6 MeV Van de Graaff accelerator and a deuterium gas target. The front of the shielding cone was made of iron while the back was made of lead. For neutrons between 9.3 and 10.0 MeV, neutrons from the $Be^9(\alpha, n)C^{12}$ reaction were used, and in this case the entire shield was made of lead so that the 4.43-MeV gamma radiation from the Be^9 target would be almost completely absorbed.

In the C^{12} experiment the scatterer was made from a piece of Hanford graphite having a density of 1.50 g/cm^3. The dimensions of the scatterer were 0.87 inches thick in a radial direction, and 1.5 inches in a direction parallel to the beam. It was machined in the form of a truncated cone having a base O.D. of 4.5. inches and a top O.D. of 4.12 inches. For the experiment with O^{16}, the scatterer was water contained in a thin aluminium container having the same dimensions as the graphite scatterer. For the N^{14} experiment, the scatterer was Be_3N_2 contained in an aluminium and Mylar holder of the same dimensions as the graphite scatterer. The total weight of the empty holder was 10.6 g, 4.8 g of aluminium and 5.8 g of 0.001 inch thick Mylar tape. In the C^{12} and O^{16} experiments, the scatterer was placed around an aluminium guide

fastened to the shield. In the N^{14} experiment, the scatterer was suspended by two wires to reduce the background due to the aluminium.

When using the $H^2(d, n)He^3$ neutron source, the absolute value of the energy of the average neutron striking the scatterer was known to ± 25 keV. The principal source of this estimated error arises from non-uniformities in the 0.000 025-inch nickel foil, which introduces an uncertainty in the energy loss in the foil.

The energy spread of the neutrons impinging on the scatterer is due primarily to the loss in energy of the deuteron beam in the finite length of the gas target and the solid angle subtended by the scatterer. In the C^{12} experiment the calculated neutron energy spread at 4.8-MeV neutron energy due to the gas target length of 4.3 cm at a gas pressure of 0.2 atmospheres was 54 keV. The spread in energy due to the solid angle of the scatterer was 12 keV, giving a total calculated neutron spread of 66 keV at a neutron energy of 4.8 MeV. Above 6 MeV, the calculated energy spread was essentially constant at 55 keV. Data were also taken in the C^{12} experiment from 6.1 to 6.7-MeV neutron energy using a 28-inch target to scatterer spacing rather than the 14-inch spacing shown in fig. 1. With this geometry and with a lower gas pressure in the target the calculated energy spread of the neutrons was reduced to 31 keV.

In the O^{16} and N^{14} experiments a gas pressure of 0.33 atmospheres was used. This increased the spread due to the gas correspondingly and gives a total spread at 8.1 MeV of 62 keV.

When using the $Be^9(\alpha, n)C^{12}$ reaction as a neutron source, the absolute value of the energy of the average neutrons striking the scatterer is known to approximately ± 30 keV, and the total neutron energy spread due to the solid angle of the scatterer and the thickness of the Be^9 target was calculated to be 39 keV at a neutron energy of 9.5 MeV.

3. The Reaction $C^{12}(n, n'\gamma)C^{12}$

3.1. RESULTS

The cross section for the production of 4.43-MeV γ-radiation by neutron inelastic scattering in C^{12} as a function of neutron energy was obtained by observing the difference in the number of counts with the carbon scatterer in and out of position in those channels corresponding to electron energies from 3.0 to 4.5 MeV. Below a neutron energy of 4.85 MeV, which is the threshold for γ-radiation production, the scatterer produced a 15 % increase in the number of counts in these channels. This background is believed to be due to the effect of scattered neutrons in the NaI crystal and surrounding materials. Typical data with and without the scatterer is shown in fig. 2; the data were taken at a neutron energy of 7.88 MeV.

The absolute cross section for the production of the 4.43-MeV γ-radiation in

C^{12} was measured at 6.94-MeV neutron energy. This was done by comparing the number of counts in the 3.0—4.5-MeV electron energy range obtained with the carbon scatterer to those obtained from a calibrated RaD-Be neutron source placed at the same position as the ring of carbon. The intensity of the γ-radiation from the RaD-Be source was calculated from the measured value of 0.60 ± 0.06 γ-quanta per neutron [4]). A cross section of 14.6 ± 3.6 mb/sr at 90° was obtained by this method at a neutron energy of 6.94 MeV. Day [3]) has

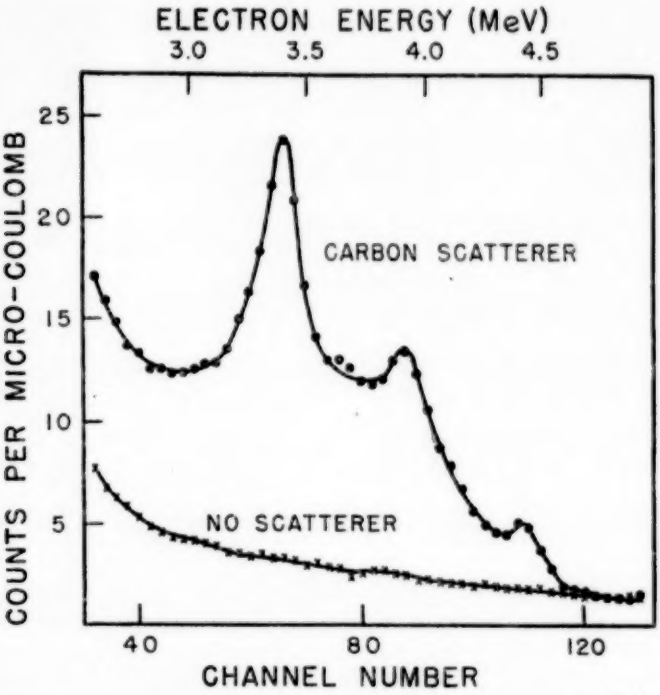

Fig. 2. Pulse-height distributions obtained with carbon scatterer and with no scatterer at a neutron energy of 7.88 MeV.

accurately measured this cross section at a neutron bombarding energy of 6.58 MeV as 28.1 ± 4.7 mb/sr at 95°. Using Day's result as a standard, the cross section at 6.94-MeV neutron bombarding energy was calculated to be 15.8 ± 2.6 mb/sr at 90°, which agrees with the first method within the estimated error. Since Day's value of the cross section is probably more accurate, our data have been normalized, using his value at 6.58 MeV. The absolute value of the cross section is thought to be correct to ±20 %.

The results of the C^{12} experiment are shown in fig. 3. The yield of γ-radiation increases sharply above the threshold at 4.83 MeV and rises to a maximum cross section of 45 mb/sr at the resonance of 8.15 MeV. The cross section of 20 mb/sr at 9.7 MeV is approximately the same as the value of 19.5 mb/sr which has been reported at 14 MeV [2]).

Since there were no total neutron cross section data for C^{12} between 7.0 and 8.1 MeV at the time this experiment was begun, a series of measurements was

carried out to determine these cross sections. The results are given in fig. 3 along with other measurements [5,6,7]) of the total cross section. There is considerable similarity in the resonances obtained in the total cross section and in those found for γ-emission. The main difference is that the 6.57-MeV resonance is very prominent for γ-emission but seems to appear as an anti-resonance in the total cross section. This shape of curve would be obtained if the neutrons which produce the resonance have $l = 1$, since a phase shift of about $-90°$ is expected

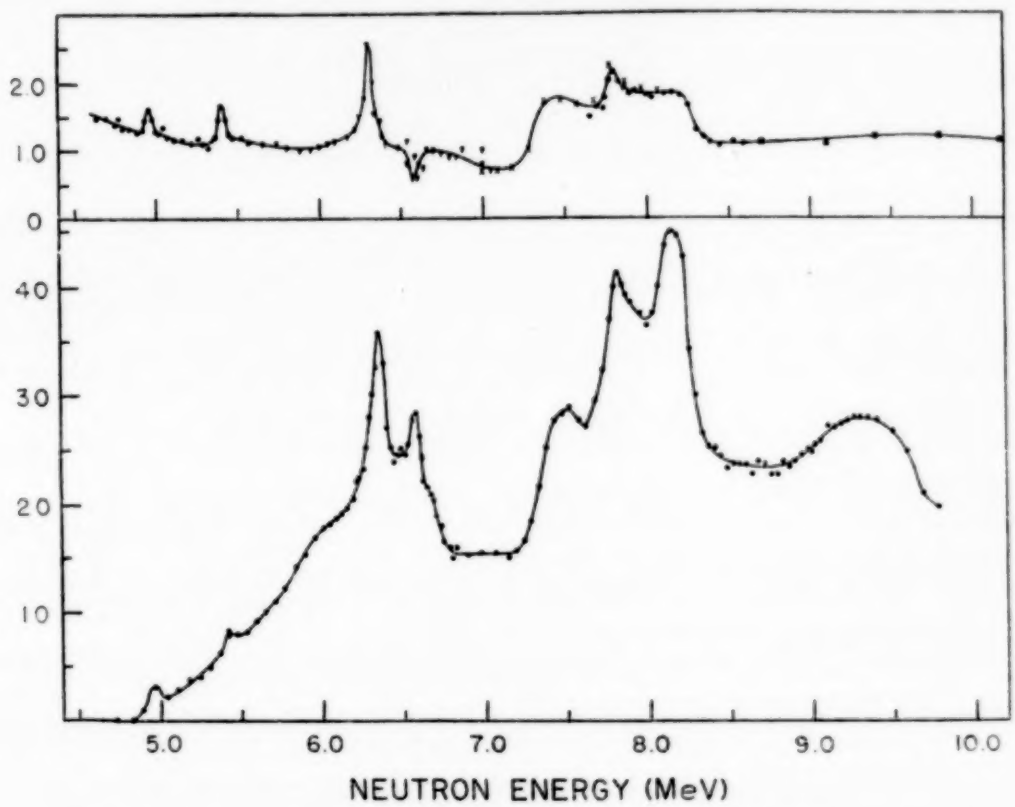

Fig. 3. Upper curve: total cross section for C^{13} (in b) versus neutron energy.
× Rice ● Becker & Barschall ▼ L. A. (unpublished) ■ Nereson
Lower curve: inelastic cross section for C^{12} (n, n'γ) C^{12} reaction, at 90°, in mb · sr^{-1}.

for hard sphere scattering of $l = 1$ neutrons in C^{12} at about this energy. Pertinent data on the resonances are given in table 1.

All the resonances which are apparent in the excitation curve of γ-radiation have been reported in other reactions except the one at a neutron bombarding energy of 5.98 MeV which corresponds to an excitation energy in C^{13} of 10.47 MeV. There are two levels known from other reactions which do not appear in the excitation curve. These levels in C^{13} at 12.08 and 13.41 MeV correspond to neutron bombarding energies of 7.70 and 9.17 MeV, respectively.

The predicted narrow resonance at a neutron energy of 9.17 MeV is quite prominent in the $Be^9(\alpha, n)C^{12}$ reaction [8]) but is much weaker in the $C^{12}(n, n'\gamma)$ reaction. The resonances at bombarding energies of 7.50 and 7.81 MeV give

TABLE 1

Data on the resonances in the $C^{12}(n, n'\gamma)C^{12}$ reaction

Energy of neutron (MeV)	Level width (keV)	Width other experiments (keV)	Excitation energy in C^{13}			
			$C^{12}(n, n', \gamma)$[e] (MeV)	Total cross (MeV)	$B^{11}(He^3, p)$ (MeV)	$Be^9(\alpha, n)$ (MeV)
4.96	<80	<10 [a]	9.53	9.53 [b]	9.52 [a]	
5.42	<80	<10 [a]	9.95	9.93 [b]	9.90 [a]	
5.98	200		10.47			
6.35	120		10.81	10.78 [a]	10.9 [a]	
6.57	<80		11.01			11.02 [d]
6.65	<80	Narrow [d]	11.09			11.08 [d]
7.50	260	200 [g]	11.87	11.87 [e]		11.96 [f,g]
		Broad			12.08 [a]	12.06 [f]
7.81	180	200 [g]	12.16	12.15 [b,e]		12.23 [f,g]
8.14	220	200 [g]	12.46	12.50 [b]		12.46 [f,g]
		60 [g]				13.41 [f,g]
9.31	500	400 [g]	13.54			13.6 [f,g]

[a]) C. D. Moak, A. Galonsky, R. L. Traughber and C. M. Jones, Phys. Rev. **110** (1958) 1369; T. E. Young, Doctoral Thesis, The Rice Institute (1958)

[b]) See ref. [5])

[c]) See ref. [7])

[d]) W. E. Bennett, P. A. Roys and B. J. Toppell, Phys. Rev. **93** (1954) 924A

[e]) Present Experiment

[f]) J. R. Risser, J. E. Price and C. M. Class, Phys. Rev. **105** (1957) 1288

[g]) T. W. Bonner, A. A. Kraus, J. B. Marion and J. P. Schiffer, Phys. Rev. **102** (1956) 1348

excitation energies which are 90 and 70 keV, respectively, lower than those indicated by the $Be^9(\alpha, n)$ reaction when the ground state neutrons are observed (table 1, ref. [f])). However, since these are broad states, the effect of the Coulomb barrier would be to displace the peak of the resonances in the α-particle reaction to higher energies.

3.2. DISCUSSION

The observed threshold for γ-radiation at 4.83 MeV corresponds to an excitation energy in C^{12} of 4.46 MeV which agrees well with the known energy of this state [9]).

The variation in the cross section as a function of energy depends upon the competing reactions as well as the nature of the resonances in the compound nucleus. The two known competing reactions are the $C^{12}(n, \alpha)Be^9$ reaction which has a threshold for 6.17-MeV neutrons and the $C^{12}(n, 3\alpha)$ reaction which has a threshold for 7.89-MeV neutrons. From knowledge of the inverse reaction $Be^9(\alpha, n)C^{12}$, the cross section for the reaction $C^{12}(n, \alpha)Be^9$ is small below a neutron energy of 7.2 MeV. In the region of 8 to 10 MeV the cross section of this reaction, as calculated by the method of detail balance, should vary from 0.8 to 10 mb/sr. The cross section of the $C^{12}(n, 3\alpha)$ reaction has been reported [10])

to be 35 ± 20 mb/sr at 10.0 MeV, with an observable threshold at approximately 8 MeV.

There is no simple theory applicable for inelastic scattering in a nucleus as light as carbon. However, one may qualitatively present some arguments on the magnitude of the cross section using the compound nucleus theory. From this theory one would expect that well above threshold the total cross section would be made up of approximately 50 % elastic scattering, 25 % compound elastic scattering, and 25 % inelastic scattering where only one excited state can be formed and no disintegrations are being produced. The experimental cross section for gamma production, assuming an isotropic distribution of the inelastically produced gamma radiation, varies between 25 % and 30 % of the total cross section for neutrons with energies from 6.5 to 9.5 MeV and drops to 21 % at 9.7 MeV. This would indicate that the competing reactions have a relatively minor effect over most of the energy range covered in this experiment.

4. The Reaction $O^{16}(n, n'\gamma)O^{16}$

4.1. RESULTS

The study of the γ-radiation from inelastic scattering in O^{16} is complicated by the fact that three γ-radiation emitting states with energies of 6.14, 6.91 and 7.12 MeV are present. Table 2 gives the known properties of the levels in O^{16}.

TABLE 2

States of O^{16}

Energy of level (MeV)	Angular momentum and parity
Ground State	0^+
6.06	0^+
6.14	3^-
6.91	2^+
7.12	1^-
8.88	2^-

All the excited states may decay with γ emission with the exception of that at 6.06 MeV which decays by nuclear pair emission. It is known also that the 8.88-MeV state decays principally through a cascade to the 6.14-MeV level and therefore only very weak γ-radiation of 8.88 MeV would be expected.

Near the threshold weak γ-radiation is more easily detected by a different technique in the presence of the continuous spectra caused by the neutron capture in iodine and other background γ-radiation. This consists of taking the ratio of the number of counts in the individual channels above the threshold for γ production to that below threshold. Since the shape of the spectrum due

to the background radiation remains nearly constant, any increase of the ratio above 1.0 corresponds to γ-radiation from the O^{16}. The ratio curve obtained with 6.83-MeV neutrons is shown in fig. 4 along with the pulse height distri-

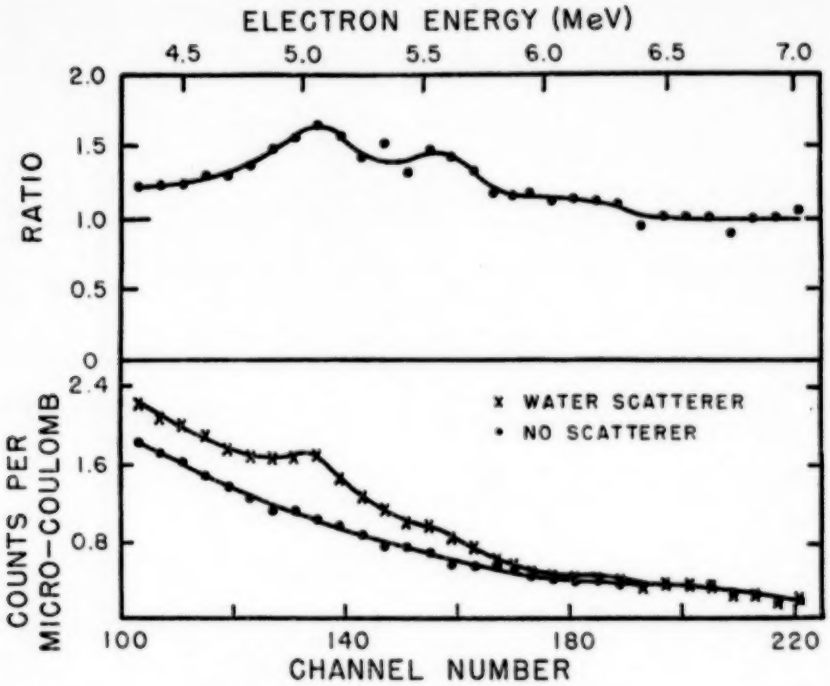

Fig. 4. Pulse-height distributions obtained with 6.83 MeV neutrons and a water scatterer. Also shown is the background observed with no scatterer at a neutron energy of 6.45 MeV, and the ratio of these two pulse-height distributions.

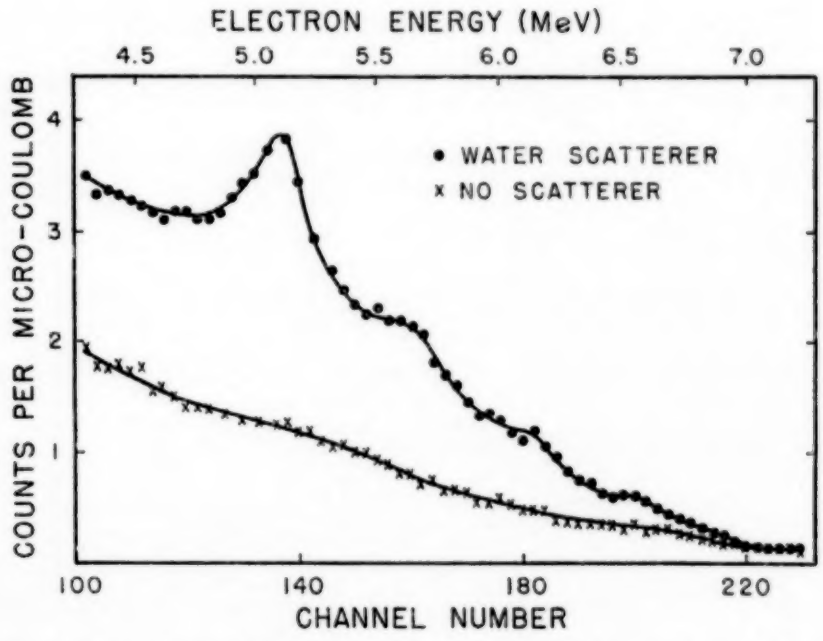

Fig. 5. Pulse-height distributions obtained with a water scatterer and with no scatterer at a neutron energy of 7.88 MeV.

butions used to determine this curve. The area above 1.0 on the ratio curve is a measure of the relative number of 6.14-MeV gamma rays present. For neutrons with energies above 7.4 MeV, the intensity of 6.14-MeV gamma rays was large enough so that they were measured by taking the difference between the pulse-height distribution curves obtained with the water and no scatterer in place. A typical set of curves is shown in fig. 5 which was obtained with a neutron energy of 7.88 MeV. The sum of those channels covering electron energies from 4.9 to 5.8 MeV was taken as a measure of the number of 6.14-MeV gamma rays. The variation of the cross section for the production of the sum of the 6.91 and 7.12-MeV gamma rays was taken in the same manner using the sum of the channels corresponding to electron energies from 6.3 MeV to 7.12 MeV.

A search was made for positrons from the 6.06 MeV 0^+ state in O^{16} by substituting a thin-wall Geiger counter for the NaI crystal shown in fig. 1. No positon emission was detected for neutrons with energies from 6.4 MeV to 8.3 MeV. An upper limit of any pair emission is 10 % of the total number of gamma quanta produced by inelastic scattering.

The absolute cross section for the production of γ radiation in O^{16} was measured at a neutron energy of 7.88 MeV by comparing the production of gamma radiation to that obtained in C^{12} at this same energy. Corrections were applied for the difference in absorption of the two different gamma radiations in the crystal and the relative number of pulses observed in the pair peaks. The pulse-height distributions for the 4.43 and 6.14-MeV gamma rays were obtained by observing the pulse-height distributions of these gamma radiations in the $N^{15}(p, \alpha)C^{12}$ and $F^{19}(p, \alpha)O^{16}$ reactions. The measured ratio of the cross section in O^{16} to that in C^{12} should be accurate to 10 %. The absolute value of the cross section for the production of 6.14-MeV gamma radiation should be correct to $\pm$ 30 %, because of the additional uncertainty in the cross section in C^{12}. At a neutron energy of 7.06 MeV, a cross section of 6.1 ± 1.8 mb/sr at 90° was obtained while Day [3]) reports a value of 8.3 ± 2.1 mb/sr at 95° at the same energy.

The differential cross section for the production at 90° of the 6.14-MeV gamma radiation, and the sum of the 6.91 and 7.12-MeV gamma radiation, is shown in fig. 6 as a function of neutron bombarding energy. The total cross section [5, 7]) is also shown in this figure for comparison. The excitation curve for the sum of the 6.91 and 7.12-MeV gamma radiation is quite similar to that for the 6.14-MeV gamma radiation, except that the higher energy radiation is much weaker. This large population of the 6.14-MeV state relative to the 6.91 and 7.12 states for neutrons up to 8.5 MeV is unexpected.

The relative intensity of the three γ-radiations were determined by using the ratio technique previously described and peel off, and the results of the analysis for a neutron energy of 8.50 MeV are given in table 3. Since all four levels are known to decay directly to the ground state, the relative intensities of the

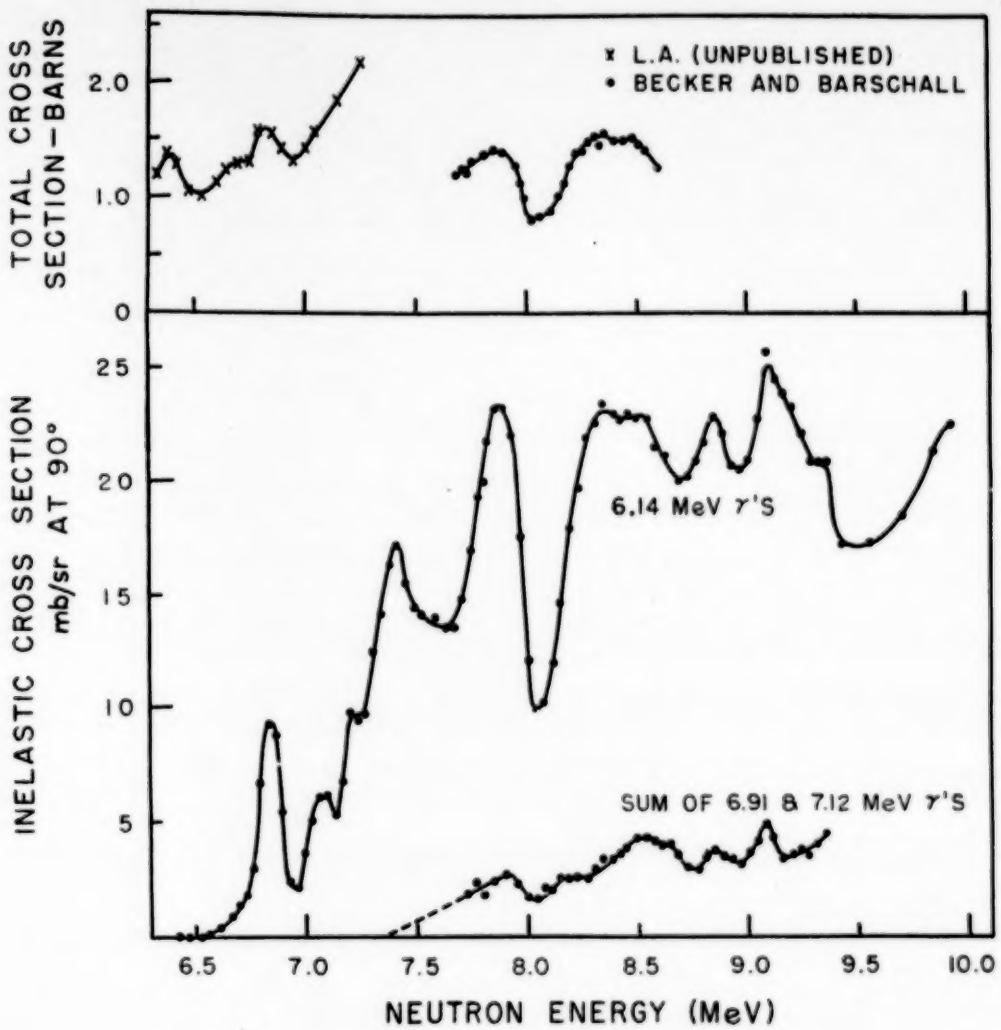

Fig. 6. Cross section for the production of 6.14, and 6.91+7.12 MeV γ-radiations in the $O^{16}(n, n'\gamma)O^{16}$ reaction and the total cross section for neutron scattering in O^{16}.

TABLE 3

The relative probability of excitation of O^{16} to the first four excited states at 8.5-MeV neutron energy

State in O^{16} (MeV)	Relative probability of excitation	Method of decay
6.06	<0.10	pairs
6.14	1.0	gamma
6.91	0.14	gamma
7.12	0.04	gamma

radiations correspond to the relative probability of excitation of the given level.

Information concerning the resonances is given in table 4 together with resonances obtained from the total cross section measurements [5, 7]). In table 4

there are six levels obtained in the present experiment in addition to those observed from the total cross section measurements.

TABLE 4

Data on the resonances in the reaction $O^{16}(n, n'\gamma)O^{16}$

Energy of neutron (MeV)	Excitation energy in O^{17}	
	Present experiment (MeV)	Total cross section (MeV)
6.83	10.57	10.56 [a]
7.07	10.80	
7.24	10.95	
7.40	11.11	
7.87	11.55	11.53 [b]
8.35	12.00	11.97 [b]
8.50	12.14	12.11 [b]
8.84	12.45	
9.10	12.71	
9.34	12.93	

[a]) See ref. [7])
[b]) See ref. [5])

4.2. DISCUSSION AND COMPARISON WITH THEORY

The observed threshold of 6.53-MeV neutron bombarding energy corresponds to an excitation energy of 6.15 MeV in O^{16} which agrees well with value 6.14 MeV given from other sources [9]).

The variation in the cross section as a function of energy depends on the cross section for competing reactions. The only known competing reaction is $O^{16}(n, \alpha)C^{13}$ which has a threshold at a neutron energy of 2.34 MeV. Unfortunately the cross section has not been measured above 5.2 MeV or below 14 MeV. At 14.1 MeV Lillie [11]) reported a cross section of 310 ± 100 mb (24.7 ± 8 mb/sr) and Walton, Clement and Boreli [12]) reported a cross section varying from 30 to 180 mb (14.4 mb/sr) for neutron energies in the range from 4 to 5.2 MeV. Therefore, it is quite probable that the $O^{16}(n, \alpha)$ cross section will be of the same order of magnitude as the inelastic cross section over the neutron energy range covered in this experiment.

In heavy nuclei the Hauser-Feshbach theory [13]) may be used to calculate the inelastic cross section. Although the assumptions of the theory are not valid for light nuclei, Feshbach has pointed out that if the nuclear radius is chosen such that the continuum model leads to the correct total cross section, then it many cases, the calculated inelastic cross section agrees well with the experimental inelastic cross section. The calculation has already been made for the total inelastic cross section [14]) from threshold to 9 MeV using this adjusted nuclear radius. A calculated (n, α) cross section in this energy region was used and any excitation of the 6.06-MeV level in O^{16} was neglected.

A comparison of the data to this calculated curve expressed as a differential cross section is shown in fig. 7. The total inelastic cross section is the sum of the 6.14, 6.91 and 7.12 MeV gamma radiations. The experimental inelastic cross section agrees qualitatively with that calculated from the theory.

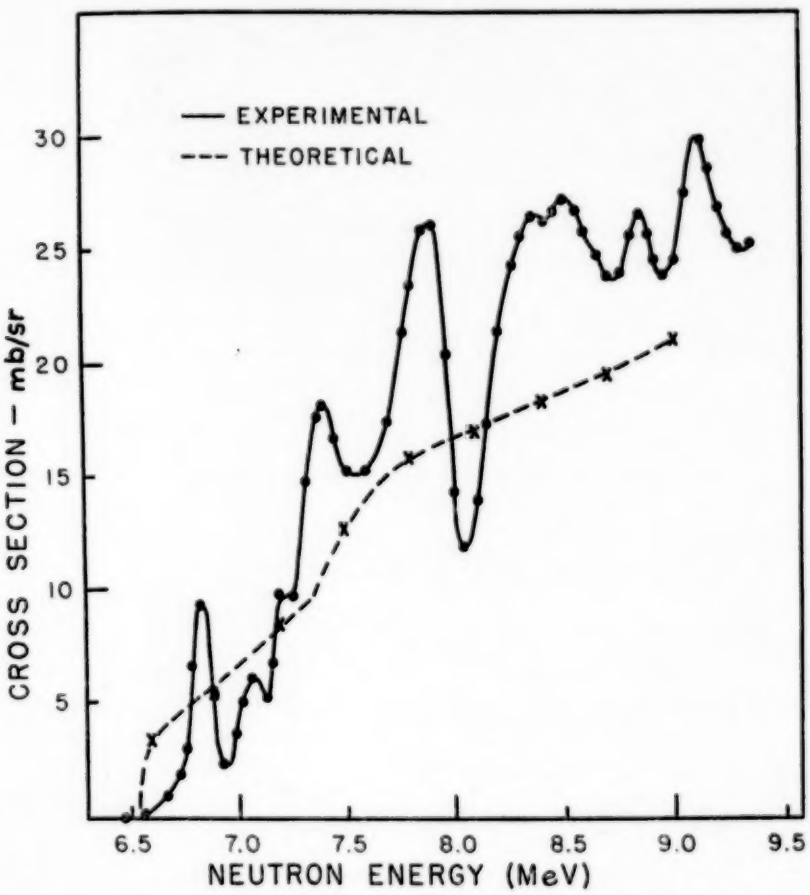

Fig. 7. Experimental cross sections for the reaction $O^{16}(n, n'\gamma)O^{16}$ compared to the theoretical values.

5. The Reactions $N^{14}+n$

5.1. RESULTS

The study of γ-radiation resulting from neutron bombardment of N^{14} is quite complicated when using a scintillation spectrometer since several states of N^{14} in the $N^{14}(n, n')N^{14*}$ reaction may be excited as well as several γ-emitting states of B^{11} through the $N^{14}(n, \alpha)B^{11*}$ reaction. Also, it would be possible to excite the first five levels in C^{14} through the $N^{14}(n, p)C^{14}$ reaction. Table 5 gives the known properties of the levels which may be excited in N^{14} and B^{11} in the present experiment.

All the excited states shown in table 1 decay either directly to the ground state or through cascades with γ-emission. The transition probabilities are known for the various excited states of N^{14} and B^{11}, and the $N^{14}(n, \alpha)B^{11*}$

cross sections for the first three excited states of B^{11} have been measured [15]) over most of the neutron energy range covered in the present experiment. From this information, the energies of the gamma radiations to be expected at any given neutron energy are known.

Typical pulse height distribution curves obtained with and without the Be_3N_2 scatterer at 7.4-MeV neutron energy are shown in fig. 8. There are recognizable peaks in the pulse-height distribution curve with no scatterer present at electron energies of 1.75, 2.2 and 5.1 MeV corresponding to 1.75, 2.2, and 6.1-MeV γ-radiations. The 6.1-MeV γ-radiation is probably due to neutron

TABLE 5

States of N^{14} and B^{11}

N^{14}			B^{11}	
Energy of level (MeV)	Angular momentum and parity	Isobaric spin	Energy of level (MeV)	Angular momentum and parity
Ground state	1^+	0	Ground state	$\frac{3}{2}^-$
2.31	0^+	1	2.14	$\frac{1}{2}^-$
3.95	1^+	0	4.46	$\frac{5}{2}^{(-)}$
4.91	(0^-)		5.03	$(\frac{3}{2}^-)$
5.10	2		6.76	$(\frac{7}{2}^-)$
5.68	(1)	0	6.81	$(\frac{3}{2}^-)$
5.83	$3^{(-)}$		7.30	$(\frac{5}{2}^-)$
6.23	(1^-)	0		
6.44	(3)	0		

inelastic scattering in O^{16}, since the variation in its magnitude correlated well with the $O^{16}(n, n', \gamma)O^{16}$ cross section. O^{16} is present in the Al_2O_3 light reflector, in the glass envelope of the photomultiplier tube, and to a minor extent in the Mylar tape. The 2.2-MeV radiation and part of the 1.75-MeV γ-radiation in the background curve are probably due to inelastic scattering in Al^{27}. With an aluminium scatterer at 7.8-MeV neutron energy, prominent peaks of approximately equal magnitudes were observed at 1.72 and 2.22-MeV electron energy. A thin aluminium cap was used to cover the crystal, and Al_2O_3 was used as the light reflector. Part of the 1.75-MeV γ-radiation is probably due to the 1.78-MeV γ-radiation accompanying the decay of Al^{28} which results from the $Si^{28}(n, p)Al^{28}$ reaction. Silicon is present in the glass envelope of the photomultiplier tube.

The peaks in the pulse-height distribution curve obtained with the Be_3N_2 scatterer, other than those mentioned above, are primarily due to γ-radiations resulting from the interaction of neutrons with N^{14}. There was no detectable γ-radiation other than that observed as background when a Be scatterer was

used. For γ-radiations above 2 MeV, the first and second anihilation radiation escape peaks are present in addition to the full energy peaks.

The quality of the pulse-height curve is not good enough to pick out all the energies of the various γ-radiations by inspection. However it was possible to obtain the intensity of the known γ-radiation by suitable analysis. The method used consisted essentially of making a least squares fit to the pulse-height distribution curve obtained using the Be_3N_2 scatterer at each neutron energy.

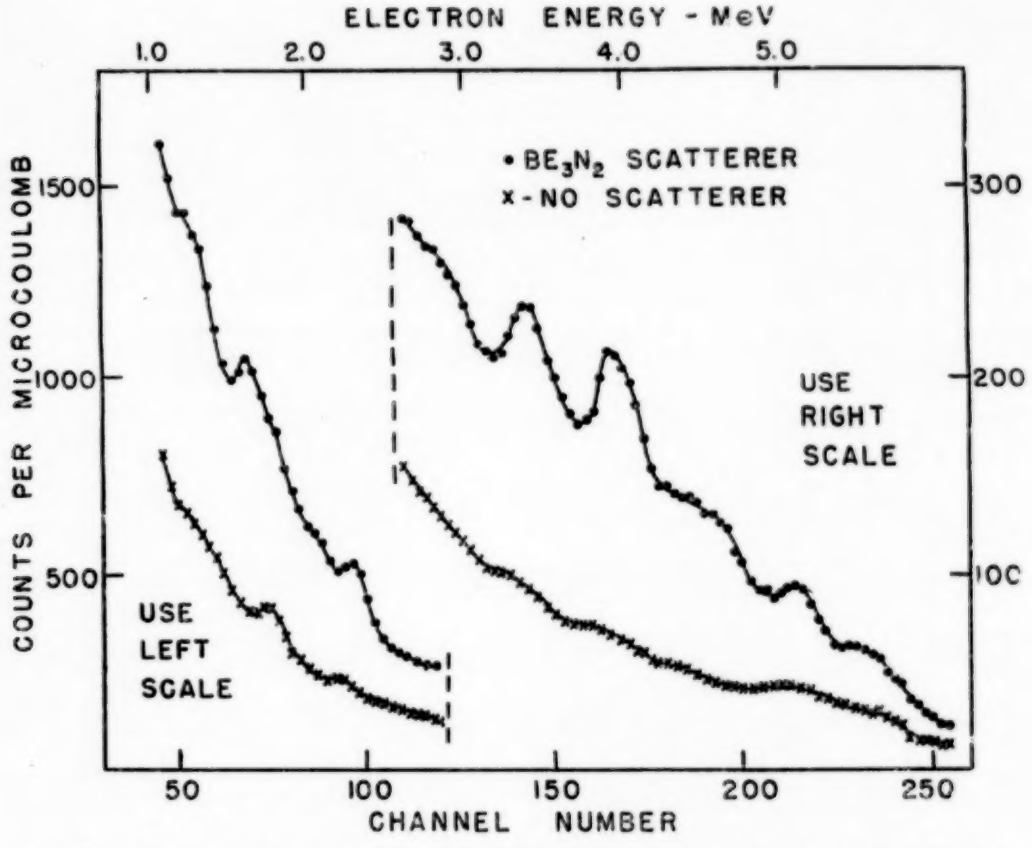

Fig. 8. Pulse-height distributions obtained with a Be_3N_2 scatterer and with no scatterer at a neutron energy of 7.40 MeV.

The variables introduced were the amplitude coefficients of the pulse-height curves for each of the various γ-radiations present, an amplitude coefficient for the pulse-height curve obtained with no scatterer present, and a constant. Experimental pulse-height distribution curves were obtained for monoenergetic γ-radiations of 1.12, 2.22, 4.43 and 6.14 MeV, and interpolations were made for pulse height curves corresponding to γ-radiations of intermediate energies. The coefficients thus determined for the amplitude of the no scatterer pulse-height curve ranged from 1.25 to 1.50, which is probably due to neutrons scattered into the crystal and surrounding material by the Be_3N_2 scatterer. An additional complication is that this coefficient is not a constant over the complete range of

electron energies from 1 to 6 MeV. For this reason, fits were made in two energy ranges, from 1.0 to 2.4 MeV, and from 2.4 to 5.2 MeV electron energies. Least square fits were made on an Elecom 120A Computer for the data obtained for neutron energies above 5.8 MeV.

Below 5.8 MeV variations in the cross section for the production of the 2.31-MeV γ-radiation were determined using a different technique. The background

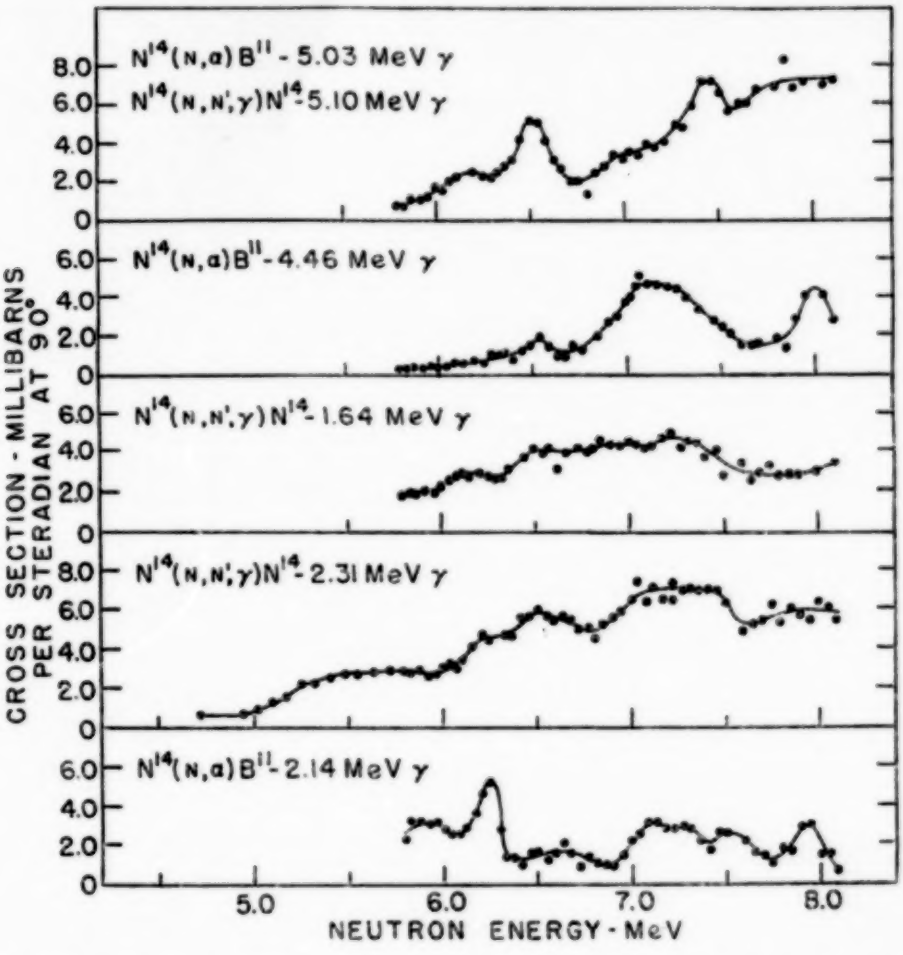

Fig. 9. Cross section for the production of 1.64, 2.14, 2.31, 4.46 and 5.06 MeV γ-radiation as a function of neutron energy.

was subtracted from the Be_3N_2 pulse-height curve after multiplying the no scatterer pulse height curve by 1.33. Using this corrected curve, the difference between the sum of the channels over the 2.31-MeV peak and the sum of an equal number of channels at 2.50-MeV electron energy was taken to be a measure of the 2.31-MeV γ-radiation present.

The absolute cross section for the production of the γ-radiation in N^{14} was measured at several neutron energies between 6.5 and 7.5-MeV neutron energy by comparing the production of gamma radiation in N^{14} to the 4.43-MeV γ-radiation obtained from C^{12} at the same energy. Corrections were applied for

the variation in crystal efficiency with the energy of the gamma radiation. The measured ratio of the cross section in N^{14} for comparable energy γ-radiations to the cross section of C^{12} should be accurate to ± 10 % The absolute value of the cross section for these γ-radiations should be accurate to ± 30 %, because of the additional uncertainty in the cross section of C^{12}. For γ-radiations below 3 MeV. the absolute cross sections should be accurate to within ± 40 % due to the additional uncertainty in the crystal efficiency.

The differential cross section for the production of the 2.14, 2.31, 1.64, 4.46 and the sum of the 5.03 and 5.10 MeV γ-radiations is shown in fig. 9. The excitation curve for the 2.14-MeV γ-radiation resulting from the $N^{14}(n, \alpha)B^{11*}$ reaction is quite similar to that obtained by observing the α particles [15]). The cross section for the production of the 2.31 MeV γ-radiation is quite low from 4.7 to 5.0 MeV, being 0.6 mb/sr at 90° at 4.7 MeV. Day [3]) obtained a value of 0.5 mb/sr at 95° at 3.95 MeV. Both these values indicate that the cross section for the direct excitation of the 2.31-MeV level in N^{14} is quite low for neutrons with an energy of 4 to 5 MeV.

The 1.64-MeV γ-radiation results from a cascade from the 3.95-MeV level of N^{14} to the 2.31-MeV level. By subtraction of the cross section of the 1.64-MeV γ-radiation from that of the 2.31-MeV γ-radiation, it is seen that the cross section for the direct excitation of the 2.31-MeV level is still quite low at 5.9-MeV neutron energy, namely, 0.7 mb/sr.

The 5.03-MeV γ-radiation resulting from the $N^{14}(n, \alpha)B^{11*}$ reaction and the 5.10-MeV γ-radiation resulting from the $N^{14}(n, n')N^{14*}$ reaction were unresolved.

The magnitude of the cross section for the production of the 4.46 MeV γ-radiation would be influenced by any C^{12} which is present since the 4.43 and 4.46-MeV γ-radiations would be unresolved. Approximately 4.5 g of C^{12} are present in the Mylar tape used as part of the holder for the Be_3N_2 scatterer. The 4.46-MeV γ-radiation cross section curve has been corrected for this amount of C^{12}.

A summary of the experimentally determined cross sections for the various γ-radiations involved in $N^{14}(n, n', \gamma)N^{14}$, $N^{14}(n, \alpha)B^{11*}$ and $N^{14}(n, p)C^{14*}$ reactions is given in table 6 for 7.3-MeV neutron energy. The cross sections listed as experimental are those obtained for γ-radiation having that energy corresponding to the excited states listed in the first column. The magnitude of the cross sections for the various γ-radiations were determined using the peel off method in addition to the least squares fit. The cross sections listed as calculated are those calculated from the measured cross section of the cascade γ-radiation using the transition probability given in table 6. The calculated cross section of 1.6 mb/sr listed for the 5.10-MeV radiation in the $N^{14}(n, n')N^{14*}$ reaction was obtained by subtracting the cross section of 3.7 mb/sr for the 5.03-MeV γ-radiation obtained by Gabbard *et al.*[15]), in the $N^{14}(n, \alpha)B^{11*}$ reaction. Any 3.95-MeV γ-radiation from the second excited state of N^{14} to the ground state

would be unresolved from the 3.92-MeV γ-radiation resulting from a cascade from the 6.23-MeV level to the 2.31-MeV level of N^{14}.

The cross section for the sum of γ-radiations between 5.6 and 7.0 MeV was measured to be 1.5 ± 0.8 mb/sr at 7.30-MeV neutron energy. This includes γ-radiation from the 5.68, 5.83, 6.23 and 6.44 MeV levels in N^{14}, and the

TABLE 6

Cross section for γ-radiations produced by interaction of 7.3-MeV neutrons with N^{14}

γ-radiation (MeV)	Assignment	Transition probability [a]) (%)	Cross section exper. (mb/sr)	Cross section calcul. [b]) (mb/sr)
1.64	$N^{14}: 3.95 \rightarrow 2.31$	96	4.4 ± 1.0	
2.14	$B^{11}: 2.14 \rightarrow 0$	100	2.5 ± 0.5	
2.31	$N^{14}: 2.31 \rightarrow 0$	100	6.9 ± 1.0	
2.82	$N^{14}: 5.10 \rightarrow 2.31$	26	1.5 ± 0.4	0.6 ± 0.3
	$B^{11}: 5.03 \rightarrow 2.41$	8		0.3 ± 0.1
3.37	$N^{14}: 5.68 \rightarrow 2.31$	63	<1.2	
3.93	$N^{14}: 6.23 \rightarrow 2.31$	76	1.3 ± 0.4	1.1 ± 0.4
	$N^{14}: 3.95 \rightarrow 0$	4		0.2 ± 0.05
4.46	$B^{11}: 4.46 \rightarrow 0$	100	4.5 ± 1.0	
4.91	$N^{14}: 4.91 \rightarrow 0$	100	<1.0	
5.06	$N^{14}: 5.10 \rightarrow 0$	74	5.3 ± 0.8	1.6 ± 1.0
	$B^{11}: 5.03 \rightarrow 0$	92		3.7 ± 1.0
5.68	$N^{14}: 5.68 \rightarrow 0$	37	<1.0	
5.83	$N^{14}: 5.83 \rightarrow 0$	35	<1.0	
6.09	$C^{14}: 6.09 \rightarrow 0$	100	<1.0	
6.23	$N^{14}: 6.23 \rightarrow 0$	24	<1.0	0.4 ± 0.2
6.44	$N^{14}: 6.44 \rightarrow 0$	100	<1.0	
6.59	$C^{14}: 6.59 \rightarrow 0$		<1.0	
6.72	$C^{14}: 6.72 \rightarrow 0$	100	<1.0	
6.89	$C^{14}: 6.89 \rightarrow 0$	0	<1.0	
7.35	$C^{14}: 7.35 \rightarrow 0$	50	<1.0	
5.6–7.0	N^{14} and C^{14}		1.5 ± 0.8	

[a]) ref. [9]); H. E. Gove, A. E. Litherland, E. Almquist and D. A. Bromley, Phys. Rev. **103** (1956) 835;
E. K. Warburton and H. E. Rose, Phys. Rev. **109** (1958) 1199;
F. Ajzenberg and T. Lauritsen, Nuclear Physics **11** (1959) 1

[b]) Calculated from experimental cross sections and cascade ratios

6.09, 6.59, 6.72 and 6.89 MeV levels in C^{14}. Any γ-radiation greater than 7.0 MeV was measured to have a cross section less than 0.5 mb/sr.

The cross sections for the various γ radiations may be added to obtain a cross section for the particular reaction involved. At 7.3-MeV neutron energy, the cross section for the $N^{14}(n, n'\gamma)N^{14}$ reaction, including cascades, is 16.2 mb/sr. The cross section of the $N^{14}(n, n')N^{14*}$ reaction is 10.1 mb/sr which is approximately equal to the cross section of 10.7 mb/sr for the $N^{14}(n, \alpha)B^{11*}$ reaction

leading to the first three excited states of B^{11}. The value of 10.7 mb/sr for this latter cross section compares to a value of 9.9 mb/sr obtained [15]) by observing the three groups of α particles.

The data on the prominent resonances exhibited in the cross section curves are given in table 7.

TABLE 7

Data on prominent resonances in reaction $N^{14}+n$

Neutron energy (MeV)	N^{15*} $N^{14}+n$ (MeV)	Width $N^{14}+n$ (keV)	N^{15*} $C^{13}+d$ (MeV)	Width $C^{13}+d$ (keV)
6.26	16.67	120	16.70 [a])	≈100 [a])
6.52	16.91	170	16.89 [a])	≈400 [a])
			17.10 [b,c])	Broad [b,c])
			17.22 [b])	≈200 [b])
			17.35 [b,c])	≈400 [b,c])
7.10	17.46	200	17.47 [a])	≈100 [a])
			17.57 [b])	≈200 [b])
			17.69 [a,b])	≈500 [a,b])
			17.71 [b])	48± 9 [b])
6.48	17.78	200	17.8 [d])	≈600 [d])
			18.06 [b])	19± 4 [b])
			18.08 [b,c])	45 [b,c])
7.92	18.22	170	18.28 [b,c,d])	270± 70 [b,c])
8.00	18.29	120		

[a]) J. E. Richardson, Phys. Rev. **80** (1950) 850
[b]) J. B. Marion and G. Weber, Phys. Rev. **102** (1956) 1355
[c]) J. B. Marion and G. Weber, Phys. Rev. **103** (1956) 167
[d]) J. B. Marion, T. W. Bonner and C. F. Cook, Phys. Rev. **100** (1955) 847

The resonance at 6.26-MeV neutron energy gives an excitation energy in N^{15} 30 keV lower than that obtained from the C^{13}(d, p) reaction. However, the deuteron energy is 0.63 MeV, the state is broad, and the result of the Coulomb barrier would be to shift this level to a higher energy in the (d, p) reaction.

The previously reported resonance corresponding to an excitation energy in N^{15} of 18.28 MeV with a width of 270 keV was resolved into two resonances. From the excitation curve of the 2.14-MeV γ-radiation, there is a resonance at 7.92-MeV neutron energy corresponding to an excitation energy in N^{15} of 18.22 MeV. From the excitation curve of the 4.46-MeV γ-radiation, there is a resonance at 8.00-MeV neutron energy corresponding to an excitation energy in N^{15} of 18.29 MeV.

It is possible that the five broad states previously reported, which correspond to neutron energies of 6.75, 6.86, 6.98, 7.20 and 7.31 MeV are masked by more prominent adjacent levels. There may be some evidence for the last three

resonances in the 5.03, 5.10, 1.64 and 2.14 MeV γ-radiation excitation curves respectively.

It is interesting to note that any resonances corresponding to the narrow levels in N^{15} at 17.71, 18.06 and 18.08 MeV excitation energy, which would be at 7.41, 7.77 and 7.79 MeV neutron energy, are quite weak if not missing. Resonances corresponding to the first two of these levels are also missing in the (d, p) reaction, whereas they are quite prominent in the (d, α)reaction.

5.2. DISCUSSION

In the $N^{14}(n, n')N^{14*}$ reaction at 7.30-MeV neutron energy, the 3.95 and 5.10-MeV levels in N^{14} are those which apparently have the highest probability of excitation. The cross section for the direct excitation of the state of 2.31 MeV is only 0.8 mb/sr. The ratio of the relative probability of exciting the 2.31-MeV level directly to exciting the 3.95-MeV level is 1 : 6. This is to be compared to a similar ratio of 1 : 2 observed by Buechner *et al.*[16]) in the $N^{14}(p, p')N^{14}$ reaction where the 6.92 or 7.56-MeV protons were scattered through 90 degrees. The difference may be due to the fact that in the present experiment, γ-radiation was measured over approximately π steradians at 90°, whereas the proton experiment was carried out with small angular resolution. It would be expected from isobaric spin considerations that this ratio would be the same in both experiments at this energy.

In connection with the sum of the cross sections for the various γ-radiations, it is rather unexpected that at 7.3 MeV the cross section for the $N^{14}(n, \alpha)B^{11*}$ reaction is approximately equal to the cross section for the $N^{14}(n, n')N^{14*}$ reaction. This implies that the compound nucleus (N^{15}) exists as a configuration of α particles for a large fraction of the time.

References

1) L. C. Thompson and J. R. Risser, Phys. Rev. **94** (1954) 941
2) M. E. Battat and E. R. Graves, Phys. Rev. **97** (1955) 1266
3) R. B. Day, Phys. Rev. **102** (1956) 767
4) D. E. Diller and M. F. Crouch, Phys. Rev. **93** (1954) 362A
5) R. L. Becker and H. H. Barschall, Phys. Rev. **102** (1956) 1384
6) N. Nereson and S. E. Darden, Phys. Rev. **89** (1953) 775
7) Los Alamos Data in BNL 325 (unpublished)
8) See table 1, ref. [8])
9) F. Ajzenberg and T. Lauritsen, Revs. Mod. Phys. **27** (1955) 77
10) S. S. Vasil'ev, V. V. Komarov and A. M. Popora, JETP **33** (1958) 1321
11) A. B. Lillie, Phys. Rev. **87** (1952) 716
12) R. B. Walton, J. D. Clement and F. Boreli, Phys. Rev. **107** (1957) 1056
13) W. Hauser and H. Feshbach, Phys. Rev. **87** (1952) 366
14) Lustig, Goldstein and Kalos, Interim Report on Neutron Cross Section of Oxygen, N.D.A. 086-2 (1958) (unpublished)
15) F. Gabbard, H. Bichsel and T. W. Bonner, Nuclear Physics **14** (1959/60) 277
16) C. Bockelman, C. Browne, W. Buechner and A. Sperduto, Phys. Rev. **92** (1953) 665
17) H. E. Hall and T. W. Bonner, Bull. Am. Phys. Soc. **1** (1956) 96; **4** (1959) 103

7.A *Nuclear Physics* **14** (1959/60) 314—338; © *North-Holland Publishing Co., Amsterdam*
Not to be reproduced by photoprint or microfilm without written permission from the publisher

EINE FELDTHEORETISCHE VERALLGEMEINERUNG DER IMPULSNÄHERUNG

F. KASCHLUHN

Vereinigtes Institut für Kernforschung, Laboratorium für Theoretische Physik, Dubna, USSR

Received 25 June 1959

Abstract: A generalization of Chew's impulse approximation in field theory is proposed, which may be used for an explicit evaluation of the contribution from the non-observable region in the dispersion relations for pion-deuteron scattering. The Hamilton-formalism for a non-relativistic two-nucleon system is assumed with a pseudovector coupling to the pion field for which the usual cut-off is used. The generalization to the case of more than two nucleons and to other couplings is obvious, and it should also be possible, with appropriate modifications, to extend the method to the relativistic case. We employ the time-dependent scattering formalism: the S-matrix describes transitions between the bare states of the two-nucleon system, which are defined as the projections of the corresponding real states onto the meson vacuum. This leads directly to the introduction of a field-energy operator which involves self-energies and interaction between the nucleons, and by means of which it is possible to avoid the difficulties associated in general with the bound state problem in quantum field theory. It is shown that the higher approximations to the impulse approximation correspond, also in field theory, to the potential scattering and multiple scattering corrections, which also include the absorption phenomena.

1. Einleitung

Bei der Aufstellung und Auswertung der Dispersionsbeziehungen für die elastische Streuung von π-Mesonen an Deuteronen [1, 2, 3, 4]) tauchte das Problem einer Berechnung der Strom-Matrixelemente bezüglich des Deuteron-Grundzustandes und der nicht gebundenen Zustände des kontinuierlichen Spektrums des Zwei-Nukleonen-Systems auf (bzw. der Übergangselemente für die Absorption des einlaufenden π-Mesons durch das Deuteron). In der vorliegenden Arbeit wird gezeigt, daß das in Ref. [1, 2, 3]) vorgeschlagene Näherungsverfahren genau einer feldtheoretischen Verallgemeinerung der Chewschen Impulsnäherung [5, 6, 7]) entspricht: die Übergangsmatrix für den in Frage stehenden Prozeß am Deuteron wird durch die Summe der Ein-Nukleon-Übergangsmatrizen approximiert, wobei die einzelnen freien Nukleonen Impulsverteilungen haben, die genau ihrer Impulsverteilung in den nackten Zuständen des Zwei-Nukleonen-Systems entsprechen. Hierbei sind die nackten Zustände des Zwei-Nukleonen-Systems als die Projektionen der entsprechenden reellen Zustände auf das Mesonvakuum definiert. Die höheren Näherungen der Impulsnäherung entsprechen auch im feldtheoretischen Falle der Potential- und Vielfachstreukorrektur, die auch den Absorptionseffekt korrigieren.

Unseren Untersuchungen wird der zeitabhängige Streuformalismus zugrunde gelegt. Der Hamilton-Operator beschreibt die nichtrelativistische Bewegung zweier Nukleonen, die in pseudovektorieller Wechselwirkung mit dem π-Mesonfeld stehen, für das die übliche Abschneidung vorausgesetzt wird. Elektromagnetische Wechselwirkung und der Massenunterschied der verschieden geladenen Teilchen werden vernachlässigt. Die S-Matrix selbst beschreibt Übergänge zwischen den nackten Zuständen der Teilchen. Die Definition der nackten Zustände des Zwei-Nukleonen-Systems als der Mesonvakuum-Projektionen der entsprechenden reellen Zustände führt zwangsläufig zur Einführung eines Feldenergieoperators, der Selbstenergie und Wechselwirkung der Nukleonen enthält. Mit Hilfe dieses Operators, dessen Eigenschaften in Abschnitt 2 genauer untersucht werden, können die Schwierigkeiten explizit überwunden werden, die sonst der Formulierung einer Feldtheorie mit gebundenen Zuständen im Wege stehen und die bekanntlich mit der Adiabaten-Konzeption zusammenhängen (da diese — in üblicher Weise interpretiert — zum Zerfall des gebundenen Zustandes führt). Der S-Matrix-Formalismus wird im einzelnen im Abschnitt 3 entwickelt, wobei wir in Anlehnung an Bogolubov und Mitarbeiter [8, 9]) Variationsableitungen der S-Matrix verwenden, die in unserem Falle aber zweckmäßigerweise bezüglich des Hamiltonoperators der Wechselwirkung gebildet werden (was im übrigen auch eine einfache Formulierung der Kausalitätsbedingung in unserer bezüglich der Nukleonen nichtrelativistischen Theorie gestattet). Im Abschnitt 4 wird die Impulsnäherung formuliert, wobei die Bedeutung der höheren Näherungen sich zwangsläufig an Hand zweckmäßig geschriebener allgemeiner Ausdrücke ergibt. In der Schlußbemerkung in Abschnitt 5 werden kurz einige Probleme erörtert, die mit den Dispersionsbeziehungen für die Streuung von π-Mesonen an Deuteronen im Zusammenhang stehen (insbesondere wird auf die Frage nach der Abweichung des Massenspektrums der intermediären Zustände vom normalen Spektrum eingegangen).

Die Verallgemeinerung der vorliegenden Untersuchungen auf den Fall von mehr als zwei Nukleonen und anderer Kopplungsarten ist offensichtlich und sollte — bei geeigneten Modifikationen — auch auf den relativistischen Fall möglich sein.

2. Feldenergieoperator und die Zustände der nackten Teilchen

Wir setzen den Hamilton-Formalismus für zwei nichtrelativistisch bewegte Nukleonen voraus, die in pseudovektorieller Wechselwirkung mit dem π-Mesonfeld stehen, für das die übliche Abschneidung vorausgesetzt wird. Bezüglich der Nukleonen wird keine zweite Quantisierung durchgeführt, und elektromagnetische Wechselwirkung und der Massenunterschied der

verschieden geladenen Teilchen werden vernachlässigt. Weiterhin setzen wir voraus, daß das Gesamtsystem nur einen gebundenen Zustand hat, den Deuteron-Grundzustand. Wir schreiben den Gesamt-Hamiltonoperator in der Form

$$H = H_0 + H_1, \tag{1}$$

wo H_0 der Hamiltonoperator des ungekoppelten Systems und H_1 die Wechselwirkung ist. Es gilt

$$H_0 = \sum_{j=1}^{2}\left(M_0 + \frac{\mathbf{p}_j^2}{2M_0}\right) + \sum_{\rho=1}^{3}\sum_{\mathbf{q}} \omega_q a_{\rho\mathbf{q}}^* a_{\rho\mathbf{q}}, \tag{2}$$

wo $\mathbf{p}_j$ der Impulsoperator des Nukleons j mit der nichtrenormierten Masse M_0 und $\omega_q = \sqrt{(m^2+\mathbf{q}^2)}$ die Energie eines π-Mesons der Masse m mit Isobarenspinindex ρ und Impuls $\mathbf{q}$ ist, dessen Vernichtungs- bzw. Erzeugungsoperator $a_{\rho\mathbf{q}}$ bzw. $a_{\rho\mathbf{q}}^*$ ist (wie sie in üblicher Weise für Bosonen gelten). Das Problem einer Renormierung der Mesonmasse tritt nicht auf, da im betrachteten nichtrelativistischen Fall eine Paarerzeugung von Nukleonen nicht möglich ist. Der Hamiltonoperator der Wechselwirkung besteht aus einer Summe zweier Terme, die den beiden Nukleonen entsprechen:

$$H_1 = \sum_{j=1}^{2}\sum_{\rho=1}^{3} \frac{\sqrt{4\pi} f_0}{m} \int \mathrm{d}\mathbf{x}\rho(\mathbf{x}-\mathbf{x}_j)\tau_\rho{}^j \boldsymbol{\sigma}^j \cdot \nabla\phi_\rho(\mathbf{x}); \tag{3}$$

$\rho(\mathbf{x}-\mathbf{x}_j)$ ist die Quelldichtefunktion der (räumlich ausgedehnten) Nukleonen mit den Ortskoordinaten $\mathbf{x}_j$, den Isobarenspinoperatoren $\tau_\rho{}^j$ und Spinoperatoren $\boldsymbol{\sigma}^j$ und $\phi_\rho(\mathbf{x})$ der reelle pseudoskalare Feldoperator der π-Mesonen; f_0 ist die nichtrenormierte (nicht rationalisierte) Kopplungskonstante. Wir schreiben

$$\phi_\rho(\mathbf{x}) = \frac{1}{\sqrt{V}}\sum_{\mathbf{q}} \frac{1}{\sqrt{2\omega_q}} \{a_{\rho\mathbf{q}}\, \mathrm{e}^{i\mathbf{q}\cdot\mathbf{x}} + a_{\rho\mathbf{q}}^*\, \mathrm{e}^{-i\mathbf{q}\cdot\mathbf{x}}\}, \tag{4}$$

wo V das Normierungsvolumen ist, und erhalten für (3)

$$H_1 = \sum_{\rho=1}^{3}\sum_{\mathbf{q}} \{a_{\rho\mathbf{q}} V_{\rho\mathbf{q}} + a_{\rho\mathbf{q}}^* V_{\rho\mathbf{q}}^*\}, \tag{5}$$

mit

$$V_{\rho\mathbf{q}} = \sum_{j=1}^{2} V_{\rho\mathbf{q}}^j, \quad V_{\rho\mathbf{q}}^j = \frac{i}{\sqrt{V}} \frac{\sqrt{4\pi} f_0}{m} \tau_\rho{}^j \boldsymbol{\sigma}^j \cdot \mathbf{q} v_q \frac{1}{\sqrt{2\omega_q}} \mathrm{e}^{i\mathbf{q}\cdot\mathbf{x}_j}, \tag{6}$$

wo

$$v_\mathbf{q} = \int \mathrm{d}\mathbf{x}\, \mathrm{e}^{i\mathbf{q}\cdot\mathbf{x}} \rho(\mathbf{x}) \tag{7}$$

die Abschneidefunktion ist. Im folgenden werden die Indizes ρ, $\mathbf{q}$ zu q zusammengefaßt.

Der wesentliche Punkt für den im folgenden Abschnitt zu entwickelnden S-Matrix-Formalismus, der die Streuung an stabilen gebundenen Komplexen beschreiben soll, besteht nun in einer geeigneten Definition der nackten Zustände der Teilchen, in die das System in der fernen Vergangenheit bzw. fernen Zukunft übergehen soll. Eine übliche Anwendung der Adiabaten-Konzeption in dem Sinne, daß die gesamte Wechselwirkung für $t \to \pm \infty$ verschwinden soll, ist in unserem Falle, wo die Existenz des stabilen Deuteron-Grundzustandes zu berücksichtigen ist, ganz unzweckmäßig, weil diese zum Zerfall des gebundenen Zustandes führt. Wir wollen hingegen die nackten Zustände des Zwei-Nukleonen-Systems einfach als die Projektionen der entsprechenden reellen Zustände auf das Mesonvakuum definieren, was genau dem Abschalten der Mesonwolke für $t \to \pm\infty$ entspricht (und nicht der gesamten Wechselwirkung). Mathematisch formuliert: ist der (normierte) reelle Zustand des Zwei-Nukleonen-Systems als stabiler gebundener Deuteron-Grundzustand oder als nicht gebundener Zustand des kontinuierlichen Spektrums durch

$$H\Psi_p = E_p \Psi_p \tag{8}$$

gegeben, so ist der entsprechende (normierte) nackte Zustand, in welchen das System für $t \to \pm\infty$ asymptotisch übergehen soll, durch

$$\Psi_p^{\,0} = c_p^{-1} \Lambda_0 \Psi_p \tag{9}$$

definiert, wo Λ_0 der Projektionsoperator ist, der auf das Mesonvakuum projiziert, und c_p eine Normierungskonstante ist. Wir verwenden für den reellen Zustand auch die Schreibweise

$$\Psi_p = c_p \Psi_p^{\,0} + \Lambda_c \Psi_p \tag{10}$$

wo Λ_c der Projektionsoperator ist, der weg vom Mesonvakuum projiziert; $|c_p|^2$ ist dann einfach die Wahrscheinlichkeit dafür, das nackte System im reellen Zustand anzutreffen, und der Zusatz $\Lambda_c \Psi_p$ entspricht genau der Mesonwolke. Für die Projektionsoperatoren gilt

$$\Lambda_0 + \Lambda_c = 1, \quad \Lambda_0^2 = \Lambda_0, \quad \Lambda_c^2 = \Lambda_c. \tag{11}$$

Aus (8) in Verbindung mit (1) folgt nach Multiplikation mit Λ_0 von links her und Verwendung von (10), (11) und

$$[H_0, \Lambda_0] = 0, \quad \Lambda_0 H_1 \Lambda_0 = 0, \tag{12}$$

die Beziehung

$$H_0 c_p \Psi_p^{\,0} + \Lambda_0 H_1 \Lambda_c \Psi_p = E_p c_p \Psi_p^{\,0}. \tag{13}$$

Definieren wir den Feldenergieoperator Γ_p durch

$$c_p \Gamma_p \Psi_p^{\,0} = \Lambda_0 H_1 \Lambda_c \Psi_p, \tag{14}$$

dann wird aus (13) unter Verwendung von (2)

$$(H_0+\Gamma_p)\Psi_p^0 = \left\{\sum_j \left(M_0+\frac{\mathfrak{p}_j^2}{2M_0}\right)+\Gamma_p\right\}\Psi_p^0 = E_p\Psi_p^0. \tag{15}$$

Zur Berechnung von Γ_p multiplizieren wir (8) in Verbindung mit (1) von links her mit Λ_c und erhalten unter Verwendung von (10), (11) und

$$[H_0, \Lambda_c] = 0, \quad \Lambda_c H_1 \Psi_p^0 = H_1 \Psi_p^0, \tag{16}$$

für die Mesonwolke

$$\Lambda_c \Psi_p = c_p \frac{\mathrm{P}}{E_p - H_0 - \Lambda_c H_1} H_1 \Psi_p^0, \tag{17}$$

wo P den Hauptwert bezeichnet. Zwar verbietet der Operator Λ_c im Nenner, daß ein Mesonvakuum-Zustand intermediär oder als Endzustand auftreten kann, aber wir haben (im Gegensatz zum Ein-Nukleon-Problem) die Möglichkeit instabiler Zustände des Zwei-Nukleonen-Systems in Betracht zu ziehen, die zur reellen Emission von Mesonen führen (wo dann der Energienenner verschwinden würde)†. Aus (14) und (17) folgt dann für den Operator Γ_p

$$\Gamma_p = \Lambda_0 H_1 \frac{\mathrm{P}}{E_p - H_0 - \Lambda_c H_1} H_1 \Lambda_0, \tag{18}$$

der wegen (11) rechts auch in der Form

$$\Gamma_p = \Lambda_0 H_1 \frac{\mathrm{P}}{E_p - H_0 - \Lambda_c H_1 \Lambda_c} H_1 \Lambda_0 \tag{18'}$$

geschrieben werden kann, was direkt die Hermitizität von Γ_p zeigt. Der Operator Γ_p beschreibt Selbstenergie und Wechselwirkung der beiden Nukleonen, worauf wir noch genauer eingehen.

Es ist nützlich, Γ_p noch in einer anderen Form zu bestimmen. Aus (8) in Verbindung mit (1) und der aus (15) folgenden Gleichung

$$H\Psi_p^0 = E_p\Psi_p^0 + (H_1 - \Gamma_p)\Psi_p^0 \tag{19}$$

folgt nach Standard-Methode die stationäre Lösung von (8) zu

$$\Psi_p = c_p \left\{1 + \frac{\mathrm{P}}{E_p - H}(H_1 - \Gamma_p)\right\}\Psi_p^0. \tag{20}$$

Es ist offenbar

$$c_p \frac{\mathrm{P}}{E_p - H}(H_1 - \Gamma_p)\Psi_p^0 = \Lambda_c \Psi_p, \tag{21}$$

da Γ_p nach (18) (unter anderem) diejenigen Beiträge von H_1 kompensiert, die zum Mesonvakuum als Endzustand führen†. Die Konstante c_p hat also auch denselben Wert wie in (10). Aus (14) folgt unter Verwendung von (21)

† Vgl. die Entwicklung (39).

$$\Gamma_p = \Lambda_0 H_1 \frac{\mathrm{P}}{E_p - H} (H_1 - \Gamma_p) \Lambda_0, \tag{22}$$

was natürlich identisch mit obigem Ausdruck (18) bzw. (18′) ist (Γ_p auf der rechten Seite bedingt, daß kein intermediärer Mesonvakuum-Zustand auftritt). Glg. (22) lässt sich nach (21) auch in der symmetrischen Form schreiben

$$\Gamma_p = \Lambda_0 (H_1 - \Gamma_p) \frac{\mathrm{P}}{E_p - H} (H_1 - \Gamma_p) \Lambda_0. \tag{22'}$$

Die (normierten) reellen Zustände, die zusätzlich zum Vorhandensein der beiden Nukleonen noch die Existenz von einem oder mehreren π-Mesonen beschreiben, sind dann gegeben durch

$$H \Psi_{p,\, qq' \ldots} = (E_p + \omega_q + \omega_{q'} + \ldots) \Psi_{p,\, qq' \ldots}. \tag{23}$$

Diese sollen asymptotisch für $t \to \pm\infty$ in die nackten Zustände

$$\Psi^0_{p,\, qq' \ldots} = a_q^* a_{q'}^* \ldots \Psi_p^0 \tag{24}$$

übergehen, die also das Vorhandensein eines freien Zwei-Nukleonen-Systems im nackten Zustand Ψ_p^0 und freien π-Mesonen mit den Impulsen und Isobarenspinindizes $q, q', \ldots$ beschreiben (im Falle übereinstimmender $q, q', \ldots$ sind die bekannten Normierungsfaktoren anzubringen). Definieren wir den allgemeinen Feldenergieoperator Γ des Zwei-Nukleonen-Systems durch

$$\Gamma = \sum_{p,\, qq' \ldots} a_q^* a_{q'}^* \ldots \Gamma_p |\Psi_p^0\rangle\langle\Psi^0_{p,\, qq' \ldots}| \tag{25}$$

wo Γ_p durch (18) oder (22) gegeben ist und die Summe in (25) über alle Zustände des Systems zu erstrecken ist, so genügen die Zustände (24) trivialerweise der Gleichung (vgl. (15))

$$(H_0 + \Gamma) \Psi^0_{p,\, qq' \ldots} = (E_p + \omega_q + \omega_{q'} + \ldots) \Psi^0_{p,\, qq' \ldots}. \tag{26}$$

Insbesonders gilt natürlich auch

$$(H_0 + \Gamma) \Psi_p^0 = E_p \Psi_p^0, \tag{15'}$$

da diese Gleichung mit (15) identisch ist. Die Voraussetzungen zur Aufstellung des Streuformalismus sind nun nahezu vollständig: die asymptotischen Zustände sind durch (24), (26) gegeben und stellen ein vollständiges Orthonormalsystem dar, wobei die Energieeigenwerte sich in der Tat additiv aus den Beiträgen des Zwei-Nukleonen-Systems und der π-Mesonen zusammensetzen, während die Wechselwirkung dann durch

$$H_1 - \Gamma \tag{27}$$

gegeben ist. Es ist noch nötig zu zeigen, daß die Eigenwerte von (23) und (26) wirklich zusammenfallen, d.h. daß auch für die reellen Zustände gilt,

daß ihre Energieeigenwerte sich in der angegebenen Form additiv zusammensetzen †.

Dazu schreiben wir z.B. für den Fall eines zusätzlichen Mesons

$$\Psi_{p,q} = \Lambda_q \Psi_{p,q} + \Lambda_{qc} \Psi_{p,q}, \tag{28}$$

wo Λ_q der Projektionsoperator ist, der auf den Ein-Meson-Zustand q projiziert, und Λ_{qc} derjenige, der von diesem weg projiziert. Der zweite Term in (28) repräsentiert gewissermaßen die „Mesonwolke" (mit Einschluß des Mesonvakuumbeitrages) des Ein-Meson-Zwei-Nukleonen-Zustandes. Die Entwicklung von (28) nach dem System (24) zeigt, daß

$$\Lambda_q \Psi_{p,q} = c_{p,q} a_q^* \Psi_p^0, \tag{29}$$

worin Ψ_p^0 zunächst eine allgemeine Superposition der Eigenfunktionen von (15) und $c_{p,q}$ eine Entwicklungskonstante ist. Aus der Annahme

$$H\Psi_{p,q} = (E_p + \omega_q)\Psi_{p,q} \tag{30}$$

und (29) folgt nun analog den Überlegungen, die zu (15) führen,

$$\begin{aligned}(H_0 + \Gamma_{p,q}) a_q^* \Psi_p^0 &= \left\{ \sum_j \left(M_0 + \frac{\mathbf{p}_j^2}{2M_0} \right) + \omega_q + \Gamma_{p,q} \right\} a_q^* \Psi_p^0 \\ &= (E_p + \omega_q) a_q^* \Psi_p^0,\end{aligned} \tag{31}$$

wo

$$\Gamma_{p,q} = \Lambda_q H_1 \frac{\mathrm{P}}{E_p + \omega_q - H_0 - \Lambda_{qc} H_1} H_1 \Lambda_q \tag{32}$$

der Feldenergieoperator des Zustandes $\Psi_{p,q}$ ist, der Selbstenergie und Wechselwirkung der Nukleonen beschreibt, und der in der Tat in dem allgemeinen Feldenergieoperator (25) enthalten ist. Denn wegen

$$a_q^* \Lambda_0 = \Lambda_q a_q^*, \quad a_q^* \Lambda_c = \Lambda_{qc} a_q^*, \tag{33}$$

gilt

$$\Gamma_{p,q} a_q^* = a_q^* \Gamma_p, \tag{34}$$

wo Γ_p durch (18) definiert ist (vgl. auch (25)), wobei Glieder unterdrückt sind, die aus (vgl. (5))

$$[H_1, a_q^*] = V_q \tag{35}$$

folgen und die gegenüber (34) wie $1/V$ für wachsendes Normierungsvolumen $V \to \infty$ gegen Null gehen. (Um (34) zu beweisen, verwende man die Identität

$$\begin{aligned}(E_p + \omega_q - H_0 - \Lambda_{qc} H_1)^{-1} a_q^* &= H a_q^* (E_p - {}_0 - \Lambda_c H_1)^{-1} \\ &+ (E_p + \omega_q - H_0 - \Lambda_{qc} H_1)^{-1} \Lambda_{qc} V_q (E_p - H_0 - \Lambda_c H_1)^{-1},\end{aligned}$$

die einfach durch Multiplikation mit einem der Energienenner zu beweisen ist). Aus (34) folgt aber, daß die Gleichungen (15) und (31) identisch sind.

† Daß die Energien der reellen und der nackten Zwei-Nukleonen-Zustände gleich sind, ist gemäß (8) und (15) klar.

Dieses zeigt, daß der Eigenwert von (30) die vorausgesetzte Form haben muß und daß im übrigen Ψ_p^0 in (29) direkt Eigenfunktion von (15) (und keine Superposition) ist.

Oder anders ausgedrückt: wir haben gezeigt (für Zustände mit mehr als einem Meson gehen die Überlegungen ganz analog), daß die Wechselwirkung (27) keine Energieeigenwertänderung bewirkt, sondern nur noch Einfluß auf die Zustandsvektoren selbst hat †, was im übrigen auch dann der Fall ist, wenn wir vom gesamten Feldenergieoperator Γ den Wechselwirkungsanteil der beiden Nukleonen abtrennen (so daß nur der reine Selbstenergieanteil verbleibt), da dieser ebenfalls keine Energieeigenwertänderung bewirkt (wie das etwa beim gewöhnlichen Potential der Fall ist). Dann würde Ψ_p^0 den Zustand zweier freier nackter Nukleonen beschreiben. Jedoch hat in unserem Falle dieses Vorgehen keinen Sinn, da wir explizit die Existenz des gebundenen Zustandes zu berücksichtigen haben.

Der Zustandsvektor Ψ_p^0 des nackten Zwei-Nukleonen-Systems hat nun die allgemeine Form

$$\Psi_p^0 = \int \mathrm{d}\mathbf{x}_1 \mathrm{d}\mathbf{x}_2 \psi_p(\mathbf{x}_1, \mathbf{x}_2) |\mathbf{x}_1, \mathbf{x}_2; s\rangle \tag{36}$$

wo

$$\psi_p(\mathbf{x}_1, \mathbf{x}_2) = \langle \mathbf{x}_1, \mathbf{x}_2; s | \Psi_p^0 \rangle \tag{37}$$

die übliche Schrödingersche Wellenfunktion ist; s soll den Spin- und Isobarenspin-Zustand des Zwei-Nukleonen-Systems bezeichnen, der ansonsten mit durch p charakterisiert sein soll. Aus (15) folgt nun nach Multiplikation mit $\langle \mathbf{x}_1, \mathbf{x}_2; s|$ von links her direkt die Schrödinger-Gleichung für das Zwei-Nukleonen-System

$$\sum_j \left(M_0 + \frac{\mathbf{p}_j^2}{2M_0} \right) \psi_p(\mathbf{x}_1, \mathbf{x}_2) + \int \mathrm{d}\mathbf{x}'_1 \mathrm{d}\mathbf{x}'_2 \langle \mathbf{x}_1, \mathbf{x}_2; s | \Gamma_p | \mathbf{x}'_1, \mathbf{x}'_2; s \rangle \psi_p(\mathbf{x}'_1, \mathbf{x}'_2) = E_p \psi_p(\mathbf{x}_1, \mathbf{x}_2). \tag{38}$$

Es ist gut bekannt, daß (38) als Ausgangspunkt für eine nichtrelativistische Theorie der Kernkräfte verwandt werden kann. Im allgemeinen ist das resultierende Potential impulsabhängig und nichtlokal. Das hängt damit zusammen, daß Γ_p die Nukleonenimpulse enthält, d.h. von den Impulseigenwerten und Impulsoperatoren abhängt, und damit auch nichtdiagonal in den Nukleonenkoordinaten ist. Wir zeigen, daß aber im gesamten nichtrelativistischen Bereich diese Abhängigkeit nur an den Selbstenergien und nicht an dem Wechselwirkungsanteil wesentlich sein kann (sofern dieser

† d.h. es ist $\Delta E_n = \langle \Psi_n^0 | (H_1 - \Gamma) | \Psi_n \rangle = 0$, was natürlich auch direkt an diesem Ausdruck gezeigt werden kann.

klein gegen die Nukleonenmasse M ist) †. Zu diesem Zwecke beachten wir, daß bei einer Entwicklung von (18) nach $(\Lambda_c H_1 - \Gamma)$ oder Iteration von (22) und Entwicklung nach $(H_1 - \Gamma)$ gemäß ††

$$\Gamma_p = \Lambda_0 H_1 \frac{\mathrm{P}}{E_p - (H_0+\Gamma)} H_1 \Lambda_0 + \Lambda_0 H_1 \frac{\mathrm{P}}{E_p - (H_0+\Gamma)} \Lambda_c H_1 \frac{\mathrm{P}}{E_p - (H_0+\Gamma)} H_1 \Lambda_0 + \ldots \quad (39)$$

in allen Gliedern kein intermediärer Mesonvakuum-Zustand auftreten kann, so daß also die Zwischenzustände mindestens ein Meson enthalten müssen. (Die in den höheren Ordnungen auftretenden Beiträge von Γ denken wir uns unter Verwendung von (25) durch (39) selbst ausiteriert; sie lassen sich analog dem Folgenden behandeln.) Die Energienenner sind bei Entwicklung nach dem System (24) Differenzen der Form

$$E_p - E_{p'} - \omega_q, \quad E_p - E_{p''} - \omega_{q'} - \omega_{q''}, \ldots \quad (40)$$

und enthalten also mindestens die Energie eines Mesons (wobei die Untersuchung dieses Falles genügt). Daneben tritt die Differenz der Energien des Zwei-Nukleonen-Systems im gebundenen Zustand oder in den nicht gebundenen Zuständen auf. Wir betrachten zunächst letztere, so daß also gilt

$$E_p = \left(M + \frac{\mathbf{p}_1^2}{2M}\right) + \left(M + \frac{\mathbf{p}_2^2}{2M}\right) \quad (41)$$

und entsprechend für $E_{p'}$, wo M die renormierte Nukleonenmasse ist. Für hinreichend hohe Energien der Relativbewegung der Nukleonen sind ihre Eigenfunktionen ebene Wellen, so daß der Impulssatz beim einzelnen Emissionsakt (bzw. Absorptionsakt) am betreffenden Nukleon gelten muß. Dann gilt

$$E_p - E_{p'} = \frac{\mathbf{p}_j^2}{2M} - \frac{(\mathbf{p}_j - \mathbf{q})^2}{2M} \qquad (j = 1 \text{ oder } 2). \quad (42)$$

Es ist aber leicht zu zeigen, daß

$$\frac{\mathbf{p}_j^2}{2M} - \frac{(\mathbf{p}_j - \mathbf{q})^2}{2M} \ll \omega_q = \sqrt{m^2 + \mathbf{q}^2} \quad (43)$$

sofern

$$\frac{\mathbf{p}_j^2}{2M} \ll M \quad (44)$$

† Lökalität bezüglich der (ortsunabhängigen) Selbstenergien bedeutet, dass die Anwendung der Selbstenergieoperatoren auf die Wellenfunktionen lediglich zu einer Multiplikation dieser mit einem Faktor führt.

†† Bei Iteration von (22) tritt zunächst $(1 - \Lambda_0)$ im zweiten und in den höheren Gliedern auf. Es gilt aber nach (11) $1 - \Lambda_0 = \Lambda_c$.

(denn (43) ist äquivalent

$$\frac{\mathbf{p}_j^2}{2M} \ll \left(\frac{|\mathbf{q}|}{2} + \frac{M}{|\mathbf{q}|}\sqrt{m^2+\mathbf{q}^2}\right)^2 \Big/ 2M$$

und die rechte Seite ist — wie sich leicht zeigen läßt — stets $\gtrsim M$).

Bei niedrigen Energien der Relativbewegung gilt der Impulssatz nur genähert, aber die Korrekturen sind nur von der Art, daß sich $(E_p - E_{p'})$ von (42) nur durch einen nichtrelativistischen Betrag unterscheidet. Dasselbe gilt auch für den gebundenen Zustand. Insgesamt haben wir also

$$E_p - E_{p'} \ll \omega_q. \tag{45}$$

Damit ist klar, daß die Impulsabhängigkeit und Nichtlokalität des Potentials nur eine relativistische Korrektur darstellen, während sie an den Selbstenergien (sofern diese — im Unterschied zum Wechselwirkungsanteil — groß von der Ordnung M sind) bereits nichtrelativistische Korrekturen geben, was (jedenfalls bezüglich der Impulsabhängigkeit) allgemein nötig ist für den Übergang von den nichtrenormierten zu den renormierten Nukleonenenergien

$$\sum_j \left(M_0 + \frac{\mathbf{p}_j^2}{2M_0}\right) \to \sum_j \left(M + \frac{\mathbf{p}_j^2}{2M}\right). \tag{46}$$

3. *S*-Matrix-Formalismus

Die S-Matrix ist für die Wechselwirkung (27) gegeben durch

$$S = \mathrm{T}\exp\left\{-i\int_{-\infty}^{+\infty} H_1(t)\mathrm{d}t\right\} \tag{47}$$

mit

$$H_1(t) = \mathrm{e}^{i(H_0+\Gamma)t}(H_1-\Gamma)\mathrm{e}^{-i(H_0+\Gamma)t} = \sum_p \{a_q V_q(t) + a_q^* V_q^*(t)\} - \Gamma(t) \tag{48}$$

wo nun (vgl. (5) und (6))

$$V_q(t) = \sum_j \frac{i}{\sqrt{V}} \frac{\sqrt{4\pi}f_0}{m} \tau_\rho{}^j \boldsymbol{\sigma}^j \cdot \mathbf{q} v_{\mathbf{q}} \frac{1}{\sqrt{2\omega_q}} \mathrm{e}^{iH_N t}\mathrm{e}^{i\mathbf{q}\cdot\mathbf{x}_j}\mathrm{e}^{-iH_N t}\mathrm{e}^{-i\omega_q t},\ \Gamma(t) = \mathrm{e}^{iH_N t}\Gamma\mathrm{e}^{-iH_N t} \tag{49}$$

$$H_N = \sum_j \left(M_0 + \frac{\mathbf{p}_j^2}{2M_0}\right) + \Gamma.$$

Hierbei haben wir von der Tatsache Gebrauch gemacht, daß Γ bzw. $\Gamma(t)$ gemäß (25) eine mit a_q^* und a_q kommutierende Größe ist. Das T-Symbol in (47) ordnet die einzelnen Terme in der Entwicklung nach $H_1(t)$ in der bekannten Weise. Jedoch werden wir keinen expliziten Gebrauch von einer störungstheoretischen Entwicklung machen, sondern nur einige allgemeine Beziehungen brauchen, die aus der Darstellung (47) folgen.

Die unitäre S-Matrix (47) geht nun durch einen Grenzübergang aus der Transformationsmatrix

$$U(t, t_0) = \mathrm{T} \exp\left\{-i \int_{t_0}^{t} H_1(t)\mathrm{d}t\right\} \tag{50}$$

hervor, die den Differentialgleichungen

$$\frac{\partial U(t, t_0)}{\partial t} = -iH_1(t)U(t, t_0), \quad \frac{\partial U(t, t_0)}{\partial t_0} = iU(t, t_0)H_1(t_0) \tag{51}$$

mit der Anfangsbedingung $U(t_0, t_0) = 1$ bzw. den Integralgleichungen

$$U(t, t_0) = 1 - i \int_{t_0}^{t} \mathrm{d}t' H_i(t')U(t', t_0) = 1 + i \int_{t}^{t_0} \mathrm{d}t' U(t, t')H_1(t') \tag{51'}$$

genügt. Der Grenzübergang ist dabei so vorzunehmen, daß die in t oszillierenden Terme in (50) für $t_0 \to -\infty$, $t \to +\infty$ verschwinden, damit sich ein definierter Grenzwert ergibt. Wir ersetzen dazu

$$H_1(t) \to \mathrm{e}^{-\varepsilon|t|} H_1(t), \tag{52}$$

wo $\mathrm{e}^{-\varepsilon|t|}$ ein Dämpfungsfaktor in dem Sinne ist, daß nach Ausführung der Rechnung der Grenzübergang $\varepsilon \to 0$ vorzunehmen ist. Dann erhalten wir gemäß der zweiten Gleichung (51') in Anwendung auf einen nackten Zustand (24), (26) die Chew-Gell-Mann-Goldberger-Darstellung für den uns wichtigen Operator $U(0, \mp\infty)$ [7, 11])

$$\begin{aligned} U(0, \mp\infty)\Psi_n^0 &= \left\{1 + i \int_0^{\mp\infty} \mathrm{d}t \mathrm{e}^{\pm\varepsilon t} \mathrm{e}^{i(H - E_n)t}(H_1 - \Gamma)\right\} \Psi_n^0 \\ &= \left\{1 + \frac{1}{E_n - H \pm i\varepsilon}(H_1 - \Gamma)\right\} \Psi_n^0 \end{aligned} \tag{53}$$

wo wir (vgl. (48) und (50))

$$U(0, t)H_1(t) = \mathrm{e}^{iHt}(H_1 - \Gamma)\mathrm{e}^{-i(H_0 + \Gamma)t} \tag{54}$$

benutzt haben, was aus einfacher Anwendung der bekannten Additionstheoreme für Exponentialoperatoren folgt. Glg. (53) ergibt aber

$$(H - E_n)U(0, \mp\infty)\Psi_n^0 = 0, \tag{55}$$

d.h. die Zustände

$$\Psi_n^{(\pm)} = U(0, \mp\infty)\Psi_n^0 \tag{56}$$

sind Eigenfunktionen des Gesamt-Hamiltonoperators in dem Sinne, daß der Operator $U(0, \mp\infty)$ einen nackten Zustand Ψ_n^0 in einen Eigenzustand $\Psi_n^{(\pm)}$ des Gesamt-Hamiltonoperators überführt, wobei Ψ_n^0 die einlaufenden bzw. auslaufenden Teilchen beschreibt. Es ist wichtig zu bemerken, daß auch in unserem Falle, wo die Existenz eines gebundenen Zustandes zu berücksichtigen ist, $U(0, \mp\infty)$ ein unitärer Operator ist (wobei insbesondere

eine Normierungskonstante in (53) zu berücksichtigen ist, da $U(0, \mp\infty)\Psi_n^0$ im allgemeinen kein normierter Zustandsvektor ist, was wir aber nicht explizit ausschreiben wollen). Wegen

$$U^*(0, \mp\infty) = U(\mp\infty, 0) \tag{57}$$

lautet die Unitaritätsbeziehung

$$U(\mp\infty, 0)U(0, \mp\infty) = 1, \quad U(0, \mp\infty)U(\mp\infty, 0) = 1. \tag{58}$$

Der Grund ist der, daß die von uns definierten asymptotischen Zustände (24) und die reellen Zustände das gleiche Eigenwertspektrum besitzen, da die von uns benutzte Asymptotenbedingung nicht zum Zerfall des gebundenen Zustandes führt, weil die Wechselwirkung zwischen den Nukleonen im nackten Zustand nicht abgeschaltet wird (sondern nur die Mesonwolke). Bei üblicher Verwendung der Adiabaten-Konzeption, die die gesamte Wechselwirkung abschaltet, zerfällt zwangsläufig der gebundene Zustand und die zweite Gleichung in (58) ist ungültig [11]).

Im folgenden verwenden wir den S-Matrix-Formalismus unter Benutzung von Variationsableitungen, wie er von Bogolubov [8, 9]) vorgeschlagen wurde. Die Tatsache, daß wir das Nukleonenfeld nicht ein zweites Mal quantisiert haben, bedingt, daß der Operator der kinetischen Energie der Nukleonen nicht mit dem Feldoperator der Mesonen am Ort der Nukleonen kommutiert, was wir aber im einzelnen zu beachten haben, wenn wir die Vertauschungsrelationen für die Vernichtungs- und Erzeugungsoperatoren der Mesonen mit der S-Matrix durch Variationsableitungen dieser bezüglich des Mesonfeldes $\phi_\rho(x)$ formulieren wollen. Es erscheint in unserem Falle aber zweckmäßiger, direkt Variationsableitungen von S bezüglich des Wechselwirkungsoperators $H_1(t)$ in (47) zu bilden. Aus (48) folgt

$$[a_q, H_1(t)] = V_q^*(t), \quad [H_1(t), a_q^*] = V_q(t), \tag{59}$$

und hieraus, da die S-Matrix gemäß (47) ein Funktional in $H_1(t)$ ist,

$$\begin{aligned} [a_q, S] &= \mathrm{T}[a_q, \mathrm{e}^{-i\int H_1(t)\,dt}] = \mathrm{T}\int dt V_q^*(t)\,\frac{\delta}{\delta H_1(t)}\,\mathrm{e}^{-i\int H_1(t)\,dt} \\ &= \int dt\,\mathrm{T}\,V_q^*(t)\,\frac{\delta S}{\delta H_1(t)}, \\ [S, a_q^*] &= \int dt \mathrm{T} V_q(t)\,\frac{\delta S}{\delta H_1(t)}, \end{aligned} \tag{60}$$

wo die Operatoren $V_q^*(t)$ und $V_q(t)$, die bei verschiedenen Zeiten nicht vertauschbar sind und demgemäß auch nicht mit dem Operator S und seinen Variationsableitungen nach $H_1(t)$, innerhalb des als T-Produkt geordneten

Endausdruckes stehen müssen (innerhalb eines T-Produktes haben sie die Eigenschaften von c-Zahlen, was die übliche Herleitung in (60) möglich macht). Natürlich ist das T-Symbol durch das $\overline{\mathrm{T}}$-Symbol für das antichronologische Produkt in (60) zu ersetzen, falls die S-Matrix durch dieses ausgedrückt wird.

Die Kausalitätsbedingung, die von Bogolubov [8, 9]) als „Retardierungs-" bzw. „Avancierungseigenschaft" des Stromoperators $j(x)$ in dem Sinne formuliert wurde, daß dieser nicht von den einlaufenden Mesonfeldern mit Zeiten $t' > t$ bzw. nicht von den auslaufenden mit Zeiten $t' < t$ abhängen soll, ist in unserem Falle zu schreiben

$$\frac{\delta}{\delta H_1(t')}\left[S^*\left(\mathrm{T}V_q(t)\frac{\delta S}{\delta H_1(t)}\right)\right] = 0 \quad \text{für} \quad t' > t, \tag{61}$$

$$\frac{\delta}{\delta H_1(t')}\left[\left(\mathrm{T}V_q(t)\frac{\delta S}{\delta H_1(t)}\right)S^*\right] = 0 \quad \text{für} \quad t' < t, \tag{61'}$$

wo natürlich $V_q(t)$ auch durch $V_q{}^*(t)$ ersetzt werden kann. Wegen (vgl. (47))

$$\mathrm{T}V_q(t)\frac{\delta S}{\delta H_1(t)} = -iU(+\infty, t)V_q(t)U(t, -\infty) \tag{62}$$

und

$$S^*U(+\infty, t) = U(-\infty, t), \quad U(t, -\infty)S^* = U(t, +\infty)$$

(wo wir die Unitarität von $U(t, \pm\infty)$ benutzen) sind die Beziehungen (61), (61') in unserem Hamilton-Formalismus trivialerweise erfüllt.

Im folgenden benutzen wir die Bezeichnung

$$\bar{V}_q(t) = i\left(\mathrm{T}V_q(t)\frac{\delta S}{\delta H_1(t)}\right)S^* = U(+\infty, t)V_q(t)U(t, +\infty), \tag{63}$$

wodurch $V_q(t)$ in der Heisenberg-Darstellung ausgedrückt wird, die für $t \to +\infty$ mit der Wechselwirkungsdarstellung übereinstimmt, was fürs Folgende zweckmäßig ist. Durch einfaches Ableiten folgt die wichtige Beziehung

$$\left(\mathrm{T}V_{q'}^*(t')\frac{\delta}{\delta H_1(t')}\right)\bar{V}_q(t) = i\theta(t'-t)[\bar{V}_q(t), \bar{V}_{q'}^*(t')] \tag{64}$$

welche im übrigen die Bedingung (61') enthält. Ein Ausdruck der Form (64) ist aus der Theorie der Dispersionsbeziehungen bekannt [12]).

Genau so einfach leitet man die Beziehung (vgl. (62))

$$\left[\left(\mathrm{T}V_{q'}^*(t')\frac{\delta}{\delta H_1(t')}\right)\left(\mathrm{T}V_q(t)\frac{\delta S}{\delta H_1(t)}\right)\right]S^* = -\mathrm{T}\bar{V}_{q'}^*(t')\bar{V}_q(t) \tag{65}$$

ab, die genau dem in einer kovarianten Formulierung auftretenden T-Produkt der Ströme entspricht. Wir werden (65) aber nicht brauchen.

Unser Streuformalismus ist nun so weit fertig, daß wir unmittelbar zur Formulierung der Impulsnäherung für den Fall der Streuung von π-Mesonen an Deuteronen übergehen können.

4. Impulsnäherung

Wir betrachten das S-Matrixelement für die (elastische oder unelastische) Streuung von π-Mesonen an Deuteronen

$$\langle p', q'|S|p, q\rangle = \langle \Psi^0_{p',q'}|S|\Psi^0_{p,q}\rangle = \langle a^*_{q'}\Psi^0_{p'}|S|a_q{}^*\Psi_p{}^0\rangle, \tag{66}$$

wo $\Psi^0_{p,q}$ den Anfangszustand beschreibt, in dem sich ein Deuteron im Grundzustand $\Psi_p{}^0$ und ein π-Meson im Zustand q befindet, und entsprechend $\Psi^0_{p',q'}$ den Endzustand, in dem das Zwei-Nukleonen-System im Zustand $\Psi^0_{p'}$ und das π-Meson im Zustand q' ist. Die Anwendung der Vertauschungsrelation (60) auf das einlaufende Meson führt auf

$$\langle p', q'|S|p, q\rangle = \delta_{q'q}\langle \Psi^0_{p'}|S|\Psi_p{}^0\rangle + \int \mathrm{d}t \langle a^*_{q'}\Psi^0_{p'}|\left(\mathrm{T}V_q(t)\,\frac{\delta S}{\delta H_1(t)}\right)|\Psi_p{}^0\rangle. \tag{67}$$

Wir verwenden nun die Tatsache, daß das Zwei-Nukleonen-System sich im Anfang im stabilen Deuteron-Grundzustand befindet, für den (bis auf einen Phasenfaktor) gilt

$$S\Psi_p{}^0 = S^*\Psi_p{}^0 = \Psi_p{}^0, \tag{68}$$

so daß sich (67) bei Anwendung einer Vertauschungsrelation vom Typ (60) auf das auslaufende Meson und Verwendung von (63) weiter reduziert auf

$$\langle p', q'|S|p,q\rangle = \delta_{p',q';p,q} - i\int \mathrm{d}t\mathrm{d}t' \langle p'|\left(\mathrm{T}V^*_{q'}(t')\,\frac{\delta}{\delta H_1(t')}\right)\bar{V}_q(t)|p\rangle. \tag{69}$$

Definieren wir die R-Matrix durch

$$S = 1 + R \tag{70}$$

und verwenden wir (64), so folgt

$$\langle p', q'|R|p, q\rangle = -\int \mathrm{d}t\mathrm{d}t'\,\theta(t'-t)\langle p'|[\bar{V}^*_{q'}(t'), \bar{V}_q(t)]|p\rangle. \tag{71}$$

Die Funktion $\bar{V}_q(t)$ läßt sich auch in der von (63) verschiedenen Form schreiben

$$\bar{V}_q(t) = U(+\infty, 0)\mathrm{e}^{iHt}V_q\mathrm{e}^{-i\omega_q t}\mathrm{e}^{-iHt}U(0, +\infty), \tag{72}$$

wo V_q durch (6) gegeben ist, so daß unter Verwendung von (55), nach einfacher Rechnung wird

$$\langle p', q'|R|p, q\rangle = -2\pi\delta(E_{p'} + \omega_{q'} - E_p - \omega_q)\int \mathrm{d}t\theta(t)\langle p'|[\bar{V}^*_{q'}(t), \bar{V}_q(0)]|p\rangle. \tag{73}$$

Definieren wir die T-Matrix durch

$$\langle \mathfrak{p}', q'|S|\mathfrak{p}, q\rangle = \delta_{\mathfrak{p}', q'; \mathfrak{p}, q} - 2\pi i \delta(E_{\mathfrak{p}'} + \omega_{q'} - E_{\mathfrak{p}} - \omega_q)\langle \mathfrak{p}', q'|T|\mathfrak{p}, q,\rangle, \quad (74)$$

so gilt nach (70) und (73)

$$\langle \mathfrak{p}', q'|T|\mathfrak{p}, q\rangle = -i \int \mathrm{d}t \theta(t) \langle \mathfrak{p}'|[\bar{V}_{q'}^*(t), \bar{V}_q(0)]|\mathfrak{p}\rangle. \quad (75)$$

Wir entwickeln (75) nach dem Funktionensystem (24), (26) und erhalten †

$$\begin{aligned}\langle \mathfrak{p}', q'|T|\mathfrak{p}, q\rangle &= -i \sum_n \int \mathrm{d}t \theta(t) \{\langle \mathfrak{p}'|\bar{V}_{q'}^*(t)|n\rangle\langle n|\bar{V}_q(0)|\mathfrak{p}\rangle - \langle \mathfrak{p}'|\bar{V}_q(0)|n\rangle\langle n|\bar{V}_{q'}^*(t)|\mathfrak{p}\rangle\} \\ &= \sum_n \left\{ \frac{\langle \mathfrak{p}', q'|T^*|n\rangle\langle n|T|\mathfrak{p}, q\rangle}{E_{\mathfrak{p}'} + \omega_{q'} - E_n + i\varepsilon} + \frac{\langle \mathfrak{p}', q|T|n\rangle\langle n|T^*|\mathfrak{p}, q'\rangle}{E_{\mathfrak{p}} - \omega_{q'} - E_n - i\varepsilon} \right\}, \end{aligned} \quad (76)$$

wobei wir die Tatsache verwandt haben, daß gemäß (vgl. (67), (68), (63) und (72))

$$\begin{aligned}\langle n|S|\mathfrak{p}, q\rangle = \langle n|S|a_q^* \Psi_{\mathfrak{p}}^0\rangle &= \delta_{n; \mathfrak{p}, q} - i \int \mathrm{d}t \langle n|\bar{V}_q(t)|\mathfrak{p}\rangle \\ &= \delta_{n; \mathfrak{p}, q} - 2\pi i \delta(E_n - E_{\mathfrak{p}} - \omega_q)\langle n|\bar{V}_q(0)|\mathfrak{p}\rangle \end{aligned} \quad (77)$$

allgemein für die T-Matrix gilt

$$\langle n|T|\mathfrak{p}, q\rangle = \langle n|\bar{V}_q(0)|\mathfrak{p}\rangle. \quad (78)$$

Wir bemerken, daß im Gegensatz zur statischen Ein-Nukleon-Theorie von Chew und Low [13]) die Abhängigkeit vom Impuls des einkommenden Mesons in (78) nichttrivial ist, weil diese gemäß (6) zusätzlich in den Exponentialfaktoren $e^{i\mathfrak{q}\cdot\mathfrak{x}_j}$ steckt. Dennoch definiert der Ausdruck (78) eine bestimmte Extrapolation von der Energieschale, und es ist klar, daß (76) dieselbe Extrapolation hat. Der Beweis in der statischen Ein-Nukleon-Theorie von Chew und Low ist bekanntlich trivial, weil sich die Abhängigkeit vom Impuls des einfallenden Mesons auf beiden Seiten der zu (76) analogen Chew-Low-Gleichung als Faktor einfach heraushebt. Im allgemeinen Fall folgt die Möglichkeit der Extrapolation einfach aus der Tatsache, daß (76) eine mathematische Identität ist, denn (75) und (76) folgen unter Verwendung einer zu (60) analogen Vertauschungsrelation unmittelbar aus der Definition (78) (unabhängig davon, ob die Werte der Impulse auf der Energieschale liegen oder nicht; es ist klar, daß in den Energienennern in (76) $E_{\mathfrak{p}'} + \omega_{q'}$ bzw. $E_{\mathfrak{p}} - \omega_{q'}$ nur dann durch $E_{\mathfrak{p}} + \omega_q$ bzw. $E_{\mathfrak{p}'} - \omega_q$ ersetzt werden darf, wenn Werte auf der Energieschale betrachtet werden, s.a. Ref. [10])).

Der antihermitische Teil der Übergangsmatrix folgt nun aus (76) in der Form

† Falls wir die S-Matrix gemäß (65) reduziert hätten, so wären wir auf einen Ausdruck der Form (76) gestoßen, in dem im zweiten Glied $-i\varepsilon$ durch $+i\varepsilon$ ersetzt ist, und der also ganz andere analytische Eigenschaften hat.

$$\langle p', q'|A|p, q\rangle = \frac{1}{2i}\langle p', q'|T-T^*|p, q\rangle$$
$$= -\pi \sum_n \{\langle p', q'|T^*|n\rangle\langle n|T|p, q\rangle\delta(E_{p'}+\omega_{q'}-E_n) \qquad (79)$$
$$-\langle p', q|T|n\rangle\langle n|T^*|p, q'\rangle\delta(E_p-\omega_{q'}-E_n)\},$$

der für den Fall der elastischen Vorwärtsstreuung in bekannter Weise mit dem totalen Wirkungsquerschnitt zusammenhängt gemäß dem optischen Theorem

$$\sigma_t = \frac{2\pi}{v} V \sum_n \delta(E_p+\omega_q-E_n)|\langle n|T|p, q\rangle|^2 = -\frac{2}{v} V\langle p, q|A|p, q\rangle, \quad (80)$$

worin V das Normierungsvolumen und v die Relativgeschwindigkeit ist, für die im Laboratoriumssystem gilt $v = |\mathbf{q}|/\omega_q$, das wir im folgenden voraussetzen wollen. Hierbei ist zu beachten, daß im beobachtbaren Bereich ($\omega_q \geqq m$) der zweite Summand in (79) auf Grund der Stabilität des Anfangszustandes (Deuteron-Grundzustand) verschwindet, weil keine Emission eines oder mehrerer Mesonen möglich ist ($E_p \neq E_n+\omega_{q'}$). Die Beziehung (79) war Gegenstand der Untersuchungen in Ref. [1, 2, 3]) bei der Aufstellung und Auswertung der Dispersionsbeziehungen für den Fall der elastischen Vorwärtsstreuung von π-Mesonen an Deuteronen. Besonderes Interesse hatte der Absorptions-bzw. Emissionsprozeß mit $|n\rangle = |p''\rangle$ in (79), der genähert ausgerechnet und in den nichtbeobachtbaren Bereich analytisch fortgesetzt wurde. Der Grundgedanke dieses naheliegenden Näherungsverfahrens, das auch von Ioffe, Pomeranchuk und Rudik [14]) und für den Fall der statischen Theorie von Lichtenberg [15]) in ähnlichem Zusammenhang verwandt wurde, ist einfach der: man ersetze beim Emissions- bzw. Absorptionsprozeß die reellen Zustandsvektoren des Zwei-Nukleonen-Systems durch die Wellenfunktionen der entsprechenden nackten Zustände unter gleichzeitiger Ersetzung der nichtrenormierten Kopplungskonstanten durch die renormierte. Dieses Näherungsverfahren soll hier nun im einzelnen untersucht werden, was uns ganz zwangsläufig zu einer feldtheoretischen Verallgemeinerung der Chewschen Impulsnäherung führen wird.

Dazu betrachten wir genauer die T-Matrix (78) unter Verwendung von (63) und (6):

$$\langle n|T|p, q\rangle = \langle n|\bar{V}_q(0)|p\rangle = \langle n|U(+\infty, 0)V_q U(0, +\infty)|p\rangle$$
$$= \sum_j \langle n|U(+\infty, 0)V_q^j U(0, +\infty)|p\rangle, \qquad (81)$$

wo nach (49)

$$U(0, +\infty) = \mathrm{T}\exp\left\{-i\int_{+\infty}^{0} H_1(t)\mathrm{d}t\right\} = \exp_+\left\{-i\int_{+\infty}^{0} H_1(t)\right\}\mathrm{d}t; \quad (82)$$

$H_1(t)$ ist durch (48) gegeben und das $+$-Symbol soll im folgenden die chronologische Ordnung der Operatoren angeben und entsprechend das

—-Symbol die antichronologische. Wir schreiben unter Verwendung der Additionstheoreme für Exponentialoperatoren

$$\begin{aligned}\exp_+\left\{-i\int_\infty^0 H_1(t)\mathrm{d}t\right\} &= \exp\left\{-i\int_\infty^0 H\mathrm{d}t\right\}\exp\left\{i\int_\infty^0 (H_0+\Gamma)\mathrm{d}t\right\}\\ &= \exp_+\left\{-i\int_\infty^0 [H_1{}^1(t)+H_1{}^2(t)]\mathrm{d}t\right\}\exp\left\{-i\int_\infty^0 (H_0+\Gamma_1+\Gamma_2)\mathrm{d}t\right\}\exp\left\{i\int_\infty^0 (H_0+\Gamma)\mathrm{d}t\right\} \qquad (83)\\ &= \exp_+\left\{-i\int_\infty^0 [H_1{}^1(t)+H_1{}^2(t)]\mathrm{d}t\right\}\exp_+\left\{-i\int_\infty^0 \Gamma_P{}^{12}(t)\mathrm{d}t\right\}\end{aligned}$$

mit

$$\Gamma_P{}^{12}(t) = \mathrm{e}^{i(H_0+\Gamma)t}\Gamma_P{}^{12}\mathrm{e}^{-i(H_0+\Gamma)t}, \qquad \Gamma_P{}^{12} = \Gamma_P{}^{21} = \Gamma_1+\Gamma_2-\Gamma, \qquad (84)$$

worin Γ_j die Selbstenergieoperatoren für die einzelnen Nukleonen, gebildet analog (25) für die Ein-Nukleon-Systeme, und Γ der Feldenergieoperator (25) ist und (vgl. (6) und (48), (49))

$$H_1{}^j(t) = \sum_q \{V_q{}^j(t)a_q+V_q{}^{j*}(t)a_q{}^*\}-\Gamma_j(t) \qquad (85)$$

mit

$$\begin{aligned}V_q{}^j(t) &= \mathrm{e}^{iH_N{}^jt}V_q{}^j\mathrm{e}^{-i\omega_q t}\mathrm{e}^{-iH_N{}^jt}, \quad \Gamma_j(t) = \mathrm{e}^{iH_N{}^jt}\Gamma_j\mathrm{e}^{-iH_N{}^jt},\\ H_N{}^j &= \left(M_0+\frac{\mathbf{p}_j{}^2}{2M_0}\right)+\Gamma_j\end{aligned} \qquad (86)$$

die Wechselwirkungsoperatoren für die entsprechenden Ein-Nukleon-Systeme sind.

Weiterhin formen wir um

$$\exp_+\left\{-i\int_\infty^0 [H_1{}^1(t)+H_1{}^2(t)]\mathrm{d}t\right\} = \begin{cases}\exp_+\left\{-i\int_\infty^0 \Gamma_M{}^{12}(t)\mathrm{d}t\right\}U^1(0,+\infty)U^2(0,+\infty)\\ \exp_+\left\{-i\int_\infty^0 \Gamma_M{}^{21}(t)\mathrm{d}t\right\}U^2(0,+\infty)U^1(0,+\infty)\end{cases} \qquad (87)$$

mit

$$U^j(0,+\infty) = \exp_+\left\{-i\int_\infty^0 H_1{}^j(t)\mathrm{d}t\right\} \qquad (88)$$

als den Transformationsoperatoren für die entsprechenden Ein-Nukleon-Systeme und

$$\Gamma_M{}^{12}(t) = -i\sum_q U^1(0,t)\left\{V_q{}^1(t)\int_0^t \mathrm{d}t'\,\bar{V}_q{}^{2*}(t')-V_q{}^{1*}(t)\int_0^t \mathrm{d}t'\,\bar{V}_q{}^2(t')\right\}U^1(t,0), \qquad (89)$$

wo

$$\bar{V}_q{}^j(t) = U^j(0,t)V_q{}^j(t)U^j(t,0), \qquad U^j(t,0) = \exp_+\left\{-i\int_0^t H_1{}^j(t')\mathrm{d}t'\right\}. \qquad (90)$$

Insgesamt wird damit

$$U(0,+\infty) = \begin{cases}\exp_+\left\{-i\int_\infty^0 \Gamma_M{}^{12}(t)\mathrm{d}t\right\}U^1(0,+\infty)U^2(0,+\infty)\exp_+\left\{-i\int_\infty^0 \Gamma_P{}^{12}(t)\mathrm{d}t\right\},\\ \exp_+\left\{-i\int_\infty^0 \Gamma_M{}^{21}(t)\mathrm{d}t\right\}U^2(0,+\infty)U^1(0,+\infty)\exp_+\left\{-i\int_\infty^0 \Gamma_P{}^{12}(t)\mathrm{d}t\right\}.\end{cases} \qquad (91)$$

Glg. (91) ist nun unmittelbar geeignet für eine Definition der Impulsnäherung. Wir definieren diese durch

$$\exp_+\left\{-i\int_{\infty}^{0}\Gamma_P^{12}(t)\mathrm{d}t\right\}\to 1, \tag{92}$$

$$\exp_+\left\{-i\int_{\infty}^{0}\Gamma_M^{\binom{12}{21}}(t)\mathrm{d}t\right\}\to 1, \tag{93}$$

so daß

$$U(0,+\infty)\to\begin{cases}U^1(0,+\infty)U^2(0,+\infty)\\ U^2(0,+\infty)U^1(0,+\infty).\end{cases} \tag{94}$$

Die Näherung (92) entspricht gemäß (84) der Vernachlässigung der Potentialeffekte, da $\Gamma-(\Gamma_1+\Gamma_2)$ im wesentlichen die Wechselwirkung zwischen den Nukleonen beschreibt (der Feldenergieoperator Γ enthält ja Selbstenergie und Wechselwirkung des Zwei-Nukleonen-Systems †) und (93) entspricht der Vernachlässigung der Vielfachstreueffekte, welche gemäß (87) aus der Tatsache folgen, daß der Mesonfeldoperator $\phi_\rho(x)$ am Ort des einen Nukleons im allgemeinen nicht mit dem am Ort des anderen Nukleons vertauschbar ist. Durch Berücksichtigung beider Effekte wird dann auch der Absorptionseffekt korrigiert. In dieser Weise erhalten wir eine direkte Korrespondenz zur Arbeit von Chew und Goldberger [7]) über eine Verallgemeinerung der Impulsnäherung im Falle des einfacheren Potentialproblems, wo die höheren Näherungen ebenfalls durch die Berücksichtigung der Potential- und Vielfachstreukorrekturen bestimmt sind.

Die T-Matrix (81) kann damit in der Impulsnäherung gemäß (94) durch

$$\langle n|T|p,q\rangle=\sum_j\langle n|U^j(+\infty,0)V_q{}^jU^j(0,+\infty)|p\rangle \tag{95}$$

approximiert werden. Wir können (95) auch in der Form

$$T=\sum_j T^j \tag{95'}$$

schreiben, wo T^j die Übergangsmatrizen für die Ein-Nukleon-Systeme sind. Hierbei ist natürlich der Anfangszustand durch $|p,q\rangle$ zu fixieren.

Wir betrachten zunächst den Absorptionsprozeß mit $|n\rangle=|p'\rangle$ und untersuchen

$$\langle p'|T|p,q\rangle=\sum_j\langle\Psi_{p'}^0|U^j(+\infty,0)V_q{}^jU^j(0,+\infty)|\Psi_p{}^0\rangle. \tag{96}$$

Nach (36), (37) wird dieser Ausdruck

$$\sum_j\int \mathrm{d}\mathbf{x}'_1\mathrm{d}\mathbf{x}'_2\psi^*_{p'}(\mathbf{x}'_1,\mathbf{x}'_2)\langle\mathbf{x}'_1,\mathbf{x}'_2;s'|U^j(+\infty,0)V_q{}^jU^j(0,+\infty)|\mathbf{x}_1,\mathbf{x}_2;s\rangle\psi_p(\mathbf{x}_1,\mathbf{x}_2)\mathrm{d}\mathbf{x}_1\mathrm{d}\mathbf{x}_2. \tag{97}$$

† Wir bemerken aber, daß sich die Selbstenergieanteile in Γ auf das Zwei-Nukleonen-System beziehen, im Unterschied zu den Γ_j.

Wir führen die Fourier-Transformierte zu $\psi_p(\mathbf{x}_1, \mathbf{x}_2)$ ein:

$$\psi_p(\mathbf{x}_1, \mathbf{x}_2) = \frac{1}{(2\pi)^3}\int d\mathbf{p}_1 d\mathbf{p}_2 g_p(\mathbf{p}_1, \mathbf{p}_2) e^{i(\mathbf{p}_1\cdot\mathbf{x}_1+\mathbf{p}_2\cdot\mathbf{x}_2)} \tag{98}$$

und entsprechend zu $\psi_{p'}(\mathbf{x}_1, \mathbf{x}_2)$, so daß (97) die Form annimmt

$$\int d\mathbf{p}'_1 d\mathbf{p}'_2 g^*_{p'}(\mathbf{p}'_1, \mathbf{p}'_2)\{\langle \mathbf{p}'_1; s'|T^1|\mathbf{p}_1, q; s\rangle \delta(\mathbf{p}'_2-\mathbf{p}_2) + \langle \mathbf{p}'_2; s'|T^2|\mathbf{p}_2, q; s\rangle \delta(\mathbf{p}'_1-\mathbf{p}_1)\} g_p(\mathbf{p}_1, \mathbf{p}_2) d\mathbf{p}_1 d\mathbf{p}_2, \tag{99}$$

worin

$$\langle \mathbf{p}'_j; s'|T^j|\mathbf{p}_j, q; s\rangle = \langle \mathbf{p}'_j; s'|U^j(+\infty, 0) V_q{}^j U^j(0, +\infty)|\mathbf{p}_j; s\rangle \tag{100}$$

mit

$$|\mathbf{p}_j; s\rangle = \frac{1}{(2\pi)^{\frac{3}{2}}}\int d\mathbf{x}_j e^{i\mathbf{p}_j\cdot\mathbf{x}_j}|\mathbf{x}_j; s\rangle \tag{101}$$

die entsprechenden T-Matrizen für die Ein-Nukleon-Systeme sind, deren Spin- und Isobarenspin-Zustände sich aber auf das Zwei-Nukleonen-System beziehen. Die Interpretation der Beziehung (99), die vollkommen analog der Chewschen Beziehung (13) in Ref. [5]) für Potentialstreuung ist, ist folgende: das einfallende Meson wird jeweils von einem freien Nukleon bestimmter Impulsverteilung absorbiert, wobei die Störung durch das Vorhandensein des anderen vernachlässigt wird und dieses nur die Rolle eines Zuschauers spielt (δ-Funktionen in (99)). Hierbei hat das absorbierende freie Nukleon im Anfangs- und Endzustand eine Impulsverteilung, die genau derjenigen in den entsprechenden nackten Zuständen des Zwei-Nukleonen-Systems entspricht. Wir erwarten, daß angesichts der schwachen Bindung der Nukleonen im Deuteron-Grundzustand und der relativ hohen kinetischen Energie der Mesonen diese Näherung brauchbar ist.

Wir untersuchen nun die wichtige Frage nach der Abhängigkeit der T^j-Matrizen (100) von den Impulsen der einzelnen Nukleonen. Dazu betrachten wir den Ein-Nukleon-Zustandsvektor

$$\Psi_{p_j} = U^j(0, \pm\infty)\Psi^0_{p_j}, \tag{102}$$

wo die $\pm$-Zeichen bedeutungslos sind angesichts der Stabilität der nackten Ein-Nukleon-Zustände $\Psi^0_{p_j}$. Wir wählen den Hauptwert, und Glg. (102) kann analog (20) in der Form geschrieben werden

$$U^j(0, \pm\infty)\Psi^0_{p_j} = U^j\Psi^0_{p_j} = c_{p_j}\left\{1+\frac{\mathrm{P}}{E_{p_j}-H^j}(H_1{}^j-\Gamma_j)\right\}\Psi^0_{p_j}, \tag{103}$$

$$|c_{p_j}|^2 = \left[1+\langle\Psi^0_{p_j}|(H_1{}^j-\Gamma_j)\frac{\mathrm{P}}{E_{p_j}-H^j}\frac{\mathrm{P}}{E_{p_j}-H^j}(H_1{}^j-\Gamma_j)|\Psi^0_{p_j}\rangle\right]^{-1}, \tag{104}$$

wo wir die Normierungskonstante nun explizit mitnehmen. Ganz analog den Überlegungen am Ende von Abschnitt 2 läßt sich zeigen, daß die U^j im

ganzen nichtrelativistischen Bereich vom Nukleonenimpuls unabhängig sind (was dann natürlich auch von der Normierungskonstanten gelten muß). Denn der Operator

$$\frac{\mathrm{P}}{E_{p_j}-H^j}(H_1{}^j-\Gamma_j) \tag{105}$$

enthält weder als End- noch intermediären Zustand das Mesonvakuum, so daß bei einer Entwicklung analog (39) die Energienenner mindestens die Energie eines Mesons enthalten müssen (hier kommt noch der Umstand hinzu, daß der Impulssatz streng gilt).

Der Ausdruck (100) läßt sich nun auf Beiträge reduzieren, deren Spin- und Isobarenspinzustände sich auf das einzelne Nukleon beziehen, und wir schreiben

$$\langle p'_j|T^j|p_j, q\rangle = \langle \Psi_{p'_j}|V_q{}^j|\Psi_{p_j}\rangle = Z\langle p'_j|V_q{}^j|p_j\rangle \tag{106}$$

mit der Renormierungskonstante

$$Z = \frac{\langle U^j\Psi^0_{p'_j}|V_q{}^j|U^j\Psi^0_{p_j}\rangle}{\langle \Psi^0_{p'_j}|V_q{}^j|\Psi^0_{p_j}\rangle}. \tag{107}$$

Aus der Tatsache, daß U^j im ganzen nichtrelativistischen Bereich vom Nukleonenimpuls unabhängig ist, folgt, daß die Grösse (107) wirklich konstant ist †, so daß wir die renormierte Kopplungskonstante einführen können gemäß

$$f = Zf_0. \tag{108}$$

Es ist gut bekannt, daß die renormierte Kopplungskonstante in der Theorie der Dispersionsbeziehungen für solche Werte der Nukleonenimpulse $\mathbf{p}$, $\mathbf{p}'$ und des Mesonimpulses $\mathbf{q}$ definiert wird, für die Energie- und Impulssatz bei der Absorption erfüllt sind. Hierbei ist $\mathbf{q}$ notwendig komplex und entspricht im Laboratoriumssystem der Mesonenergie

$$E = \sqrt{m^2+\mathbf{q}^2} = \frac{m^2}{2M} \ll m, \tag{109}$$

was im einzelnen bedeutet, daß eine solche Definition der Kopplungskonstanten nur auf dem Wege einer analytischen Fortsetzung möglich ist. Wichtig ist die Tatsache, daß hierdurch die Kopplungskonstante für solche Werte der Nukleonenimpulse definiert wird, die nichtrelativistisch sind (wobei die entsprechenden kinetischen Energien sogar klein gegen die

† Wir beachten, daß (107) allgemein nur von den Impulsen des Nukleons und des Mesons (die im übrigen durch den Impulssatz verknüpft sind) und nicht von Spin- und Isobarenspin abhängen kann (vgl. Ref. [10]). Man überlegt sich dann leicht (unter Verwendung des im Anschluss an (107) Gesagten), dass sich die gesamte Impulsabhängigkeit in (107) wegkürzt. Der Index j kann dann natürlich auch weggelassen werden.

Mesonmasse sind), so daß also nach den obigen Überlegungen die Kopplungskonstante in diesem ganzen Energiebereich gar nicht von den Impulsen des Nukleons abhängt.

Damit wird also (100) unter Verwendung von (106) und der Darstellung (101)

$$\langle \mathbf{p}'_j; s'|T^j|\mathbf{p}_j, q; s\rangle = Z\langle \mathbf{p}'_j; s'|V_q{}^j|\mathbf{p}_j; s\rangle = \langle s'|M_q{}^j|s\rangle\delta(\mathbf{p}'_j-\mathbf{p}_j-\mathbf{q}) \quad (110)$$

mit (vgl. (6))

$$M_q{}^j = \frac{i}{\sqrt{V}}\,\frac{\sqrt{4\pi f}}{m}\,\tau_\rho{}^j\boldsymbol{\sigma}^j\cdot\mathbf{q}v_\mathbf{q}\,\frac{1}{\sqrt{2\omega_q}}, \quad (111)$$

wo $|s\rangle$ den Spin- und Isobarenspin-Zustand des Zwei-Nukleonen-Systems bezeichnet und f die renormierte Kopplungskonstante (108) ist. Glg. (96) wird dann über (99) und (110)

$$\langle p'|T|p, q\rangle = \delta(\mathbf{p}'-\mathbf{p}-\mathbf{q})\{\sum_j \langle s'|M_q{}^j|s\rangle F^j_{p'_r p_r}\} \quad (112)$$

mit den Formfaktoren

$$F^j_{p'_r p_r} = \int \chi^*_{p'_r}(\mathbf{x}_r)\mathrm{e}^{\pm\frac{1}{2}i\mathbf{q}\cdot\mathbf{x}_r}\chi_{p_r}(\mathbf{x}_r)\mathrm{d}\mathbf{x}_r \quad \text{für} \quad j = \begin{cases}1\\0,\end{cases} \quad (113)$$

wo gemäß

$$\psi_p(\mathbf{x}_1, \mathbf{x}_2) = \frac{1}{(2\pi)^{\frac{3}{2}}}\mathrm{e}^{i\mathbf{p}\cdot\mathbf{x}_c}\chi_{p_r}(\mathbf{x}_r), \qquad \mathbf{x}_c = \tfrac{1}{2}(\mathbf{x}_1+\mathbf{x}_2), \qquad \mathbf{x}_r = \mathbf{x}_1-\mathbf{x}_2, \quad (114)$$

Schwerpunkts- und Relativbewegung abseparierт wurden. Die Approximation (112) ist in Ref.[1, 3]) bei der Berechnung des Beitrags des nichtbeobachtbaren Bereichs in den Dispersionsbeziehungen verwandt worden.

Entsprechend läßt sich die T-Matrix für den Streuprozeß in einer zu (99) analogen Form schreiben:

$$\langle p', q'|T|p, q\rangle = \int \mathrm{d}\mathbf{p}'_1\mathrm{d}\mathbf{p}'_2 g^*_{p'}(\mathbf{p}'_1, \mathbf{p}'_2)\{\langle \mathbf{p}'_1, q'; s'|T^1|\mathbf{p}_1, q; s\rangle\delta(\mathbf{p}'_2-\mathbf{p}_2) + \langle \mathbf{p}'_2, q'; s'|T^2|\mathbf{p}_2, q; s\rangle\delta(\mathbf{p}'_1-\mathbf{p}_1)\}g_p(\mathbf{p}_1, \mathbf{p}_2)\mathrm{d}\mathbf{p}_1\mathrm{d}\mathbf{p}_2, \quad (115)$$

wo analog (100)

$$\langle \mathbf{p}'_j, q'; s'|T^j|\mathbf{p}_j, q; s\rangle = \langle \mathbf{p}'_j; s'|a_{q'}U^j(+\infty, 0)V_q{}^jU^j(0, +\infty)|\mathbf{p}_j; s\rangle \quad (116)$$

die entsprechenden T-Matrizen für die Ein-Nukleon-Systeme sind, deren Spin- und Isobarenspin-Zustände sich aber wiederum auf das Zwei-Nukleonen-System beziehen, und für die sich Ausdrücke der Form (76) herleiten lassen (Chew-Low-Gleichungen für den Fall eines bewegten Nukleons).

In der gleichen Weise wie im Falle der Absorption begründen wir die Unabhängigkeit der U^j-Matrizen in (116) von den Nukleonenimpulsen für die Anfangszustände (da im Deuteron-Grundzustand die enthaltenen Impulse ja nichtrelativistisch sind). Wir können also in (116) $\mathbf{p}_1 = \mathbf{p}_2 = 0$

setzen. Bezüglich der Endzustände, wo die Dinge nicht so einfach liegen, haben wir zwischen elastischer und unelastischer Streuung zu unterscheiden.

Allgemein gilt für diese

$$U^j(0, +\infty)a^*_{q'}\Psi^0_{p'_j}$$
$$= \left\{1 + \frac{\mathrm{P}}{E_{p'_j}+\omega_{q'}-H^j}(H_1{}^j - \Gamma_j) + i\pi\delta(E_{p'_j}+\omega_{q'}-H^j)(H_1{}^j-\Gamma_j)\right\} a^*_{q'}\Psi^0_{p'_j} \quad (117)$$

worin aber nur auf die ersten beiden Terme die obigen Überlegungen bezüglich der Unabhängigkeit von den Nukleonenimpulsen verallgemeinert werden können, während der dritte Term — der wegen der Instabilität des betrachteten Zustandes nicht verschwindet — vom Nukleonenimpuls abhängen wird. Es ist aber klar, daß für kleine Nukleonenimpulse, d.h. für

$$\frac{\mathbf{p}'^2_j}{2M} \ll \omega_{q'}, \quad (118)$$

die Abhängigkeit auch dieses Terms vom Nukleonenimpuls unwesentlich sein wird, so daß dann die T^j-Matrizen in (115) (bis auf die den Impulssatz bedingenden δ-Funktionen) vor die Integrale gezogen werden können.

Wir zeigen (118) zunächst für den Fall der elastischen Streuung. Dazu beachten wir, daß die Beiträge in (115) für große $\mathbf{p}'_j$ klein sind, weil jeweils $\mathbf{p}'_2 = \mathbf{p}_2 = 0$ bzw. $\mathbf{p}'_1 = \mathbf{p}_1 = 0$ gilt und $g_{p'}(\mathbf{p}'_1, \mathbf{p}'_2)$ als Fourier-Transformierte des Deuteron-Grundzustandes für größere $(\mathbf{p}'_1 - \mathbf{p}'_2)$ verschwindet, d.h. es wird praktisch (118) gelten.

Im Falle der unelastischen Streuung beachten wir, daß für größere $\mathbf{p}'_j$, wo (118) nicht mehr gilt, die Beziehung

$$g_{p'}(\mathbf{p}'_1, \mathbf{p}'_2) \sim \delta[\mathbf{p}'_1 - \mathbf{p}'_2 - (\mathbf{p}''_1 - \mathbf{p}''_2)] \quad (119)$$

richtig ist (etwa für eine Energie der Relativbewegung oberhalb 10 MeV, s. auch Ref. [5]), da die Wellenfunktion des Endzustandes dann durch ebene Wellen approximiert werden kann

$$\psi_{p'}(\mathbf{x}_1, \mathbf{x}_2) = \frac{1}{(2\pi)^3} e^{i(\mathbf{p}''_1 \cdot \mathbf{x}_1 + \mathbf{p}''_2 \cdot \mathbf{x}_2)} \quad (120)$$

(von der notwendigen Symmetrisierung in den Raumkoordinaten abgesehen). Denn dann muß die Energie der Relativbewegung der Nukleonen wie im Falle der elastischen Streuung hoch sein, weil auch hier jeweils $\mathbf{p}'_2 = \mathbf{p}_2 = 0$ bzw. $\mathbf{p}'_1 = \mathbf{p}_1 = 0$ gilt. In diesem Falle ist also die Integration über die $\mathbf{p}'_j$ für solche Werte, für die nicht mehr (118) gilt, durch δ-Funktionen festgelegt, so daß insgesamt die T^j-Matrizen (bis auf die δ-Funktionen in (123)) vor die Integrale gezogen werden können.

Damit folgt aus (115)

$$\langle p', q'|T|p, q\rangle = \delta(\mathbf{p}'+\mathbf{q}'-\mathbf{p}-\mathbf{q})\{\sum_j \langle s'|M^j_{q'q,\mathbf{p}'_j}|s\rangle G^j_{\mathbf{p}'_\tau \mathbf{p}_\tau}\} \qquad (121)$$

mit den Formfaktoren (vgl. 112))

$$G^j_{\mathbf{p}'_\tau \mathbf{p}_\tau} = \int \chi^*_{\mathbf{p}'_\tau}(\mathbf{x}_\tau) e^{\pm i\frac{1}{2}(\mathbf{q}-\mathbf{q}')\cdot \mathbf{x}_\tau} \chi_{\mathbf{p}_\tau}(\mathbf{x}_\tau) d\mathbf{x}_\tau \quad \text{für} \quad j = \begin{cases} 1 \\ 2 \end{cases} \qquad (122)$$

wo analog (110) †

$$\langle \mathbf{p}'_j, q'; s'|T^j|\mathbf{p}_j, q; s\rangle = \langle s'|M^j_{q'q,\mathbf{p}'_j}|s\rangle \delta(\mathbf{p}'_j+\mathbf{q}'-\mathbf{p}_j-\mathbf{q}). \qquad (123)$$

In dem von uns benutzten Laboratoriumssystem ist sowohl in (121) $\mathbf{p} = 0$ als auch in (123) $\mathbf{p}_j = 0$ zu setzen, d.h. die Streuamplitude für die Streuung von π-Mesonen an Deuteronen im Laboratoriumssystem ist durch die für Streuung von π-Mesonen an freien Nukleonen im Laboratoriumssystem ausgedrückt worden. Glg. (121) entspricht genau der Beziehung, die in Ref. [2]) und [3]) für die Berechnung der totalen Wirkungsquerschnitte im beobachtbaren Bereich verwandt wurde, wo auch der Näherungscharakter diskutiert wurde.

Wir bemerken, daß der (intermediäre) Beitrag des Absorptionsprozesses von π-Mesonen an Deuteronen in (121) im beobachtbaren Bereich fehlt, da freie Nukleonen auf Grund der Erhaltungssätze nicht π-Mesonen absorbieren oder emittieren können, während im nichtbeobachtbaren Bereich ein reiner Polbeitrag auftritt. Dagegen liefert der strenge Ausdruck (76) einen (experimentell allerdings nur kleinen) Absorptionsbeitrag im beobachtbaren Bereich, während im nichtbeobachtbaren Gebiet ein kontinuierlicher Beitrag auftritt. Diese Verhältnisse sind im Rahmen der Theorie der Dispersionsbeziehungen in Ref. [1, 2, 3]) im einzelnen untersucht worden.

5. Schlußbemerkung

Die obigen Untersuchungen zeigten, daß es möglich ist, die Chewsche Impulsnäherung auf den feldtheoretischen Fall in durchsichtiger Weise zu verallgemeinern. Hierbei wurde der Hamilton-Formalismus für zwei nichtrelativistisch bewegte Nukleonen zugrunde gelegt, die in pseudovektorieller Wechselwirkung mit dem π-Mesonfeld stehen, für das die übliche Abschneidung vorausgesetzt wurde. Die höheren Näherungen der Impulsnäherung entsprechen auch hier der Potential- und Vielfachstreukorrektur, wobei durch diese auch der Absorptionseffekt korrigiert wird. Die Verallgemeinerung auf den Fall von mehr als zwei Nukleonen und anderer Kopplungsarten ist offensichtlich und sollte auch — bei geeigneten Modifikationen — auf den

† Der Index $\mathbf{p}'_j$ von M bezieht sich auf die unelastische Streuung.

relativistischen Fall möglich sein. Bei unserer Formulierung wurde der zeitabhängige Streuformalismus gewählt, in dem die Anfangs- und Endzustände die Situation der nackten Teilchen beschreiben. Die nackten Zustände des Zwei-Nukleonen-Systems bildeten die Projektionen der entsprechenden reellen Zustände auf das Mesonvakuum. Das führte zwangsläufig zur Einführung eines Feldenergieoperators, der Selbstenergie und Wechselwirkung der Nukleonen beschreibt und mit dessen Hilfe sich explizit die Schwierigkeiten beheben ließen, die sonst der Formulierung einer Feldtheorie mit gebundenen Zuständen im Wege stehen.

Die Anwendung der Ergebnisse dieser Untersuchungen ist bereits in Ref. [1,2,3]) bei der Aufstellung und Auswertung der Dispersionsbeziehungen für die elastische Vorwärtsstreuung von π-Mesonen an Deuteronen gegeben worden. Bei der expliziten Berechnung des Beitrags des nichtbeobachtbaren Bereichs, wo die Übergangsmatrix für die Absorption des einfallenden π-Mesons auftritt, wurde die Beziehung (112) in Verbindung mit (111) verwandt, wobei die renormierte Kopplungskonstante im ganzen in Frage kommenden nichtrelativistischen Bereich der Nukleonenbewegung wirklich als konstant und in Übereinstimmung mit der Goldbergerschen Kopplungskonstante vorausgesetzt werden konnte. Die Matrixelemente des Stromes mußten wegen der auftretenden Divergenzen explizit in den nichtbeobachtbaren Bereich analytisch fortgesetzt werden, wozu genäherte Wellenfunktionen des Zwei-Nukleonen-Systems verwandt wurden, was anschließend gerechtfertigt werden konnte. Die Dispersionsbeziehungen waren in Übereinstimmung mit den Ergebnissen der Impulsnäherung, gemäß derer für die Streuamplituden im beobachtbaren Bereich die Beziehung (121) benutzt werden konnte. Aus der Dispersionsbeziehung für Spinflip-Streuung, wo der Beitrag des nichtbeobachtbaren Bereichs hinreichend groß ist, folgte insbesonders ein Wert für die Kopplungskonstante, der nur um weniger als 10 % von demjenigen abweicht, der sich aus der entsprechenden Dispersionsbeziehung für π-Meson-Streuung an freien Nukleonen ergibt. Diese Untersuchungen machen es sehr wahrscheinlich, daß die Theorie der Dispersionsbeziehungen nicht an die Voraussetzung derElementarteilchen-Konzeption gebunden ist, sondern eine natürliche Ausdehnung auf den Fall der gebundenen Zustände erlaubt.

Wir machen noch folgende wichtige Anmerkung im Hinblick auf das in Ref. [1,2,3]) verwandte Massenspektrum der intermediären Zustände. Von Nambu [16]) wurde auf der 1958 Annual International Conference on High Energy Physics at CERN die Frage aufgeworfen, ob bei der Streuamplitude für π-Meson-Deuteron-Streuung nicht ähnliche Verhältnisse wie beim Deuteron-Formfaktor vorliegen, wo sich störungstheoretisch eine (physikalisch vernünftige) Abweichung des Massenspektrums der intermediären Zustände vom normalen Spektrum ergibt (und zwar liegt der störungs-

theoretische Schwellenwert tiefer als der normale). In unserem Falle würde das besagen, daß unser Massenspektrum nicht — wie vorausgesetzt — bei $(2M)^2$ beginnt (zwei ruhende Nukleonen im intermediären Zustand), sondern störungstheoretisch einen etwas tieferen Schwellenwert hat. Inzwischen ist von Karplus, Sommerfield und Wichmann [17]) und Nambu [18]) gezeigt worden, daß störungstheoretisch der Schwellenwert bei $(2M)^2 - 0.002\ M^2$ liegt (was einer Verschiebung um 0.61 MeV unterhalb der normalen Schwelle entspricht), so daß die Abweichung also praktisch ganz unwesentlich ist, denn die Integration über das nichtbeobachtbare Gebiet geht über einen Bereich von 140 MeV.

Ich habe Herrn Dr. Nambu für eine Diskission des zuletzt erörterten Problems und ihm und den Herren Dr. Oehme, Dr. Karplus, Dr. Sommerfield und Dr. Wichmann für die Zusendung von damit in Zusammenhang stehenden Manuskripten bzw. Preprints sehr zu danken.

Literatur

1) F. Kaschluhn, Zs. f. Naturforsch. **13a** (1958) 183
2) F. Kaschluhn, Nuclear Physics **8** (1958) 303
3) F. Kaschluhn, Nuclear Physics **9** (1958/59) 347
4) Chew, Vortrag in Proceedings of the 1958 Annual International Conference on High Energy Physics at CERN, p. 99
5) G. F. Chew, Phys. Rev. **80** (1950) 196
6) G. F. Chew und G. C. Wick, Phys. Rev. **85** (1952) 636
7) G. F. Chew und M. L. Goldberger, Phys. Rev. **87** (1952) 778
8) N. N. Bogolubov, B. V. Medvedev und M. K. Polivanov, Probleme der Theorie der Dispersionsbeziehungen (Gostekhisdat Moskau, 1958), gekürzte deutsche Übersetzung in Fortschr. d. Phys. **6** (1958) 169
9) F. Kaschluhn, Nuovo Cimento **12** (1959) 541
10) G. C. Wick, Revs. Mod. Phys. **27** (1955) 339
11) M. Gell-Mann und M. L. Goldberger, Phys. Rev. **91** (1953) 398
12) M. L. Goldberger, Phys. Rev. **99** (1955) 979
13) G. F. Chew und F. E. Low, Phys. Rev. **101** (1956) 1570
14) B. L. Ioffe, I. Ya. Pomeranchuk und A. P. Rudik, Exp. Theor. Phys. USSR **4** (1956) 712
15) D. B. Lichtenberg, Phys. Rev. **100** (1955) 303
16) Diskussion zum Goldberger-Vortrag in Proceedings of the 1958 Annual International Conference on High Energy Physics at CERN, p. 212
17) R. Karplus, C. M. Sommerfield und E. H. Wichmann, Preprint
18) Y. Nambu, Preprint

8.A *Nuclear Physics* **14** (1959/60) 339—341; © *North-Holland Publishing Co., Amsterdam*
Not to be reproduced by photoprint or microfilm without written permission from the publisher

β-DECAY OF NEGATIVE PIONS

YU. A. BUDAGOV, S. WIKTOR, V. P. DZHELEPOV, P. F. YERMOLOV and V. I. MOSKALEV

Laboratory of Nuclear Problems, Joint Institute for Nuclear Research, Dubna, USSR

Received 28 August 1959

All the experiments on pion β-decay performed up till now refer to the investigation of β-decay of stopping π^+ mesons [1–6]). In two recent papers [5–6]) the following result for the relative probability of this process is obtained:

$$\frac{\pi^+ \to e^+ + \nu}{\pi^+ \to \mu^+ + \nu} \approx 1 \times 10^{-4} \pm (20\,\% - 40\,\%).$$

This value is in agreement with the value 1.3×10^{-4} which follows from the universal V—A theory of β-decay [7]). For negative pions, as follows from the relativistic invariance (CPT-theorem) [8]) this process must have the same relative probability as for positive ones. However, it is important to determine directly from experiment the relative probability of π^--meson β-decay.

The $\pi^- \to e^-$ decay, unlike the $\pi^+ \to e^+$ decay, can be found only in flight. Therefore, to detect β-decay of π^--mesons we used the data obtained in a diffusion cloud chamber operating in a magnetic field of 9000 gauss and used for the investigation of 130 and 160 MeV π^--meson interaction with protons and rare modes of π^0-meson decay [9–11]). As a result of triple scanning of about 100 000 stereophotographs, 29 decays were found in which a secondary particle was deflected by an angle $\theta > 20°$ (the maximum angle for $\pi \to \mu$ decay for the energy 130 MeV is equal to 10°). In all events the primary and the secondary particles, according to visual estimations, had the minimum ionization. As a result of measurements (the method of measuring the momenta and angles is similar to that described in ref.[11])) 26 events were identified as $\mu^- \to e^-$ decays and 3 events were attributed to $\pi^- \to e^-$ decays. It should be noted that the conditions of momentum separation of $\pi \to e$ and $\mu \to e$ decays in flight is rather better than when π and μ mesons come to rest, since the ratio of the momentum of an electron produced in $\pi \to e$ decay to the maximum possible momentum, at the given angle, of an electron from $\mu \to e$ decay exceeds in a wide angle region the ratio of the indicated momenta for π and μ-mesons coming to rest. The lower background of $\mu \to e$ decays is also favourable. Fig. 1 represents the momentum distribution of electrons produced in $\pi^- \to e^-$ and

$\mu^- \to e^-$ decays in the rest system of π^- and μ^--mesons. The indicated errors are the maximum errors of measuring the curvature radius of π^- and μ^--mesons and electrons. The picture of one of $\pi^- \to e^-$-decays is given in fig. 2.

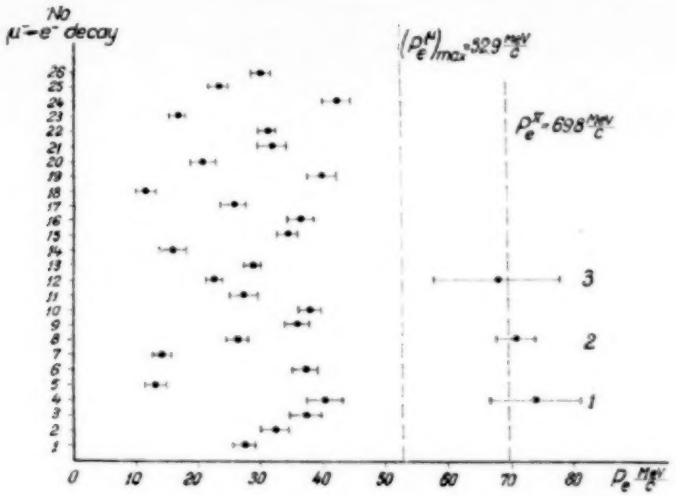

Fig. 1. Momentum distribution of electrons from $\pi^- \to e^-$ and $\mu^- \to e^-$ decays (in the rest system of π^- and μ^--mesons).

TABLE 1

Number of $\pi^- \to e^-$ event	Lab. system			Rest system of π^- meson	
	π^- meson momentum (MeV/c)	electron momentum (MeV/c)	θ (degrees)	electron momentum (MeV/c)	θ (degrees)
1	228±10	104± 8	42.5±0.5	74± 7	108±2
2	207±11	103± 3	42 ±0.5	71± 4	102±2
3	266± 6	156±26	26 ±0.5	68±11	86±1

The data of the $\pi^- \to e^-$ decay measurements are shown in table 1. As is seen from fig. 1 and the table, the electron momenta in the rest system of the π^--meson have values close to 69.8 MeV/c. If one would assume that the primary particle is a μ^--meson, then, in the rest system of the μ^--meson, the electrons for these three events would have the momenta 80±8, 77±4 and 70±11 MeV/c, respectively, whereas the maximum electron momentum in $\mu \to e$ decay is equal to 52.9 MeV/c.

The other possible processes which can imitate $\pi^- \to e^-$ decays (inelastic scattering of π^--mesons on complex nuclei of impurities in the gas of the chamber, electron bremsstrahlung radiation, a $\pi^- \to \mu^- \to e^-$ decay in flight with a short track of μ^--meson) are of very small probability.

To determine the relative probability of π^--meson β-decay it is necessary to

Fig. 2. Picture of $\pi^- \to e^- + \tilde{\nu}$ decay obtained in the diffusion cloud chamber.

know the total number of $\pi^- \to \mu^-$-decays. This number, equal to $(5.6 \pm 0.3) \times 10^4$, was calculated from the known total length of π^--meson path in the chamber, equal to $(7.8 \pm 0.4) \times 10^7$ cm, and the mean momentum $P_\pi = 253$ MeV/c. Assuming the efficiency of observation of $\pi^- \to e^-$ decays equal to that of $\mu^- \to e^-$ decay observation, which according to estimations is equal to 70 % and taking into account the contribution from the angular region $\theta < 20°$, the following value was obtained for the relative probability of π^--meson β-decay:

$$\frac{\pi^- \to e^- + \tilde{\nu}}{\pi^- \to \mu^- + \tilde{\nu}} = (1.2 \pm 0.7) \times 10^{-4}.$$

Within the experimental errors this value is in agreement with the probability of β-decay of positive mesons as well as with the above value calculated on the basis of universal V—A theory of β-interaction.

The authors wish to thank T. S. Sazhneva, L. I. Krasnoslobodtseva and Yu. L. Saikina for help in scanning the photographs.

References

1. H. L. Friedman and J. Rainwater, Phys. Rev. **84** (1951) 684
2. S. Lokanathan and J. Steinberger, Nuovo Cimento **10** (1955) 151
3. H. L. Anderson and C. M. G. Lattes, Nuovo Cimento **6** (1957) 1356
4. T. Fazzini, G. Fidecaro, A. W. Merrison, H. Paul and A. V. Tollestrup, Phys. Rev. Lett. **1** (1958) 247
5. G. Impeduglia, R. Plano, A. Prodell, N. Samios, M. Schwartz and J. Steinberger, Phys. Rev. Lett. **1** (1958) 249
6. H. L. Anderson, T. Fujii, R. H. Miller and L. Tau, Phys. Rev. Lett. **2** (1959) 53
7. M. Ruderman and R. Finkelstein, Phys. Rev. **76** (1949) 1458
8. G. Lüders and B. Zumino, Phys. Rev. **106** (1957) 385
9. Yu. A. Budagov, S. Wiktor, V. P. Dzhelepov, P. F. Yermolov and V. I. Moskalev, Proceedings of Conference on cloud, diffusion and bubble chambers, JINR, Dubna, 1958
10. Yu. A. Budagov, S. Wiktor, V. P. Dzhelepov, P. F. Yermolov and V. I. Moskalev, JETP **35** (1958) 1575
11. Yu. A. Budagov, S. Wiktor, V. P. Dzhelepov, P. F. Yermolov and V. I. Moskalev, JETP **36** (1959) 1080

8.B *Nuclear Physics* **14** (1959/60) 342—348; © *North-Holland Publishing Co., Amsterdam*
Not to be reproduced by photoprint or microfilm without written permission from the publisher

ZUR DEPOLARISATION DER μ-MESONEN BEIM AUGER-EINFANG IN WASSERSTOFF

J. VON BEHR † und H. MARSCHALL
Physikalisches Institut der Universität Freiburg i.B.

Eingegangen am 7. August 1959

Abstract: Depolarization of polarized muons by Auger-capture in hydrogen atoms has been estimated. Assuming that the velocity of the muons is distributed randomly with respect to the centre of capture, the degree of polarization of the captured muons is found to be approximately $\frac{1}{3}$.

1. Einleitung

In einem durch Pionenzerfall entstandenen Myonenstrahl definiere die Spinrichtung der Teilchen die z-Achse des im folgenden benutzten Koordinatensystems. Die μ-Mesonen sind longitudinal polarisiert und bewegen sich längs der positiven oder längs der negativen z-Achse [1]). Gelangt der Myonenstrahl in die Nähe von Wasserstoffatomen, so kann immer dann ein Auger-Austausch mit dem Atomelektron eintreten, wenn ein hinreichend stark gebremstes Meson in unmittelbare Nähe der K-Schale des Elektrons kommt. Ohne wesentliche Abstandsänderung zum Proton wird dann der Austausch Elektron gegen Meson erfolgen, so daß dieses auf der K-Schale landet. Das Meson befindet sich damit im Quantenzustand $n \approx 14$, d.h. es ist ein hochangeregtes Mesonenatom entstanden. Infolge der nun über sehr viele Umläufe wirksamen Spin-Bahn-Kopplung wird der Erwartungswert des Spins reduziert, so daß eine Depolarisation des Mesons stattfindet. Die vor dem Einfang bereits mögliche Depolarisation sei vernachlässigt: Solange das Myon vor dem Einfang nur der Einwirkung der durch die Elektronen abgeschirmten Coulombfelder ausgesetzt ist, existiert sicher nur eine sehr kleine Spin-Bahn-Wechselwirkung. Gelangt das Teilchen jedoch in Atomnähe ohne eingefangen zu werden, so wächst zwar die Spin-Bahn-Kraft, die Flugzeit innerhalb dieses Bereiches ist dann jedoch so kurz, daß eine merkliche Drehung des Spinvektors nicht eintreten wird. Im nicht gebundenen Zustand des Myons lassen wir daher neben l und $s = \frac{1}{2}$ auch m und m_s als gute Quantenzahlen zu.

Für den Anfangszustand eines Myons mit dem Impuls $\mathbf{k}$ notieren wir

$$|i_\mu\rangle = \sum_{l,m} (2l+1) i^l g_l(r_\mu) C_m^{(l)*}\left(\frac{\mathbf{k}}{k}\right) C_m^{(l)}(\theta_\mu)\chi_{\frac{1}{2}\frac{1}{2}} \quad \text{mit} \quad C_m^{(l)} = \left(\frac{4\pi}{2l+1}\right)^{\frac{1}{2}} Y_{lm}; \quad \text{(1a)}$$

† Zur Zeit bei CERN (Genf).

r_μ, θ_μ sind Mesonenkoordinaten (θ_μ steht für Polar- und Azimutalwinkel) und $\chi_{\frac{1}{2}\frac{1}{2}}$ kennzeichnet den Spinzustand des Teilchens. Treffen die Myonen isotrop auf das Wasserstoffatom, bei welchem der Auger-Einfang geschieht, so treten alle Impulse **k** mit gleicher Wahrscheinlichkeit auf und bei der Durchführung der Rechnung ist über alle **k** zu mitteln. Ist dagegen bei dem Einfangprozeß die ursprüngliche Mesonenrichtung noch ausgezeichnet, so reduziert sich (1a) etwa auf die in z-Richtung laufende Welle

$$|i_\mu\rangle = \sum_l (2l+1) i^l g_l(r_\mu) C_0^{(l)}(\theta_\mu) \chi_{\frac{1}{2}\frac{1}{2}}. \tag{1b}$$

Eine Richtungsmittelung entfällt und $m = 0$. Im folgenden behandeln wir zunächst die zu einfacheren Aussagen führende isotrope Impulsverteilung, auf den zweiten Fall gehen wir am Schluß der Arbeit kurz ein.

2. Die allgemeine Formulierung

Infolge der elektrostatischen Wechselwirkung

$$W = \frac{e^2}{|\mathbf{r}_\mu - \mathbf{r}_e|} = e^2 \begin{cases} r_\mu^{-1} \sum_\lambda \left(\frac{r_e}{r_\mu}\right)^\lambda P_\lambda(\cos \widehat{\mu e}) & \text{für} \quad r_\mu < r_e \\ r_e^{-1} \sum_\lambda \left(\frac{r_\mu}{r_e}\right)^\lambda P_\lambda(\cos \widehat{\mu e}) & \text{für} \quad r_\mu > r_e \end{cases} \tag{2}$$

zwischen Meson und Elektron — $\widehat{\mu e}$ bedeutet den Winkel zwischen den Ortsvektoren $\mathbf{r}_\mu$ und $\mathbf{r}_e$ — kommt es zu einem Austausch mit dem im Anfangszustand

$$|i_e\rangle = \varphi(r_e)|\tfrac{1}{2} m_s\rangle = \varphi(r_e)\psi_{\frac{1}{2}m_s} \tag{3}$$

befindlichen Elektron, so daß das Myon in den gebundenen Zustand

$$|f_\mu\rangle = G_{nL}(r_\mu)[(LM_L\tfrac{1}{2}\tfrac{1}{2}|JML) Y_{LM_L}(\theta_\mu)\chi_{\frac{1}{2}\frac{1}{2}} + (LM_L\tfrac{1}{2}-\tfrac{1}{2}|JML) Y_{LM_L+1}(\theta_\mu)\chi_{\frac{1}{2}-\frac{1}{2}}] \tag{4}$$

übergeht und das Elektron in den Zustand

$$|f_e\rangle = \phi_\Lambda(r_e)|\Lambda M_\Lambda \tfrac{1}{2} M_s\rangle = \phi_\Lambda(r_e) Y_{\Lambda M_\Lambda}(\theta_e)\psi_{\frac{1}{2}M_s} \tag{5}$$

frei gesetzt wird; r_e, θ_e sind Elektronenkoordinaten, $\psi_{\frac{1}{2}m_s}$ und $\psi_{\frac{1}{2}M_s}$ bezeichnen Spinzustände. Anfangs-und Endzustand des Gesamtsystems bezeichnen wir mit

$$|i\rangle = |i_\mu\rangle|i_e\rangle, \quad |f\rangle = |f_\mu\rangle|f_e\rangle. \tag{6}$$

Solange sich das Myon im Zustand $|i_\mu\rangle$ befindet, unterliegt es der Einwirkung des durch das gebundene Elektron abgeschirmten Coulombfeldes. Ebenso erfährt das frei gesetzte Elektron im Zustand $|f_e\rangle$ die Wirkung des durch das nun gebundene Myon abgeschirmten Feldes. Mithin sind die Radialfunktionen $g_l(r_\mu)$ und $\phi_\Lambda(r_e)$ Lösungen der Wellengleichung für abgeschirmte Coulomb-

felder. Ferner sind $\varphi(r_e)$ und $G_{nL}(r_\mu)$ die Coulombwellenfunktionen für den 1s-Zustand des Elektrons und den hochangeregten Zustand $n \approx 14$ des Mesonenatoms.

Die Depolarisation des Mesons geschieht nun beim Übergang $|i_\mu\rangle$ nach $|f_\mu\rangle$. Der Spinerwartungswert $\langle\vec{s}\rangle = \langle s_z\rangle = \frac{1}{2}$ des Ausgangszustandes ist im Endzustand infolge der Spin-Bahn-Wechselwirkung kleiner. Mit (4) findet man nämlich das bekannte Resultat

$$\langle f_\mu|s_z|f_\mu\rangle = \langle JML|s_z|JML\rangle = \begin{cases} \dfrac{M}{2J} & \text{für} \quad J = L+\frac{1}{2} \\ -\dfrac{M}{2(J+1)} & \text{für} \quad J = L-\frac{1}{2} \end{cases} \tag{7}$$

welches auch mit Hilfe des Vektorgerüstes qualitativ verständlich ist. Da die Myonen in alle möglichen Endzustände gelangen, ist (7) experimentell natürlich nicht kontrollierbar. Vielmehr müssen wir jeden der Erwartungswerte (7) mit derjenigen Wahrscheinlichkeit w_{f_μ} multiplizieren, mit welcher der Endzustand $|f_\mu\rangle$ erreicht wird. Der Spinerwartungswert, welcher die Polarisation nach dem Einfang angibt, lautet dann

$$\langle s_z\rangle = \frac{\sum\limits_{f_\mu} w_{f_\mu}\langle f_\mu|s_z|f_\mu\rangle}{\sum\limits_{f_\mu} w_{f_\mu}}. \tag{8}$$

Da die Übergangswahrscheinlichkeit w_{f_μ} nur den Mesonenendzustand fixieren soll, ist zu ihrer Berechnung über die Elektronenanfangs- und Endzustände zu summieren. Ebenso ist über die Einfallsrichtungen $\mathbf{k}$ des Mesons zu mitteln, also die Integration $(4\pi)^{-1}\int d\Omega_{\mathbf{k}} \ldots$ durchzuführen. Mithin ist

$$w_{f_\mu} = \tfrac{1}{2}\frac{2\pi}{\hbar}\frac{dZ}{dE}\sum_{f_e, i_e}(4\pi)^{-1}\int d\Omega_{\mathbf{k}}|\langle f|W|i\rangle|^2. \tag{9}$$

Der Faktor $\frac{1}{2}$ rührt von der Mittelung über die beiden durch $m_s = \pm\frac{1}{2}$ festgelegten Anfangszustände $|i_e\rangle$ des Elektrons her. Die Dichte dZ/dE der Elektronenendzustände findet man mit Hilfe einer hinreichend großen Kugel des Radius ρ und mit Hilfe des asymptotisch dargestellten Radialanteils $\phi_\Lambda(r_e)$ zu

$$\frac{dZ}{dE} = \frac{\rho}{\pi}\frac{m_e}{\hbar^2 k_e}$$

also unabhängig von der Drehimpulsquantenzahl Λ; m_e und k_e bedeuten Elektronenmasse und Elektronenimpuls.

Die Übergangswahrscheinlichkeiten folgen aus (9) in 1. Näherung. Es sei jedoch nochmals daran erinnert, daß Meson und Elektron in den nichtgebundenen Zuständen nicht als kräftefreie Teilchen anzusehen sind, die Einwirkung des abgeschirmten Coulombfeldes soll berücksichtigt werden.

3. Die Übergangswahrscheinlichkeiten in den Mesonenendzustand

Zur Berechnung der w_{f_μ} führen wir in den Winkelfunktionen $P_\lambda(\cos\widehat{\mu e})$ der Wechselwirkung die Lagekoordinaten beider Teilchen ein. Die in (2) notierte Fallunterscheidung umgehen wir durch Benutzung der Symbole $r_<$ und $r_>$ für das kernnahe und kernferne Teilchen und erhalten dann

$$W = e^2 \sum_{\lambda,q} \frac{r_<^{\lambda}}{r_>^{\lambda+1}} (-1)^q C_{-q}^{(\lambda)}(\theta_e)\, C_q^{(\lambda)}(\theta_\mu) = \sum_{\lambda,q} W_e^{\lambda,q} W_\mu^{\lambda,q}. \tag{10}$$

Diese Zerlegung führt dann mit (6) zu dem Ausdruck

$$w_{f_\mu} = \tfrac{1}{2} \frac{2\pi}{\hbar} \frac{\mathrm{d}Z}{\mathrm{d}E} \sum_{f_e, i_e} (4\pi)^{-1} \int \mathrm{d}\Omega_{\mathbf{k}} | \sum_{\lambda,q} \langle f_e | W_e^{\lambda,q} | i_e \rangle \langle f_\mu | W_\mu^{\lambda,q} | i_\mu \rangle |^2. \tag{11}$$

Setzen wir den Mesonenzustand (1a) in (11) ein, so läßt sich die Integration über $\mathbf{k}$ durchführen und wir erhalten

$$w_{f_\mu} = \tfrac{1}{2} \frac{2\pi}{\hbar} \frac{\mathrm{d}Z}{\mathrm{d}E} \sum_{m_s M_s \Lambda M_\Lambda} \sum_{lm} (2l+1)$$
$$| \sum_{\lambda q} \langle \Lambda M_\Lambda \tfrac{1}{2} M_s | (-1)^q C_{-q}^{(\lambda)} | \tfrac{1}{2} m_s \rangle \langle JM | C_q^{(\lambda)} | C_m^{(l)} \chi_{\frac{1}{2}\frac{1}{2}} \rangle K(\Lambda L \lambda l) |^2, \tag{12}$$

wobei die verschiedenen Zustände definierenden Quantenzahlen explizite eingeführt sind; K bezeichnet das Radialintegral

$$K(\Lambda L \lambda l) = \int_0^\infty \phi_\Lambda(r_e) G_{nL}(r_\mu) \frac{r_<^{\lambda}}{r_>^{\lambda+1}} g_l(r_\mu) q(r_e) r_\mu^2 \mathrm{d}r_\mu r_e^2 \mathrm{d}r_e. \tag{13}$$

Für den Elektronenanteil von (12) findet man mit Hilfe von (5) und (3) †

$$\langle \Lambda M_\Lambda \tfrac{1}{2} M_s | (-1)^q C_{-q}^{(\lambda)} | \tfrac{1}{2} m_s \rangle = \delta_{M_s m_s} \delta_{\Lambda\lambda} (2\Lambda+1)^{\frac{1}{2}} \begin{pmatrix} \Lambda & \lambda & 0 \\ 0 & 0 & 0 \end{pmatrix} a,$$
$$a = \begin{pmatrix} \Lambda & \lambda & 0 \\ M_\Lambda & q & 0 \end{pmatrix} \delta_{q,-M_\Lambda}. \tag{14}$$

Ebenso ergibt sich für den Mesonenanteil unter Beachtung von (4)

$$\langle JML | C_q^{(\lambda)} | C_m^{(l)} \chi_{\frac{1}{2}\frac{1}{2}} \rangle = (4\pi)^{\frac{1}{2}} (-1)^{M_L} (L M_L \tfrac{1}{2}\tfrac{1}{2} | JML) (2L+1)^{\frac{1}{2}} \begin{pmatrix} L & \lambda & l \\ 0 & 0 & 0 \end{pmatrix} b,$$
$$b = \begin{pmatrix} L & \lambda & l \\ -M_L & q & m \end{pmatrix} \delta_{q,\, M_L - m}. \tag{15}$$

† Die Auswertung der Matrixelemente geschieht am einfachsten mit Hilfe einer der nachstehenden Monographien: A. R. Edmonds (Princeton, 1957); M. E. Rose (New York, London, 1957); Fano U. und G. Racah (New York, 1959).

Mit diesen Resultaten vereinfacht sich die Summation in (12): Zunächst erhält man wegen $\delta_{M_s m_s}$ in (14) eine Summation über die beiden Spinzustände des Anfangszustandes $|i_e\rangle$, also wegen der Unabhängigkeit der Summanden von m_s einfach den Faktor 2 in (12). Die Summe λ, q läßt wegen $\delta_{\Lambda\lambda}\,\delta_{q,-M_\Lambda}$ in (14) jeweils nur ein Wertepaar $\lambda = \Lambda$, $q = -M_\Lambda$ zu, welches nach Vorschrift (12) zu quadrieren ist. Wir erhalten so

$$w_{f_\mu} = 4\pi \frac{2\pi}{\hbar} \frac{\mathrm{d}Z}{\mathrm{d}E} (LM_L \tfrac{1}{2}\tfrac{1}{2}|JML)^2$$

$$\cdot \sum_{\Lambda l} (2l+1)(2\Lambda+1)(2L+1) \begin{pmatrix} \Lambda & \Lambda & 0 \\ 0 & 0 & 0 \end{pmatrix}^2 \begin{pmatrix} L & \Lambda & l \\ 0 & 0 & 0 \end{pmatrix}^2 K^2(\Lambda L \Lambda l) \tag{16}$$

$$\times \sum_{M_\Lambda m} \begin{pmatrix} \Lambda & \Lambda & 0 \\ M_\Lambda & -M_\Lambda & 0 \end{pmatrix}^2 \begin{pmatrix} L & \Lambda & l \\ -M_L & -M_\Lambda & m \end{pmatrix}^2 \delta_{-M_\Lambda, M_L - m}.$$

Wegen

$$\begin{pmatrix} \Lambda & \Lambda & 0 \\ 0 & 0 & 0 \end{pmatrix}^2 = \begin{pmatrix} \Lambda & \Lambda & 0 \\ M_\Lambda & -M_\Lambda & 0 \end{pmatrix}^2 = (2\Lambda+1)^{-1}$$

reduziert sich die letzte Summe auf die Orthogonalitätseigenschaft

$$\sum_{M_\Lambda m} \begin{pmatrix} L & \Lambda & l \\ -M_L & -M_\Lambda & m \end{pmatrix}^2 = (2L+1)^{-1}, \quad -M_L - M_\Lambda + m = 0,$$

so daß sich (16) zu

$$w_{f_\mu} = 4\pi \frac{2\pi}{\hbar} \frac{\mathrm{d}Z}{\mathrm{d}E} (LM_L \tfrac{1}{2}\tfrac{1}{2}|JML)^2 \sum_{\Lambda l} \frac{2l+1}{2\Lambda+1} \begin{pmatrix} L & \Lambda & l \\ 0 & 0 & 0 \end{pmatrix}^2 K^2(\Lambda L \Lambda l| \tag{17}$$

vereinfacht.

Bei gegebenem Λ und L folgen die erlaubten l-Beträge aus der „Dreiecksrelation" $\Delta(L\Lambda l)$, wobei $\left(\begin{smallmatrix} L & \Lambda & l \\ 0 & 0 & 0 \end{smallmatrix}\right)$ immer dann verschwindet, wenn $L+\Lambda+l$ ungerade ist (Auswahlregeln).

Eine Abhängigkeit der Übergangswahrscheinlichkeit in den Endzustand $|JML\rangle$ von der Quantenzahl M ist also nur über den vor der Summe stehenden Clebsch-Gordan Koeffizienten vorhanden. Wir schreiben daher

$$w_{f_\mu} = 4\pi \frac{2\pi}{\hbar} \frac{\mathrm{d}Z}{\mathrm{d}E} (LM_L \tfrac{1}{2}\tfrac{1}{2}|JML)^2 S(L) \tag{18a}$$

mit

$$S(L) = \sum_{\Lambda l} \frac{2l+1}{2\Lambda+1} \begin{pmatrix} L & \Lambda & l \\ 0 & 0 & 0 \end{pmatrix}^2 K^2(\Lambda L \Lambda l). \tag{18b}$$

4. Die Polarisation nach dem Auger-Einfang

Zur Durchführung der für die Berechnung von $\langle S_z\rangle$ in (8) vorgeschriebenen Summation unterscheiden wir die beiden Fälle

$$J = L+\tfrac{1}{2} \quad \text{mit} \quad (LM_L\tfrac{1}{2}\tfrac{1}{2}|JML)^2 = \frac{J+M}{2J}, \tag{19a}$$

$$J = L-\tfrac{1}{2} \quad \text{mit} \quad (LM_L\tfrac{1}{2}\tfrac{1}{2}|JML)^2 = \frac{J-M+1}{2(J+1)} \tag{19b}$$

und bilden mit Hilfe von (18) sowie (7) den Spinerwartungswert (8):

$$\langle S_z\rangle = \tfrac{1}{2}\frac{\sum\limits_J\left[S(L=J-\tfrac{1}{2})\sum\limits_M\frac{M(J+M)}{J^2} - S(L=J+\tfrac{1}{2})\sum\limits_M\frac{M(J-M+1)}{(J+1)^2}\right]}{\sum\limits_J\left[S(L=J-\tfrac{1}{2})\sum\limits_M\frac{J+M}{J} + S(L=J+\tfrac{1}{2})\sum\limits_M\frac{J-M+1}{J+1}\right]}. \tag{20}$$

Die Summationen über M sind elementar durchführbar, im einzelnen ist

$$\sum_M\frac{M(J+M)}{J^2} = \tfrac{1}{3}\frac{(J+1)(2J+1)}{J}, \quad \sum_M\frac{M(J-M+1)}{(J+1)^2} = -\tfrac{1}{3}\frac{(2J+1)J}{J+1}$$

$$\sum_M\frac{J+M}{J} = \sum_M\frac{J-M+1}{J+1} = 2J+1.$$

Das Ergebnis notieren wir in der Form

$$p = \frac{\langle S_z\rangle}{\frac{1}{2}} = \tfrac{1}{3}\frac{\sum\limits_J(2J+1)\left[\frac{J+1}{J}S(L=J-\tfrac{1}{2}) + \frac{J}{J+1}S(L=J+\tfrac{1}{2})\right]}{\sum\limits_J(2J+1)[S(L=J-\tfrac{1}{2})+S(L=J+\tfrac{1}{2})]}, \tag{21}$$

wo p den Prozentsatz der Polarisation angibt.

Zur Berechnung der Summe $S(L)$ summiert man für jede Quantenzahl $\Lambda = 0, 1, 2, \ldots$ über die mit L und Λ verträglichen l. Da die Übergangswahrscheinlichkeiten von dem drehimpulslosen Elektronenzustand $|i_e\rangle$ nach $|f_e\rangle$ mit wachsendem Λ sicher rasch abnimmt, genügt die Beschränkung auf kleine Λ-Beträge, sagen wir $\Lambda = 0, 1, 2$. Die Numerische Abschätzung der in $S(L)$ auftretenden Radialintegrale ist vermutlich fragwürdig, deshalb verzichten wir darauf (18b) ausführlich zu notieren. Nun wird ein merklicher Auger-Austausch beider Teilchen nur dann stattfinden, wenn der Stoßparameter des heranfliegenden Myons von der Größenordnung des Bohrschen Radius ist; aus dieser Forderung schließt man leicht auf eine notwendige Drehimpulsquantenzahl $l \approx k/k_e$ für das Meson. Da ferner die Mesonenenergie beim Einfang etwa die Größenordnung der Energie des gebundenen Elektrons haben

wird, folgt weiter $l \approx (m_\mu/m_e)^{\frac{1}{2}} \approx 14$. Wegen der Beschränkung auf kleine Λ-Beträge ist dann aber auch $L \approx l \approx 14$, so daß das Meson vorzugsweise in einer Zirkularbahn oder in einer nahezu zirkularen Bahn eingefangen wird. Für die damit erlaubte Beschränkung auf große L- und damit auch große J-Beträge folgt dann aus (21) sofort $p = \frac{1}{3}$, ohne daß wir Absolutabschätzungen der $S(L)$ benötigen.

Läßt man die bisher benutzte Voraussetzung der isotropen Impulsverteilung fallen, so ist (1b) in (11) einzusetzen. Die Mittelungen über die Impulsrichtungen entfällt, weshalb in den folgenden Rechnungen eine Doppelsumme $\sum_l \sum_{l'}$ auftritt. Wegen $m = 0$ entfallen ferner die Summationen über m und M_Λ. Statt (17) erhält man

$$w_{f_\mu} = 4\pi \frac{2\pi}{\hbar} \frac{\mathrm{d}Z}{\mathrm{d}E} (LM_L \tfrac{1}{2}\tfrac{1}{2} | JML)^2 \sum_{\Lambda l l'} (2l+1)(2l'+1) \frac{2L+1}{2\Lambda+1} \times \begin{pmatrix} L & \Lambda & l \\ 0 & 0 & 0 \end{pmatrix} \begin{pmatrix} L & \Lambda & l' \\ 0 & 0 & 0 \end{pmatrix} \begin{pmatrix} L & \Lambda & l \\ -M_L & M_L & 0 \end{pmatrix} \begin{pmatrix} L & \Lambda & l' \\ -M_L & M_L & 0 \end{pmatrix} K(\Lambda L \Lambda l) K(\Lambda L \Lambda l'). \tag{22}$$

Im Gegensatz zu (17) treten jetzt auch nichtdiagonale Terme l, l' auf, insbesondere ist aber jetzt die Abhängigkeit der Übergangswahrscheinlichkeit von $M = M_L + \frac{1}{2}$ nicht mehr so bequem wie früher, da diese jetzt nicht durch den Clebsch-Gordan Koeffizienten allein gegeben ist. Begnügt man sich für eine rohe Abschätzung mit $\Lambda = 0$ (das Elektron wird von dem drehimpulslosen Anfangszustand in den kugelsymmetrischen Endzustand $\phi_0(r_e)$ befördert), so ist nach (22) $l = l' = L$, $M_L = 0$, also $M = \frac{1}{2}$ und man erhält

$$w_{f_\mu} = 4\pi \frac{2\pi}{\hbar} \frac{\mathrm{d}Z}{\mathrm{d}E} (L0 \tfrac{1}{2}\tfrac{1}{2} | J \tfrac{1}{2} L)^2 (2L+1) K^2(0L0L). \tag{23}$$

Mit (7) kontrolliert man nun leicht, daß — in Übereinstimmung mit den Aussagen des Vektordiagramms — die zu (23) gehörige Polarisation mit wachsendem J verschwindet, so daß für $L \approx 14$ das Meson praktisch völlig depolarisiert wird. Vermutlich ändert sich an dieser Aussage auch dann nichts wesentliches, wenn in (22) weitere Terme $\Lambda = 1, 2 \ldots$ berücksichtigt werden. Es wäre denkbar, daß man die Depolarisation erheblich verringern kann ($p > \frac{1}{3}$), wenn man durch eine geeignete experimentelle Anordnung dafür sorgt, daß Spin und Flugrichtung aufeinander senkrecht stehen.

Wünschenswert für eine vollständige theoretische Beschreibung scheint die Beantwortung der Fragen nach der Impulsverteilung des Mesons beim Auger-Einfang und damit nach der Depolarisation des aus einer beliebigen **k**-Richtung heranfliegenden Mesons.

Literatur

1) R. Garwin, L. Ledermann und M. Weinrich, Phys. Rev. **105** (1957) 1415;
D. Berley, T. Coffin, R. Garwin, L. Ledermann und M. Weinrich, Phys. Rev. **106** (1957) 835

NORTH - HOLLAND BOOKS

Bruno Vitale

CERN-GENEVA

A Bibliography

on

Heavy Mesons and Hyperons

1946-1958

It has become difficult nowadays either to find a useful information or a pertinent reference in the field of "strange" particles. Now the aim of this bibliography is to classify and arrange in chronological order all the available papers on this matter. The book could be used also as a list of the problems that have been, or are at present discussed about "strange" particles.

6½×9½" VIII + 142 p. Guilders 9.50 19s. $2.50

NORTH-HOLLAND PUBLISHING COMPANY — AMSTERDAM

NORTH - HOLLAND BOOKS

Paul Ehrenfest

COLLECTED SCIENTIFIC PAPERS

XII + 632 pages

Guilders 45.00 (90s.)

This volume makes widely scattered publications readily available. All Dutch articles appear here in English; the German publications in the original language.

Sole Agency for U.S.A.:
Interscience Publishers Inc.— New York

NORTH-HOLLAND PUBLISHING COMPANY-AMSTERDAM